

# **Unraveling novel and evolutionarily conserved regulators of cell wall integrity signaling in tip- growing plant cells**

Inaugural-Dissertation

zur

Erlangung des Doktorgrades

der Mathematisch-Naturwissenschaftlichen Fakultät

der Universität zu Köln

vorgelegt von

**Jens Westermann**

aus Schwalmstadt, Deutschland

Köln, 2018

Berichterstatte:r:                      Dr. Aurélien Boisson-Dernier  
Prof. Dr. Martin Hülskamp

Prüfungsvorsitzender:                Prof. Dr. Siegfried Roth

Tag der mündlichen Prüfung:        10. Januar, 2019

## ZUSAMMENFASSUNG

Pflanzenzellen sind auf die ständige Wahrnehmung von Umweltreizen angewiesen um essentielle Prozesse, wie zum Beispiel Zellwachstum, zu gewährleisten. Dies gilt im Besonderen für Zellen mit polarem Spitzenwachstum (engl. "tip-growth"), wie Pollenschläuche und Wurzelhaare, die über das Zusammenspiel von lokalen Veränderungen ihrer Zellwandelastizität und des intrazellulären Turgordrucks unidirektional expandieren. Hierzu haben Pflanzen eine fein abgestimmte molekulare Maschinerie extra- und intrazellulärer Regulatoren entwickelt, welche die Aufrechterhaltung der Zellwandintegrität während des polaren Spitzenwachstums kontrollieren. In der Ackerschmalwand (*Arabidopsis thaliana*) wurden die Malectin-ähnlichen Rezeptoren (MLRs) ANXUR1/2 (ANX1/2) und ihr direktes Schwesterhomolog FERONIA (FER), welche zur Überfamilie Rezeptor-ähnlicher Kinasen (RLKs) gehören, als Mediatoren extrazellulärer Signale in das Zellinnere von Pollenschläuchen bzw. Wurzelhaaren identifiziert. Weiter stromabwärts dieses Signaltransduktionsweges aktivieren sowohl ANX1/2 als auch FER NADPH-Oxidasen der 'REACTIVE BURST OXIDASE'-HOMOLOG (RBOH)-Untergruppe, sowie die Rezeptor-ähnliche zytoplasmatische Kinase (RLCK) MARIS (MRI). Wie dieser Signalweg in eine Zellantwort umgewandelt wird, ist hingegen nur schlecht verstanden.

Vor diesem Hintergrund ist ein Hauptanliegen dieser Arbeit die Identifizierung der fehlenden Bindeglieder des Zellwandintegritätssignalweges, vor allem im Hinblick auf die Frage, wie (genetische) Signale in ein mechanistisches Programm umgewandelt werden. Im Rahmen der vorgelegten Arbeit wurden mehrere mögliche Regulatoren des polaren Spitzenwachstums untersucht. Dies beinhaltet (i) durch zyklische Nukleotide gesteuerte Ionenkanäle (CNGCs), die den Influx von Calcium, einem zentralen Regulator der molekularen Zellwandrestrukturierung und der Wachstumsgeschwindigkeit, steuern, (ii) die Proteinphosphatasen ATUNIS1/2 (AUN1/2), welche die ersten negativen Regulatoren des MLR-medierten Zellwandintegritätssignalweges darstellen, (iii) die Typ-VII-RLCK VEIVE (VEI) und (iv) zwei RLK-Homologe des Brunnenlebermooses *Marchantia polymorpha*, welche eine nahe Verwandtschaft zu *Arabidopsis* MLRs und RLCKs aufweisen und somit ein konserviertes Signalmodul zur Kontrolle der Zellwandintegrität in *Marchantia*-Rhizoiden (spezialisierten Wurzelzellen mit polarem Spitzenwachstum) bilden könnten.

Aufgrund der möglicherweise konservierten Funktion von MLRs und ihrer in *Arabidopsis* bekannten Stromabwärtsregulatoren im Laufe der Evolution von Algen bis hin zu Blütenpflanzen, mag die Kombination solch neuer Entdeckungen daher zu einem besseren Verständnis der generellen Regulationsmechanismen zur Aufrechterhaltung der Zellwandintegrität von Zellen mit polarem Spitzenwachstum beitragen. Zum anderen bieten diese Ergebnisse auf lange Sicht möglicherweise wertvolle Einblicke im Hinblick auf die gezielte Manipulation von Zellwandkomposition, Ernteertrag und Fruchtbarkeit von Pflanzen, welche mittels Disziplinen wie der grünen Biotechnologie und der Agronomie ausgenutzt werden könnten.

## ABSTRACT

Plant cells are in a constant need of sensing their environment to guarantee essential processes such as cell growth. This accounts especially for tip-growing cells, such as pollen tubes or root hairs, which expand unidirectionally via an interplay of local changes in cell wall (CW) elasticity and turgor-driven cell expansion. Therefore, plants have developed a fine-tuned molecular machinery of extra- and intracellular regulators which control the maintenance of cell wall integrity (CWI) during tip-growth. In the thale cress (*Arabidopsis thaliana*), the malectin-like receptors (MLRs) ANXUR1/2 (ANX1/2) and their closest homolog FERONIA (FER), all of which belong to the superfamily of receptor-like kinases (RLKs), have been shown to function as mediators of extracellular signals into the cytoplasm of pollen tubes and root hairs, respectively. Further downstream, ANX1/2 and FER both activate a signaling pathway which includes reactive oxygen (ROS)-producing NADPH-oxidases of the REACTIVE BURST OXIDASE HOMOLOG (RBOH) subfamily and the receptor-like cytoplasmatic kinase (RLCK) MARIS (MRI). However, how downstream signaling is converted into a cell response is only poorly understood.

Against this background, a major aim of this work is the identification of the missing links in CWI signaling regarding the question how (genetic) signaling is transmitted into a mechanistical program. In the scope of this thesis several putative regulators of tip-growth control were studied. This includes the study of (i) cyclic nucleotide-gated ion channels (CNGCs) which control the influx of  $\text{Ca}^{2+}$ , a central regulator of molecular CW remodeling and growth rate, (ii) the protein phosphatases ATUNIS1/2 (AUN1/2) which represent the first negative regulators of MLR-mediated CWI signaling, (iii) the type-VII receptor-like cytoplasmic kinase VEIVE (VEI) and (iv) two RLK-homologs of the liverwort *Marchantia polymorpha*, which are closely related to *Arabidopsis* MLRs and RLCKs and could build a conserved signaling module to control growth of *Marchantia* rhizoids, specialized tip-growing rooting cells.

As the function of MLRs and their *Arabidopsis* downstream regulators appear to be conserved from algae to angiosperms, the combination of such findings may aid our understanding of the general regulatory mechanisms maintaining CWI in the tip-growing cell, ultimately holding valuable insights for targeted manipulation of CW composition, crop yield and plant fertility to be exploited via green biotechnology and agronomy.



# INDEX OF CONTENTS

<b>1. INTRODUCTION</b>	<b>8</b>
1.1. Forms of growth are various in eukaryotic cells	8
1.2. Tip-growing cells are ideal models to study a multitude of functions in plants.	9
1.3. The primary cell wall and intracellular cytoskeleton build a dynamic scaffold which shapes the tip-growing cell.	10
1.4. A tip-focused proton gradient recruits CW remodeling enzymes to the pollen tube.	12
1.5. Calcium represents a versatile regulator of tip-growth control.	14
1.6. Transmembrane signal transduction - How to control the tip-growth control machinery? ....	16
1.7. What does it take to build a tube? - Evolution and functional conservation of tip-growth control during land plant evolution	18
1.8. Functional conservation of RLK-mediated CWI control in streptophytes	21
1.9. <i>Marchantia polymorpha</i> as a genetic model to study tip-growth	26
<b>2. RESEARCH OUTLINE</b>	<b>28</b>
2.1. Has RLK-mediated tip-growth control been conserved in a common signaling module during land plant evolution?	28
2.2. How do plants regulate CWI? - Understanding the regulatory mechanism of tip-growth control	28
2.2.1. Type-one protein phosphatases ATUNIS1/2.	29
2.2.2. Cyclic nucleotide-gated ion channel18 (CNGC18).	29
2.2.3. Type-VII-receptor-like cytoplasmic kinase VEIVE	30
<b>3. MATERIALS AND METHODS</b>	<b>31</b>
3.1. Materials	31
3.1.1. Plant lines and bacterial strains	31
3.1.1.1. <i>Arabidopsis thaliana</i> and <i>Marchantia polymorpha</i>	31
3.1.1.2. <i>Escherichia coli</i> and <i>Agrobacterium tumefaciens</i>	34
3.1.2. Vectors	34
3.1.3. Oligonucleotide sequences	37
3.1.4. Chemicals and solutions	39
3.1.5. Preparation kits	42
3.1.6. Software	42
3.2. Methods	43
3.2.1. Plant cultivation	43
3.2.1.1. Axenic cultivation setup	43
3.2.1.2. Far-red light-induced sporogenesis in <i>Marchantia</i>	43
3.2.1.3. Long-term cultivation of vegetative and reproductive <i>Marchantia</i> stages	44
3.2.2. Molecular biology, cloning and transformation	44
3.2.2.1. Genomic DNA-extraction	44

3.2.2.2.	PCR-based genotyping .....	44
3.2.2.3.	Gender-specific <i>Marchantia</i> genotyping PCR .....	46
3.2.2.4.	Genotyping for point mutations via dCAPS-assay .....	46
3.2.2.5.	RNA-extraction from <i>Marchantia</i> thalli .....	47
3.2.2.6.	Complementary DNA synthesis .....	47
3.2.2.7.	PCR-based amplification of promoter and ORF sequences .....	48
3.2.2.8.	Gel elution of PCR-fragments .....	49
3.2.2.9.	Gateway-Cloning system .....	49
3.2.2.10.	Plasmid-modification via restriction and ligation .....	50
3.2.2.11.	Site-directed mutagenesis.....	50
3.2.2.12.	Heat-shock transformation of <i>Escherichia coli</i> .....	51
3.2.2.13.	Extraction of plasmid DNA .....	51
3.2.2.14.	Plasmid verification .....	52
3.2.2.15.	Long-term storage of bacterial strains in glycerol .....	53
3.2.2.16.	Transformation of electro-competent <i>Agrobacterium tumefaciens</i> .....	53
3.2.2.17.	<i>Agrobacterium</i> -mediated plant transformation and transformant selection .....	53
3.2.3.	Phenotypic analyses .....	55
3.2.3.1.	<i>In vitro</i> pollen germination assay.....	55
3.2.3.2.	Pollen tube length measurements.....	56
3.2.3.3.	Seed set assay.....	56
3.2.3.4.	Reciprocal crossing of <i>Arabidopsis</i> .....	57
3.2.3.5.	Root hair growth assay.....	57
3.2.3.6.	Rhizoid growth assay .....	58
3.2.3.7.	Microscopic analyses .....	58
3.2.3.8.	Detection of RFP signals in autofluorescent tissue of <i>M. polymorpha</i> .....	59
3.2.3.9.	Live-imaging of cytosolic [Ca <sup>2+</sup> ]-dynamics in tip-growing cells .....	60
4.	<b>RESULTS</b> .....	62
4.1.	Functional conservation of a RLK-dependent cell wall integrity signaling module .....	62
4.1.1.	The <i>Marchantia</i> homologs <i>MpPTI</i> and <i>MpTHE1</i> regulate cell wall integrity in tip-growing rhizoids .....	62
4.1.2.	<i>AtMRI</i> is capable of rescuing the loss of integrity phenotype of <i>Mppti</i> rhizoids.....	67
4.1.3.	<i>MpPTI</i> is capable of rescuing the <i>mri-1</i> -induced loss of CWI in both, <i>Arabidopsis</i> PTs and RHs. ....	69
4.1.4.	Overexpression of <i>Marchantia</i> and <i>Arabidopsis</i> MLRs and PTI-like genes leads to growth inhibition in tip-growing cells.....	75
4.1.4.1.	PTI-like- and MLR-homologs inhibit <i>Marchantia</i> rhizoid growth .....	75
4.1.4.2.	<i>MpPTI</i> and <i>MpPTI</i> <sup>[R240C]</sup> inhibit tip-growth in <i>Arabidopsis</i> . ....	80
4.1.5.	Does <i>MpPTI</i> act genetically downstream of <i>MpTHE1</i> in a rhizoid CWI signaling pathway? .....	84

4.1.6.	Is <i>MpPTI</i> <sup>[R240C]</sup> capable of rescuing the loss of CWI in <i>fer-4</i> root hairs and <i>amiRRALF4/19</i> pollen tubes? .....	84
4.1.7.	Do <i>Mppti</i> and <i>Mpthe1</i> govern further functions in <i>Marchantia</i> ? .....	85
4.2.	The protein phosphatases AUN1/2 regulate cell wall integrity in tip-growing cells.....	88
4.2.1.	Former work .....	88
4.2.2.	Establishment and phenotypic analysis of the independent mutant alleles <i>aun1-2</i> and <i>aun2-2</i> .....	88
4.2.3.	Cloning of AUN2 ORF and <i>proAUN1</i> .....	91
4.2.4.	Subsequent work.....	92
4.3.	Role of CNGCs and Ca <sup>2+</sup> signaling in tip-growth control .....	93
4.3.1.	Loss of CNGC18 function leads to pollen tube bursting <i>in vitro</i> . ....	93
4.3.2.	The CNGC18 <sup>[R491Q]</sup> amino acid substitution in <i>cngc18-17</i> is truly linked to pollen bursting.....	96
4.3.3.	Overexpression of GFP-CNGC18 inhibits pollen tube growth <i>in vitro</i> . ....	98
4.3.4.	Knockdown of both, CNGC18 and MRI, leads to irregular [Ca <sup>2+</sup> ] <sub>cyt.</sub> -oscillations and unsteady pollen tube growth <i>in vitro</i> .....	101
4.3.5.	Expression of YFP-CNGC18 under <i>proLat52</i> does not rescue male transmission of the <i>anx-2</i> allele in the <i>anx1-1/anx1-1 anx2-1/ANX2</i> background. ....	104
4.3.6.	Does introduction of <i>proACA9::GFP-CNGC18</i> via crossing rescue male transmission of <i>anx2-1</i> in the <i>anx1-1/anx1-1 anx2-1/ANX2</i> background? .....	107
4.4.	The role of the class VII-RLCK VEIVE in plant reproduction .....	108
4.4.1.	VEIVE is a pollen-expressed member of class VII RLCKs. ....	108
4.4.2.	VEIVE loss of function does not cause obvious phenotypes linked to male fertility. ..	109
4.4.3.	VEIVE does not have any close <i>Arabidopsis</i> homologs. ....	113
5.	<b>DISCUSSION</b> .....	114
5.1.	RLK-mediated CWI signaling during tip-growth is conserved amongst land plants. ....	114
5.1.1.	The evolution of tip-growth – Homology or convergence? .....	117
5.1.2.	Future directions.....	119
5.2.	The protein phosphatases AUN1/2 negatively regulate MLR-mediated tip-growth control. ....	123
5.2.1.	AUN1/2 and their putative up- and downstream targets.....	125
5.3.	Do CNGCs regulate the tip-focused Ca <sup>2+</sup> -gradient in response to RLK-mediated CWI signaling? .....	127
5.3.1.	Alternative models for RLK-dependent and -independent Ca <sup>2+</sup> -signaling .....	128
5.4.	May Rho-GTPases be the missing link between the establishment of pollen tube polarity and the Ca <sup>2+</sup> -dependent regulation of growth speed? .....	132
5.5.	VEIVE does not exert an obvious pollen-specific function during plant reproduction.....	134
6.	<b>SUPPLEMENTAL FIGURES AND TABLES</b> .....	135
7.	<b>REFERENCES</b> .....	137
8.	<b>INDEX OF ABBREVIATIONS</b> .....	152
9.	<b>INDEX OF FIGURES</b> .....	156

10.	<b>INDEX OF TABLES</b> .....	158
11.	<b>ACKNOWLEDGEMENTS</b> .....	159
12.	<b>EIGENSTÄNDIGKEITSERKLÄRUNG</b> .....	161
13.	<b>LEBENS LAUF</b> .....	162

# 1. INTRODUCTION

## 1.1. Forms of growth are various in eukaryotic cells.

Growth of multicellular organisms relies on cellular expansion. Plants have developed a fascinating variety of cellular forms and shapes during evolution. The majority of plant cells shows a diffuse, three-dimensional, uniform growth behavior based on the equally distributed (isobaric) intracellular turgor-pressure, an example being fruit parenchyma cells (Fig. 1A). In contrast, some tissues and single cells depend on anisotropic growth modes given their specialized functions in the context of the whole plant. Epidermal hypocotyl cells, for instance, need to expand bidirectionally to allow the plant seedling to grow against the gravitropic vector (Fig. 1B). An extreme form of polar growth is tip-growth. Tip-growing cells, such as pollen tubes, root hairs and rhizoids expand unidirectionally at the apical dome, a strictly defined region at the distal cellular end (Fig. 1C). In addition, some cell types, such as trichomes and leaf epidermal cells, have developed a hybrid form of diffuse, bi- and/or unidirectional growth (Fig. 1D; Geitmann and Ortega, 2009; Guerriero et al., 2014).

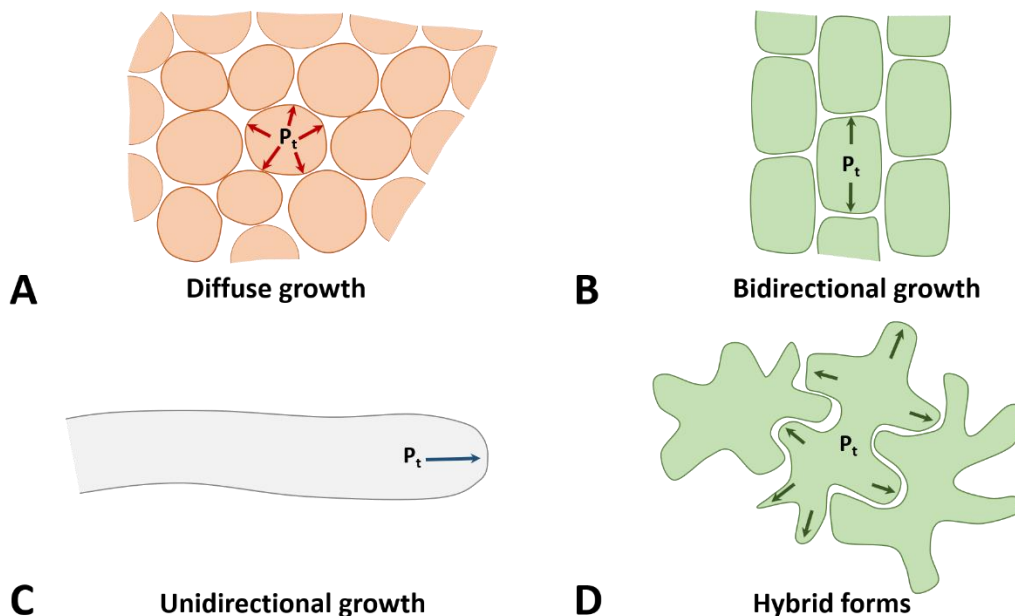


**Fig. 1: The variety of growth modes in plant cells.** Schematic representations of (A) diffuse, isotropic growth (e.g. fruit parenchyma cells), (B) bidirectional growth (epidermal hypocotyl cells), (C) tip-growth (pollen tubes and root hairs) and (D) hybrid forms employing both, unidirectional and multidirectional/ diffuse growth (e.g. leaf epidermal cells; trichomes). Arrows depict the effective cellular growth directions promoted by the isobaric turgor pressure ( $P_t$ ); schemes are based on the descriptions of Geitmann and Ortega, 2009.

## 1.2. Tip-growing cells are ideal models to study a multitude of functions in plants.

Tip-growing cells have been studied best in flowering plants, such as *Lillium longiflorum* (lily) and the genetic model plant *Arabidopsis thaliana* (thale cress), but also in agronomically important species such as rice (*Oryza sativa*) or maize (*Zea mays*), in all of which they govern a multitude of functions. Root hairs represent unidirectional outgrowths of root epidermal cells, which serve as additional contact surface to facilitate water and nutrient uptake from and anchorage to the substrate (Jones and Dolan, 2012; Fig. 2A and B). Pollen tubes represent specialized male-gametophytic cells, which penetrate the pistillar tissue for sperm cell delivery and fertilization (Dresselhaus and Franklin-Tong, 2013; Fig. 2C - E).

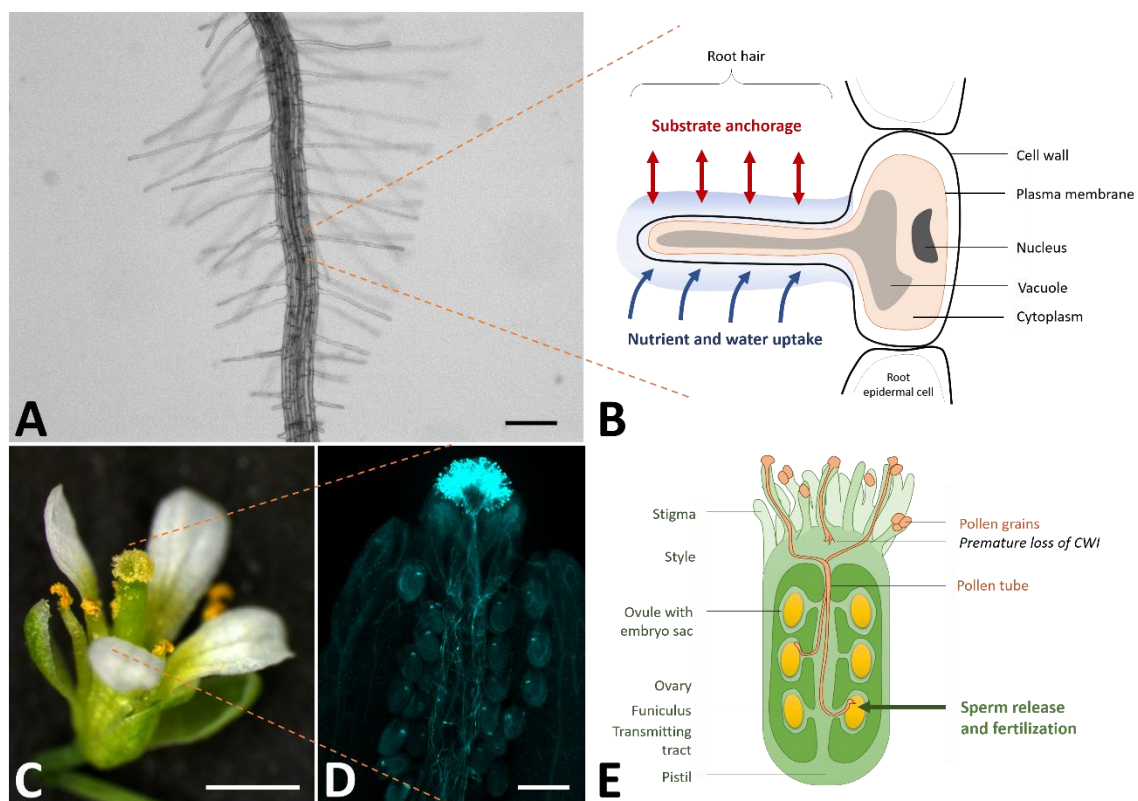


**Fig. 2: The functions of root hairs and pollen tubes in flowering plants.** (A) Root hairs on the primary root of *Arabidopsis thaliana*. Scale bar: 200  $\mu$ m. (B) Schematic representation of the root epidermis which gives rise to root hairs, unicellular evaginations of the cellular border. Root hairs govern several functions, including anchorage to the substrate, as well as water and nutrient uptake from the soil, both via surface area extension. (C) A flower of the model plant *Arabidopsis thaliana* with a pollinated pistil (marked with orange dashed lines); scale bar: 1 mm. (D) Microscopic image of a pollinated pistil visualized via Aniline Blue staining; scale bar: 200  $\mu$ m (Franck, 2018). (E) Schematic representation of the male and female gametophytes during reproduction: Pollen grains germinate upon attachment to the stigma of the female pistil. They build pollen tubes which penetrate the style, grow through the transmitting tract and the funiculi towards the ovules (containing embryo sacs). Upon arrival, the pollen tube loses its cell wall integrity in a controlled manner to release its cargo, two sperm cells, which fertilize the female egg cell (giving rise to the embryo) and the central cell (giving rise to the endosperm, *i.e.* a tissue nourishing the developing embryo).

Tip-growing cells are ideal models to study control of cell growth and polarity as they display extraordinarily high growth rates, while cellular expansion is restricted to only one distinct region. Growth-related phenotypes are thus thought to be easily observable and recordable. Furthermore, they are amenable to genetic and “omics”-based approaches, pharmacological treatments, *in vitro* cultivation and live-cell imaging via fluorescence microscopy (Michard et al., 2017).

### 1.3. The primary cell wall and intracellular cytoskeleton build a dynamic scaffold which shapes the tip-growing cell.

Different hypotheses have been introduced in the quest for the driving force of tip-growth. While the “cell wall model” suggests that spatiotemporally well-organized cell wall (CW) remodeling leads to oscillatory changes in CW stiffness and thus, turgor-driven, unidirectional cellular expansion, the “hydrodynamic model” acts on the assumption that changes in turgor pressure alone account for cellular expansion (Zonia and Munnik, 2011). However, the cell wall model has largely been favored by plant scientists based on experimental evidence. In assumption of the cell wall model, the isobaric turgor pressure always requires a local, intra- or extracellular counterforce to allow for anisotropic, unidirectional growth. Indeed, plant cells have acquired an intra- and extracellular, stable yet dynamic framework which is mainly composed of proteins and polysaccharides: (i) An extracellular matrix (ECM), mainly composed of pectin, cellulose and hemicellulose, but also structural, remodeling, synthesis and signal transduction proteins, builds the primary CW. Cellulose fibres are the main carbohydrates, which are linked via hemicellulose molecules, such as xyloglucan, functioning as “tethers”. The cellulose-hemicellulose-network is embedded in a matrix of pectins, which determine the extent of CW elasticity or stiffness (Fry and Stephan, 1989; Cosgrove, 2005; Gu and Nielsen, 2013). (ii) The intracellular cytoskeletal framework of actin filaments and microtubules is arranged longitudinally in the tube shank region, with actin filaments being increasingly scattered towards the apex (Cai et al., 2015), allowing for tip-directed growth. Furthermore, vesicles are transported along actin filaments via motor proteins, such as myosin, in order to deliver CW material to the pollen tube tip (Cai and Cresti, 2009). Another motor protein, the Armadillo repeat-containing kinesin 1 (ARK1) is required for directed tip-growth in the *Arabidopsis* root hair. Both, the ECM and the cytoskeleton, shape the cell and guarantee stability against positive and negative pressures. In turn, unidirectional growth relies on the delicate balance between

secretion of adequate amounts of CW components to be integrated into the CW mesh, CW crosslinking and local, tip-focused CW loosening. The close spatiotemporal regulation of these processes causes a selective pliability at the pollen tube apex, allowing for turgor-driven cellular expansion, while maintaining cell wall integrity (CWI) (Goriely and Tabor, 2003; Rounds and Bezanilla, 2013; Fig. 3).

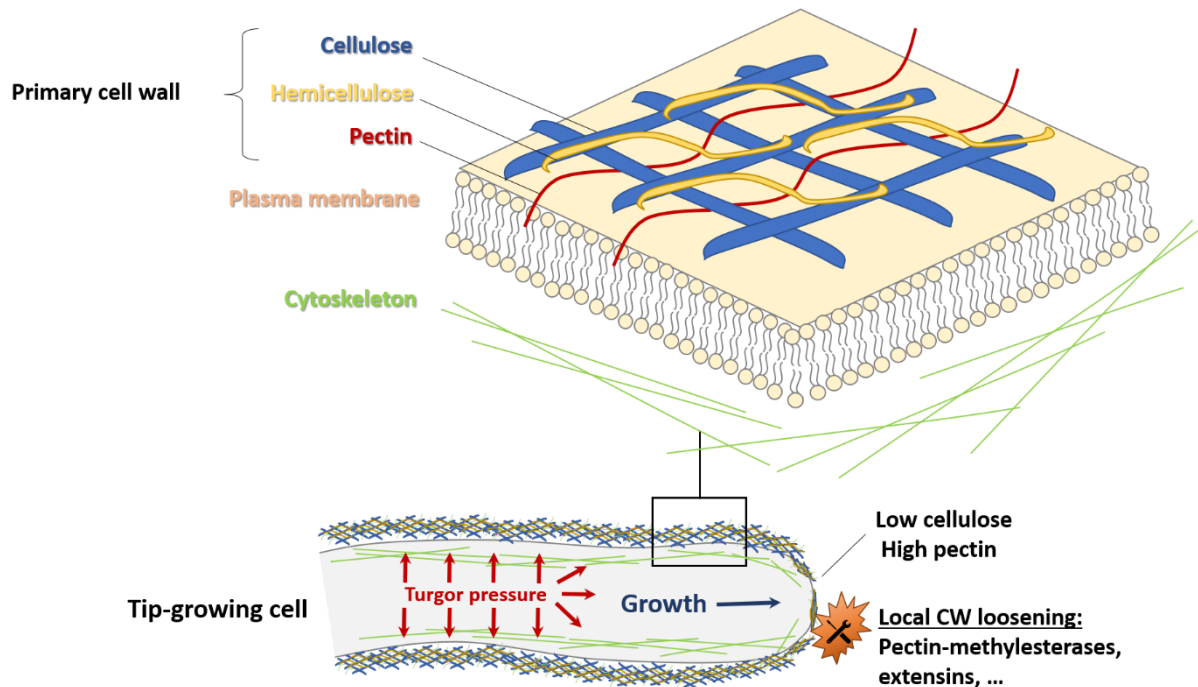


**Fig. 3: Structural composition of the extracellular matrix and intracellular cytoskeleton of the tip-growing cell.** A schematic representation. The extracellular matrix (ECM), also referred to as primary cell wall (CW), is mainly composed of several layers of cellulosic microfibrils, embedded in a matrix of hemicellulose and braided with pectins, as well as a variety of CW remodeling proteins. The intracellular cytoskeleton is composed of actin and microtubules, which are arranged longitudinally along the shank region. The cellular tip contains comparatively large amounts of pectins, which can be remodelled via pectin-methylesterases (PMEs), and which are thought to influence CW elasticity, leading to local CW loosening and turgor-driven, unidirectional growth (Cosgrove, 2005; Gu and Nielsen, 2013; Cai et al., 2015).

A variety of CW and cytoskeleton remodeling factors has been described, including extensins, expansins, glucanases, glycosylases, pectin-methylesterases and actin-binding proteins (Rounds and Bezanilla, 2013; Cosgrove, 2016; Bedinger, 2018). All these factors, however, need to be directed in a spatiotemporal manner. It has been demonstrated that tip-growing cells, such as pollen tubes, possess an intracellular tip-focused pH- and calcium gradient, both of which are crucial for steady pollen tube growth (Holdaway-Clark et al., 2003; Steinhorst and Kudla, 2013 A; Steinhorst and Kudla, 2013 B, Michard et al., 2017).



#### 1.4. A tip-focused proton gradient recruits CW remodeling enzymes to the pollen tube.

The pH-gradient of pollen tubes is thought to be maintained via an interplay between a constant apical proton influx via proton/cation-permeable channels and subapical proton efflux via proton pumps, respectively, forming an acidic tip and an alkaline band in the shank region of the tube (Feijó et al., 1999; Cárdenas et al., 2005). While subapical alkalinization was proposed to positively regulate actin filament formation via pH-sensitive actin-binding proteins, apical acidification is thought to foster binding of pollen-specific alkaline pectin methylesterases (PMEs) (Feijó et al., 1999; Bosch and Hepler, 2005). Even though such pH-gradients have not directly been observed in root hairs, high cytoplasmic pH can lead to root hair growth inhibition, while high apoplastic proton concentrations can trigger loss of cell wall integrity (Bibikova et al., 1998). Regulation of proton flux in tip-growing cells has been hypothesized to be governed by proton pumps ( $H^+$ -ATPases) (Monshausen et al., 2007). In pollen tubes of *Nicotiana tabacum*, absence of the AUTOINHIBITED PLASMA MEMBRANE  $H^+$ -ATPase (*NtAHA*) from the tube apex is crucial for cell polarity and growth (Cortal et al., 2008), while root (hair)-specific AHA2 and AHA7 control root cell expansion and root hair growth in *Arabidopsis* (Hoffmann et al., 2018), underpinning the general role of AHA homologs during tip-growth.

##### **Pectin methylesterases**

The pollen tube apex is mainly coated with pectins, which are secreted as pectin methoxyesters and in turn demethylesterified by co-secreted PMEs. Freshly secreted, pectin methoxyesters mixed with deesterified pectins are building a comparatively loose CW which allows for tip-growth. At the tip, PME-induced pectin demethylesterification is blocked via co-secreted PME inhibitors (PMEIs). In the shank region, however, absence of active PMEIs leads to conversion of methylesterified pectins into their acid form by PMEs and thus CW stiffening and decreased growth rate (Li et al., 1996; Kroeger et al., 2008; Hepler et al., 2012; Kroeger and Geitmann, 2012). Alternation between acidic and mixed (esterified and deesterified) pectins can be visually traced in lily pollen tubes in form of apical “pectin rings” (Li et al., 1996) and the balance between PMEs and PMEIs was experimentally shown to determine the distribution of esterified and deesterified pectins at the tube apex (Röckel et al., 2008). Furthermore, the known roles of the pollen-expressed pectin methylesterase VANGUARD1 (VGD1) in promotion of pollen tube growth in the transmitting tract during plant reproduction in *Arabidopsis* and the regulation of pollen tube morphology and growth

rate via the pollen-specific PME1 (*AtPPME1*) support this model (Bosch and Hepler, 2005; Jiang et al., 2005; Tian et al., 2006).

### **Extensins**

Extensins are known as structural CW glycoproteins which are exocytosed via the secretory pathway (Hawes et al., 1991) and can covalently crosslink with the primary cell wall (Draeger et al., 2015). They have been identified and characterized in several plant species, including *Arabidopsis* and maize (Rubinstein et al., 1995, Bedinger, 2018). The Leucin-rich-repeat extensin chimera 1 and -2 (LRX1/2) are tightly associated with the root hair cell wall and were shown to regulate root hair development in *Arabidopsis* (Baumberger et al., 2001; Baumberger et al., 2003), while the pollen-expressed LRX8/9/10/11 regulate cell wall development and integrity signaling in *Arabidopsis* pollen tubes (Fabrice et al., 2018; Mecchia et al., 2017; Sede et al., 2018). It is currently unknown how LRXs exert their role precisely.

### **Cellulose synthases**

Unlike hemicelluloses and pectins, which are secreted via vesicles at the growing tip of the cell, cellulosic microfibrils are synthesized by plasma membrane (PM)-localized cellulose synthetases (CESAs). In *Arabidopsis*, at least 3 different CESA genes are required to form a functional cellulose synthesizing complex (Cosgrove, 2005; Gu and Nielsen, 2013). CESAs are required for (bidirectional) cell elongation in hypocotyl and root tissue (Fagard et al., 2000). Similarly, mutant versions of CESA and CESA-like (CSL) genes, both of which show polar localization to the plasma membrane of the cell apex (Cai et al., 2011; Wang et al., 2011 A), are known to cause strong defects in pollen germination and pollen tube growth (Persson et al., 2007; Bernal et al., 2008; Wang et al., 2011 A). Accordingly, CESAs/CSLs were shown to be required for root hair tip-growth as well (Bernal et al., 2008; Galway et al., 2011; Park et al., 2011; Yoo et al., 2012). However, CSLs have also been shown to localize to the endoplasmic reticulum (ER) suggesting a possible further role in synthesis of non-cellulosic, secreted polysaccharides such as hemicelluloses (Foreman and Dolan, 2001; Cosgrove, 2005).

## 1.5. Calcium represents a versatile regulator of tip-growth control.

Calcium ions ( $\text{Ca}^{2+}$ ) are a central messenger in a variety of developmental processes across eukaryotes. It has long been known that pollen tube growth relies on tip-focused  $\text{Ca}^{2+}$  accumulation and (trans-membrane) flux (Brewbaker and Kwack, 1963; Kwack, 1967; Jaffe et al., 1975; Kühtreiber and Jaffe, 1990; Miller et al., 1992; Hepler et al., 2012; Steinhorst and Kudla, 2013 A; Demidchik et al., 2018; Fig. 4). Furthermore,  $\text{Ca}^{2+}$  controls pollen tube growth direction (Malhó and Trewavas, 1996), while  $\text{Ca}^{2+}$  concentrations below  $10\mu\text{M}$  were reported to lead to pollen tube bursting (Picton and Steer, 1983). While initial discovery and measurement of  $\text{Ca}^{2+}$  fluxes mainly relied on electrophysiological approaches (e.g. the patch-clamping method) (Véry and Davies, 2000; Demidchik et al., 2018), contemporary studies on intracellular  $\text{Ca}^{2+}$  dynamics often rely on genetically-encoded ratiometric  $\text{Ca}^{2+}$ -biosensors, like the Yellow CaMeleon 3.60 (YC3.60) sensor, allowing for spatiotemporal visualization of relative intracellular  $\text{Ca}^{2+}$  concentrations and dynamics (Monshausen et al., 2008; Boisson-Dernier et al., 2013; Franck et al., 2017; Schoenaers et al., 2017; Kwon et al., 2018). One important role of  $\text{Ca}^{2+}$  is the regulation of CW elasticity via crosslinking of CW-localized acidic pectin (Hepler et al., 2012). Pectin methoxyesters and PME (see 1.3.) were shown to be secreted at the pollen tube apex via exocytosis in an oscillatory pattern which precedes oscillatory, yet regular changes in growth rate (McKenna et al., 2009). Similarly, periodic oscillations in cytosolic  $\text{Ca}^{2+}$  concentrations, followed by changes in growth rate, have frequently been reported for *Arabidopsis* wild-type pollen tubes (Weisenseel et al., 1975; Holdaway-Clark et al., 1997; Messerli et al., 1997; Holdaway-Clark et al., 2003; Cárdenas et al., 2008; Kroeger et al., 2008; Frank et al., 2017) and root hairs (Monshausen et al., 2008), while a similar correlation between tip-growth rate and intracellular ROS- and  $\text{H}^+$ -oscillations has been observed (Monshausen et al., 2007). Irregular oscillations in growth rate and cytosolic  $[\text{Ca}^{2+}]$  ( $[\text{Ca}^{2+}]_{\text{cyt.}}$ ), however, have been linked to growth cessation and premature pollen bursting, supposedly caused by an imbalance of  $\text{Ca}^{2+}$ -activated ROS production (Boisson-Dernier et al., 2013; Kaya et al., 2014; Lassig et al., 2014; Franck et al., 2017). Furthermore, experiments with pollen of several different species link the cytosolic  $\text{Ca}^{2+}$  gradient to cytoskeletal dynamics and exocytosis (Roy et al., 1999; Camacho and Malhó, 2003; Lee et al., 2008). Altogether,  $\text{Ca}^{2+}$  appears to be a central signaling ion, not only for CW crosslinking, but for intracellular regulation of tip-growth in response to exocytosis, possibly in a self-regulatory manner.

Despite the profound knowledge on the role of  $\text{Ca}^{2+}$  dynamics during tip-growth, it is still debated which proteins create and regulate the  $\text{Ca}^{2+}$  flux of tip-growing cells (Steinhorst and

Kudla, 2013 A; Steinhorst and Kudla, 2013 B; Mangano et al., 2016). While cation channels such as glutamate receptor-like proteins (GLRs) and cyclic nucleotide-gated ion channels (CNGCs) have been suggested to establish a tip-focused  $\text{Ca}^{2+}$  gradient,  $\text{Ca}^{2+}$  exchangers ( $\text{Ca}^{2+}$  pumps) such as the Autoinhibited  $\text{Ca}^{2+}$  ATPase 9 (ACA9) are thought to regulate its efflux (Hepler et al., 2012).

### **Glutamate receptor-like channels (GLRs)**

GLRs are glutamate-responsive  $\text{Ca}^{2+}$  channels (Qi et al., 2006) out of which six have been shown to be specifically expressed in pollen grains (Pina et al., 2005) and one in pollen tubes (Song et al., 2009). Indeed, GLRs represent  $\text{Ca}^{2+}$ -permeable channels, which function in response to D-serine (Michard et al., 2011) amongst other amino acids (Qi et al., 2006). Knockout of GLR1 or GLR3 was described to lead to partial male sterility, as indicated by a decreased number of seeds per silique and a moderate decrease of male transmission efficiency, possibly due to a partial loss of pollen tube polarity phenotype. Furthermore, D-serine treatment induced an increase in tip-focused  $\text{Ca}^{2+}$  concentration and magnitude of oscillation, as could be shown in ratiometric  $\text{Ca}^{2+}$  imaging experiments (Michard et al., 2011). Ultimately, the further characterization of the role of pollen-expressed GLRs will be awaited.

### **Cyclic nucleotide-gated ion channels (CNGCs)**

The non-selective,  $\text{Ca}^{2+}$ -permeable, pollen-expressed CNGCs 7, 8 and 18 have been identified as essential regulators of pollen tube growth (CNGC18) and male reproductive fertility through tip-growth initiation (CNGC7/8) (Chang et al., 2007; Frietsch et al., 2007; Tunc-Ozdemir et al., 2013 A; Gao et al., 2014; Gao et al., 2016; Gu et al., 2017). Knockout alleles of CNGC18 display a severe male-gametophytic transmission defect (Frietsch et al. 2007), while knockdown was described to lead to increased pollen grain and tube bursting and pollen tube branching in response to decreased extracellular  $\text{Ca}^{2+}$  concentrations as compared to wild-type pollen (Gao et al., 2016). Similarly, a recent publication suggests the root hair-expressed CNGC14 as regulator of  $\text{Ca}^{2+}$  influx during root hair growth (Zhang et al., 2017). Furthermore, the physical interaction between  $\text{Ca}^{2+}$ -binding Calmodulin (CaM) and the C-terminus of most of the 20 *Arabidopsis* CNGCs (Fischer et al., 2017) and the regulatory function of the CaM-binding domain (CaMBD) of CNGCs (DeFalco et al., 2016) have recently been demonstrated, representing a possible target for their regulation. CNGC18 was shown to be activated by the calcium-dependent protein kinase 32 (CPK32), possibly representing a positive signaling loop for increase of tip-focused  $\text{Ca}^{2+}$  during the elevation phase of  $\text{Ca}^{2+}$  oscillation (Zhou et al., 2014). A recent study also demonstrated the functional connection between  $\text{Ca}^{2+}$ - and anion homeostasis in an antagonistically oscillating pattern via  $\text{Ca}^{2+}$ - and CPK2/6/20-dependent anion channel recruitment to the pollen tube tip

(Gutermuth et al., 2018), putatively offering a possibility to negatively feed back on CNGC18-/CPK32-induced  $\text{Ca}^{2+}$  oscillation.

### Calcium ATPases

The autoinhibited  $\text{Ca}^{2+}$ -ATPase 9 (ACA9) is a pollen-specific, plasma membrane-localized  $\text{Ca}^{2+}$ -pump which is activated by  $\text{Ca}^{2+}$ /CaM. ACA9 was shown to be essential for pollen tube growth and male fertility, as loss of ACA9 function led to a decreased growth and fertilization potential, leading to a decreased number of seeds per silique. Thus, it was hypothesized to be a possible missing link in shuttling of  $\text{Ca}^{2+}$  back into the periplasm, where it may be recycled for  $\text{Ca}^{2+}$  import or retained in the ECM for CW remodeling (Schiøtt, et al., 2004). Interestingly, ACA8/10 and CNGC2/4 are common targets of CaM-binding in plant immunity signaling, however being antagonistically regulated, pointing towards a possible collective regulatory function (Cheval et al., 2013).

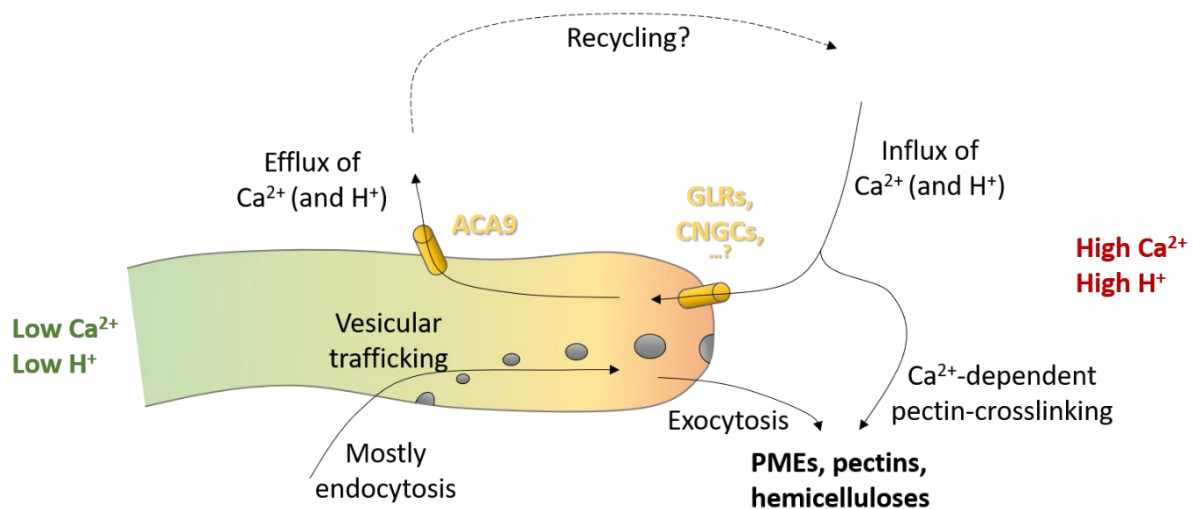


**Fig. 4: The internal growth machinery relies on close interplay between exocytosis and ion fluxes.** Tip-focused  $\text{Ca}^{2+}$ - and  $\text{H}^{+}$  gradients are established via influx through tip-localized cation channels and shank-localized efflux. CW components (hemicellulose and pectin) and CW remodeling factors (PMEs, PMEIs, extensins, etc.) are secreted via tip-focused exocytosis, where CW components are crosslinked in a  $\text{Ca}^{2+}$ -dependent manner.

## 1.6. Transmembrane signal transduction - How to control the tip-growth control machinery?

Despite the major advances in understanding CW remodeling factors and their (known) direct regulators - mainly ions and kinases - it has remained comparatively obscure for many years, how the tip-growth machinery is regulated on a genetic level: How are extracellular

cues transmitted into the inner cell and processed to regulate the intracellular growth machinery? Transmembrane receptor kinases have been described as wide-spread signal transduction factors, not only in plants, but throughout eukaryotes (Shiu and Bleecker, 2001). Malectin-like receptors (MLRs) represent a subfamily of Receptor-like kinases (RLKs) which regulate various developmental and house-keeping processes throughout land plants, often in a pleiotropic manner (Franck et al., 2018 A). Loss of function of the MLRs ANXUR1 and -2 (ANX1/2) and their closest homolog FERONIA (FER), both of which localize to the plasma membrane, was shown to lead to pollen tube and root hair bursting, respectively, while overexpression of ANX1 led to growth inhibition, linked to CW material over-accumulation and plasma membrane invagination. Thus, ANX1/2 and FER represent positive regulators of tip-growth in *Arabidopsis* pollen tubes and root hairs, respectively (Boisson-Dernier et al., 2009; Duan et al., 2010). Short peptides, namely RAPID ALKALINIZATION FACTORS (RALFs), have recently been demonstrated to physically bind to and regulate ANX1/2 and FER in both, fertilization, root growth and immunity signaling (Haruta et al., 2014; Mang et al., 2017; Ge et al., 2017; Mecchia et al., 2017; Stegmann et al., 2017). Loss of function of the pollen-expressed RALF4/19 was found to induce loss of CWI in pollen tubes, just like *anx1 anx2* mutants. The LRR-extensins LRX8/9/10/11, whose function is crucial for pollen tube CWI as well, were furthermore shown to form a supramolecular, heteromeric ligand-binding complex for RALF4 (and RALF19) binding during CWI signaling in the growing pollen tube (Mecchia et al., 2017). This complex likely includes two further pollen-expressed MLRs, namely BUDDHA'S PAPER SEAL1 and -2 (BUPS1/2), which bind to ANX1/2 via their endodomains (Ge et al., 2017). On an intracellular level, ANX1/2 positively influence activity of the two redundant ROS-producing NADPH-oxidases and positive regulators RESPIRATORY BURST OXIDASE H and -J RBOHH/J (Boisson-Dernier et al., 2013), whose loss of function leads to a severe loss of CWI phenotype in pollen and thus, strongly decreased fertility. RBOHH/J, in turn, lead to activation of the PTI-like receptor-like cytoplasmic kinase (RLCK) MARIS (MRI), a positive CWI regulator (Boisson-Dernier et al., 2015), and the two redundant protein phosphatases ATUNIS1 and -2 (AUN1/2), two negative CWI regulators (Franck et al., 2018 B). Both, MRI and AUN1/2 were found in the course of a suppressor screen for rescue of *anx1 anx2* male sterility. Knockdown and knockout of MARIS were found to lead to loss of integrity in pollen tubes, while MARIS overexpression triggered growth inhibition (Boisson-Dernier et al., 2015), just like described for ANX1 overexpression before (Boisson-Dernier et al., 2009), further underpinning their close relation in pollen tube growth control and the need for close fine-tuning of this process. Fascinatingly, the genetic program which regulates *Arabidopsis* pollen tube growth is strongly mirrored in root hairs, whose signaling program relies on signal transduction via the same genes or their close homologs (Boisson-Dernier et al.,

2013; Boisson-Dernier et al., 2015; Franck et al., 2018 B; Fig. 8). However, how MRI and AUN1/2 convert the transduced signal into a cellular response remains to be further elucidated.

### 1.7. What does it take to build a tube? - Evolution and functional conservation of tip-growth control during land plant evolution

When plants first colonized terrestrial habitats more than 470 mya they were confronted with a multitude of major novel problems such as the need for sufficient water and nutrient uptake, strong substrate anchorage, vegetative growth against the gravitational vector and the guarantee of efficient reproductive propagation (Kenrick and Crane, 1997; Bateman et al., 1998; Raven and Edwards, 2001; Ligrone, et al., 2012; Ambrose and Purugganan, 2012). For these purposes, plants have developed a series of morphological adaptations, many of which are based on the unique properties of tip-growing cells (Fig. 5). Rooting cells such as rhizoids and root hairs facilitate water and nutrient uptake via root surface extension, as well as substrate anchorage via intrusion of the soil. They are thought to have occurred comparatively early during land plant evolution and are found in all major extant plant clades, such as bryophytes (mosses *sensu latu*), monilophytes (ferns) and spermatophytes (seed plants), but also in charophycean algae (Carol and Dolan, 2002; Jones and Dolan, 2012). Rooting cells are known to appear in either the gametophytic or sporophytic life phase, an exception being lycophytes and monilophytes, which possess both, gametophytic rhizoids and sporophytic root hairs (Jones and Dolan, 2012; Fig.5B). A comparatively young, evolutionary adaptation to terrestrial habitats was fertilization via passive sperm cell delivery by pollen tubes ('siphonogamy'), which allowed reproduction irrespective of the presence of watery environments, in contrast to active movement (swimming) of flagellate sperm cells towards the female egg-cell (as found in early-diverging land plants). Thus, pollen tubes represent a seed plant-exclusive, gametophytic invention, as specialized male-gametophytic cells to allow for sperm cell delivery to the female gametophyte (Friedmann, 1993; Doyle, 2006). A further mechanism which relies on tip-growth is the vegetative horizontal dispersal via gametophytic multicellular protonema filaments in leafy mosses (Reski, 1998; Menand et al., 2007 A) such as *Physcomitrella patens*, however they are strongly reduced in liverworts such as *Marchantia polymorpha* and absent from hornworts (Gibson, 2006). Protonemata strongly resemble the morphology of filamentous algae and may thus represent one of the earliest tip-growing cell types of land plants.

Despite their dissimilar functions, tip-growing cells rely on the same mode of cellular growth and have been suggested to share a common set of molecular regulators (Boisson-Dernier et al., 2015; Franck et al., 2018 A and B). One approach to assess such hypothetical conservation is the functional comparison of homologous (structurally similar) genes between related cell types, tissues and species, aiming to understand the evolution of developmental mechanisms ('evo devo') over time (Carroll, 2008; Harrison, 2016; Kramer et al., 2017). In the last decade, advances have been made to elucidate evolutionary relationships of unidirectional growth control during plant (and eukaryotic) evolution.

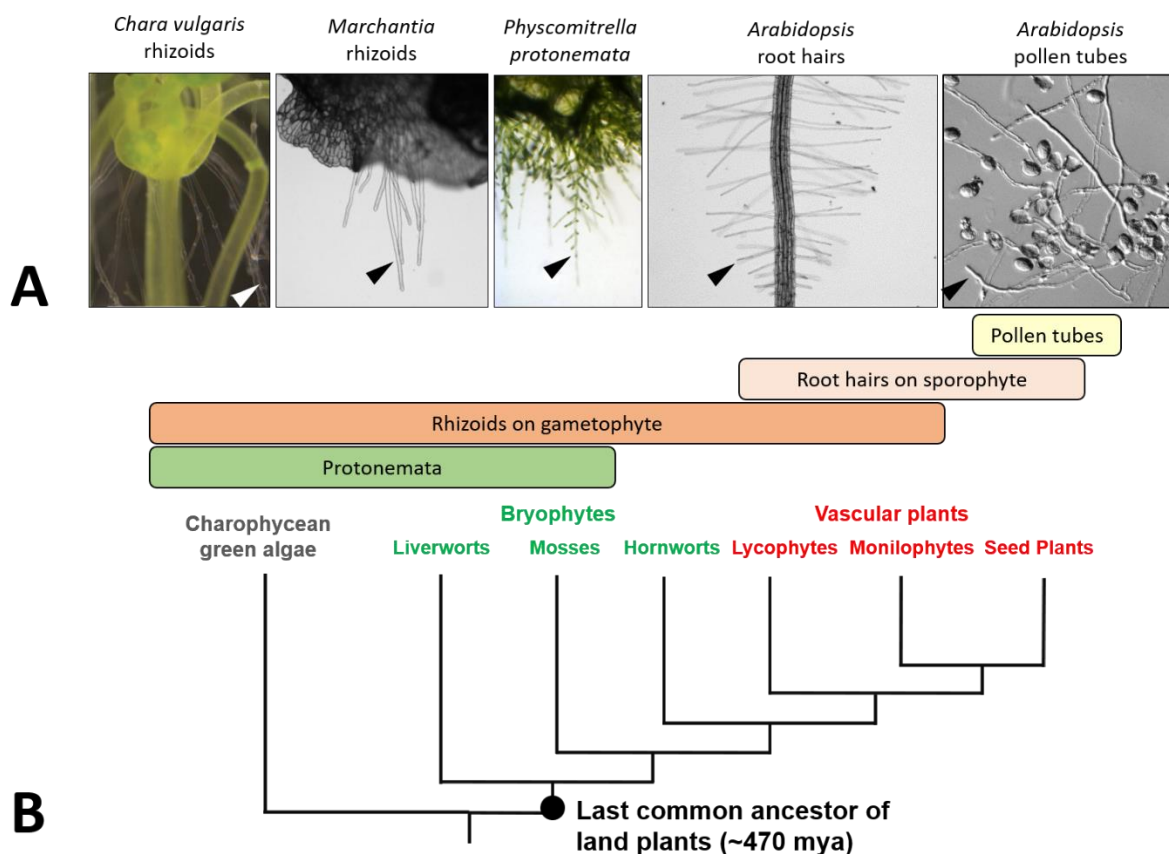


**Fig. 5: Occurrence of tip-growing cells during land plant evolution.** (A) Examples of the most important tip-growing cell types across charophytes. The tip-growing cells are marked with an arrowhead. The picture of *Chara vulgaris* rhizoids is from Jones and Dolan, 2012. (B) Phylogenetic representation of the major land plant lineages and the occurrence and presence of tip-growing cell types in these lineages. Based on the descriptions of Jones and Dolan, 2012; Harrison, 2016.

### Rho-GTPase signaling

Ras-homolog GTPases (Rho-GTPases) belong to the superfamily of small GTPases, whose various functions have been well studied in animals. Rho-GTPases of plants (ROPs) represent their respective plant homologs which are thought to have evolved from a common



progenitor gene in early eukaryotes (Fort, 2017). Rho GTPases have been reported to regulate tip-growth in land plants and fungal hyphae, but also polar expansion of neuronal axons in animals. Furthermore, all these processes appear to rely on a common set of growth regulatory processes and mechanisms, including upstream regulation of Rho-GTPases via activating guanine exchange factors (GEFs) and inhibiting RhoGAP (GTPase-activating proteins),  $\text{Ca}^{2+}$  signaling, cytoskeletal remodeling and exocytosis (Palanivelu and Preuss, 2000; Brand et al., 2014; Takeshita et al., 2014; Sun et al., 2015; Schoenaers et al., 2017).

Concerning tip-growth *in planta*, *AtROP1* has been demonstrated to regulate *Arabidopsis* pollen tube polarity; Excessive *AtROP1* activation was described to induce pollen tube tip enlargement, while depolarizing the tube and reducing tube elongation (Hwang et al., 2010). Accordingly, overexpression of its activating guanine exchange factor *AtROP-GEF1* was found to lead to loss of pollen tube polarity, likely due to disruption of the longitudinally well-organized actin-filament network (Cheung et al., 2008). Both, *AtROP1* and *AtROP-GEF1* form a complex with the *Arabidopsis* POLLEN-SPECIFIC RECEPTOR KINASE 2 (*AtPRK2*), which prevents autoinhibition of *AtROP-GEF1* and allows for positive *AtROP1*-mediated regulation of pollen tube growth (Chang et al., 2013). Interestingly, the MLR FERONIA (FER) is also known to physically interact with *AtROP2* to control root hair growth and CWI (Duan et al., 2010). Tip-growth control via ROP-signaling has been reported in a variety of flowering plant species, such as *Brassica napus* (Wang et al., 2011 B), *Medicago truncatula* (Lei et al., 2015), but also in bryophytes. The *Physcomitrella* ROP2 (*PpROP2*) and the *Physcomitrella* Guanine exchange factor 3 (*PpRopGEF3*) regulate polarity in tip-growing protonema filaments. Overexpression of either *PpROP2* or *PpRopGEF3*, however, induces loss of anisotropic growth behaviour and inflation of apical protonema cells. Overexpression of *PpROP2* additionally leads to malformation of the protonemal cross wall (Ito et al., 2014). Interestingly, this strongly reminds of the role of ROPs in regulation of cell polarization and asymmetric cell division of stomatal cells in maize (Humphries et al., 2011). Furthermore, RNA interference (RNAi) lines against all four *PpROPs* displayed an increase in actin dynamics in protonema cells, while forming a random mesh of actin filaments (as compared to the predominant orientation of actin filaments along the longitudinal cell axis in wild-type protonema cells). This severe actin-related phenotype was found to lead to the formation of spherical protonema cells which failed to initiate polar growth, as contrasted to tip-growing, branching wild-type protonema (Burkart et al., 2015). Altogether, these findings strongly support a general, functionally conserved role of ROPs in anisotropic growth and polarity signaling via regulation of actin dynamics.

### Transcriptional regulation

The two *Arabidopsis* basic helix-loop-helix (bHLH) transcription factors *AtRHD6* and *AtRSL1* control root hair development, as double knockout leads to absence of root hair initiation. Accordingly, double knockout of their *Physcomitrella* orthologs *PpRSL1/2* leads to decreased growth of caulonemal protonema filaments and rhizoids, (i) indicating that both genes redundantly regulate the development of both, rhizoids and caulonemal protonema filaments and (ii) pointing towards an ancient control switch for rooting cell initiation and/ or growth (Menand et al., 2007 B). Interestingly, the unique *Marchantia* ‘*Lotus japonicus*-ROOTHAIRLESS-LIKE’ (LRL) bHLH transcription factor is crucial for emergence of rhizoids and thus acts as a general, positive regulator of rhizoid growth, whereas *AtLRL* genes act in antagonistic groups during *Arabidopsis* root hair growth (Breuninger et al., 2016). It is noteworthy, that rooting cells, unlike pollen tubes, emerge from polar cell expansion of an epidermal cell, which requires cell-type specific signaling to determine or suppress the identity as tip-growing cell. Consequently, it is likely that the transcriptional program of pollen tubes and rooting cells (*i.e.* of tissue-derived and -independent cells) may differ significantly.

### Protein (de)phosphorylation

NEVER IN MITOSIS A (NIMA)-related kinases (NEKs) represent plant homologs of eukaryotic kinases which regulate mitotic events such as spindle formation in animals and fungi (Fry et al., 2012). While NEKs in general have been shown to regulate directional cell growth in the plant epidermis, NEK6 in particular was shown to phosphorylate  $\beta$ -tubulin resulting in microtubule depolymerization. In addition, *nek6* mutants were shown to display ectopic epidermal outgrowths (Motosé et al., 2008; Sakai et al., 2008; Motosé et al., 2011). Similarly, the fungal NIMA kinase of *Aspergillus nidulans* (*AnNIMA*) and the closest *AtNEK6*-homolog of *Marchantia polymorpha* (*MpNEK1*) were both shown to be crucial for the determination of tip-growth direction in hyphae and rhizoids, respectively, both via regulation of microtubule organization in the apical dome of the tip-growing cell (Govindaraghavan et al., 2014; Otani et al., 2018).

## 1.8. Functional conservation of RLK-mediated CWI control in streptophytes

### Malectin-like receptors

Plant Malectin-like receptors (MLRs) represent a subfamily of receptor-like kinases (RLKs) (Franck et al., 2018 A). Besides a transmembrane- and an intracellular Ser/Thr-kinase domain, which is shared amongst the majority of RLKs, MLRs possess an extracellular malectin-like domain (MLD) which shows structural homology to the disaccharide-binding malectin of animals (Schallus et al., 2008). Thus, MLRs are thought to bind carbohydrate-rich ligands, which may be cell wall components or glycosylated proteins (Franck et al., 2018 A). While *Marchantia* THESEUS1 (*MpTHE1*) represents the unique *Marchantia* MLR, the *Arabidopsis* genome contains 17 MLRs out of which 10 have been characterized to date (Fig. 6). MLR functions are widespread, including plant development, cell morphogenesis, abiotic stress tolerance and pathogen defense. One major function which is governed by MLRs throughout different cell types is polar growth. *Arabidopsis* THESEUS1 (*AtTHE1*) controls bidirectional expansion of hypocotyl and root cells (Hémathy et al., 2007), while FER controls root hair growth (Duan et al., 2010). Similarly, the closest FER homologs ANX1/2 control pollen tube-mediated sperm cell delivery through steady, directed tip-growth and subsequent coordinated loss of CWI (Boisson-Dernier et al., 2009; Miyazaki et al., 2009; Ge et al., 2017). Functional studies in further species of flowering plants have confirmed similar roles during plant reproduction and regulation of CWI in tip-growing cells via orthologous MLRs (Franck et al, 2018 A). Fascinatingly, a putative MLR of the charophycean alga *Closterium* (*CpRLK*) has been characterized as a regulator of CWI during fertilization and sperm release via conjugatory papillae (Hirano et al., 2014), representing the first published evidence for the possible evolutionary conservation of MLRs as CW sensors throughout streptophytes (*i.e.* charophycean algae and embryophytes).

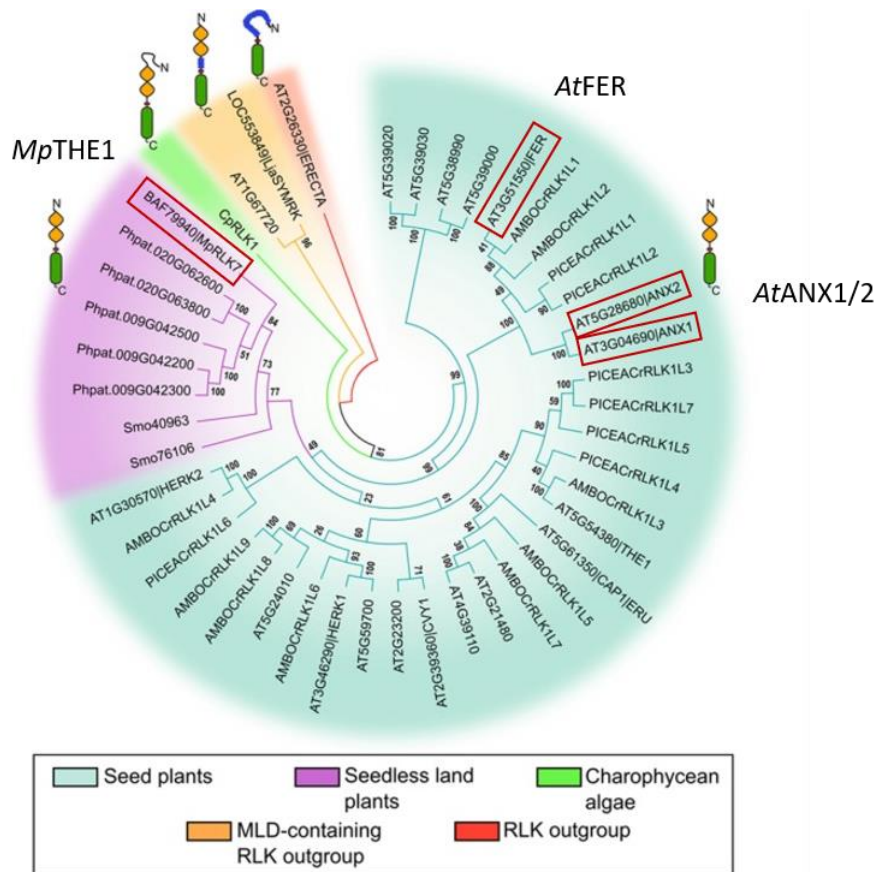


**Fig. 6: Phylogeny of Malelectin-like receptors.** Red boxes mark the MLRs of interest, *MpTHE1*, *AtFER* and *AtANX1/2*, all of which share the same domain structure comprised of extracellular MLDs (orange) and an intracellular kinase domain (green). Figure modified from Galindo-Trigo et al., 2016.

### PTI-like receptor-like cytoplasmic kinases

PTO-interacting (PTI)-like proteins represent the type VIII-subfamily of receptor-like cytoplasmic kinases (RLCKs), which possess a conserved Ser/Thr-kinase, but lack transmembrane- and extracellular domains (Franck et al., 2018 A). Their name was originally derived from the tomato (*Solanum lycopersicum*) resistance gene PTO against the *Pseudomonas syringae* pathovar tomato avirulence protein (AvrPto). Upon binding of AvrPto, PTO binds to *Solanum lycopersicum* PTI1 (SPTI1) to initiate plant defense mechanisms (Bogdanove and Martin, 2000). In contrast to MLRs, the majority of *Arabidopsis* PTI-like RLCKs has not been well characterized to date, an exception being MARIS (MRI) in the control of pollen tube and root hair growth (Boisson-Dernier et al., 2015). Interestingly, five out of the 11 *At*PTI-likes (including MRI) were found to physically interact with the kinase OXI1 (Anthony et al., 2006; Forzani et al., 2011; Liao et al., 2016), itself being a possible regulator of root hair growth (Anthony et al., 2004). The unique *Marchantia* PTI-like homolog *Mp*PTI forms a phylogenetic cluster with several *Arabidopsis* PTI-likes, including *At*MRI, thus forming the ‘*At*MRI-like subgroup’ (Fig. 7).

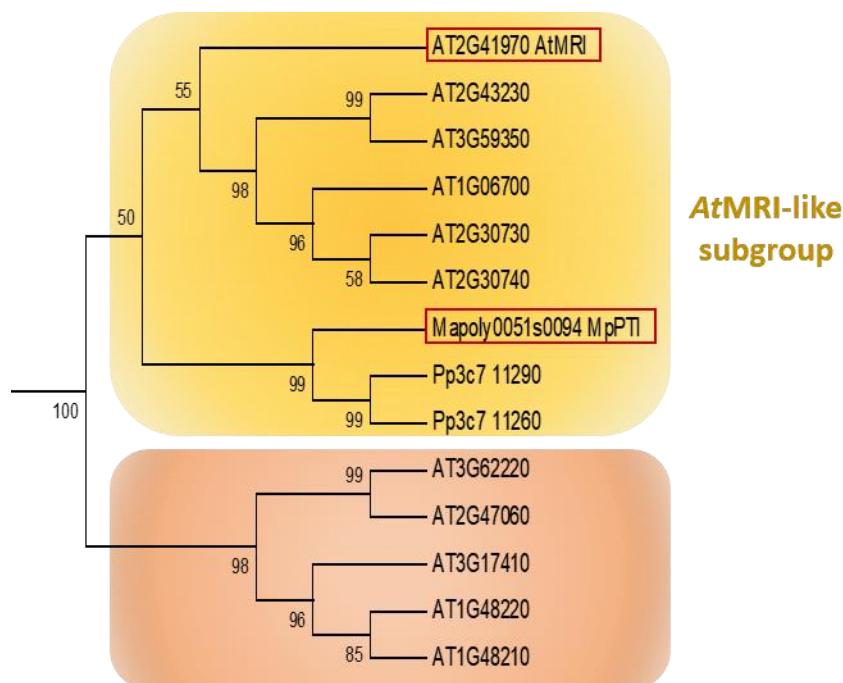


**Fig. 7: Phylogeny of *Arabidopsis* and bryophytic PTI-like homologs.** Red boxes mark the PTI-like genes of interest, *At*MRI and *Mp*PTI, both of which cluster in the ‘*At*MRI-like subgroup’ (in yellow). Phylogeny is as shown in this study, section 4.1.4.

### Conservation of MLR-/PTI-like signaling?

A recent extensive phenotypic screen of T-DNA insertion mutants of the liverwort *Marchantia polymorpha* identified 33 genes which control rhizoid growth while representing orthologs of

known *Arabidopsis* tip-growth regulators (Honkanen et al., 2016). Intriguingly, this finding included the MLR *MpTHE1* (homolog to *AtANX1/2* and *AtFER*) and the PTI-like RLCK *MpPTI* (homolog to *AtMRI*). Based on this finding, it has been hypothesized that plant cells may have acquired an evolutionarily conserved signaling module based on MLRs and PTI-like genes, possibly amongst other conserved regulators, which controls steady tip-growth by mediating downstream signaling and regulation of the intracellular tip-growth machinery (Fig. 8).

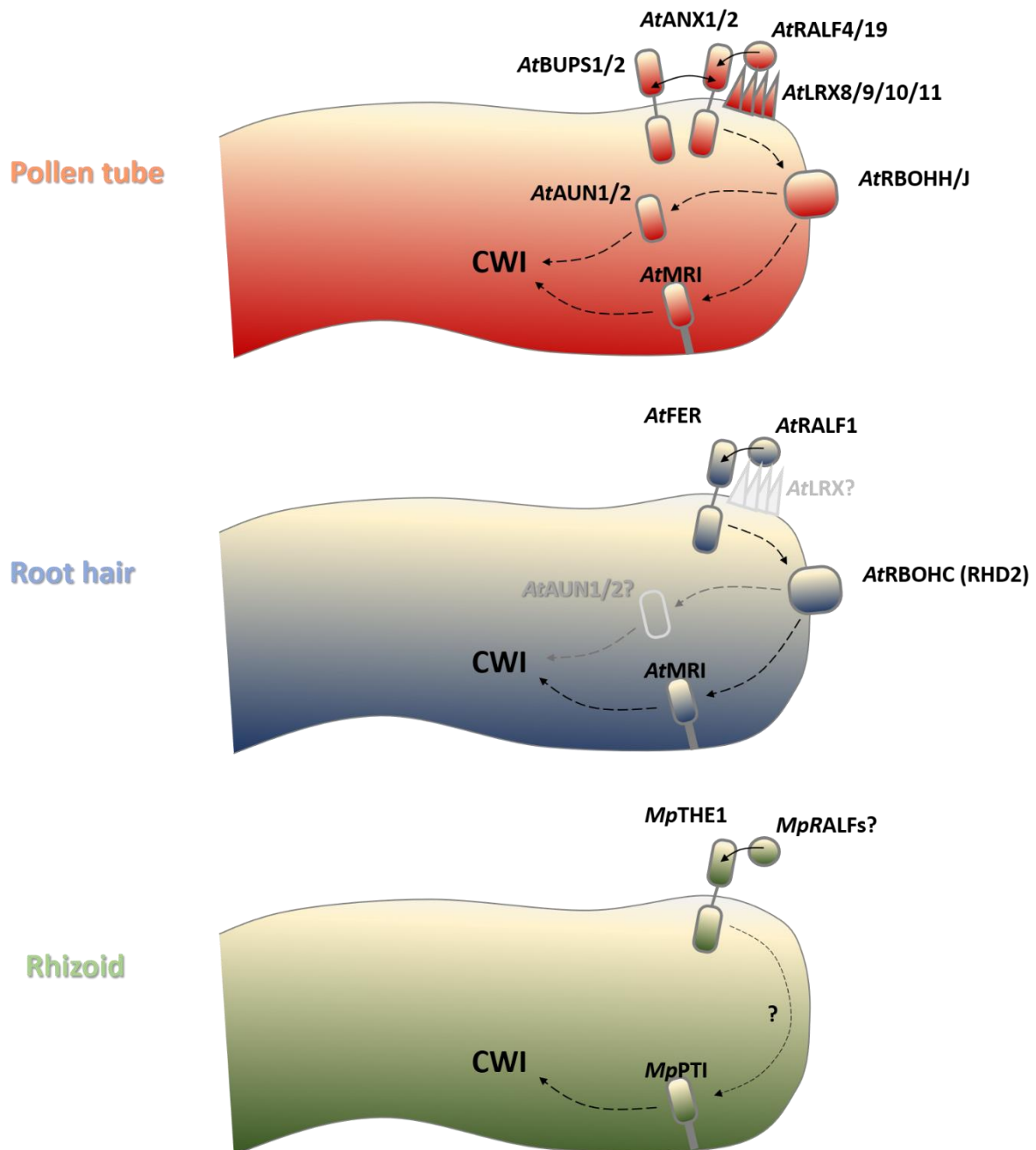
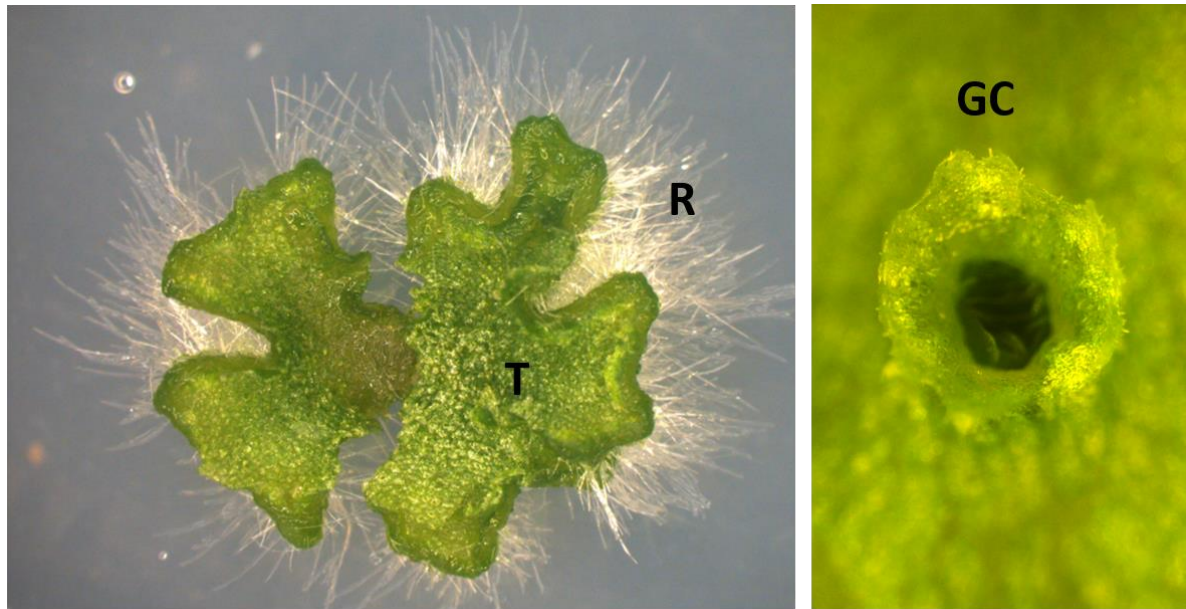


**Fig. 8: Cell wall integrity signaling in tip-growing cells of *Arabidopsis* and *Marchantia*.** The schematic representation of the RLK-mediated CWI signal transduction pathway of tip-growing cells strongly suggests the functional conservation of its key regulators between (A) the *Arabidopsis* pollen tube, (B) the *Arabidopsis* root hair and (C) the *Marchantia* rhizoid.

### 1.9. *Marchantia polymorpha* as a genetic model to study tip-growth

*Marchantia polymorpha* is a thallose liverwort which is found in moist terrestrial habitats ranging from arctic to tropical environments (Fig. 9). Within few years *Marchantia polymorpha* has emerged as a highly useful model organism due to its low genetic redundancy and amenability to reverse and forward genetic approaches. The scientific *Marchantia* community profits from a recently fully sequenced genome (Bowman et al., 2017) and a variety of well-established experimental protocols including strategies for CRISPR-Cas9-based genome editing and gene targeting via homologous recombination, T-DNA insertion tools, GUS-based promoter activity analyses, plastid and nuclear genome transformation. Its dominant gametophytic (haploid) generation phase allows time-efficient reverse genetic analysis in T1 plants. Furthermore, *Marchantia* vegetative and reproductive stages can be cultivated both, axenically and in soil-based culture systems. Mature plants can be crossed easily with a complete life cycle of approximately 3 months. Finally, *M. polymorpha* holds a key-position in the phylogenetic tree of plants: As an early-diverging land plant it is predestined as a model to address questions on early plant evolution and to understand the conquest of terrestrial habitats by plants (Ishizaki et al., 2015).





*Marchantia* thallus (T), rhizoids (R) and gemmae cup (GC)



Male and female gametangia

Spore-harboring  
sporangia on a female  
gemetangium

**Fig. 9: *Marchantia polymorpha* developmental stages.** The *M. polymorpha* thalloid habitus represents the predominant, gametophytic life phase. Epidermal cells give rise to ventral rhizoids for substrate attachment and water/nutrient uptake. Influenced by environmental conditions (e.g. light qualities), the thallus gives rise to gemmae cups (harboring clonal propagules, called 'gemmae', for vegetative propagation) or gametangia (sexual reproductive organs). *Marchantia* is a diecious plant, thus male and female gametangia (antheridiophores and archegoniophores, respectively) emerge from individual thalli. Fertilization in *Marchantia* is water-dependent, as the male spermatozoids, which are released from the antheridium, actively swim towards the female egg cell (not shown). The obligate gametophyte-dependent sporophyte includes sporogenous cells, which undergo meiosis to give rise to spores. Sporangia harbor and release the spores, which develop into sporelings and subsequently, new thalli.



## 2. RESEARCH OUTLINE

### 2.1. Has RLK-mediated tip-growth control been conserved in a common signaling module during land plant evolution?

Rooting cells are thought to have evolved comparatively early during land plant evolution (Raven and Edwards, 2001; Ambrose and Purugganan, 2012; Jones and Dolan, 2012; Franck et al., 2018 A). It is thus interesting to assess if and to which extent crucial genes for (gametophytic) rhizoid growth control were recruited during the evolution of (sporophytic) root hairs. Furthermore, such well-established genetic tool kits may have been ‘rediscovered’ during evolution of comparatively young tip-growing cells such as pollen tubes of flowering plants, instead of the invention of a whole new genetic signaling program (Rensing, 2016). Recent findings indicate that loss of function of the *Marchantia* MLR homolog *MpTHE1* or PTI-like homolog *MpPTI* leads to a similar loss of cell wall integrity phenotype (Honkanen et al., 2016) as observed in the respective *Arabidopsis* mutants of tip-growth regulators (*i.e.* the MLRs *AtANX1/2* and *AtFER*, as well as the PTI-like *AtMRI*) (Boisson-Dernier et al., 2009; Duan et al., 2010; Boisson-Dernier et al., 2015), thus implying that MLRs and PTI-like genes may govern tip-growth control throughout plant evolution. Accordingly, one aim of this study is the investigation of such putatively conserved functions between *Arabidopsis* and *Marchantia* MLR and PTI-like homologs via genetic complementation and rescue studies. Discovery of such conservation would aid our understanding of (i) early rooting structures, (ii) the evolution of sporophytic dominance and (iii) the emergence of seed plants and (iv) ultimately hold precious outlines for green biotechnology in the face of increasing demand for highly productive crop plants (Franck et al., 2018 A).

### 2.2. How do plants regulate CWI? - Understanding the regulatory mechanism of tip-growth control

In the past decade, major advances have been made in unraveling of CWI regulators and in understanding how they interact both, genetically and physically, to guarantee efficient tip-growth control. However, our understanding of how such regulation works on a mechanistic level remains comparatively sparse. Thus, the second aim of this study is the identification of further signaling constituents of the RLK-mediated CWI signaling pathway, including the

characterization of their possible intracellular function and position within the signaling pathway.

### 2.2.1. Type-one protein phosphatases ATUNIS1/2.

A former suppressor screen for rescue of the *anx1 anx2*-induced pollen tube bursting revealed 32 *impotence rescue (ipr)* mutants in *Arabidopsis*, which display rescue of pollen bursting and thus, male fertility (Boisson-Dernier et al., 2015). A single nucleotide polymorphism (SNP) inducing a non-synonymous substitution of aspartic acid to asparagine at codon 94 [D94N] in the ORF of AT3G05580 was shown to be causative for rescue of fertility in *ipr7*. AT3G05580 codes for the Type One Protein Phosphatase 9 (TOPP9), which possesses a close sister homolog (AT5G27840 = TOPP8; 89.9 % sequence identity), both of which were named ATUNIS1/2 (AUN1/2). The role of AUN1/2 in pollen tube and root hair tip-growth control was studied via analysis of *aun1 aun2* loss-of-function mutants and, subsequently, their rescue via AUN1/2-expression. To assess whether AUN1/2 truly are part of the MLR-governed growth control pathway, we then tested for genetic interaction with known tip-growth regulators. The AUN1/2 project has meanwhile been finished and our insights have been published recently (Franck et al., 2018). In the scope of my thesis I will present all related data which were obtained under my participation.

### 2.2.2. Cyclic nucleotide-gated ion channel18 (CNGC18).

Cyclic nucleotide-gated ion channels (CNGCs) have been demonstrated to represent functional  $\text{Ca}^{2+}$  channels which may control pollen tube growth and thus, plant fertility, via regulation of  $\text{Ca}^{2+}$ -flux (Frietsch et al. 2007; Gao et al., 2016). Based on the loss of CWI and growth inhibition phenotypes in *Arabidopsis* pollen tubes of knockout/knockdown and overexpression lines of CNGC18, it was hypothesized that CNGC18 may be the missing link in  $\text{Ca}^{2+}$ /ROS-dependent regulation of RLK-mediated tip-growth control. To test this hypothesis, we revisited the role of CNGCs during tip-growth, compared intracellular  $\text{Ca}^{2+}$ -dynamics in growth-defective mutants and finally tested for genetic interactions between CNGCs and members of RLK-mediated CWI signaling.

### 2.2.3. Type-VII-receptor-like cytoplasmic kinase VEIVE.

The locus AT2G07180 encodes a putative, pollen-expressed RLCK which we named VEIVE (VEI). VEI belongs to subfamily VII of RLCKs (Ranf et al., 2014) and was shown to be pollen-expressed (Wang et al., 2008). Type VII RLCKs are known to govern important biological functions such as pollen tube guidance (Liu et al., 2013). Against this background it was hypothesized that VEI may be a further regulator of plant reproduction, possibly being inflicted in pollen tube tip-growth control. To test this hypothesis, we screened two T-DNA lines (*vei-1/2*) for possible defects in pollen tube growth and plant fertility via phenotypic analyses and determination of transmission efficiency.

### 3. MATERIALS AND METHODS

#### 3.1. Materials

##### 3.1.1. Plant lines and bacterial strains

###### 3.1.1.1. *Arabidopsis thaliana* and *Marchantia polymorpha*

All used *Arabidopsis thaliana* and *Marchantia polymorpha* genotypes are listed in Tab. 1 and Tab. 2, respectively. If not stated otherwise in the text, usage of the genus names *Arabidopsis* and *Marchantia* exclusively refer to *Arabidopsis thaliana* and *Marchantia polymorpha*, respectively.

**Tab. 1: Genetically modified *Arabidopsis thaliana* lines.** Lines are separated into mutant and transgenic lines. (A) Mutant lines, including targeted genetic locus, plant ecotype and molecular markers. (B) Transgenic lines, including transformed construct, genotyping primers and plant selection markers. T-DNA and transposon insertion lines as found on <http://signal.salk.edu/>. Marked lines were received from: [1] Prof. Dr. Yong-Fei Wang, Chinese Academy of Sciences, Shanghai, China; [2] Prof. Dr. Jeffrey Harper, University of Nevada, Reno, USA.

(A) Mutant lines	Targeted locus	Ecotype	Molecular markers
<i>amiRNA RALF 4/19</i> (Mecchia et al., 2017)	AT1G28270 AT2G33775	Col-0	Selection: Hygromycin
<i>anx1-1/anx1-1 anx2-1/ANX2</i> (Boisson-Dernier et al., 2013)	AT3G04690 AT5G28680	Col-0	PCR (ANX2): ABD603/ABD604 PCR ( <i>anx2-1</i> ): ABD603/ABD600
<i>aun1-1</i> (SALK_045433C; Franck et al., 2018 B)	AT3G05580	Col-0	PCR (AUN1): ABD728/ABD729 PCR ( <i>aun1-1</i> ): ABD728/ABD600
<i>aun1-1 aun2-1</i> (from crosses of <i>aun1-1</i> x <i>aun2-1</i> )	AT3G05580 AT5G27840	Col-0	see single mutants
<i>aun1-2</i> (GABI_600E08; Franck et al., 2018 B)	AT3G05580	Col-0	PCR (AUN1): ABD728/ABD731 PCR ( <i>aun1-2</i> ): ABD731/ABD600
<i>aun1-2 aun2-2</i> (from crosses of <i>aun1-2</i> x <i>aun2-2</i> )	AT3G05580 AT5G27840	Col-0	see single mutants
<i>aun2-1</i> (SALK_137888; Franck et al., 2018 B)	AT5G27840	Col-0	PCR (AUN2): ABD779/ABD731 PCR ( <i>aun2-1</i> ): ABD779/ABD600
<i>aun2-2</i> (SALK_125184; Franck et al., 2018 B)	AT5G27840	Col-0	PCR (AUN2): ABD779/ABD731 PCR ( <i>aun2-2</i> ): ABD779/ABD600
<i>cngc18-1/CNGC18 (qrt)</i> (Fritsch et al., 2007; Gao et al., 2016; [1+2])	AT5G14870	Col-0	PCR (CNGC18): ABD792/ABD793 PCR ( <i>cngc18-1</i> ): ABD794/ABD793 Selection: Basta
<i>cngc18-2 (qrt)</i> (Fritsch et al., 2007; Gao et al., 2016; [1+2])	AT5G14870	Col-0	Selection: Sulfadiazine
<i>cngc18-17</i> (Gao et al., 2016; [1])	AT5G14870	Col-0	dCAPS: JW23/JW24
<i>fer-4</i>	AT3G51550	Col-0	-

(GABI_106A06; Duan et al., 2010)			
<i>mri-1</i> /MRI ( <i>qrt</i> ) (CSHL_GT21229; Boisson-Dernier et al., 2015)	AT2G41970	Ler	PCR (MRI): ABD681/ABD682 PCR ( <i>mri-1</i> ): ABD682/ABD747 Selection ( <i>mri-1</i> ): Kanamycin
<i>mri-2</i> (GABI_820D05; Boisson-Dernier et al., 2015)	AT2G41970	Col-0	PCR (MRI): ABD735/ABD736 PCR ( <i>mri-2</i> ): ABD735/ABD614
<i>rbohH-3 rbohJ-3</i> (Boisson-Dernier et al., 2013)	AT5G60010 AT3G45810	Col-0	-
<i>vei-1</i> (SK26869)	AT2G07180	Col-0	PCR (VEI): JW06/JW07 PCR ( <i>vei-1</i> ): JW06/ABD006
<i>vei-2</i> (SK29099)	AT2G07180	Col-0	PCR (VEI): JW06/JW07 PCR ( <i>vei-2</i> ): JW06/ABD006
<b>(B) Transgenic lines</b>	<b>Transformed construct</b>	<b>Genotyping primers</b>	<b>Plant selection markers</b>
<i>amiRNA RALF4/19</i> with <i>proLAT52::MpPTI<sup>[R240C]</sup>-CFP</i>	pJW37	Construct: JW34/ABD699	Construct: Basta Mutant: Hygromycin
<i>anx1-1/anx1-1 anx2-1/ANX2</i> with <i>proLat52::YFP-CNGC18</i>	pJW15	ANX2: ABD603/ABD604 <i>anx2-1</i> : ABD603/ABD600 Construct: ABD698/JW16	Construct: Hygromycin
<i>aun1-1 aun2-1</i> with <i>proLat52::AUN2-YFP</i>	pCMF3	JW15/ABD630	Construct: Basta
<i>cngc18-17</i> with <i>proLAT52::YC3.60</i> (obtained from [1])	-	-	not described
Col-0 with <i>proACA9::GFP-CNGC18</i> (obtained from [2])	-	-	Construct: Hygromycin
Col-0 with <i>proAct1::YC3.60</i> (obtained from [1])	-	-	Construct: Kanamycin
Col-0 with <i>proLAT52::YC3.60</i> (obtained from [1])	-	-	not described
Col-0 with <i>proMRI::AtMRI<sup>[R240C]</sup>-YFP</i>	pABD85	Construct: ABD766/ABD736	Construct: Basta
Col-0 with <i>proMRI::MpPTI-YFP</i>	pJW20	Construct: ABD766/JW35	Construct: Basta
Col-0 with <i>proMRI::MpPTI<sup>[R240C]</sup>-YFP</i>	pJW36	Construct: ABD766/JW35	Construct: Basta
<i>fer-4</i> with <i>proMRI::MpPTI<sup>[R240C]</sup>-YFP</i>	pJW36	Construct: ABD766/JW35	Construct: Basta
<i>mri-1 (qrt)</i> with <i>proLat52::AtMRI-CFP</i>	pABD47	<i>mri-1</i> : ABD682/ABD747	Construct: Basta Mutant: Kanamycin
<i>mri-1 (qrt)</i> with <i>proLat52::AtMRI<sup>[R240C]</sup>-CFP</i>	pABD49	<i>mri-1</i> : ABD682/ABD747	Construct: Basta Mutant: Kanamycin
<i>mri-1 (qrt)</i> with <i>proMRI::AtMRI-YFP</i>	pABD84	<i>mri-1</i> : ABD682/ABD747 Construct: ABD766/ABD736	Construct: Basta Mutant: Kanamycin

<i>mri-1 (qrt)</i> with <i>proMRI::MpPTI</i> -YFP	pJW20	<i>mri-1</i> : ABD682/ABD747 Construct: ABD766/JW35	Construct: Basta Mutant: Kanamycin
<i>mri-1</i> /MRI with <i>proLat52::YFP</i> -CNGC18	pJW15	MRI: ABD681/ABD682 <i>mri-1</i> : ABD682/ABD747 Construct: ABD698/JW16	Construct: Hygromycin
<i>mri-2</i> with <i>proAct1::YC3.60</i> (obtained via crossing)	-	-	Construct: Kanamycin
<i>rbohH rbohJ</i> with <i>proLat52::YFP</i> -CNGC18	pJW15	Construct: ABD698/JW16	Construct: Hygromycin

**Tab. 2: Genetically modified *Marchantia polymorpha* lines.** Lines are separated into mutant and transgenic lines. (A) Mutant lines, including targeted genetic locus, plant ecotype and molecular markers. (B) Transgenic lines, including transformed construct, genotyping primers and plant selection markers. Marked lines were obtained from [1] Prof. Liam Dolan, University of Oxford, United Kingdom and [2] Susanna Streubel, Dolan Lab, University of Oxford, United Kingdom.

(A) Mutant lines	Targeted locus	Ecotype	Molecular markers
<i>Mppti</i> (Honkanen et al., 2016; [1])	<i>MpPTI</i>	Tak-2 x Tak-1	PCR ( <i>Mppti</i> ): JW60/JW63 Selection (T-DNA): Hygromycin
<i>Mpthe1</i> (Honkanen et al., 2016; [1])	<i>MpTHE1</i>	Tak-2 x Tak-1	PCR ( <i>MpTHE1</i> ): JW52/JW59 PCR ( <i>Mpthe1</i> ): JW52/JW64 Selection (T-DNA): Hygromycin
(B) Transgenic lines	Transformed construct	Genotyping primers	Plant selection markers
<i>Mppti</i> with <i>proMpEF1α::AtMRI</i> -RFP	pJW10	<i>Mppti</i> : JW60/JW63 Construct: JW17/ABD736	Construct: Chlorsulfuron Mutant: Hygromycin
<i>Mppti</i> with <i>proMpEF1α::MpPTI</i> -RFP	pJW28	<i>Mppti</i> : JW60/JW63 Construct: JW17/JW35	Construct: Chlorsulfuron Mutant: Hygromycin
<i>Mpthe1</i> with <i>proMpEF1α::MpPTI</i> <sup>[R240C]</sup> -RFP	pJW51	<i>Mpthe1</i> : JW52/JW64 Construct: JW17/JW35	Construct: Chlorsulfuron Mutant: Hygromycin
<i>Mpthe1</i> with <i>proMpEF1α::MpTHE1</i> -3xCitrine ( <i>MpTHE1</i> sequence obtained from [2])	pJW45	<i>Mpthe1</i> : JW52/JW64 Construct: JW17/JW41	Construct: Chlorsulfuron Mutant: Hygromycin
Tak-2 x Tak-1 with <i>proMpEF1α::AtANX1</i> -3xCitrine	pJW21	Construct: JW17/ABD547	Construct: (Gentamicin)
Tak-2 x Tak-1 with <i>proMpEF1α::AtFER</i> -3xCitrine	pJW25	Construct: JW17/ABD569	Construct: (Gentamicin)
Tak-2 x Tak-1 with <i>proMpEF1α::AtMRI</i> -3xCitrine	pJW09	Construct: JW17/ABD736	Construct: (Gentamicin)
Tak-2 x Tak-1 with <i>proMpEF1α::AtMR</i> <sup>[R240C]</sup> - 3xCitrine	pJW11	Construct: JW17/ABD736	Construct: (Gentamicin)
Tak-2 x Tak-1 with	pJW27	Construct: JW17/JW35	Construct: (Gentamicin)

<i>proMpEF1α::MpPTI-3xCitrine</i>			
Tak-2 x Tak-1 with <i>proMpEF1α::MpTHE1-RFP</i>	pJW46	Construct: JW17/JW41	Construct: (Gentamicin)

### 3.1.1.2. *Escherichia coli* and *Agrobacterium tumefaciens*

All cloned Gateway (GW)-Entry- and GW-Expression vectors used in this study were transformed into and amplified in *Escherichia coli* Dh5α-cells. Destination vectors, carrying a GW-compatible cassette, were kept in *E. coli* DB3.1-cells. Expression vectors were transformed into *Agrobacterium tumefaciens*. All bacterial strains were kept as a glycerol stock culture at -80 °C.

### 3.1.2. Vectors

All GW-Entry-, GW-Destination- and GW-Expression vectors used in this study are listed in Tab. 3, Tab. 4 and Tab. 5, respectively. All pJW-vectors were created in the course of this study, while pABD- and pCMF-vectors were received from Dr. Aurélien Boisson-Dernier and Dr. Christina Maria Franck, respectively.

**Tab. 3: Entry vectors and clones.**

Vector ID	Full name	Purpose	Bacterial selection marker	Vector type
pABD038	pDONR207 (ThermoFisher)	Generation of GW-compatible Entry-clones	Gentamicin	Entry vector
-	pENTR11 (ThermoFisher)	Generation of GW-compatible Entry-clones	Kanamycin	Entry vector
-	pJet1.2 (ThermoFisher)	GW-independent cloning	Carbenicillin	Entry vector
pABD43	MRI (without stop) in pDONR207	Cloning of MRI ORF	Gentamicin	Entry clone
pABD44	MR <sup>[R240C]</sup> (without stop) in pDONR207	Cloning of MR <sup>[R240C]</sup> ORF	Gentamicin	Entry clone

pABD50	ANX1 (without stop) in pDONR207	Cloning of ANX1 ORF	Gentamicin	Entry clone
pABD52	FER (without stop) in pDONR207	Cloning of FER ORF	Gentamicin	Entry clone
pCMF1	AUN1 (without stop) in pDONR207	Cloning of AUN1 ORF	Gentamicin	Entry clone
pJW01	<i>proAUN1</i> in pJet1.2	Cloning of <i>proAUN1</i>	Carbenicillin	Entry clone
pJW03	AUN2.1 ORF (with stop) in pDONR207	Cloning of AUN2.1 ORF	Gentamicin	Entry clone
pJW04	CNGC18 ORF (without stop) in pDONR207	Cloning of CNGC18 ORF	Gentamicin	Entry clone
pJW18	<i>MpPTI</i> ORF (without stop) in pDONR207	Cloning of <i>MpPTI</i> ORF	Gentamicin	Entry clone
pJW35	<i>MpPTI</i> <sup>[R240C]</sup> (without stop) in pDONR207	Cloning of <i>MpPTI</i> <sup>[R240C]</sup>	Gentamicin	Entry clone
pJW42	<i>MpTHE1</i> (without stop) in pDONR207	Cloning of <i>MpTHE1</i>	Gentamicin	Entry clone

**Tab. 4: Destination vectors.**

Vector ID	Full name	Purpose	Bacterial selection marker	Plant selection marker
pABD34	<i>proLat52::GW-YFP</i>	Pollen-specific expression in <i>Arabidopsis</i>	Spectinomycin	Basta
pABD35	<i>proLat52::GW-CFP</i>	Pollen-specific expression in <i>Arabidopsis</i>	Spectinomycin	Basta
pABD83	<i>proMRI::GW-YFP</i>	pollen- and root hair-specific expression in <i>Arabidopsis</i>	Spectinomycin	Basta
pABD94	<i>proLat52::YFP-GW</i>	pollen-specific expression in <i>Arabidopsis</i>	Spectinomycin	Hygromycin
pABD106	<i>proMpEF1α::GW-3xCitrine</i>	ubiquitous expression in <i>Marchantia</i>	Spectinomycin	Gentamicin
pABD107	<i>proMpEF1α::GW-RFP</i>	ubiquitous expression in <i>Marchantia</i>	Spectinomycin	Chlorsulfuron
pJW02	<i>proAUN1::GW-YFP</i>	expression of AUN1/2-YFP under native <i>proAUN1</i> in <i>Arabidopsis</i>	Spectinomycin	Basta



**Tab. 5: Expression vectors.**

Vector ID	Full name	Entry clone and destination vector	Bacterial selection marker	Plant selection marker
pABD47	<i>proLat52::AtMRI</i> -CFP	pABD43/pABD35	Spectinomycin	Basta
pABD49	<i>proLat52::AtMRI<sup>[R240C]</sup></i> -CFP	pABD44/pABD35	Spectinomycin	Basta
pABD84	<i>proMRI::AtMRI</i> -YFP	pABD43/pABD83	Spectinomycin	Basta
pABD85	<i>proMRI::AtMRI<sup>[R240C]</sup></i> -YFP	pABD44/pABD83	Spectinomycin	Basta
pCMF3	<i>proLat52::AUN1</i> -YFP	pCMF01/pABD34	Spectinomycin	Basta
pJW05	<i>proAUN1::AUN1</i> -YFP	pCMF01/pJW02	Spectinomycin	Basta
pJW06	<i>proAUN1::AUN2.1</i> -YFP	pJW03/pJW02	Spectinomycin	Basta
pJW07	<i>proLAT52::AUN2.1</i> -YFP	pJW03/pABD34	Spectinomycin	Basta
pJW09	<i>proMpEF1α::AtMRI</i> -3xCitrine	pABD43/pABD106	Spectinomycin	Gentamicin
pJW10	<i>proMpEF1α::AtMRI</i> -RFP	pABD43/pABD107	Spectinomycin	Chlorsulfuron
pJW11	<i>proMpEF1α::AtMRI<sup>[R240C]</sup></i> -3xCitrine	pABD44/pABD106	Spectinomycin	Gentamicin
pJW15	<i>proLAT52::YFP</i> -CNGC18	pJW04/pABD94	Spectinomycin	Hygromycin
pJW20	<i>proMRI::MpPTI</i> -YFP	pJW18/pABD83	Spectinomycin	Basta
pJW21	<i>proMpEF1α::AtANX1</i> -3xCitrine	pABD50/pABD106	Spectinomycin	Gentamicin
pJW25	<i>proMpEF1α::AtFER</i> -3xCitrine	pABD52/pAB106	Spectinomycin	Gentamicin
pJW27	<i>proMpEF1α::MpPTI</i> -3xCitrine	pJW18/pABD106	Spectinomycin	Gentamicin
pJW28	<i>proMpEF1α::MpPTI</i> -RFP	pJW18/pABD107	Spectinomycin	Chlorsulfuron
pJW36	<i>proMRI::MpPTI<sup>[R240C]</sup></i> -YFP	pJW35/pABD83	Spectinomycin	Basta
pJW37	<i>proLAT52::MpPTI<sup>[R240C]</sup></i> -CFP	pJW35/pABD35	Spectinomycin	Basta
pJW45	<i>proMpEF1α::MpTHE1</i> -3xCitrine	pJW42/pABD106	Spectinomycin	Gentamicin
pJW46	<i>proMpEF1α::MpTHE1</i> -RFP	pJW43/pABD107	Spectinomycin	Chlorsulfuron
pJW51	<i>proMpEF1α::MpPTI<sup>[R240C]</sup></i> -RFP	pJW35/pJW107	Spectinomycin	Chlorsulfuron

### 3.1.3. Oligonucleotide sequences

All oligonucleotide sequences used in this study are listed in Tab. 6. JW-oligonucleotides were designed in the course of this study, while ABD-oligonucleotides were designed by Dr. Aurélien Boisson-Dernier.

**Tab. 6: Oligonucleotide sequences.**

Primer ID	Full name	Nucleotide Sequence (5' to 3')	Purpose
ABD006	SKC12	TTGACAGTGACGACAAATCG	Genotyping of SK-T-DNA insertion lines
ABD547	FERL2-R4	CGCCGTGTCAAACAATTCCGGC	Genotyping of ANX1 ORF
ABD569	FERO-RTR	GACATCGGAGATCCATATACGG	Genotyping of FER ORF
ABD600	LBa1	TGGTTCACGTAGTGGGCCATCG	Genotyping of SALK T-DNA insertion lines
ABD603	ANX2-F	TTTAAGCAATGGATGGTCGAG	Genotyping of anx2-1/ANX2
ABD604	ANX2-R	TAAGATCATTAGCAGCCACGG	Genotyping of anx2-1/ANX2
ABD626	SKc12	TTGACAGTGACGACAAATCG	Genotyping of VEI/ <i>vei-1</i> and VEI/ <i>vei-2</i>
ABD630	eYFP-R	AAGCACTGCAGGCCGTAGC	Genotyping of ORF-YFP fusions
ABD681	GT21229-F1	TTCGGCTACCACGCTCCAGA	Genotyping of MRI/ <i>mri-1</i>
ABD682	GT21229-R1	GGACCGGCCGGTTTAGAGTT	Genotyping of MRI/ <i>mri-1</i>
ABD698	mCFP-F	CGAGGAGCTGTTACCGGGG	Genotyping of CFP- or YFP-ORF fusions
ABD699	mCFP-R	CCTCGAACTTCACCTCGGCGC	Genotyping of ORF-CFP fusions
ABD728	AUN1-F1	CGATCTCATTTGCAGAGGCC	Genotyping of AUN1/ <i>aun1</i>
ABD729	AUN1-R1	CTTCTCCATTGCAGTTTGCC	Genotyping of AUN1/ <i>aun1</i>
ABD731	AUN2-R1	CTTAGCATCCTCATGGTTCCC	Genotyping of AUN2/ <i>aun2</i>
ABD735	820D05-F	GTTCTATTCTTCGACCAAATGG	Genotyping of <i>mri-2</i>
ABD736	820D05-R	CTGCATACTGGTTTGCGGG	Genotyping of MRI ORF/ <i>mri-2</i>
ABD747	Ds5-2	TCCGTTCCGTTTTCGTTTTTAC	Genotyping of <i>mri-1</i> /MRI
ABD766	pMRI-F	TTGTTTCCCGACTTTATCGCGG	Genotyping of <i>pro</i> MRI-ORF fusions
ABD776	AUN1-BPs	GGGGACAAGTTTGTACAAAAAGCAGGC TTAATGATGACGAGTATGGAAGGGAT	Amplification of AUN2.1 ORF with attB1-site
ABD779	AUN2-F2	ATACTAAACGTTTCCCCACTTGG	Genotyping of AUN2/ <i>aun2</i>
ABD792	CNGC18-F	GTGTCCAAGTACTTGTATTGTCTTTG	Genotyping of <i>cngc18-</i>

			1/CNGC18
ABD793	CNGC18-R	AGGCCCATGTAAGAAGTTCTTCCC	Genotyping of <i>cngc18-1</i> /CNGC18
ABD794	LB3_Sail	TAGCATCTGAATTTTCATAACCAATCTCGA TACAC	Genotyping of <i>cngc18-1</i> /CNGC18
ABD796	AUN2.1-BPas	GGGGACCACTTTGTACAAGAAAGCTGGG TTGCAAGACTTCCCATCTTCGGTA	Amplification of AUN2.1 ORF with attB2-site and without stop-codon
ABD798	CNGC18-BPs	GGGGACAAGTTTGTACAAAAAAGCAGGC TTAATGAATAAAATCCGGTCTCTCCG	Amplification of CNGC18 ORF with attB1-site
ABD799	CNGC18-BPas	GGGGACCACTTTGTACAAGAAAGCTGGG TTTTAAACGTCTTCTTTATCTATAG	Amplification of CNGC18 ORF with attB2-site and with stop-codon
JW06	VEI-F3	GGTTTGCCATTGGCTCCAAA	Genotyping of <i>vei-1</i> and <i>vei-2</i>
JW07	VEI-R3	CCCGGTATATGATGGAGCGTTC	Genotyping of <i>vei-1</i> and <i>vei-2</i>
JW10	pAUN1-F-Sac	CAATTTTAGGGAGCTCTTACTTCCTCC	Amplification of <i>proAUN1</i> with Sac restriction site
JW11	pAUN1-R-Spe	CTTCCTACTACTAGTCATTCTTCCTC	Amplification of <i>proAUN1</i> with Spe restriction site
JW15	AUN1/2-F	GGTCTTCTTTGTGATTTACTTTGG	Genotyping of AUN2-YFP
JW16	CNGC18-R	AACTCCTCGCGACGAACGC	Genotyping of YFP-CNGC18 fusion
JW17	Mp_pEF1-F	GCAGTGGAGCGTCTGGCTTA	Genotyping of <i>proMpEF1α</i> -ORF fusions
JW23	<i>cngc18-17_dCaps_Fwd_Eco88I</i>	GATCCGGTGAATGAGATGCTATTTGTGA CCC	dCAPS assay to genotype for <i>cngc18-17</i> /CNGC18
JW24	<i>cngc18-17_dCaps_Rev_199 bp</i>	CAGAGAGGGCACGGACGCT	dCAPS assay to genotype for <i>cngc18-17</i> /CNGC18
JW25	<i>MpPTI_fwd_w/attB1</i>	GGGGACAAGTTTGTACAAAAAAGCAGGC TTAATGGCATGGTGTGTTGCTG	Amplification of <i>MpPTI</i> ORF with attB1-site
JW26	<i>MpPTI_rev_w/attB2</i>	GGGGACCACTTTGTACAAGAAAGCTGGG TTTCCATCCCGTGTGGGTGATC	Amplification of <i>MpPTI</i> ORF with attB2-site and without stop-codon
JW27	<i>MpTHE_fwd_w/attB1</i>	GGGGACAAGTTTGTACAAAAAAGCAGGC TTAATGAGGCGTTCGTCTTGTTT	Amplification of <i>MpTHE1</i> ORF with attB1-site
JW28	<i>MpTHE_rev_w/attB2</i>	GGGGACCACTTTGTACAAGAAAGCTGGG TTTAACCTTCCTTGAGGGTTCA	Amplification of <i>MpTHE1</i> ORF with attB2-site and without stop-codon
JW34	<i>MpPTI_CDS_F1</i>	GCAACTCCAAGGCTGAGTGA	Genotyping of <i>MpPTI</i> ORF
JW35	<i>MpPTI_CDS_R1</i>	CCTTGTCCACCTCCATGCAT	Genotyping of <i>MpPTI</i> ORF
JW41	<i>MpTHE_CDS_R1</i>	GGGAATGAACGAGGCAGTGT	Genotyping of <i>MpTHE1</i> -ORF
JW45	<i>Mp_rbm27_F1</i>	CCAAGTGCGGGCAGAATCAAGT	Genotyping of male Marchantia plants
JW46	<i>Mp_rbm27_R1</i>	TTCATCGCCCGCTATCACCTTC	Genotyping of male Marchantia plants

JW47	Mp_rhf73_F1	TGACGACGAAGATGTGGATGAC	Genotyping of female Marchantia plants
JW48	Mp_rhf73_R1	GAAACTTGCCCGTGTGACTGA	Genotyping of female Marchantia plants
JW52	MpTHE_3'UTR_R1	CACTCCCAAATGAACGCACG	Genotyping of <i>Mpthe1</i> / <i>MpTHE1</i>
JW59	MpTHE1_3'UTR_F2	CGTGCCCTCTGTCTCCTGTTCC	Genotyping of <i>Mpthe1</i> / <i>MpTHE1</i>
JW60	MpPTI_5'UTR_R1	GCGGGCCTTGACTGCCTCT	Genotyping of <i>Mppti</i> / <i>MpPTI</i>
JW63	pCambia1300_RB1	CCTGCAGGCATGCAAGCTTGG	Genotyping of <i>Mppti</i> / <i>MpPTI</i>
JW64	pCambia1300_RB2	GCTGGCGTAATAGCGAAGAGG	Genotyping of <i>Mpthe1</i> / <i>MpTHE1</i>

### 3.1.4. Chemicals and solutions

Growth media and antibiotics used in this study are listed in Tab. 7 and Tab. 8, respectively.

**Tab. 7: Common media.**

Solutions	Ingredients	Further remarks
Gamborg B5 medium "M1"	3163.98 g/ L Gamborg B5	adjust pH to 5.7 with KOH; autoclave
	0.5 g/ L MES	
	0.8 % Micro agar	
Gamborg B5 medium "M2"	3163.98 g/ L Gamborg B5	adjust pH to 5.7 with KOH; autoclave
	10 g/ L Sucrose	
	0.8 % Micro agar	
Johnson's medium	20 mL Stock A (30.3 g/ L KNO <sub>3</sub> ; 6.15 g/ L MgSO <sub>4</sub> )	adjust pH to 5.6 with 1M KOH; autoclave
	20 mL Stock B (47.2 g/ L Ca(NO <sub>3</sub> ) <sub>2</sub> *4 H <sub>2</sub> O)	
	100 mg Inositol	
	1 mL Stock C (1.864 g/ L KCl; 0.773 g/ L H <sub>3</sub> BO <sub>4</sub> ; 0.223 g/ L MnSO <sub>4</sub> *4 H <sub>2</sub> O; 0.288 g/ L ZnSO <sub>4</sub> *7 H <sub>2</sub> O; 0.0624 g/ L CuSO <sub>4</sub> *5 H <sub>2</sub> O;	

	0.309 g/ L $(\text{NH}_4)_6\text{Mo}_7\text{O}_{24} \cdot 4 \text{H}_2\text{O}$	
	1 mL Stock D (6.95 g/ L $\text{FeSO}_4 \cdot 7 \text{H}_2\text{O}$ ; 9.365 g/ L $\text{Na}_2\text{EDTA}$ )	
	535,2 mg/ L $(\text{NH}_4)_2\text{SO}_4$	
	69 mg/ L $\text{NH}_4\text{H}_2\text{PO}_4$	
	533 mg MES	
	10 g/ L Sucrose	
	0.8 % Micro agar	
	ad 1 L with $\text{ddH}_2\text{O}$	
LB medium	5 g/ L Yeast extract	adjust pH to 7.0; autoclave
	10 g/ L Trypton	
	10 g/ NaCl	
	(15 g/ L Agar)	
M51C medium	2 g/ L $\text{KNO}_3$	autoclave  (Ono et al., 1979; Ishizaki et al., 2008)
	0.4 g/ L $\text{NH}_4\text{NO}_3$	
	0.37 g/ L $\text{MgSO}_4 \cdot 7 \text{H}_2\text{O}$	
	0.3 g/ L $\text{CaCl}_2 \cdot 2 \text{H}_2\text{O}$	
	0.275 g/ L $\text{KH}_2\text{PO}_4$	
	0.04 g/ L EDTA-NaFe(III)	
	B5 micronutrients (0.25 mg $\text{NaMoO}_4 \cdot 2 \text{H}_2\text{O}$ ; 0.025 mg $\text{CuSO}_4 \cdot 5 \text{H}_2\text{O}$ ; 0.025 mg $\text{CoC}_2 \cdot 6 \text{H}_2\text{O}$ ; 2 mg $\text{ZnSO}_4 \cdot 7 \text{H}_2\text{O}$ ; 10 mg $\text{MnSO}_4 \cdot 7 \text{H}_2\text{O}$ ; 3 mg $\text{H}_3\text{BO}_3$ )	
	B5 vitamins (100 mg Inositol; 1 mg Nicotinic Acid; 1 mg Pyridoxine-HCl; 10 mg Thiamine-HCl)	
	0.75 mg/ L KI	

	20 g/ L Sucrose	
	0.3 g/ L L-Glutamine	
	1 g/ L Casamino-Acids	
	ad 1 L with $\text{ddH}_2\text{O}$	
Magic Buffer	50 mM Tris/HCl pH7.2 (v/v)	-
	300 mM NaCl (v/v)	
	10 % Sucrose (w/v)	
	dissolve in $\text{ddH}_2\text{O}$	
MS medium	4.3 g/ L Murashige and Skoog (MS)*	adjust pH to 5.7 with 1 M KOH; autoclave  *2.15 g/ L for 1/2 strength *0.43 g/ L for 1/10 strength
	10 g/ L Sucrose	
	0.5 g/ L MES	
	(8 g/ L Micro Agar)	
PG medium	5 mM KCl	adjust pH to 7.5 with 0.1 M NaOH; add 1.5 % low-melting point agarose; boil and pour microscopic PG slides (500 - 550 $\mu\text{L}$ / slide)  (Boavida and McCormick, 2007)
	1 mM $\text{MgSO}_4$	
	0.01 % (w/v) $\text{H}_3\text{BO}_3$	
	5 mM $\text{CaCl}_2$	
	10 % Sucrose	

**Tab. 8: Antibiotics.** Shown are the final bacteria- and plant-specific concentrations.

Antibiotic	Concentration (Bacteria)	Concentration (Plants)
Basta	-	10 $\mu\text{g/ mL}$
Carbenicillin	50 $\mu\text{g/ mL}$	-
Cefotaxime	100 $\mu\text{g/ mL}$	-
Chloramphenicol	34 $\mu\text{g/ mL}$	-
Chlorsulfuron	-	0.5 $\mu\text{M}$
Gentamicin	30 $\mu\text{g/ mL}$	50 - 150 $\mu\text{g/ mL}$

Hygromycin	-	25 µg/ mL
Kanamycin	50 µg/ mL	30 µg/ mL
Rifampicin	10 µg/ mL	-
Spectinomycin	50 µg/ mL	-
Sulfadiazine	-	11.25 µg/ mL

### 3.1.5. Preparation kits

All preparation kits used in this study are shown in Tab. 9.

**Tab. 9: Preparation kits.** Shown are the kits used in this study, including purpose and brand.

Purpose	Preparation Kit	Company
cDNA synthesis	RevertAid H Minus First Strand cDNA Synthesis Kit	Thermo Scientific
Gel elution	QIAEX II® Gel Extraction Kit	Qiagen
Plasmid preparation	GeneJET Plasmid Miniprep Kit	Thermo Scientific
RNA extraction	Direct-Zol RNA Mini-Preparation Kit	Zymo Research

### 3.1.6. Software

All software used in this study is shown in **Tab. 10**.

**Tab. 10: Software.** Shown is the software name, including version (in brackets) and purpose.

Software (Version)	Purpose
CLC DNA Workbench (5)	<i>in silico</i> cloning
ClustalX (2.1)	Generation of multiple sequence alignments
GeneDoc (2.7)	Editing of multiple sequence alignments
ImageJ (1.50e)	Image processing and analysis
MEGA (7.0.14)	Phylogenetic analysis of multiple sequence alignments
Microsoft Office365	Image and text processing, figure design, statistical testing
RStudio (0.99.892)	Boxplot design

## 3.2. Methods

### 3.2.1. Plant cultivation

#### 3.2.1.1. Axenic cultivation setup

Axenic *Arabidopsis* and *Marchantia* cultures were grown under long day conditions (16/8 h day/night cycle under cool white light; photosynthetic photon flux density (PPFD):  $80 \mu\text{mol m}^{-2} \text{s}^{-1}$ ; 21°C) if not stated otherwise. *Arabidopsis* seedlings were cultivated on ½ strength MS medium supplemented with 1 % sugar and 0.8 % micro agar for 7-10 days and subsequently transferred onto soil. Axenic *Marchantia* thallus cultures were cultivated on Johnson's medium with 0.8 % micro agar under identical ambient conditions. *Marchantia* thalli were routinely propagated vegetatively via cultivation of asexual propagules ("gemmae"), representing clonal multicellular disks that are produced in excess by the mature (at least 3-4 weeks old) thallus.

#### 3.2.1.2. Far-red light-induced sporogenesis in *Marchantia*

To induce reproductive growth, 3-4 weeks old *Marchantia* thalli were transferred from axenic growth medium into a semi-sterile soil-based Microbox growth system (<https://saco2.com/>). Plants were then cultivated under a modified long day setup (16/8 h day/night cycle under cool white light (PPFD:  $40 \mu\text{mol m}^{-2} \text{s}^{-1}$ ) supplemented with far-red (FR) light (700-880 nm; PPFD:  $15 \mu\text{mol m}^{-2} \text{s}^{-1}$ ; 21°C; 30 % humidity) for at least 3-4 weeks (modified from Ishizaki et al., 2008), as FR light is known to induce transition from the vegetative to the reproductive growth phase (Nakazato et al., 1999). Male and female plants were kept separately to be able to cross mature plants in a controlled manner. Therefore, a droplet of sterile water was allowed to rest on a mature antheridiophore (male gametangiophore) for 5 min. The water droplet was then transferred onto one or several mature archegoniophore(s) (female gametangiophore) and plants were further cultivated for 2-3 weeks. Plants were checked regularly for the emergence of sporophytes that would give rise to sporangia. Archegoniophores with mature, yet closed sporangia were harvested and the single sporangia were transferred into 1.5 mL Eppendorf reaction tubes containing 500  $\mu\text{L}$  of sterile water. Harvested sporangia were kept in the dark at 4°C for up to 1 week. Harvested archegoniophores were kept in a semi-sterile moisture box under regular long day conditions to allow emergence of further sporangia within 1-3 days.



### 3.2.1.3. Long-term cultivation of vegetative and reproductive *Marchantia* stages

For long-term storage of *Marchantia* lines gemmae were grown on solid Johnson's medium in a short day setup (8/16 h day/night cycle under cool white light; PPFD: 50  $\mu\text{mol m}^{-2} \text{s}^{-1}$  ; 16°C). It is important to prevent the axenic cultivation plates from excessive drying, as *Marchantia* reacts sensitively to drought stress. Alternatively, precious lines can be crossed with the respective (male or female) wild-type accession and spores can be stored at -20 °C for several months.

## 3.2.2. Molecular biology, cloning and transformation

### 3.2.2.1. Genomic DNA-extraction

For genomic DNA (gDNA)-extraction, a 1 cm<sup>2</sup>-sized young *Arabidopsis* leaf or *Marchantia* thallus fragment was cut from the plant and transferred into a 2.0 mL Eppendorf reaction tube with 300  $\mu\text{L}$  of gDNA extraction buffer ('Magic buffer'). The tissue was then mechanically disrupted in a high-speed homogenizer (QIAGEN tissue-lyser) at 30 Hz for 1.5 min using glass (*Arabidopsis*) or ceramic beads (*Marchantia*). For genotyping PCRs 1-2  $\mu\text{L}$  of the extract were added to the PCR mix. The gDNA extracts were stored at 4°C and used up to 1 week after preparation.

### 3.2.2.2. PCR-based genotyping

To determine the genotype of a single plant, a DNA fragment specific to the respective locus of interest was amplified via PCR based on the DNA extract of the individual. Based on potential DNA insertions (e.g. in a T-DNA mutant), primer pairs were designed to amplify DNA amplicons of differing lengths as compared to the native locus. PCR samples were prepared on ice as listed in Tab. 11 and then incubated with a standard PCR protocol shown in Tab. 12. PCR samples were finally separated via gel-electrophoresis (GE) on a 1 % agarose gel (120V, 45 min) and analyzed in a gel documentation system.

**Tab. 11: Standard Genotyping-PCR mix.**

Ingredient	Volume
DreamTaq™ Green PCR master mix (already contains DNA-polymerase and dNTPs)	12.5 µL
F/R-Primer [10µM]	0.3 µL each
DNA extract	1-2 µL
ddH <sub>2</sub> O	ad 25 µL

**Tab. 12: Standard PCR protocol.** The duration of the DNA extension phase (\*) was set to a standard value of 60 sec for amplicons <1 kb. For every additional 0.25 kb, 15 sec were added. No amplicons larger than 1.5 kb were amplified for the purpose of genotyping PCR.

Cycle Step	Temperature [°C]	Duration [sec]	Repetitions
Initial denaturation	94	120	-
DNA denaturation	94	15	35 x
Primer annealing	58-60	15	
DNA extension	72	60*	
Final extension	72	120	-
Storage	4	-	-

### 3.2.2.3. Gender-specific *Marchantia* genotyping PCR

The heterochromatic male and female *Marchantia* lineages possess a X-chromosome or Y-chromosome, respectively, which are thought to harbor essential genes for sex determination (Bischler, 1986; Okada et al., 2001; Ishizaki et al., 2002). To determine the gender of transformed *Marchantia* sporelings (which went through sporogenesis and thus, meiosis), two primer pairs (JW45/46 and JW47/48) were designed to amplify the male-specific *rbm27* (~600 bp fragment) and female-specific *rhf73* DNA markers (~400 bp fragment) (Fujisawa et al., 2001). The following procedure resembles the descriptions of section 3.2.2.2.

### 3.2.2.4. Genotyping for point mutations via dCAPS-assay

To detect single nucleotide polymorphisms (SNPs) in a locus (which naturally do not lead to differing DNA sequence lengths in a standard genotyping PCR) a derived cleaved amplified polymorphic sequence (dCAPS) assay was performed (Neff et al, 1998). Therefore, primers were designed (<http://helix.wustl.edu/dcaps/>) in order to add a restriction site (RS) onto either the WT- or mutant-specific amplicon at the position of the SNP of interest during PCR (settings as described previously). Both DNA templates (equal in length) were then incubated with a (methylation-sensitive) restriction enzyme (RE) specific to the introduced RS (0.4 µL RE and 2.27 µL RE-specific buffer; 37°C, O/N), however only those amplicons with an introduced RS were truly cut. Via GE the amplicons, now differing in size, were separated on a 3 % agarose gel, which can be used to resolve length differences <100 bp.

To detect the SNP in the *cngc18-17* knockdown mutant inducing the R491Q amino acid exchange (Gao et al., 2016) a RS specific to the RE Aval (Thermo Scientific) was introduced into wild-type amplicons (primers JW23/24), leading to the amplicon pattern depicted in Tab. 13 upon restriction digestion and GE.

**Tab. 13: Amplicon sizes for dCAPS-based genotyping of the *cngc18-17* and CNGC18 alleles.**

amplicon size	CNGC18/CNGC18	<i>cngc18-17</i> /CNGC18	<i>cngc18-17/cngc18-17</i>
199 bp		x	x
168 bp	x	x	
31 bp	x	x	

### 3.2.2.5. RNA-extraction from *Marchantia* thalli

RNA was extracted from *Marchantia* tissue using the Zymo Research Direct-Zol RNA Mini-preparation Kit. Therefore, approximately 10 young (7 - 10 d old) thalli were harvested and residual agar was removed completely from the mesh of rhizoids. The thalli were then shock-frozen in liquid nitrogen and manually ground to a fine powder by usage of RNase-free pestle and mortar. The whole setup was constantly cooled with liquid nitrogen to prevent quality loss of the extracted RNA. The plant powder was then aliquoted to 2.0 mL Eppendorf reaction tubes in equal amounts of <200 µg. 700 µL of Trizol were added and the samples were incubated at 56°C for 10 min and gently mixed several times. The samples were centrifuged (2 min, 13.000 rpm) and the supernatant was transferred into a fresh reaction tube. 200 µL of Ethanol were added and mixed thoroughly. The mixture was transferred into a Zymo-Spin Column including a collection tube and centrifuged (30 sec, 13.000 rpm). The precipitated RNA was cleaned up in two washing steps using the provided wash buffers and centrifuged each time (see above). Finally, the RNA was eluted in 30 µL of RNase-free water. The RNA was then stored at -80°C until further usage.

### 3.2.2.6. Complementary DNA synthesis

Using extracted RNA as a template, complementary DNA (cDNA) sequences were synthesized using the RevertAid H Minus First Strand cDNA Synthesis Kit™ (Thermo Scientific) following the protocol presented in Tab. 14. cDNA was stored at -20 °C until usage.

**Tab. 14: cDNA synthesis protocol.**

Ingredient	Volume
RNA-template (~2 µg in total)	1-11 µL
oligo-(dT) <sub>18</sub> primers	1 µL
ddH <sub>2</sub> O	ad 12 µL
<i>incubate for 5 min at 65°C (initiation step)</i>	
Incubation Buffer (5x)	4 µL
'Ribo-Lock'	1 µL
dNTPs (10mM)	2 µL
Reverse Transcriptase (RT)	1 µL
<i>incubate for 90 min at 42°C (synthesis step) and then for 5 min at 70°C (inactivation step)</i>	

### 3.2.2.7. PCR-based amplification of promoter and ORF sequences

For the purpose of promoter (*pro*) and open reading frame (ORF) amplification the Phusion High-Fidelity DNA Polymerase<sup>TM</sup> (Thermo Scientific) was used based on its proofreading function to avoid introduction of random point mutations into the sequence of interest using the following PCR mix (Tab. 15) and PCR protocol (Tab. 16). Depending on the molecular cloning system, specialized oligonucleotide primers were designed. ORF sequences were amplified with overhang-primers adding GW-compatible attB-sites to the sequence, allowing introduction into GW-Entry vectors (see section 3.2.2.9). If the ORF was to be fused to a C-terminal reporter sequence, the reverse primer was additionally designed with a mismatch abolishing the stop codon in the last ORF codon. Promoters were amplified with primers introducing restriction sites at the 5' and 3'-end of the *pro* sequence, allowing introduction into the vector of interest via restriction-ligation reaction (see section 3.2.2.10).

**Tab. 15: PCR-mix for promoter and ORF amplification.**

Ingredient	Volume
cDNA or gDNA template	1 µL
dNTPs (10 mM)	0.5 µL
F/R-Primer (10µM)	0.5 µL each
HF-Buffer	5 µL
Phusion Polymerase	0.3 µL
ddH <sub>2</sub> O	ad 25 µL

**Tab. 16: PCR protocol for promoter and ORF amplification.**

Cycle Step	Temperature [°C]	Duration [sec]	Repetitions
Initial denaturation	98	120	-
DNA denaturation	98	20	35 x
Primer annealing	62	30	
DNA extension	72	30 sec/ kb	
Final extension	72	300	-
Storage	4	-	-

#### 3.2.2.8. Gel elution of PCR-fragments

PCR-amplified DNA amplicons (promoters or ORFs) were excised from a 1 % agarose gel and eluted using the QIAEX II® Gel Extraction Kit (Qiagen). Therefore, up to 250 µg DNA gel were solubilized in 600 µL of QX1-Buffer and 10 µL of Qiaex II solution in a 2.0 mL Eppendorf reaction tube (50°C, 10 min, mild shaking). The samples were centrifuged (30 sec, 13,000 rpm), the supernatant was discarded and the pellet was washed in 500 µL of QX1-Buffer and centrifugation was repeated. Subsequently, the pellet was washed twice in PE-Buffer. After centrifugation, residual buffer was removed completely and the pellet was air-dried until it became white. Finally, the pellet was eluted in 20 µL of  $\text{ddH}_2\text{O}$ , incubated for 5-10 min and centrifuged. The supernatant (the purified DNA extract) was transferred into a fresh reaction tube and stored until usage at -20°C.

#### 3.2.2.9. Gateway-Cloning system

Molecular cloning of expression vectors can be a time-consuming undertaking. The Gateway (GW) Cloning System, however, facilitates the efficient, targeted exchange of DNA-fragments between vectors (Reece-Hoyes and Walhout, 2018). It is based on the highly specific modifications (integrations and excisions) of the *E. coli* genome by bacteriophage  $\lambda$  via “*att*”-recombination sites. The GW system requires the initial amplification of the sequence of interest (e.g. an ORF) extended by *attB*1 and *attB*2 sites at the ends of the sequence. In a BP clonase reaction the *attB*-sites of the desired sequence and the *attP*-sites of a GW ENTRY vector (pDONR207 in this study) can recombine and the sequence of interest is integrated into the vector backbone, now flanked by *attL*-sites. The recombined vector is then transformed into *E. coli* Dh5 $\alpha$  cells and bacterial GW ENTRY clones are selected by the help of a vector-mediated selection marker. After retrieval of the vector DNA in a mini-preparation procedure, it can be recombined with a GW Destination vector in a second LR-clonase reaction to generate a final expression vector. This final vector is again transformed into *E. coli* generating an expression clone which can be expressed *in planta* via *Agrobacterium*-mediated transformation.

### 3.2.2.10. Plasmid-modification via restriction and ligation

In order to exchange vector sequences in absence of flanking GW-sites, a commonly used strategy is restriction-ligation. Therefore, a sequence of interest is amplified with primers which introduce restriction sites (RS) at the sequence borders which correspond to RS in the target vector. Via restriction of the vector and subsequent enzymatic ligation reaction between the linearized vector and the (eluted) RS-flanked sequence, both sequences can be recombined and transformed efficiently into *E. coli*. Selection of transformants is based on a vector-mediated bacterial selection marker. The ligation procedure used in this study is presented in Tab. 17.

**Tab. 17: T4-Ligase-based DNA ligation protocol.**

Ingredient	Volume
Vector	8 µL (~0.25 µg)
Insert	1 µL (insert:vector ratio of 3:1)
T4-Ligase Buffer (10x)	2 µL
T4-DNA Ligase	1 µL
ddH <sub>2</sub> O	ad 20 µL
incubate at 37°C for 30 min OR at 20°C O/N	

### 3.2.2.11. Site-directed mutagenesis

A frequently used strategy to introduce point mutational changes into a vector of interest is site-directed mutagenesis (SDM) (Zheng et al., 2004). For this purpose, two primers were designed using Primer X (<http://www.bioinformatics.org/primerx/>), both of which bind in the region to be mutated and which contain the (1-3 nucleotide) mismatch of interest. Via Phusion Polymerase-based amplification (see 3.2.2.7, Tab. 15) the mutation was introduced into the vector. The PCR sample was then digested with the (methylation-sensitive) RE DpnI (see 3.2.2.14, Tab. 18) to degrade (methylated) template DNA, while maintaining the newly synthesized (non-methylated) mutagenized vectors. The remaining vectors were transformed into *E. coli* Dh5α cells and selected via a vector-mediated bacterial selection marker (see 3.1.4, Tab. 8). Positive clones were verified as usual (see 3.2.2.4).

### 3.2.2.12. Heat-shock transformation of *Escherichia coli*

To transform a vector of interest into *E. coli*, chemically competent cells were gently thawed on ice for 15 min. Afterwards, 20-50 ng of plasmid were added to the cells and allowed to attach to the cell surface for 15 min. The sample was then heat-shock-transformed at 42°C for 50 sec and then quickly transferred onto ice for 2 min. 900 µL of fresh, prewarmed LB were added to the cell suspension and the sample was incubated for 1 h at 37°C under constant shaking (220 rpm). The suspension was then centrifuged (5 min, 5.000 rpm), the pellet was resuspended in 100 µL of fresh LB and finally plated onto a LB selection plate and incubated overnight. After 12-18 h emerging colonies could be picked for further analyses.

### 3.2.2.13. Extraction of plasmid DNA

A crucial step in molecular cloning is the extraction of plasmid DNA from bacteria, which was carried out using the GeneJET Plasmid Miniprep Kit (Thermo Scientific). Therefore, a 5 mL liquid overnight culture was inoculated from bacterial colonies of interest. The densely grown culture was separated into two 2.0 mL Eppendorf reaction tubes and harvested via centrifugation (8.000 rpm, 5 min). The supernatant was discarded and the pellet was resuspended in 250 µL of 'Resuspension Solution'. The cells were then further fractured by addition of 250 µL of 'Lysis Solution' and gentle, but thorough mixing. The 'Lysis Solution' was directly neutralized by addition of 350 µL of 'Neutralization Solution' and thorough mixing. The sample was then centrifuged (13,000 rpm, 5 min) and the supernatant (up to 700 µL) were loaded onto a Thermo Scientific GeneJET Spin Column. To bind the vector DNA to the column, it was centrifuged (13,000 rpm, 1 min) and the supernatant was discarded. The DNA was then washed twice by application of 500 µL of washing buffer onto the column and subsequent centrifugation (13,000 rpm, 1 min). The column was transferred into a clean 1.5 mL Eppendorf reaction tube and 50 µL of 'Elution Buffer' were applied directly onto the column. After 2 min of incubation, the sample was again centrifuged (13,000 rpm, 1 min). The flow-through now contained the cleaned-up vector DNA whose concentration was determined photometrically. The DNA sample was stored at -20°C until further usage.



### 3.2.2.14. Plasmid verification

In order to transform and express vector DNA *in planta* it is crucial to thoroughly test for the correct DNA sequence. Therefore, all GW entry and GW expression clones were PCR-genotyped (standard settings, see 3.2.2.2) to verify the in-frame fusion of the insert (ORF) to the surrounding elements (promoter and reporter). Positive clones were further propagated and their vector DNA was analyzed by means of a restriction digestion reaction. Therefore, the vector DNA was incubated with a restriction enzyme (Tab. 18) introducing 2-5 specific incisions in the vector sequence. The digested sample was separated on a 1 % agarose gel and the specific DNA banding pattern was compared with the *in silico* prediction. 3-5 positive clones were finally sent for sequencing using primers specifically binding to and amplifying the construct to be expressed (e.g. pro::ORF-reporter). Sequencing reactions were prepared as explained in Tab. 19. Finally, one positive clone was kept and used for transformation into *Agrobacterium tumefaciens* and subsequently *in planta*.

**Tab. 18: Protocol for analytical restriction digestion reactions.**

Ingredient	Volume
Vector DNA	equivalent to 1 - 2 µg
Restriction Buffer (10x)	2 µL
Restriction enzyme	1-2 µL (~1U/µg DNA/hour of digestion)
ddH <sub>2</sub> O	ad 20 µL
<i>incubate for 3 h at 37°C (occasional gentle shaking)</i>	

**Tab. 19: Sequencing reaction protocol.** Sequencing was carried out by GATC/Eurofins Genomics (<https://www.eurofinsgenomics.eu/de.aspx>).

Ingredient	Volume
DNA	equivalent to 100 ng
Primer (10 µM)	2.5 µL
ddH <sub>2</sub> O	ad 10 µL

### 3.2.2.15. Long-term storage of bacterial strains in glycerol

Bacterial suspensions of *E. coli* or *A. tumefaciens* strains carrying a vector of interest were shock-frozen in a sterile 25 % glycerol solution (final concentration) and stored at -80 °C for several months to years.

### 3.2.2.16. Transformation of electro-competent *Agrobacterium tumefaciens*

The transformation of vector DNA into plants requires a bacterial mediator such as *Agrobacterium tumefaciens*. Therefore, the vector of interest was transformed into *A. tumefaciens* strain GV3101 via electroporation. First, an aliquot of competent *Agrobacterium* cells was gently thawed on ice (15 min). The vector DNA (20 - 50 ng) was then allowed to adsorb to the bacterial cell surface (15 min) and subsequently transformed by application of a short electro-pulse (1.25kV, 200 ohms, 25µF) in a Bio Rad Electroporator. The cells were directly transferred onto ice (2 min) and incubated for 1 h in 900 µL of fresh, prewarmed LB (28 °C, 220 rpm). Finally, 20 - 100 µL of the incubated culture were spread on a LB selection plate and incubated for 36 - 48 h. Finally, a single colony was picked, the presence of the transformation vector was verified via PCR (4.2.2.2) and used for inoculation of a plant transformation (pre)culture.

### 3.2.2.17. *Agrobacterium*-mediated plant transformation and transformant selection

#### **Transformation of *Arabidopsis***

Young, flowering *Arabidopsis* plants (~10 - 12 cm in height) were transformed via floral dipping (Clough and Bent, 1998). Therefore, a fresh *Agrobacterium* culture was inoculated with 100 µL pre-culture in 250 mL of liquid LB medium and grown over night. At OD<sub>600</sub> ~ 0.8 the culture was centrifuged at 3000 rpm for 20 min and resuspended in 150 mL of a 10 % saccharose solution for 30 - 40 min. OD<sub>600</sub> was then adjusted to ~0.8 with 10 % Saccharose and 150µL of Sylvet L-77/1 L bacterial culture were added shortly before transformation initiation to increase transformation efficiency. Plants were then dipped into the *Agrobacterium* solution for 60 seconds and allowed to recover in a humid, shady environment over-night. Plants were then grown under common greenhouse conditions and

their T1 seeds were selected by the help of the co-mediated antibiotics/ herbicide resistance of choice.

### **Transformation of *Marchantia***

For *Marchantia*, two strategies for *Agrobacterium*-mediated transformation, using either developing sporelings (Ishizaki et al., 2008) or regenerating thalli (Kubota et al., 2013) have been described to date.

For the transformation of sporelings, sporogenesis was induced as explained before (3.2.1.2). Ripe, but intact sporangia were sterilized in 500  $\mu$ L of a 2 % Sodium dichlorisocyanurate (NaDCC) solution for 5 min and then washed three times in 500  $\mu$ L of sterile water. Sporangia were mechanically disrupted to release spores, which were then incubated in 25 mL M51C medium in a cell culture flask under sterile conditions and continuous light for 5 - 7 days. The sporeling culture was then inoculated with 500  $\mu$ L of an over-night *Agrobacterium* culture ( $OD_{600} \sim 0.8$ ) carrying the construct of interest. After 2 days of co-cultivation, the sporelings were rinsed thoroughly with sterile water supplemented with 100  $\mu$ g/ mL Cefotaxime for at least 30 min to destroy remaining *Agrobacterium* and prevent undesired contaminations. Transformants were selected on Gamborg B5 medium supplemented with the respective antibiotic and 100  $\mu$ g/ mL Cefotaxime (see 3.1.4, Tab. 8). After 10 - 14 days, surviving sporelings were transferred onto a fresh selection plate and the presence of the construct of interest was verified via PCR. As all used constructs included a fluorescent protein fusion, successful transformation was validated via detection of a specific fluorescence signal.

The second transformation strategy makes use of the ability of *Marchantia* thallus fragments to regenerate and develop into whole, healthy plants. *Marchantia* gemmae were grown for 10 - 14 days on solid Gamborg B5 medium “M1” under sterile conditions and continuous white light. Thalli were divided into four pieces by cutting through their meristematically active apical notches. Thalli were allowed to regenerate on Gamborg B5 medium “M2” (supplemented with 1 % sucrose) for 3 days and then transferred into 25 mL of M51C medium. Co-cultivation, transformant selection and genotyping were carried out as described for the transformation of sporelings.

### **Vector choice and design**

For protein expression in *Arabidopsis*, the well-established pollen-specific *proLAT52* (e.g. Twell, 1990; Franck et al., 2018 B) and pollen- and root hair-specific *proMRI* (Boisson-Dernier et al., 2015; Franck et al., 2018 B) were used for the majority of experiments. For

complementation and rescue studies in *aun1 aun2* the endogenous *proAUN1* was additionally cloned (see 3.2.2.7 and 4.2.3).

For overexpression and complementation studies in the *Marchantia* backgrounds Tak-1, Tak-2, *Mppti* and *Mpthe1*, *proMpEF1α* was chosen based on a former comparison of ubiquitously active *Marchantia* promoters (Althoff et al., 2014). Four different antibiotics are commonly used for *Marchantia* transformant selection: Hygromycin, Gentamicin, Chlorsulfuron and Kanamycin/Neomycin (Ishizaki et al., 2015). Since the T-DNA insertion of both, *Mppti* and *Mpthe1* mediates a Hygromycin resistance, Hygromycin was excluded as antibiotic of choice. Two types of GW-compatible vectors were chosen, *proEF1α::GW-3xCitrine* (mediating Gentamicin resistance) and *proEF1α::GW-RFP* (mediating Chlorsulfuron resistance). All final binary vectors were created via Gateway cloning (see 3.2.2.9), as summarized in Tab. 5.

It is noteworthy, that Gentamicin-based selection of sporelings led to many false positive transformants (*i.e.* plants surviving Gentamicin-based selection despite absence of the Gentamicin-resistance gene), irrespective of the Gentamicin concentration (50 - 150 µg/mL) and the composition of the growth medium (Johnson's or Gamborg B5 medium). True transformants could however be isolated via screening for their fluorescent tag. In contrast, transformation of thalli did not yield any transformants in 3 different experiments irrespective of the transformation vector to be introduced. These observations agree with (i) the (moderately) lower selection potential of Gentamicin for *Marchantia* sporelings (as compared to further selection markers) described before (Ishizaki et al., 2015) and (ii) the insensitivity of *Marchantia* towards further (commonly used) selection markers, such as the herbicide Basta (Dr. Clement Champion, *personal communication*). Thus, alternative selection markers such as Chlorsulfuron or Hygromycin should be favored for future experiments.

### 3.2.3. Phenotypic analyses

#### 3.2.3.1. *In vitro* pollen germination assay

To assess possible defects in pollen germination or pollen tube growth *Arabidopsis* flowers were harvested in the morning. Therefore, only young, healthy, freshly opened flowers from the main plant stem were considered. The flowers were incubated under long day conditions in a highly humid environment ("moisture incubation box") for 30 min to allow pollen grains to

rehydrate. Whole stamina were then brushed onto a microscopic slide coated with 500 µL of solid pollen germination medium (Boavida and McCormick, 2007) to release the pollen. Samples were transferred to 30°C for 30 min, then incubated under long day conditions for a maximum of 3 - 6 h, both under humid conditions. Samples were finally examined under a light microscope to determine pollen germination and pollen (tube) bursting rates. Therefore, only the regions with highest germination rate were favored consistently and approximately 150 - 300 pollen grains per genotype were classified as non-germinated, germinated (intact) or germinated (not intact), respectively. The pollen germination rate  $R_g$  was calculated as

$$R_g[\%] = \frac{\text{germinated pollen grains (intact)} + \text{germinated pollen grains (burst)} }{\text{total number of pollen grains}} * 100$$

while the pollen bursting rate  $R_b$  was calculated as

$$R_b = \frac{\text{germinated pollen grains (burst)} }{\text{total number of (germinated) pollen grains}} * 100$$

Based on former publications a  $R_g > 60\%$  and  $R_b < 10\%$  were considered as valid threshold values for a wild-type reference sample (which does not display any defects in pollen germination or pollen tube growth) under *in vitro* conditions.

### 3.2.3.2. Pollen tube length measurements

To test for possible effects on the maintenance of pollen tube polarity, pollen tube width and length were determined. Therefore, pollen germination was induced *in vitro* as described before (see 3.2.3.1). The pollen tube length was measured following the grown pollen tube from the origin of germination to the pollen tube tip. As a standard, at least  $n = 200$  tubes per assay were measured in three independent experiments.

### 3.2.3.3. Seed set assay

To test whether *in vitro* pollen germination defects or premature loss of cell wall integrity affect plant fertility *in vivo*, the number of seeds per silique was determined for at least  $n =$

10 siliques per analyzed line. Therefore, ripe, but closed siliques were collected in a 2 mL Eppendorf reaction tube and fixed for 1 d in 1.5 mL of acetic acid in ethanol (v/v = 1:3).

### 3.2.3.4. Reciprocal crossing of *Arabidopsis*

In order to determine possible transmission defects caused by a single mutant allele (*a*), plants which are heterozygous for the allele of interest (*A/a*) were backcrossed with wild-type plants (*A/A*). To assess putative male- (and female-) specific defects, wild-type pistils were pollinated with pollen of the heterozygous mutant (*A/a*) (and *vice versa*). In absence of an allelic transmission defect this crossing event would lead to a theoretical mendelian distribution of 50 % wild-type (*A/A*) to 50 % heterozygous (*A/a*) offspring in F1 generation (Tab. 20).

**Tab. 20: Mendelian segregation ratios in a reciprocal crossing experiment absent from allelic transmission defects.**

	A	a
A	AA (25 %)	Aa (25 %)
A	AA (25 %)	Aa (25 %)

Given a potential transmission defect caused by the mutant allele (*a*), the segregation ratio may be shifted towards the wild-type combination (*A/A*) due to less frequent transmission of the mutant allele. The transmission efficiency ( $T_E$ ) was calculated as follows:

$$T_E [\%] = \text{number of progeny carrying allele of interest} / \text{number of progeny not carrying the allele of interest} * 100$$

In order to cross two plant lines, flowers were emasculated (*i.e.* removal of stamina, as well as surrounding sepals and petals), so that only the pistil would remain on the stem. After 24 h the pistil, which contains female egg cells - carrying the female allele of interest - would be pollinated with the pollen - carrying the male allele of interest.

### 3.2.3.5. Root hair growth assay

To test for defects in root hair growth, seeds were allowed to germinate vertically on ½ MS supplemented with 2 % sugar. 4 - 5 d old seedlings were then transferred onto a regular microscopic slide and the root was immediately covered in 100 µL of liquid 1/10 MS medium

supplemented with 2 % sucrose and covered with a glass slide. The borders of the slide were wrapped with parafilm to allow additional space for the root and to avoid mechanical stress. Seedlings were then allowed to grow for 24 - 36 h. Only healthy seedlings were considered after incubation and such one's with red/ brownish tissue, indicating anthocyanin production as stress response, were excluded. Finally, the distal end of the root was captured, as it harbors the youngest, freshly emerged root hairs. The lengths of the 10 longest root hairs per root were determined for at least  $n = 10$  individuals per line. In order to generate a more resolved representation of root hair growth over time, a root hair profile was generated: The root was digitally divided into sections of 150  $\mu\text{m}$ , starting from the first (youngest) root hair. Per section, the lengths of 5 - 10 root hairs were determined. The mean of each section was compared amongst specimen of the same genotype.

#### 3.2.3.6. Rhizoid growth assay

To analyze possible rhizoid growth defects, gemmae were grown vertically on solid Johnson's medium for 7d under continuous light. Analogous to the root hair growth assay, the length of the 10 longest rhizoids per individual plant was determined for at least  $n = 10$  plants per line. To assess whether deviations in growth speed can be traced back to either growth inhibition or loss of cell wall integrity, rhizoids were also analyzed in a liquid system. Therefore, gemmae were grown under equal ambient conditions for 3 days and then transferred onto a concave microscopic slide covered with 100  $\mu\text{L}$  of liquid Johnson's medium and grown for another 24 - 36 hours. Rhizoid growth of young, intact rhizoids was tracked for 15 - 30 min under a light microscope due to low rhizoid growth rates (as compared to pollen tubes).

#### 3.2.3.7. Microscopic analyses

Microscopic analyses were carried out with a Leica MZ 16 F fluorescence binocular and a Leica DM5000 fluorescence microscope, if not stated otherwise. Live-imaging of  $\text{Ca}^{2+}$  dynamics and detection of RFP signals were carried out with a Leica SP8 confocal laser-scanning microscope (CLSM). Fluorophores were excited and detected with the specific light spectra presented in Fig. 10.

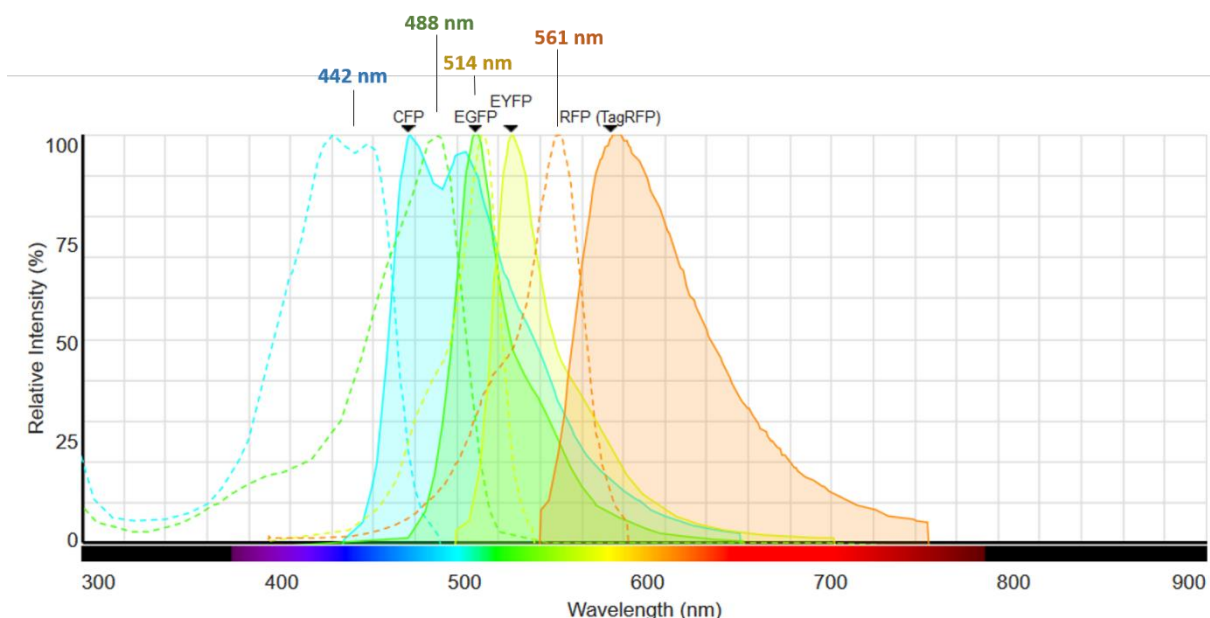


**Fig. 10: Fluorescence spectra of used fluorophores.** Excitation/emission spectra: CFP (442 nm/464-501 nm or Leica Filter Cube “CFP”), GFP (488 nm/505 - 520 nm or Leica Filter Cube “GFP”), YFP (514 nm/525-554 nm or Leica Filter Cube “YFP”), RFP (561 nm/575 - 606 nm).

### 3.2.3.8. Detection of RFP signals in autofluorescent tissue of *M. polymorpha*

In order to verify the stable, non-chimeric expression of a transformed construct, one strategy is to directly detect the fluorescence signal which is emitted by the reporter fusion. While fluorophores like YFP and CFP can be easily detected using epifluorescence microscopes (such as model Leica DM5000), RFP emission often overlaps with autofluorescent light emitted from e.g. chloroplasts. To avoid choice of false positive lines, thallus fragments of (selected and isolated) putative transformants were analyzed at a Leica SP8 CLSM with the following settings: DPSS laser (561 nm); 20 % laser intensity; channel 1: Detection of RFP signal at 575 - 606 nm (Leica ‘Smart Gain’: 200 %) , channel 2: Detection of autofluorescence signals at 650 - 700 nm (Leica ‘Smart Gain’: 10 %), channel 3: Bright field imaging. Via this procedure, PM-localized proteins tagged with RFP could be detected and easily distinguished from autofluorescent intracellular structures. In the final micrographs, both, RFP- and autofluorescent signals were differentially false-color coded (Fig. 11). The absence of (i) plasma membrane-localized autofluorescence and (ii) major regions of overlapping fluorescence signals indicate that the chosen settings are reliable for the extraction of RFP-signals from autofluorescent tissue.



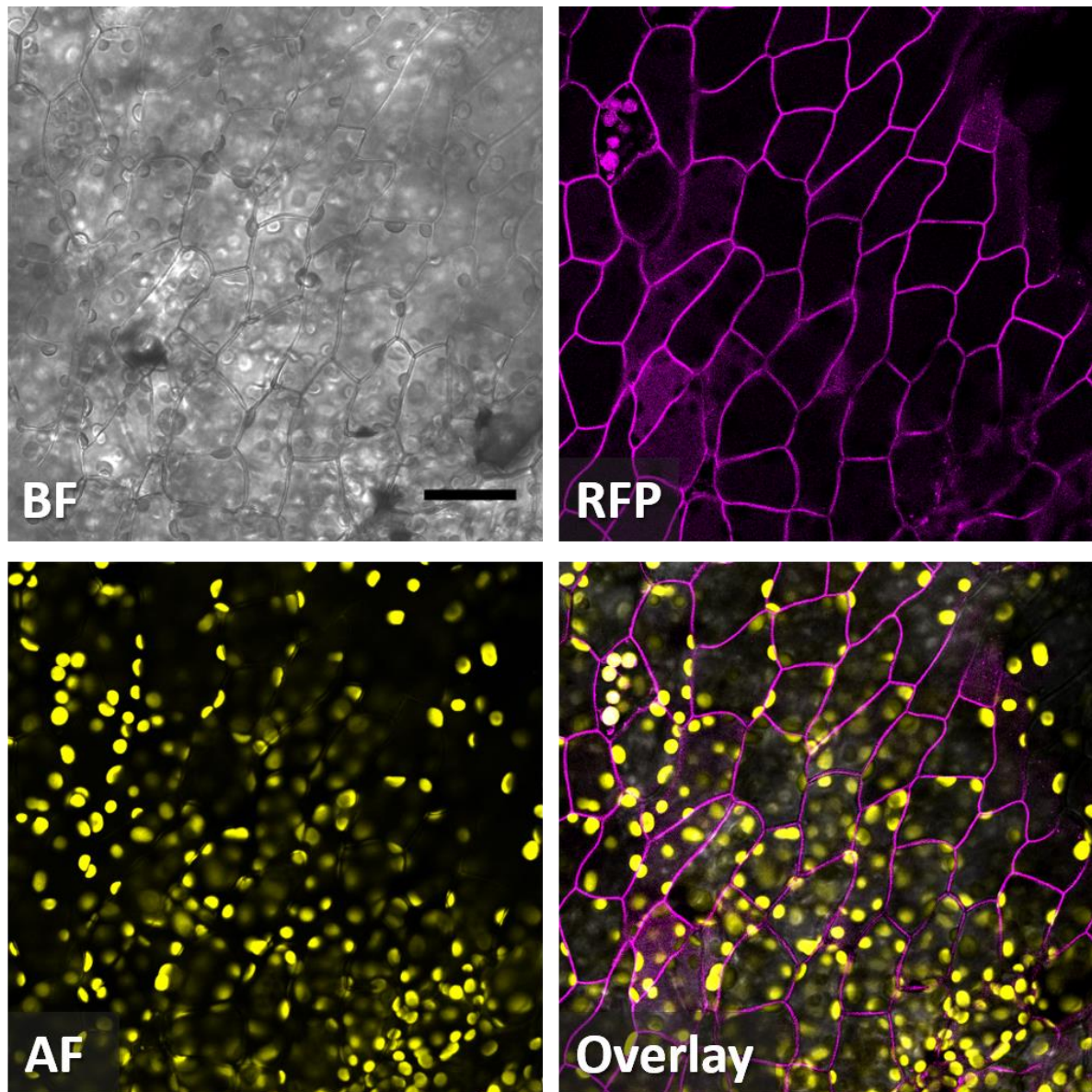


**Fig. 11: CLSM-based detection of RFP signals in autofluorescent tissue of *M. polymorpha*.** Shown are epidermal cells of a Tak-2 *Marchantia* thallus expressing plasma membrane-localized *MpPTI-RFP*; BF: Brightfield; RFP: Red fluorescent protein; AF: Autofluorescence (chloroplasts); Overlay: Composition of BF, RFP and AF channels. Settings were chosen as described above. Scale bar: 50  $\mu\text{m}$ .

### 3.2.3.9. Live-imaging of cytosolic $[\text{Ca}^{2+}]$ -dynamics in tip-growing cells

For live-imaging of intracellular  $[\text{Ca}^{2+}]_{\text{cyt}}$  dynamics the ratiometric Yellow CaMeleon 3.60 (YC 3.60)  $\text{Ca}^{2+}$ -biosensor was used, which is composed of a CFP- and a YFP-tag linked via CaM-M13 fusion. CaM then induces a protein conformational change upon  $\text{Ca}^{2+}$ -binding which brings CFP and YFP in proximity to each other. If the CFP fluorophore is excited with light at a specific wavelength of around 440 nm, it emits light at a wavelength of around 530

nm. This light can be transmitted to the proximal YFP-tag via the Förster resonance electron transfer (FRET) effect. As the ratio between CFP- and YFP emission intensity depends on  $\text{Ca}^{2+}$ -binding by CaM the YC3.60 system can be used as a ratiometric, non-cytotoxic biosensor to determine relative cytosolic  $\text{Ca}^{2+}$  concentrations and dynamics over time in tissues, as well as single cells, such as pollen tubes (Gao et al., 2016; Franck et al., 2017; this study), root hairs (Monshausen et al., 2008; Candeo et al., 2017) or fungal hyphae (Kim et al., 2012).

In the course of this study pollen tubes were analyzed via the YC3.60 system. Pollen germination of mutant lines of interest carrying the YC3.60 biosensor was induced as described before (3.2.3.1). To minimize background fluorescent noise, growing pollen tubes were analyzed with a Leica SP8 CLSM. To assess intracellular  $\text{Ca}^{2+}$ -dynamics over time pollen tube growth was captured over time (20 frames per minute) as published before (Franck et al., 2017). To analyze the steadiness of tip-growth the captured ratiometric  $\text{Ca}^{2+}$  videos were transformed into kymographs which represent an illustration of spatiotemporal information in form of a two-dimensional graph. In addition, the relative  $\text{Ca}^{2+}$ -measurements via YC3.60 allowed the annotation of  $\text{Ca}^{2+}$ -flux in a spatiotemporal manner.

## 4. RESULTS

### 4.1. Functional conservation of a RLK-dependent cell wall integrity signaling module

Two loss of function mutants of the *Marchantia* RLCK-homolog *MpPTI* and MLR-homolog *MpTHE1* have recently been described to lead to loss of CWI in *Marchantia* rhizoids (Honkanen et al., 2016), strongly reminding of the loss of function phenotypes described for the RLCK *AtMRI* (Boisson-Dernier et al., 2015) and the MLRs *AtANX1/2* and *AtFER* in *Arabidopsis* tip-growing cells. Based on these findings we hypothesized that tip-growth control may be governed by a common signaling module comprised of RLCKs and MLRs in both, *Marchantia* and *Arabidopsis*.

#### 4.1.1. The *Marchantia* homologs *MpPTI* and *MpTHE1* regulate cell wall integrity in tip-growing rhizoids

To confirm the loss of cell wall integrity phenotype in rhizoids of the two T-DNA insertional mutants ST13-3 (putative *Mppti*) and 14-3 (putative *Mpthe1*) (Honkanen, 2015; Honkanen et al., 2016; Fig. 12A) rhizoid development of young gemmae was studied *in vitro* (Fig. 12B). Both, ST13-3 and ST14-3 gemmae clearly depicted an obvious rhizoid growth defect indicated by shorter rhizoids as compared to the Tak-1 and Tak-2 wild-type accessions, as well as highly frequent loss of cell wall integrity, indicated by brownish rhizoid tips (Fig. 12B, arrowheads). The determination of maximal rhizoid length in a vertical growth setup (see 3.2.3.6.) confirmed these observations and revealed an increasing and highly significant growth defect over time as compared to Tak-1/2 (Fig. 12C). In the following, both mutant lines were PCR-genotyped for their gender with sex-specific primer combinations (see 3.2.2.3.). ST13-3 (*Mppti*) was determined to be of female gender, while ST14-3 (*Mpthe1*) was found to be male. These findings were confirmed morphologically after gametangia formation (see 3.2.1.2 and 4.1.7., Fig. 24).

To test whether the observed rhizoid growth defects in the T-DNA insertional lines ST13-3 and ST14-3 factually result from a disruption of the *MpPTI* and *MpTHE1* gene loci, respectively, mutant thalli were transformed with either a *MpPTI*-RFP or *MpTHE1*-3xCitrine/*MpTHE1*-RFP protein fusion under control of the ubiquitously active *Marchantia*

*polymorpha* Elongation-Factor1 $\alpha$  (*MpEF1 $\alpha$* ) promoter (see 3.2.2.17) (*proMpEF1 $\alpha$ ::MpPTI-RFP* and *proMpEF1 $\alpha$ ::MpTHE1-3xCitrine/-RFP*).

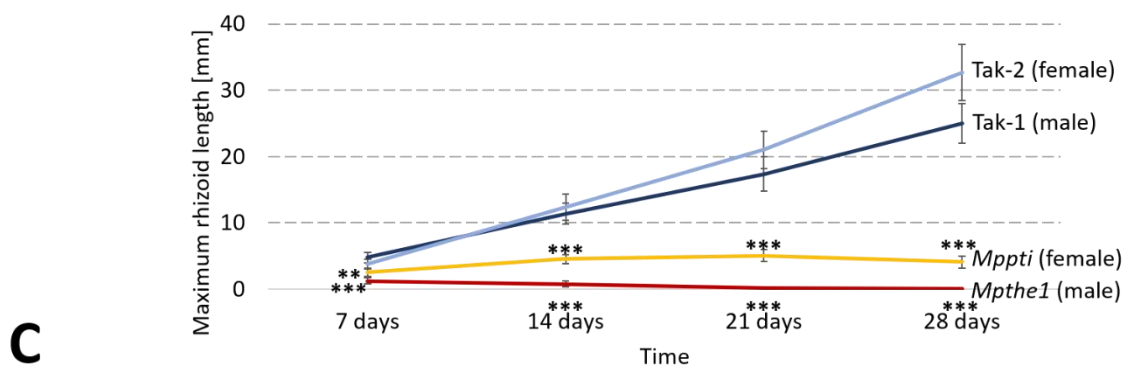
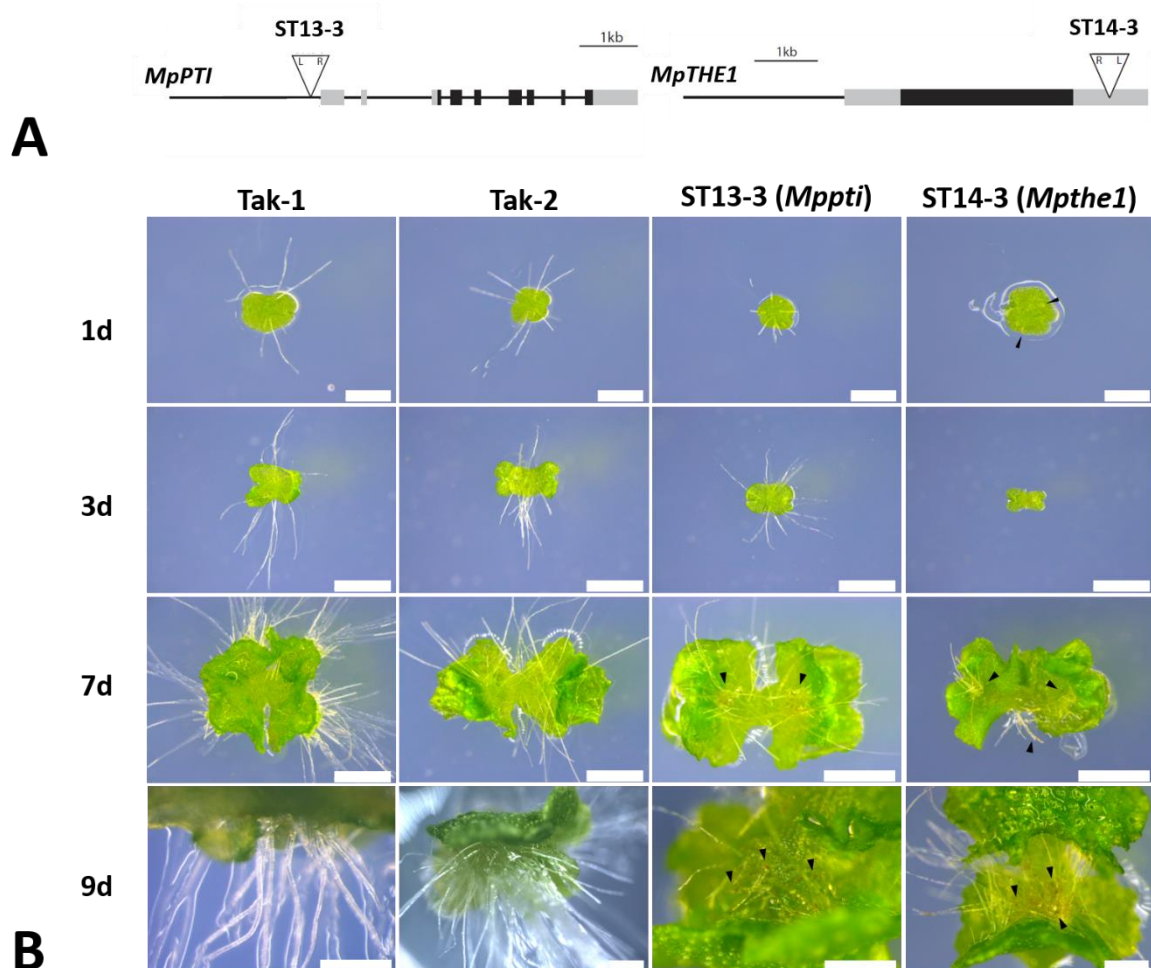


**Fig. 12: The T-DNA mutant lines ST13-3 and ST14-3 display defects in rhizoid growth.** (A) Gene models of *MpPTI* and *MpTHE1* revealing sites of T-DNA insertion in ST13-3 and ST14-3, respectively (Honkanen, 2015; Honkanen et al., 2016). Grey box: UTR; bold and thin black boxes: exons and introns, respectively. Schemes are modified from Honkanen, 2015. (B) Rhizoid growth and gemma development in *Mppti* (ST13-3) and *Mpthe1* (ST14-3) as compared to the Tak-1 and Tak-2 wild-type accessions, shown at t = 1d (scale bar: 500  $\mu$ m), 3d (scale bar: 1mm), 7d (scale bar: 1mm) and 9d (scale bar: 500  $\mu$ m) of cultivation. Arrowheads mark loss of CWI indicated by brown rhizoid tips. (C) Depiction of maximal rhizoid growth over time in a vertical rhizoid growth assay. n  $\geq$  8 thalli/genotype. Significance of *Mppti* and *Mpthe1* datasets against both, Tak-1/2 was tested with a two-tailed, unpaired student's T-test (\*\*: p <0.01, \*\*\*: p<0.001).

For ST13-3 (*Mppti*), 50 independent lines putatively expressing *MpPTI*-RFP were isolated after 3 weeks of antibiotics selection out of which 40 lines were positively PCR-genotyped for presence of the *proMpEF1α::MpPTI*-RFP construct. Seven lines were further analyzed for a putative complementation of the rhizoid growth defects through *MpPTI*-RFP expression. Therefore, the female ST13-3 (*Mppti*) mutant and transformant lines were compared to the Tak-2 (female) accession concerning rhizoid length and growth behaviour. While the untransformed ST13-3 mutant line displayed rhizoid lengths of 36 % as compared to Tak-2 (100 %), the seven tested lines displayed a restoration of rhizoid length ranging from 60 - 86 % (Fig. 13A). While rhizoids of untransformed ST13-3 plants frequently displayed an early loss of CWI in newly emerging rhizoids, the defect could not be observed in any of the complemented lines (n = 99 individuals) (Fig. 13B). Furthermore, fluorescence microscopy revealed that *MpPTI*-RFP localizes to the plasma membrane, just like *AtMRI* (Fig. 13C). These results show that loss of *MpPTI* induces loss of rhizoid CWI in *Marchantia*, just like loss of *AtMRI* induces loss of CWI in *Arabidopsis* pollen tubes and root hairs.

In order to complement T-DNA line ST14-3 (*Mpthe1*), *Mpthe1* thalli and Tak2 x *Mpthe1* spores were transformed with a *proMpEF1α::MpTHE1*-RFP and *proMpEF1α::MpTHE1*-3xCitrine construct, respectively. Mutant selection and verification are ongoing. Ultimately, the same phenotypic analyses, like described for complementation of *Mppti*, will need to be conducted, to assess whether *MpTHE1* factually controls rhizoid tip-growth, just like *AtANX1/2* and *AtFER* regulate tip-growth control in *Arabidopsis* pollen tubes and root hairs, respectively.



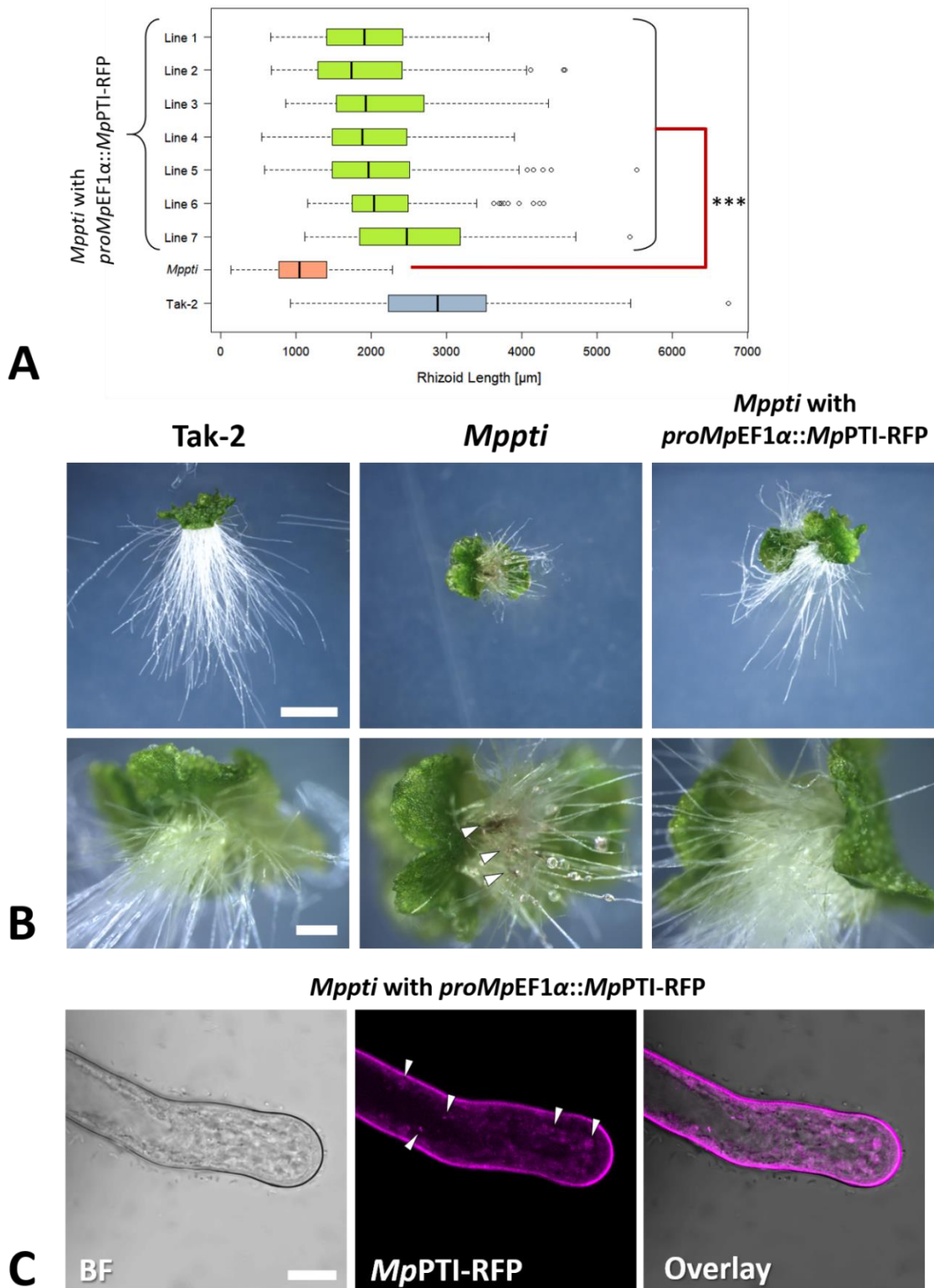


**Fig. 13: *MpPTI*-RFP complements ST13-3 (*Mppti*)-induced loss of CWI in growing *Marchantia* rhizoids.** (A) Rhizoid growth assay visualized in form of a boxplot. The female ST13-3 mutant was compared to the Tak-2 (female) wild type. Datasets of all 7 analyzed complementation lines were significantly different from the untransformed *Mppti* control (\*\*\*:  $p < 0.001$  in a two-tailed, unpaired Student's T-test). (B) Representative images of the plants analyzed in section (A). Arrowheads mark the frequent loss of CWI (brownish cells) in the untransformed *Mppti* mutant. Scale bars: upper picture series: 2mm; lower picture series: 500  $\mu\text{m}$ . (C) CLSM-images of a *Mppti* rhizoid expressing *MpPTI*-RFP. Shown are the BF (bright field) capture; corresponding *MpPTI*-RFP fluorescence signal and the digital overlay of both images. Arrowheads may indicate vesicular localization. Scale bar: 20  $\mu\text{m}$ .

#### 4.1.2. *AtMRI* is capable of rescuing the loss of integrity phenotype of *Mppti* rhizoids.

Given the fact that both, the PTI-like RLCK *AtMRI* (Boisson-Dernier et al., 2015) and its sole *Marchantia* homolog *MpPTI* (Honkanen et al., 2016; this study) are crucial to maintain CWI during tip-growth, it was hypothesized that the function of PTI-likes in regulation of tip-growth may have been conserved throughout land plant evolution. *AtMRI* and *MpPTI* share an amino acid similarity of 77.4 %, while 64.9 % of their residues are identical (Fig. 14A). To test whether the high structural similarity between *AtMRI* and *MpPTI* is sufficient to interspecifically rescue the *Mppti* rhizoid growth defect, despite their independent evolution for more than 470 million years, the *Mppti* mutant line was transformed with *AtMRI*-RFP under control of *proMpEF1α* (*proMpEF1α::AtMRI*-RFP). Three independent transformant lines showed a moderate, but significant restoration of rhizoid length in the range of 44 - 54 % as compared to Tak-2 wild-type level (100 %) (Fig. 14B). Closer analysis revealed that the loss of CWI in emerging rhizoids was drastically reduced in the transformant lines, as compared to the untransformed *Mppti* control, indicated by the emergence of less brownish (*i.e.* burst) rhizoid tips (Fig. 14D). Given the perpendicular growth axis of *Marchantia* rhizoids (in relation to the thallus), as well as their proliferative growth behaviour, it is technically complicated to image and precisely quantify the bursting rate (*i.e.* % of bursting rhizoids) of an individual. Therefore, the number of long, intact rhizoids was determined, reasoning that early loss of CWI would reduce the number of such rhizoids and thus, both values should be inversely proportional to each other. Indeed, all three transformed lines showed a moderate, but significant increase in the number of intact rhizoids per thallus. Restoration ranged between 56 and 63 %, as compared to Tak-2 (100 %) and *Mppti* (33 %) (Fig. 14C). Furthermore, fluorescence microscopy revealed, that *AtMRI*-RFP localizes to the rhizoid plasma membrane, just like *MpPTI* in rhizoids and like *AtMRI* in pollen tubes and root hairs (Fig. 14E). Taken together, these results show that *AtMRI* can, to some extent, take over the function of *MpPTI* in rhizoid growth control. The fact that both, *AtMRI*-RFP and *MpPTI*-RFP, were frequently found to localize to granules (in addition to localization to the PM), which likely represent secretory vesicles, indicate that localization of *Marchantia* and *Arabidopsis* PTI-like proteins may rely on a similar secretion system.



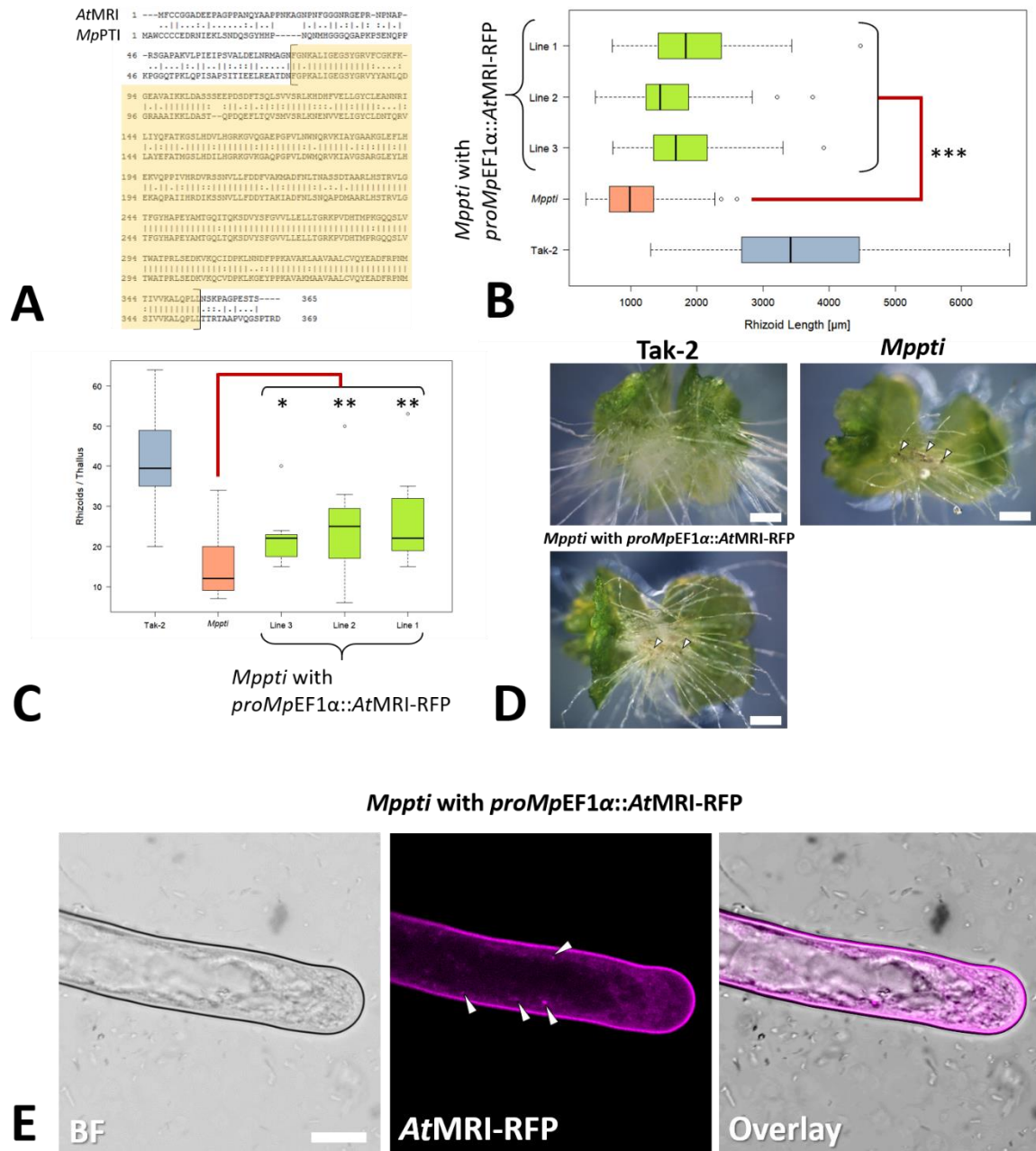


**Fig. 14: Structural and functional conservation between *AtMRI* and *MpPTI*.** (A) A pairwise sequence alignment of the *AtMRI* (AT2G41970) and *MpPTI* (Mapoly0051s0094) full-length amino acid sequences was calculated using the EMBOSS Needle alignment tool (BLOSUM62 matrix, gap open penalty: 10.0, gap extension penalty: 0.5) ([https://www.ebi.ac.uk/Tools/psa/emboss\\_needle/](https://www.ebi.ac.uk/Tools/psa/emboss_needle/)). Nomenclature: (|) identity, (:) similarity, (.) dissimilar amino acids, ( ) gap. The serine-threonine kinase domain was detected using the Prosite domain recognition tool (<https://prosite.expasy.org>) and is highlighted in yellow. (B) Rhizoid growth assay of *Mppti* transformed with *AtMRI*-RFP, in comparison with the untransformed *Mppti* and the Tak-2 wild-type lines. Datasets of all 3 independent transformant lines were significantly different from *Mppti* (\*\*\*:  $p < 0.001$  in a two-tailed, unpaired Student's T-test). (C) Number of rhizoids per thallus for  $n \geq 10$  individuals, presented as a boxplot. Significance: \*:  $p < 0.05$  and \*\*:  $p < 0.01$  in an unpaired, two-tailed student's T-test. (D) Representative images of the data presented in section (B). Arrowheads indicate the loss of CWI at the tip of rhizoids, which was strongly decreased in the transformant lines, as is also indicated by the emergence of comparatively long, intact rhizoids. Scale bar: 500  $\mu\text{m}$ . (E) Protein localization of *AtMRI*-RFP in *Mppti* rhizoids. Shown are bright field (BF) captures and corresponding *AtMRI*-RFP fluorescence images. Arrowheads indicate frequently observed fluorescent granules, which likely represent secretory vesicles. Scale bar: 20  $\mu\text{m}$ .

#### 4.1.3. *MpPTI* is capable of rescuing the *mri-1*-induced loss of CWI in both, *Arabidopsis* PTs and RHs.

Rhizoids of early-diverging land plants represent evolutionary ancient tip-growing cell types and may represent our best approximation of how rooting cells in early land plants may have looked like. In contrast to the gametophytic rhizoids of liverworts like *Marchantia*, seed plants like *Arabidopsis* develop sporophytic root hairs. Much later during evolution, seed plants evolved tip-growing pollen tubes, another gametophytic cell type, yet with a very different function. Given this evolutionary background and the universal function of *AtMRI*, irrespective of life phase or cell function, it is thus very interesting to study the degree of functional conservation between PTI-likes, *i.e.* the capability of *MpPTI* to take over the function as growth regulator in distantly related cell types (pollen tubes) or different life phases (root hairs).

##### ***MpPTI*-YFP in *mri-1* pollen**

To further address this question, *mri-1/MRI* plants were transformed with a *MpPTI*-YFP fusion under control of the endogenous MRI promoter (*proAtMRI::MpPTI*-YFP). Selected T1 seedlings were PCR-genotyped for heterozygosity of the background mutation (*mri-1/MRI*) and pollen fluorescence was determined to infer hemizygosity for the transformed construct. T2 seedlings originating from three independent T1 lines were genotyped for presence of the *mri-1* allele. Despite the severe male transmission defect of untransformed *mri-1/MRI* plants due to the *mri-1*-induced loss of pollen tube integrity that was described before (Boisson-Dernier et al., 2015), 7 out of a total number of 200 transformed plants were determined to be homozygous (*mri-1/mri-1*). Furthermore, 124 heterozygous (*mri-1/MRI*) and 69 wild-type (*MRI/MRI*) lines were identified. Comparison with the expected ratios (assuming a male transmission defect or mendelian distribution, *i.e.* full complementation of male sterility in *mri-1/MRI*) showed that the segregation ratio in the transformant lines was significantly different from both expectations (Tab. 21). This data shows that *MpPTI* is capable of partially rescuing *mri-1*-induced male sterility.

**Tab. 21: Segregation analysis of the *mri-1* allele in the *mri-1*/MRI background transformed with *proMRI::MpPTI-YFP*.** Shown are the observed numbers of T2 progeny - which were heterozygous or homozygous for the *mri-1*-allele - in dependence of presence/absence of the transformed construct *proMRI::MpPTI-YFP*. Observed values of the transformed lines were compared by means of a  $\chi^2$  test of independence with the expected values of mendelian distribution or a (male) gametophytic transmission defect. [\*] marks data from Boisson-Dernier et al., 2015.

	MRI/MRI	<i>mri-1</i> /MRI	<i>mri-1/mri-1</i>	n	Ratio	p-value (two-tailed $\chi^2$ test)
Observed ( <i>mri-1</i> /MRI) [*]	183	170	0	353	1 : 0.93 : 0	
Observed ( <i>mri-1</i> /MRI with <i>MpPTI-YFP</i> )	69	124	7	200	1 : 1.80 : 0.10	
Expected (Mendelian distribution)	50	100	50	200	1 : 2 : 1	<0.001
Expected (Male gametophytic defect)	100	100	0	200	1 : 1 : 0	<0.001

To assess if the rescue of the *mri-1*-induced transmission defect factually originated from pollen-expression of *MpPTI* and to understand, why the observed segregation of the *mri-1* allele in transformed lines was significantly different from a mendelian distribution (Tab. 21), double-homozygous *mri-1/mri-1 MpPTI-YFP* T3 plants were analyzed in an *in vitro* pollen germination assay. All three independent T3 lines of *mri-1/mri-1* homozygously expressing *MpPTI-YFP* revealed a reduction of pollen bursting from 100 % (*mri-1/mri-1*) to 27, 23 and 36 %, respectively. These reductions did not significantly differ from both, the Col-0 wild type (18 %) and *mri-1/mri-1* complemented with *proMRI::AtMRI-YFP* (21 %;  $p > 0.01$ ) (Boisson-Dernier et al., 2015; Fig. 15A). Closer analysis of *in vitro* pollen tube growth allowed the following observations: (i) All pollen tubes in *mri-1/mri-1* hemizygotously expressing *MpPTI-YFP* were fluorescent, *i.e.* expressed *MpPTI-YFP* ( $n > 50$  pollen tubes analyzed). (ii) Pollen tubes expressing *MpPTI-YFP* frequently showed a partial loss of polarity, indicated by establishment of several growth axes (*i.e.* pollen tube branching) or swollen tube apices ( $n = 56$  of 60 analyzed *mri-1 MpPTI-YFP* pollen tubes). (iii) Such pollen tubes frequently developed tip-localized lesions. (iv) Comparable phenotypic abnormalities were absent in *mri-1/mri-1* complemented with *AtMRI-YFP* (Fig. 15B).

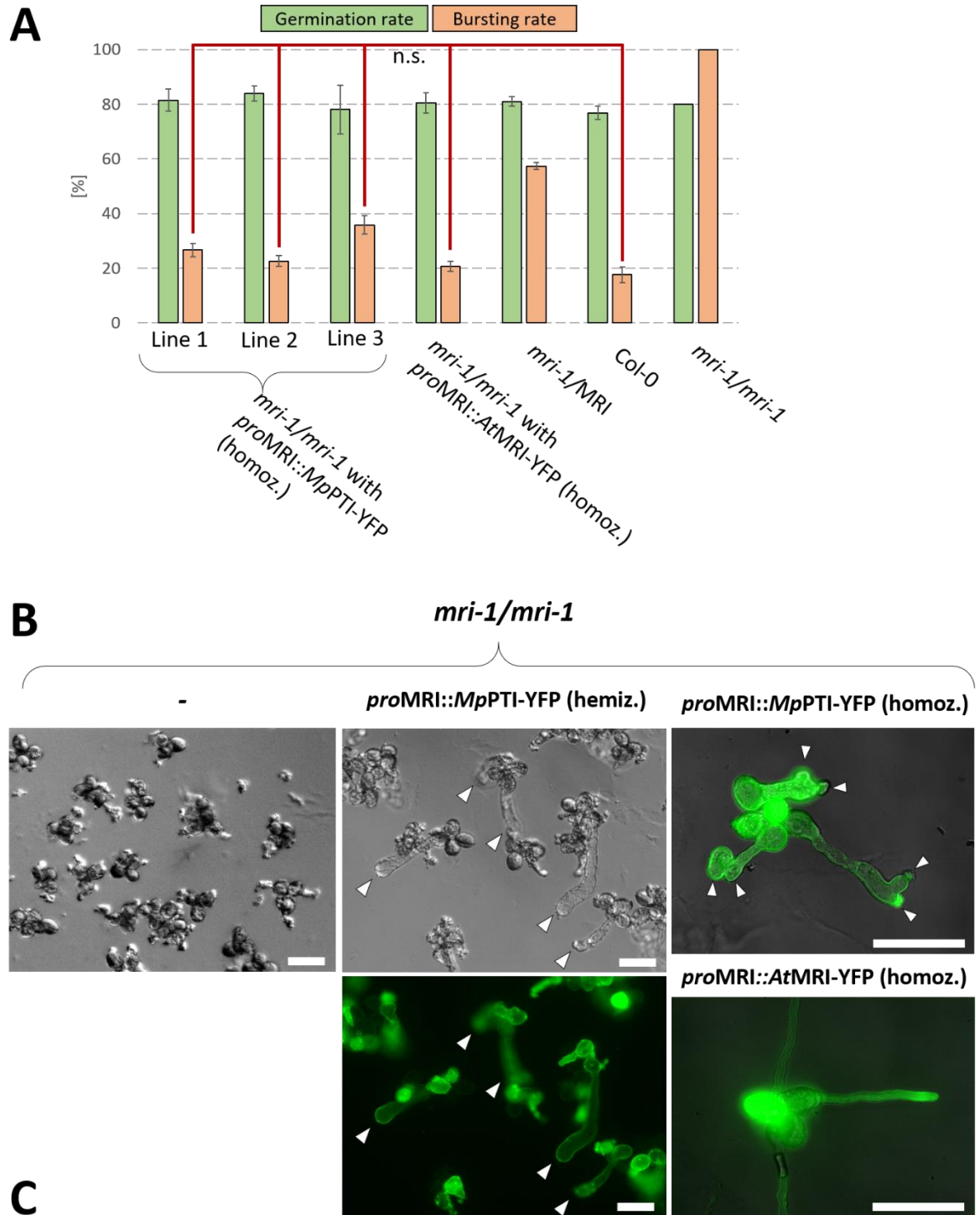


**Fig. 15: Expression of *MpPTI-YFP* rescues *mri-1*-induced loss of CWI during *in vitro* pollen germination.** (A) *In vitro* pollen germination assay of three independent T3 lines of *mri-1/mri-1* homozygously expressing *proMRI::MpPTI-YFP*, in comparison to Col-0, *mri-1/MRI*, *mri-1/mri-1* and *mri-1/mri-1* complemented with *proMRI::AtMRI-YFP*. Pollen bursting rates of all three *mri-1* lines expressing *MpPTI-YFP* were not significantly different (n.s.) from *mri-1* expressing *AtMRI-YFP* or Col-0 ( $p > 0.01$  in an unpaired, two-tailed student's T-test); a total of 600 pollen grains was analyzed in  $n = 3$  independent experiments; error bars show the standard error of the mean. (B) Representative pictures of the data shown in section (A) and described in section 4.3.1. Arrowheads indicate partial loss of polarity, i.e. pollen tube branching, swelling of tube apices and tip-focused lesions. Scale bars = 80  $\mu\text{m}$ .

To analyze whether the observed complementation of *mri-1*-induced loss of CWI *in vitro* reflects the ability to rescue fertility *in vivo*, the seed set was analyzed. The seed set of the same three independent T3 lines analyzed before was increased, ranging between 29 - 35 seeds, 18 - 25 seeds and 10 - 11 seeds per silique, as compared to 43 seeds in wild-type siliques and (close to) 0 seeds in an untransformed *mri-1* homozygous line, indicating a partial rescue of pollen bursting *in vivo*. However, the seed set of all three complemented lines was lower than in the reference line of *mri-1/mri-1* expressing *AtMRI*-YFP (42 - 44 seeds per silique). The seed set of all three lines (*mri-1* with *MpPTI*-YFP) was significantly different from untransformed *mri-1/mri-1* (Fig. 16). These results show, that *MpPTI* is capable of rescuing *mri-1*-induced sterility, not only *in vitro*, but also *in vivo*.

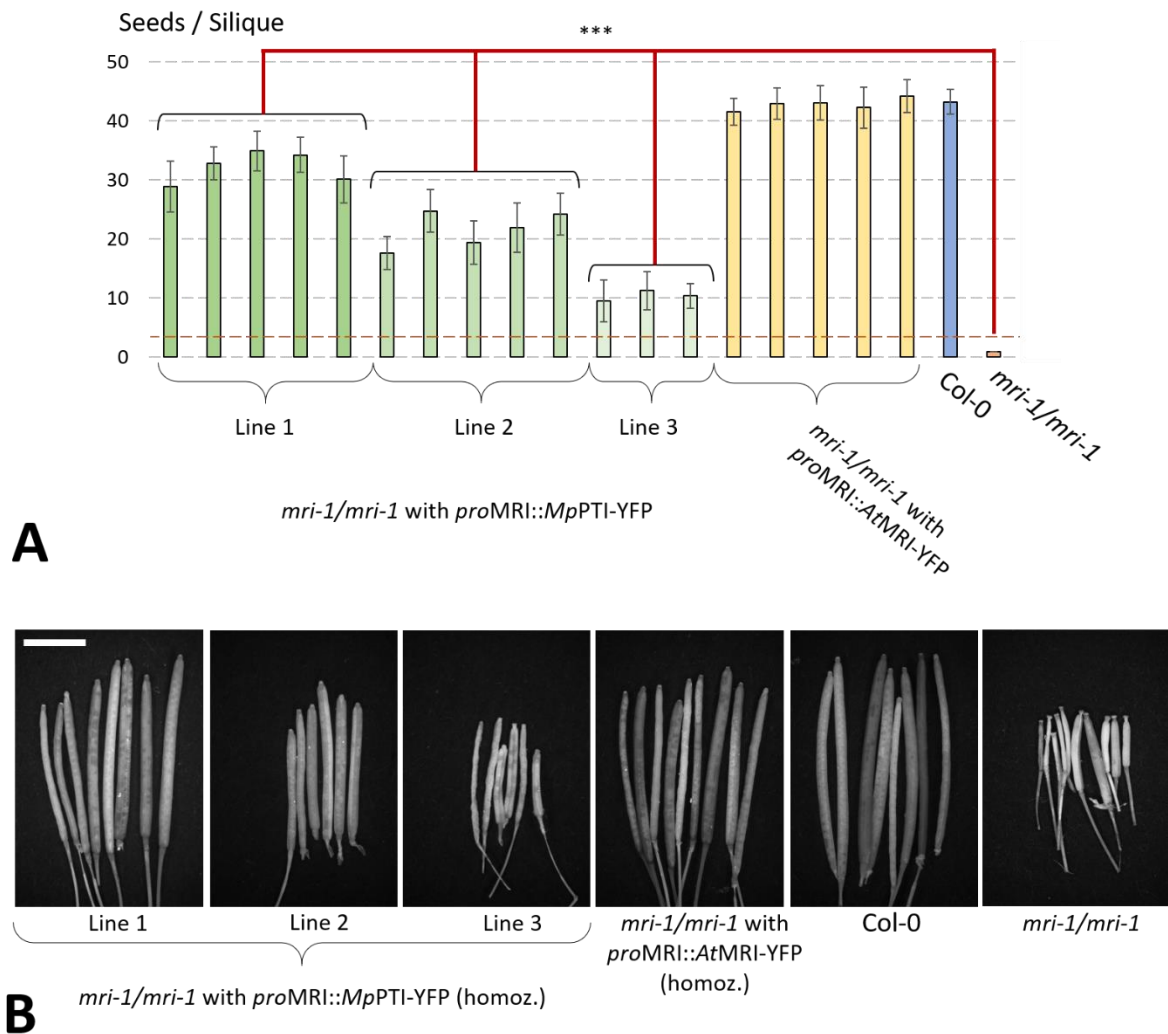


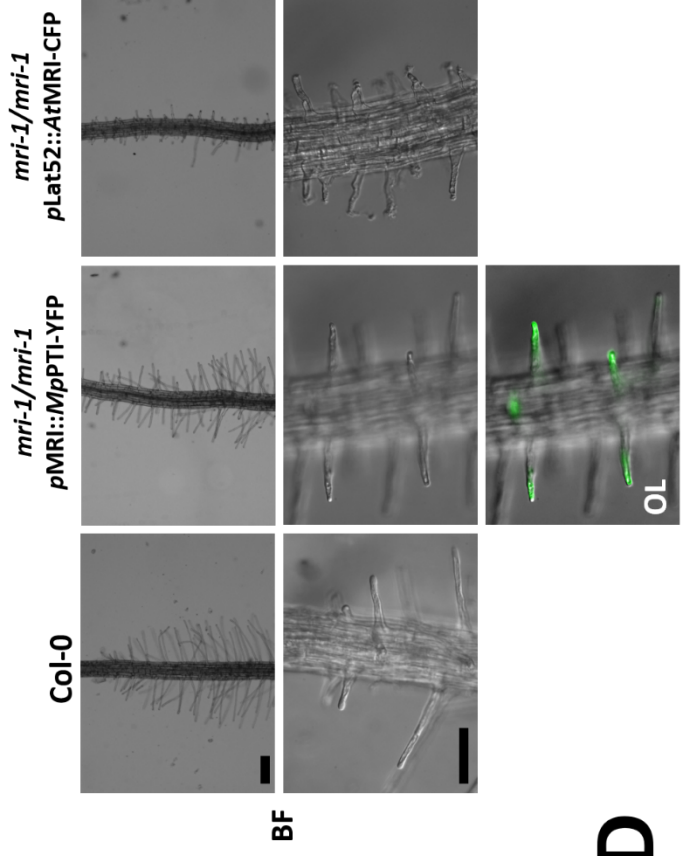
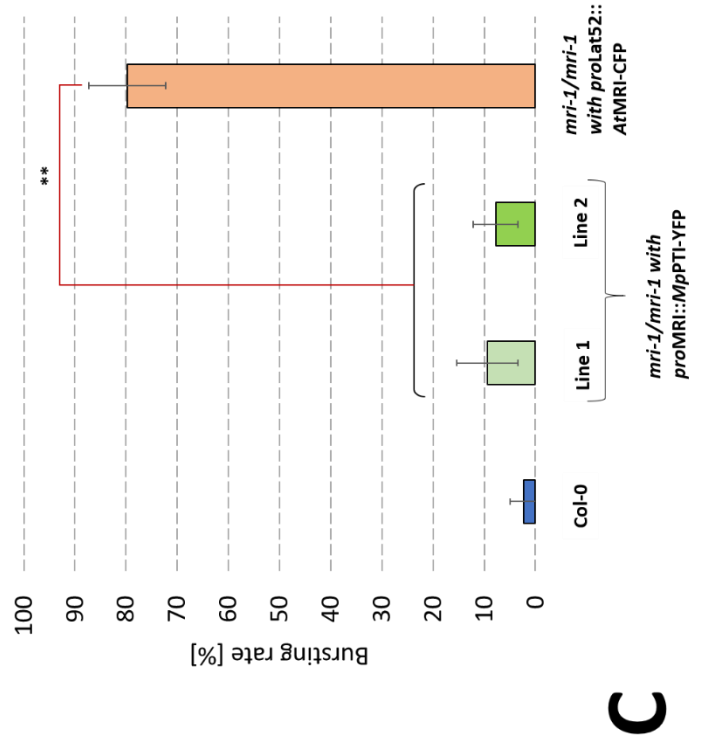
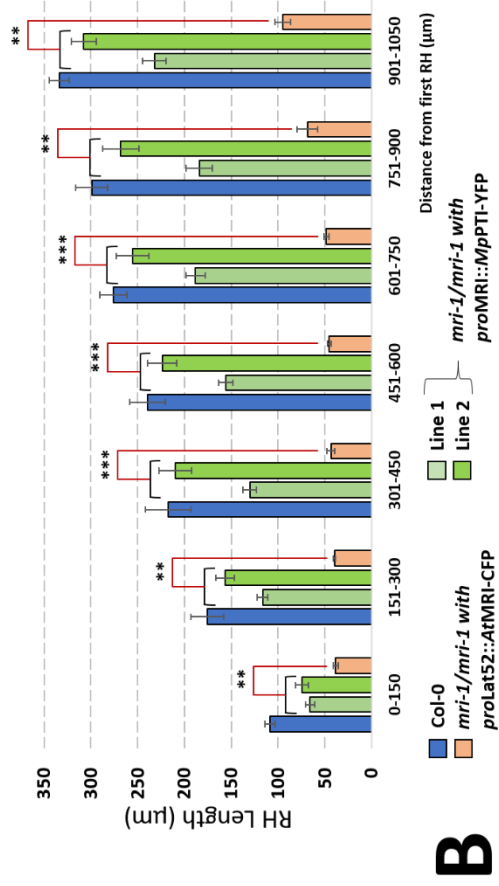
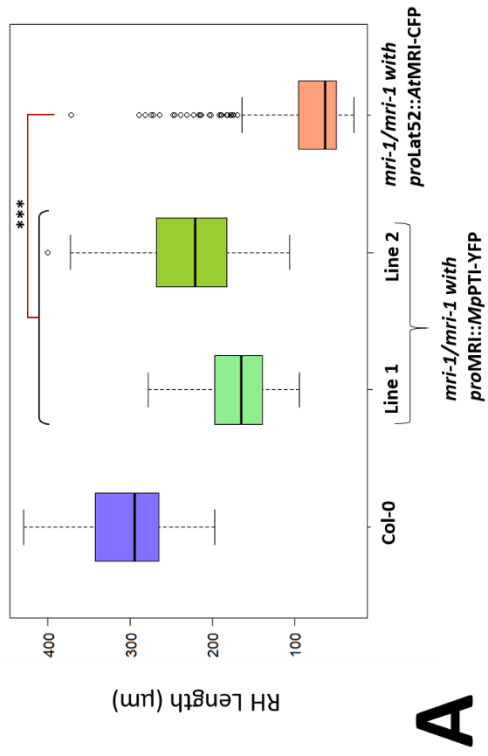
**Fig. 16: Expression of *MpPTI*-YFP partially restores the *mri-1/mri-1* seed set.** (A) Seed set assay of individuals of three independent T3 lines of *mri-1/mri-1* expressing *proMRI::MpPTI*-YFP, as compared to *mri-1/mri-1* complemented with *proMRI::AtMRI*-YFP, Col-0 and a hypothetical untransformed *mri-1/mri-1* line. All individuals of all three transformant lines were significantly different from *mri-1/mri-1* expressing *AtMRI*-YFP, Col-0 and *mri-1/mri-1* (unpaired, two-tailed student's T-test; \*\*\*:  $p < 0.001$ ;  $n = 15$  siliques per individual). (B) Representative siliques of the plants analyzed in section (A). Scale bar = 2 mm.

### ***MpPTI-YFP* in *mri-1* root hairs**

Based on the observation, that *MpPTI* - a gametophytic regulator of rhizoid growth - is able to rescue *mri-1*-induced, male gametophytic loss of CWI, we questioned whether *MpPTI* is also capable of rescuing *mri-1*-induced loss of CWI in root hairs, representing a sporophytic, yet functionally closely related cell type. Therefore, T2 seedlings originating from two of the three same lines as studied before (*mri-1 proMRI::MpPTI-YFP*) were analyzed in a root hair growth assay. Both transformant lines revealed a partial, highly significant restoration of root hair length as compared to a double-homozygous *mri-1 proLAT52::AtMRI-CFP* line (only rescued in pollen tube CWI; Boisson-Dernier et al., 2015) and the Col-0 wild type (Fig. 17A and B). Closer analysis could reveal that root hair bursting was also decreased to 8 and 9 % in the rescued lines, as compared to 80 % in the *mri-1/mri-1* control line expressing *proLAT52::AtMRI-CFP*. Compared to the wild-type control, whose root hairs burst in 2 % of all cases, this represented a nearly complete and highly significant restoration of cell wall integrity (Fig. 17C and D). Taken together, these results indicate, that *MpPTI* is capable of taking over the function of *AtMRI* in root hair growth control more efficiently than in *mri-1* pollen tubes.

**Fig. 17: Expression of *MpPTI-YFP* rescues CWI in growing *mri-1/mri-1* root hairs.** (A) Root hair length of the 10 longest root hairs per individual for  $n \geq 16$  seedlings per genotype. (B) Root hair length profile: Each primary root was digitally divided in sections of 150  $\mu\text{m}$  and root hair length was determined for 5-10 root hairs per section. Shown are the mean values of  $n = 5$  seedlings per genotype; error bars show the standard error from the mean (SEM). (C) Mean root hair bursting rate of  $n \geq 16$  seedlings; error bars show the standard deviation from the mean value. Significance of the data presented in section A - C tested with an unpaired, two-tailed student's T-test (\*\*:  $p < 0.01$ ; \*\*\*:  $p < 0.001$ ). (D) Representative captures of the data presented in sections A - C. BF = bright field; OL = Overlay of bright field image and tip-focused/PM-localized *MpPTI-YFP* fluorescence. Scale bar: 200  $\mu\text{m}$  (for both upper and lower picture series).

(Figure on following page.)



#### 4.1.4. Overexpression of *Marchantia* and *Arabidopsis* MLRs and PTI-like genes leads to growth inhibition in tip-growing cells.

In *Arabidopsis thaliana*, overexpression of the CWI regulators AtMRI and AtANX1 is known to induce growth inhibition in pollen tubes and root hairs (Boisson-Dernier et al., 2013; Boisson-Dernier et al., 2015). Based on these former findings, we hypothesized that all tip-growing cells would respond similarly to overexpression of *Arabidopsis* and *Marchantia* CWI regulators.

##### 4.1.4.1. PTI-like- and MLR-homologs inhibit *Marchantia* rhizoid growth

To test whether the overexpression of known CWI regulators has a growth inhibitory effect on *Marchantia* rhizoids, Tak-2 x Tak-1 wild-type sporelings were transformed with MpPTI-, AtMRI-, AtANX1- and AtFER-fluorescent protein fusions, all under control of *proMpEF1α*. All resulting putative transformants were PCR-genotyped for both, their gender and presence of the transformed construct, to facilitate a reliable comparison to the respective wild-type lines. The overexpression effect on rhizoid growth was then further assessed for at least three independent lines per transformed construct.

##### **PTI-like homologs in rhizoids**

Gemmae of seven independent Tak-2 x Tak-1 transformant lines expressing MpPTI-3xCitrine were analyzed concerning rhizoid growth, as compared to the Tak-1 and Tak-2 wild types, as well as an untransformed line descending from a sporeling of the same Tak-2 x Tak-1 crossing. All seven lines revealed a significant reduction of mean rhizoid length ranging between 32 and 72 % as compared to the untransformed Tak-2 x Tak-1 control line (100 %) as well as the non-crossed Tak-2 and Tak-1 lines (Fig. 18A and B). Fluorescence microscopy confirmed that MpPTI localizes to the rhizoid plasma membrane, but also less abundantly to the cytoplasm and secretory vesicles (Fig. 18C), just as observed in the *Mppti* rescue lines (Fig. 13). These findings show that MpPTI overexpression leads to inhibition of *Marchantia* rhizoid growth.



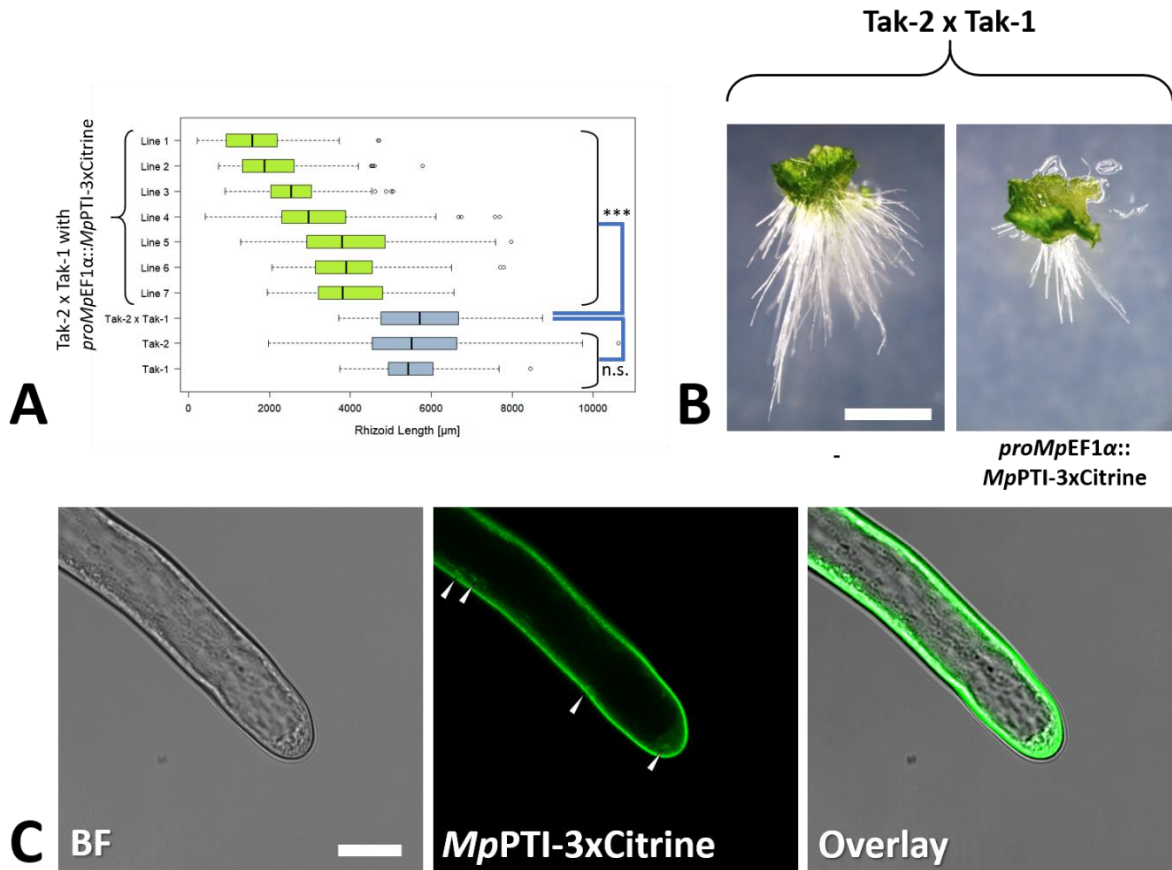


**Fig. 18: Overexpression of *MpPTI-3xCitrine* leads to growth inhibition in *Marchantia* wild-type rhizoids.** (A) Rhizoid growth assay visualized in form of a boxplot. Rhizoid lengths of the 10 longest rhizoids were determined for 10 gemmalings/genotype. Datasets of all analyzed transformant lines were significantly different from Tak-1, Tak-2 and the Tak-2 x Tak-1 untransformed line (\*\*\*:  $p < 0.001$  in a two-tailed, unpaired Student's T-test; n.s.: not significant). (B) Representative images of the data shown in (A). Scale bar: 2 mm. (E) Protein localization of *MpPTI-3xCitrine* in Tak-2 x Tak-1 rhizoids. Shown are a bright field (BF) capture, corresponding *MpPTI-3xCitrine* fluorescence image and overlay of both pictures. Arrowheads indicate frequently observed fluorescent granules, which likely represent secretory vesicles. Scale bar: 20 μm.

Similarly, the overexpression of *AtMRI-3xCitrine* in five independent *Marchantia* Tak-2 x Tak-1 wild-type lines led to a significant reduction of rhizoid length in the range of 29 to 39 % as compared to the Tak-2 x Tak-1 wild type (Fig. 19A and B). Fluorescence microscopy confirmed that *AtMRI* localizes to the rhizoid plasma membrane, but also less abundantly to the cytoplasm and secretory vesicles (Fig. 19C). These findings show that *AtMRI* overexpression leads to inhibition of *Marchantia* rhizoid growth and support the hypothesis that both homologs (and thus rhizoids and pollen tubes/root hairs) may be delivered to the PM via a common secretory system.

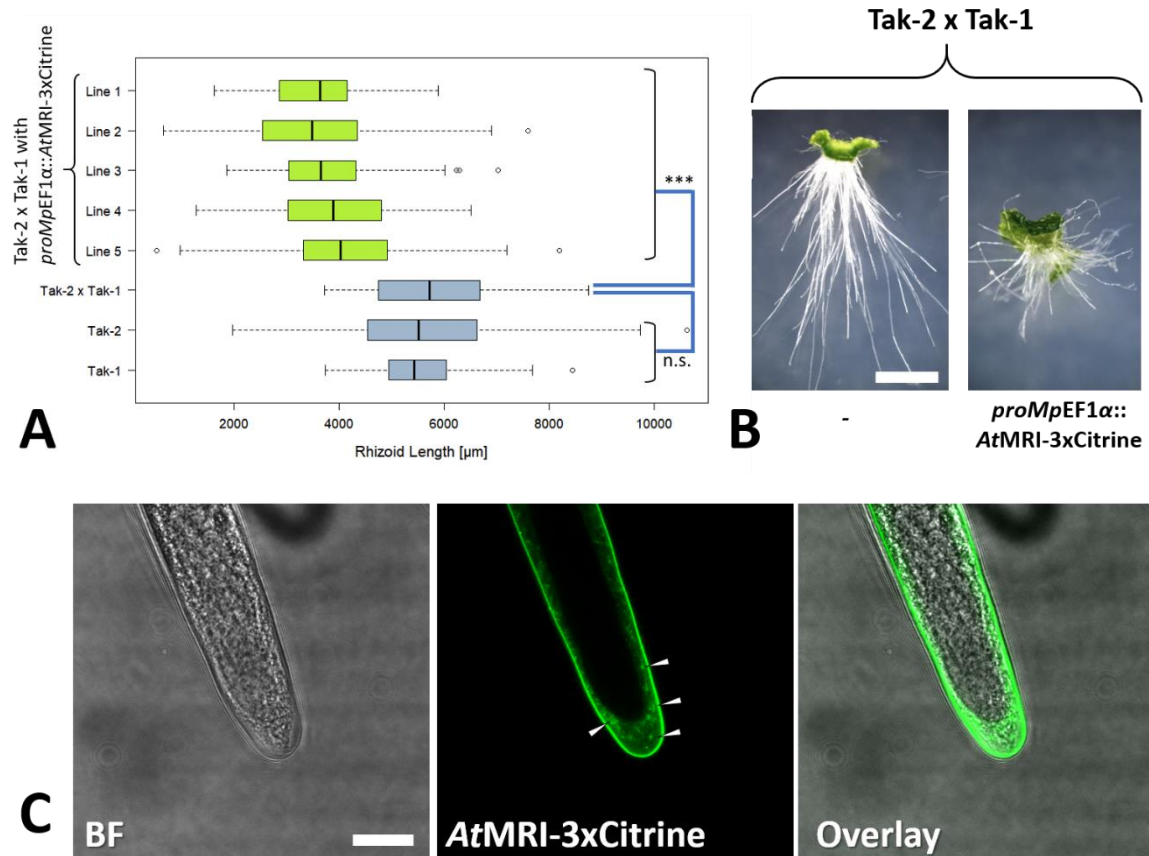


**Fig. 19: Overexpression of AtMRI-3xCitrine leads to growth inhibition in *Marchantia* wild-type rhizoids.** (A) Rhizoid growth assay visualized in form of a boxplot. Rhizoid lengths of the 10 longest rhizoids were determined for 10 gemmalings/genotype. Datasets of all analyzed transformant lines were significantly different from a Tak-2 x Tak-1 untransformed line (\*\*\*:  $p < 0.001$  in a two-tailed, unpaired Student's T-test; n.s.: not significant). (B) Representative images of the data shown in section (A). Scale bar: 2 mm. (C) Protein localization of AtMRI-3xCitrine in Tak-2 x Tak-1 rhizoids. Shown are a bright field (BF) capture, corresponding AtMRI-3xCitrine fluorescence image and overlay of both pictures. Arrowheads indicate frequently observed fluorescent granules, which likely represent secretory vesicles. Scale bar: 20 μm.

Since wild-type lines emerging from a Tak-2 x Tak-1 crossing event showed very similar (*i.e.* not significantly different) rhizoid lengths as the non-crossed wild-type accessions Tak-1 and Tak-2, non-transformed Tak-2 x Tak-1 progeny was chosen as a reliable wild-type control for further experiments.

### MLR homologs in rhizoids

Similarly to the effect of PTI-like genes, the overexpression of both, AtANX1-3xCitrine and AtFER-3xCitrine led to a highly significant reduction of rhizoid length in the range of 37 to 61 % in four independent lines and 36 to 68 % in five independent lines, respectively (Fig. 20A, C and E). Fluorescence microscopy showed that both, AtANX1 and AtFER localize to the

plasma membrane, while expression lines were also found to frequently show citrine fluorescence in granules, which may represent secretory vesicles. Furthermore, a putatively non-cytosolic volume in the pollen tube apex from which Citrine-fluorescence was absent, was frequently observed (Fig. 20B and D), which may represent an overexpression-related phenotype (as it has not been observed in any of the wild type, loss of function or complementation lines analyzed before). Taken together, these findings show that *Arabidopsis* MLRs are capable of inhibiting *Marchantia* rhizoid growth and support the hypothesis that tip-growth control via MLRs has been conserved between *Arabidopsis* and *Marchantia*. It is, however, noteworthy, that the PM-localization is different from pollen tubes, in which *AtANX1* is more abundant in the lateral tube/ shank regions (Boisson-Dernier et al., 2009). In addition, fluorescent vesicles appeared to be comparatively bigger than those observed for *MpPTI* and *AtMRI* in rhizoids (Fig. 18 and Fig. 19). Thus, PTI-like kinases are likely transported via different vesicles than MLRs.

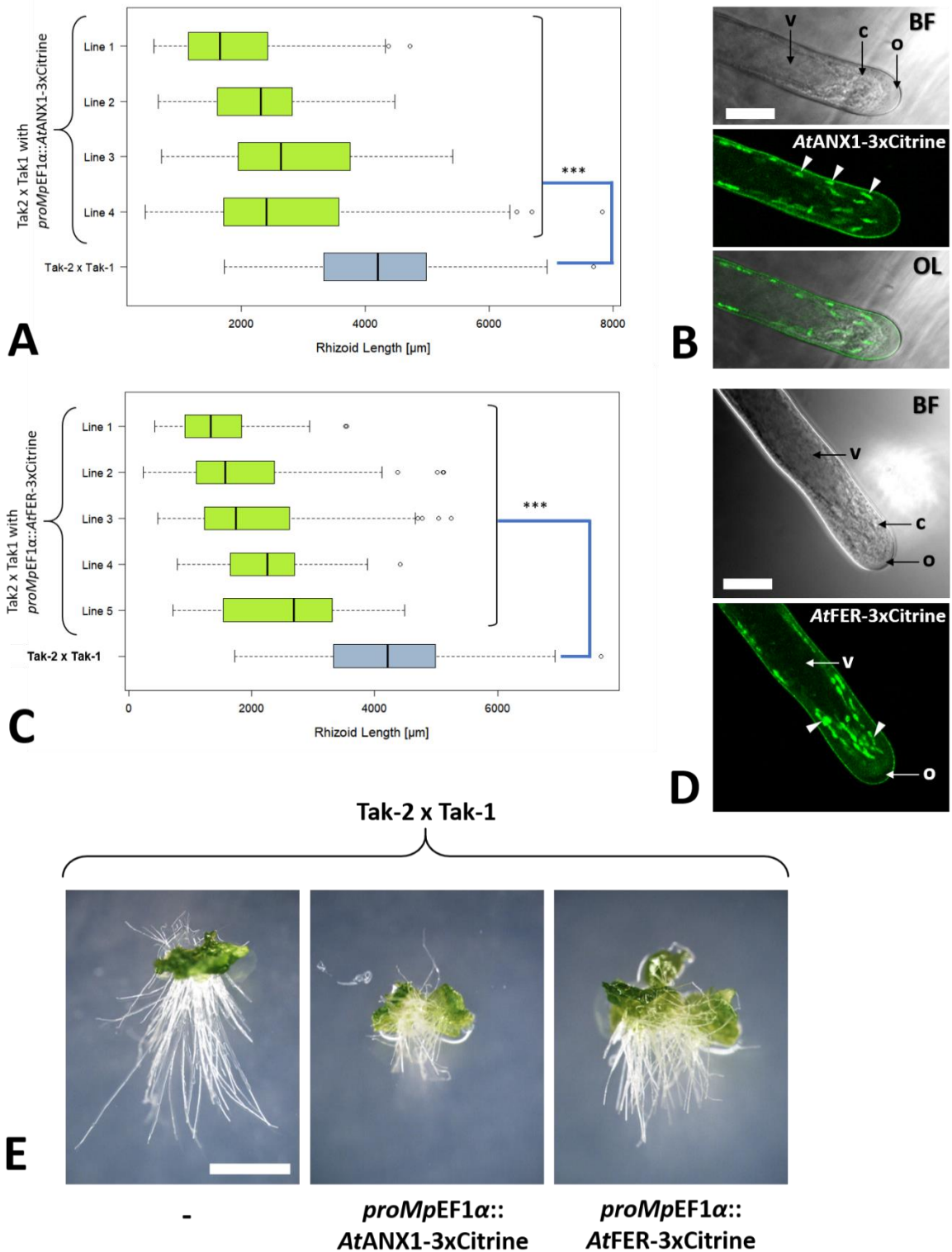


**Fig. 20: Overexpression of *AtANX1-3xCitrine* and *AtFER-3xCitrine* leads to growth inhibition in *Marchantia* rhizoids.** A; C: Rhizoid growth assays for overexpression of *AtANX1-3xCitrine* (A) and *AtFER-3xCitrine* (C), both under control of *proMpEF1α*, visualized in form of a boxplot. Rhizoid lengths of the 10 longest rhizoids were determined for 10 gemmalings/line. Datasets of all analyzed transformant lines were significantly different from a Tak-2 x Tak-1 untransformed line (\*\*\*:  $p < 0.001$  in a two-tailed, unpaired Student's T-test). B; D: CLSM captures of rhizoids expressing *AtANX1-3xCitrine* (B) or *AtFER-3xCitrine* (D). BF = Bright field capture; OL = digital overlay of bright field and fluorescence images; v = vacuole; c = cytoplasm; o = putative overaccumulation-related phenotype; arrowheads mark fluorescent granules. Scale bar: 20  $\mu\text{m}$ . (E) Representative images of the data shown in sections (A) and (B). Scale bar: 2 mm.

#### 4.1.4.2. *MpPTI* and *MpPTI*<sup>[R240C]</sup> inhibit tip-growth in *Arabidopsis*.

##### Expression of *MpPTI* inhibits *Arabidopsis* pollen tube growth

To further investigate the effect of PTI-like genes on *Arabidopsis* pollen tube growth, *in vitro* pollen germination was analyzed in three independent Col-0 wild type lines hemizygotously expressing *MpPTI*-YFP under control of *proMRI* and two reference lines hemizygotously expressing either *AtMRI*-CFP or its overactive protein version *AtMRI*<sup>[R240C]</sup>-CFP (Boisson-Dernier et al., 2015), both under control of *proLat52*. This strategy allowed direct comparison of transformed and non-transformed pollen in the same line. Initially, the percentage of fluorescent pollen grains and pollen tubes was determined. All five lines showed a percentage of fluorescent pollen grains close to 50 % (as expected for a hemizygous expression line), except for *AtMRI*<sup>[R240C]</sup>, whose proportion of transgenic pollen was mildly decreased to 39 %. To test whether the transgene influences pollen germination, indicated by a deviation from the amount of 50 % fluorescent pollen tubes, the percentage of fluorescent pollen tubes was determined for each line. The amount of fluorescent pollen tubes was drastically decreased in Col-0 expressing *AtMRI*-CFP (16 %) or *AtMRI*<sup>[R240C]</sup>-CFP (0 %), but not in any of the three lines expressing *MpPTI*-YFP (Tab. 22), indicating a strong negative correlation between *AtMRI*- and *AtMRI*<sup>[R240C]</sup>-, but not *MpPTI*-expression, and pollen germination. Upon these findings, it was hypothesized that *MpPTI* may not inhibit pollen germination (and growth), as strongly as *AtMRI* and *AtMRI*<sup>[R240C]</sup>, however, pollen tubes expressing either *MpPTI*-YFP or *AtMRI*-CFP were both significantly shorter than non-transgenic tubes ( $p < 0.001$ ; Fig. 21). These results show, that *MpPTI* indeed inhibits pollen tube growth *in vitro*, but to a lower degree than *AtMRI*.

**Tab. 22: Expression of *MpPTI*-YFP does not inhibit Col-0 wild-type pollen germination.** Shown are the percentages of fluorescent (*i.e.* transgenic) pollen grains and pollen tubes in Col-0 hemizygotously expressing *MpPTI*-YFP, *AtMRI*-CFP or *AtMRI*<sup>[R240C]</sup>-CFP.

Genotype		Fluorescent pollen grains [%]	n	Fluorescent pollen tubes [%]	n
<i>proMRI::MpPTI</i> -YFP (hemiz.)	Line 1	48	104	55	698
	Line 2	48	71	54	693
	Line 3	50	64	48	728
<i>proLat52::AtMRI</i> -CFP (hemiz.)		58	110	16	438
<i>proLat52::AtMRI</i> <sup>[R240C]</sup> -CFP (hemiz.)		39	337	0	250

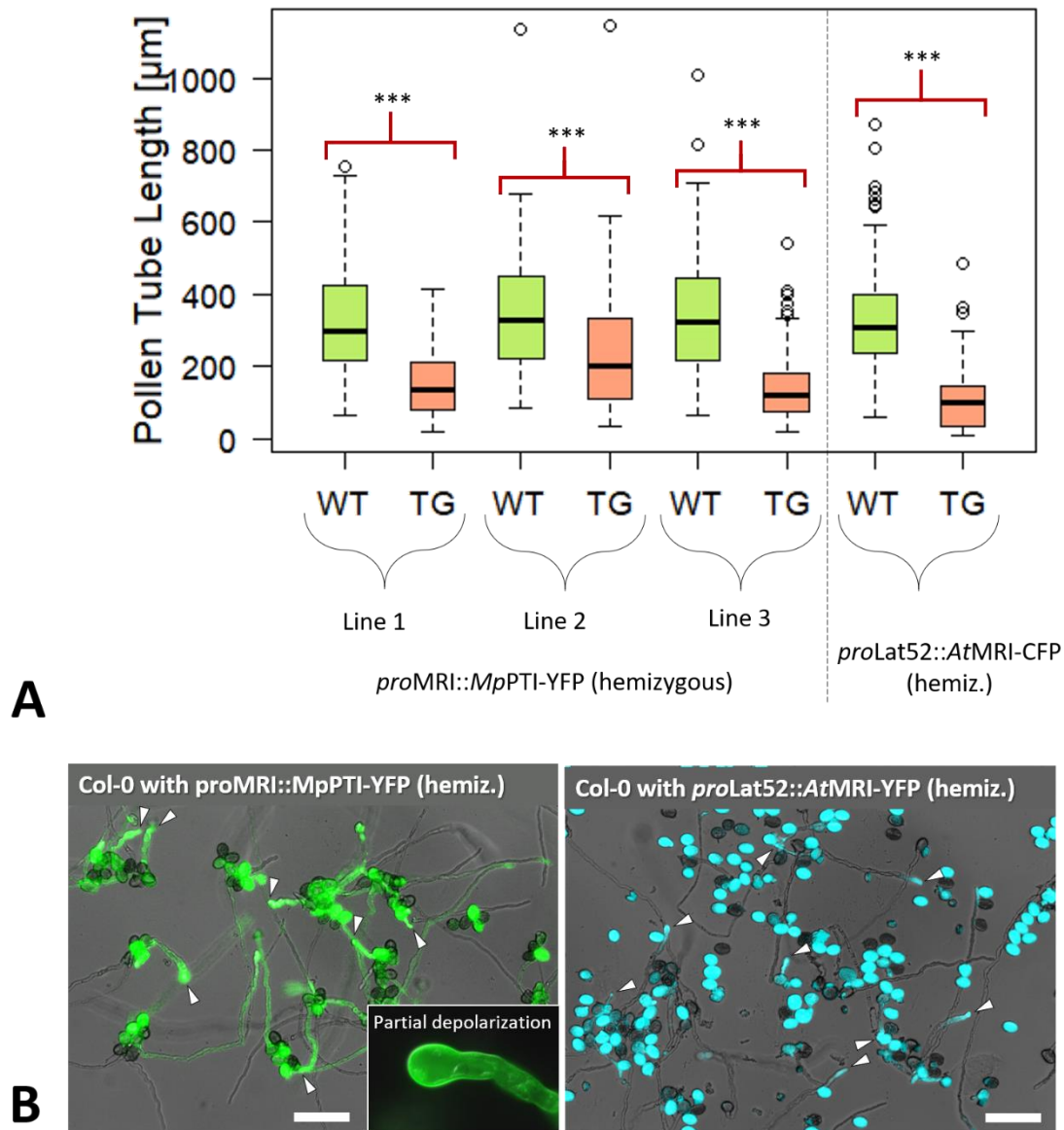


**Fig. 21: Expression of MpPTI-YFP leads to decrease of PT length *in vitro*.** (A) PTs of three independent lines of Col-0 hemizygously expressing *proMRI::MpPTI-YFP* and one line of Col-0 hemizygously expressing *proLat52::AtMRI-CFP* (Boisson-Dernier et al., 2015) were grown *in vitro*. The 10 longest wild-type (WT) and transgenic (TG) pollen tubes per capture were measured,  $n \geq 83$  pollen tubes were analyzed per line on three days and data was pooled. Data shown in form of a boxplot. Significance was tested with an unpaired, two-tailed student's T-test (\*\*\*:  $p < 0.001$ ). (B) Representative captures of the data presented in section (A). Scale bar = 80  $\mu\text{m}$ .

### Expression of *MpPTI*<sup>[R240C]</sup> inhibits growth in *Arabidopsis* root hairs

Former research on tip-growth control via *AtMRI* showed that the *AtMRI*<sup>[R240C]</sup> protein version represents an overactive form of *AtMRI* and that it is sufficient to rescue loss of CWI downstream of *AtANX1/2* and *AtFER* (Boisson-Dernier et al., 2015). Given the similar roles of both, *AtMRI* and *MpPTI* in *Arabidopsis* (Boisson-Dernier et al., 2015) and *Marchantia* tip-



growth control (Honkanen et al., 2016; this study), respectively, we argued whether a R-to-C substitution in the respective amino acid sequence of *MpPTI* would trigger similar effects. The causative arginine/cysteine residue is located in a kinase domain which has been well conserved throughout evolution of the PTI-like gene subfamily. Comparative analysis of *Arabidopsis* and bryophytic PTI-like proteins confirmed that the arginine residue, which is part of an STR-motive, is situated in an ultra-conserved kinase domain (Fig. 22).

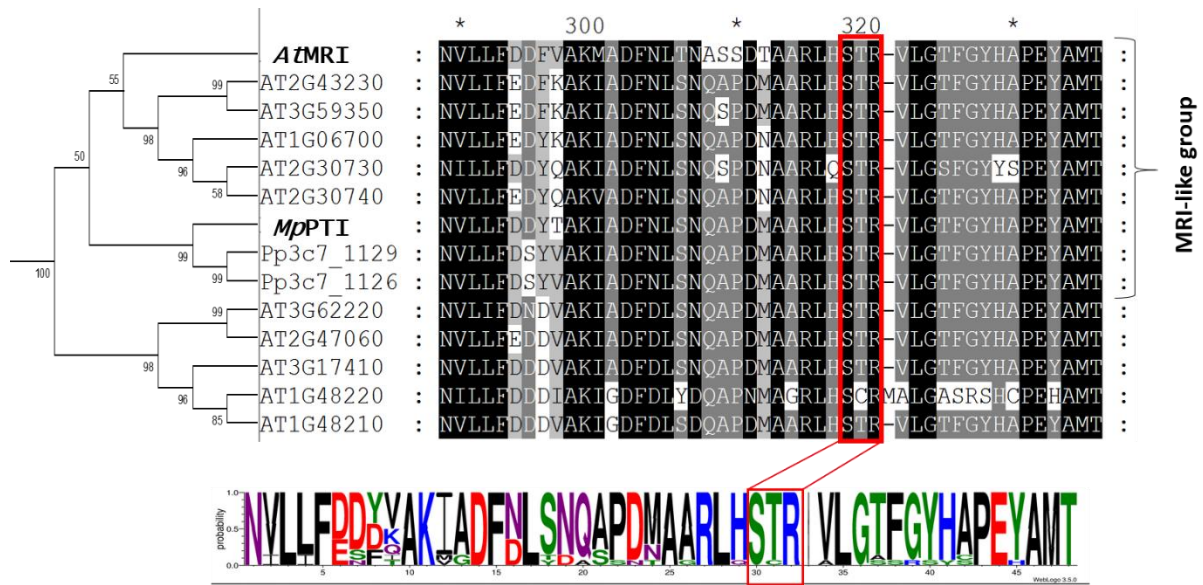


**Fig. 22: Phylogenetic analysis of PTI-like proteins from *Arabidopsis* and bryophytes.** Shown is a phylogenetic tree based on the full-length amino acid sequences of the 11 PTI-like genes from *Arabidopsis thaliana*, including *AtMRI* (AT2G41970), the unique *Marchantia polymorpha* homolog *MpPTI* (transcript Mapoly0051s0094), and the two homologs from *Physcomitrella patens* (*Pp3c7\_1129* and *Pp3c7\_1126*). The tree was generated using the Neighbor-Joining algorithm (Saitou and Nei, 1987) and tested via the bootstrap method (1000 repetitions). Labels on the nodes represent bootstrap percentages, indicating how frequently associated taxa clustered together (Felsenstein, 1985). Multiple sequence alignments and evolutionary analyses were carried out using the ClustalX (Thompson et al., 2003) and MEGA7 software (Kumar et al., 2016). A red frame highlights the highly conserved STR motif of the serine-threonine kinase domain. The frequency of amino acid usage is shown below (created using Weblogo: <http://www.weblogo.threeplusone.com/>).

Based on these findings, a comparable R-to-C substitution was generated by site-directed mutagenesis to generate a *MpPTI*<sup>[R240C]</sup>-YFP fusion under control of *proMRI* (*proMRI::MpPTI*<sup>[R240C]</sup>-YFP). To test whether this putatively overactive form of *MpPTI* can trigger similar growth inhibitory effects in *Arabidopsis* tip-growing cells like observed for *AtMRI* (Boisson-Dernier et al., 2015), it was expressed in Col-0. Root hair growth was studied in T2 seedlings originating from 3 independent T1 lines hemizygotously expressing the construct, and compared to two lines of Col-0 expressing *proMRI::AtMRI*<sup>[R240C]</sup>-YFP (Boisson-Dernier et al., 2015). All three lines expressing *MpPTI*<sup>[R240C]</sup> showed a significant decrease in root hair length as compared to the Col-0 control. The difference increased with

age of the root hairs (*i.e.* by time). Nevertheless, the effect of all three lines was less pronounced than in the reference lines expressing *AtMRI*<sup>[R240C]</sup>-YFP. Fluorescence microscopy of all five transgenic lines revealed, that both, *AtMRI*<sup>[R240C]</sup>-YFP and *MpPTI*<sup>[R240C]</sup>-YFP, are truly expressed in root hairs (Fig. 23). These results show that *MpPTI*<sup>[R240C]</sup> is capable of inhibiting Col-0 root hair growth, however, to a lower extent than *AtMRI*<sup>[R240C]</sup>.

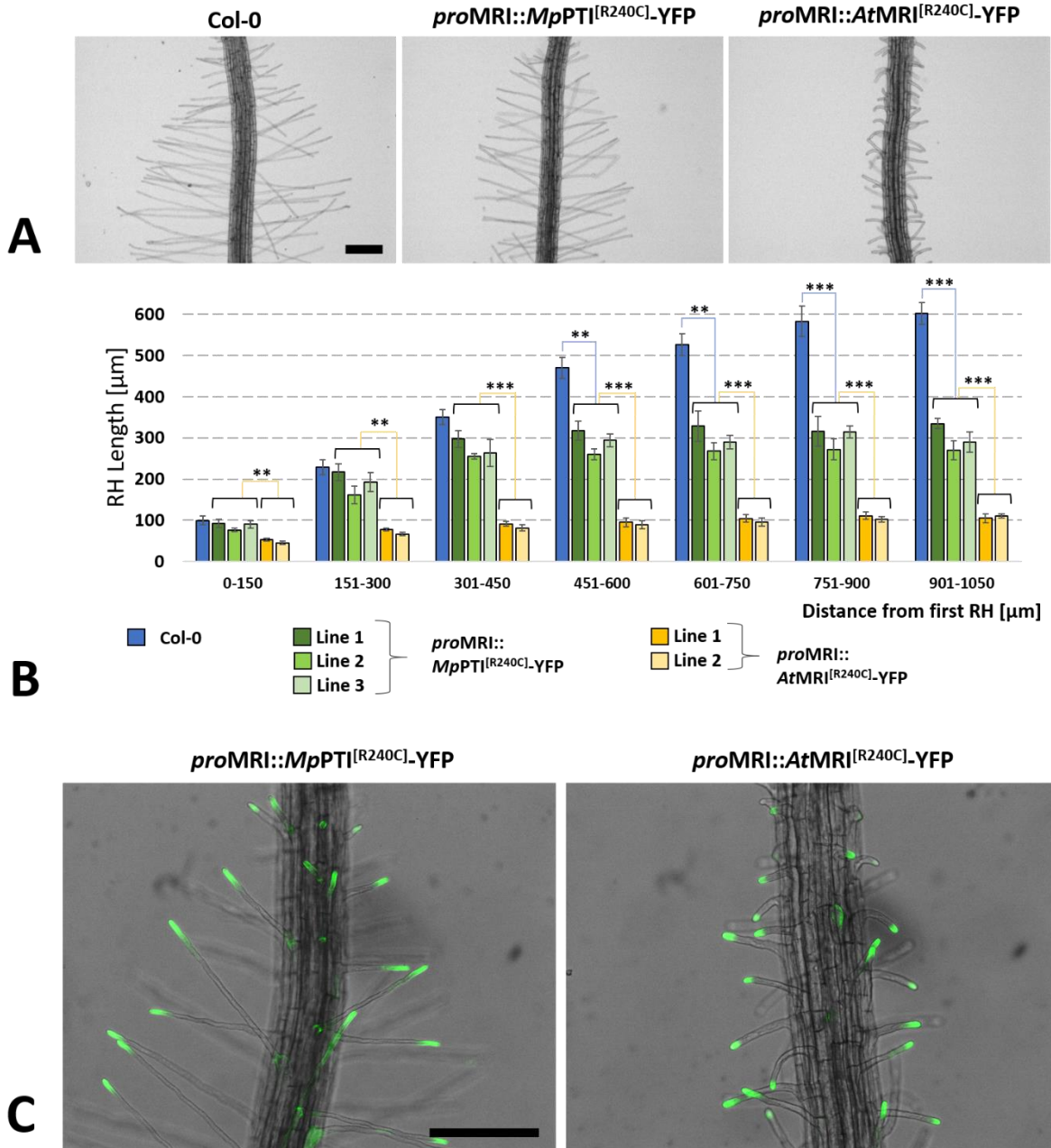


**Fig. 23: Expression of *MpPTI*<sup>[R240C]</sup>-YFP leads to growth inhibition in Col-0 root hairs.** (A) Representative captures of the data presented in section (B). Scale bar: 200  $\mu$ m. (B) Root hair length profile: Each primary root was digitally divided in sections of 150  $\mu$ m and root hair length was determined for 5-10 root hairs per section. Shown are the mean values of  $n = 5$  seedlings per genotype; error bars show the standard error from the mean (SEM). Significance tested with an unpaired, two-tailed student's T-test (\*\*:  $p < 0.01$ ; \*\*\*:  $p < 0.001$ ). (C) Protein localization of *MpPTI*<sup>[R240C]</sup> and *AtMRI*<sup>[R240C]</sup>: Shown is a digital overlay of bright field images with tip-focused YFP fluorescence.



#### 4.1.5. Does *MpPTI* act genetically downstream of *MpTHE1* in a rhizoid CWI signaling pathway?

Based on all experiments presented before, it was hypothesized whether - not only the structure and function of PTI-likes - but the RLK-mediated CWI signaling pathway as a whole may have been conserved throughout evolution of land plants. To test whether *MpTHE1* and *MpPTI* act together in a conserved CWI signaling module, just like their *Arabidopsis thaliana* homologs *AtANX1/2* and *AtFER* do with *AtMRI*, we are planning to express the (putatively) overactive *MpPTI*<sup>[R240C]</sup> gene in *Mpthe1* rhizoids. This strategy is based on the assumption that overactive *MpPTI*<sup>[R240C]</sup> may be capable of rescuing rhizoid growth to a higher extent than regular *MpPTI*, just like it is true for *AtMRI*<sup>[R240C]</sup>/ *AtMRI* in *Arabidopsis anx1 anx2* pollen and *fer-4* root hairs (Boisson-Dernier et al., 2015). Therefore, Tak-2 and *Mpthe1* plants were crossed to obtain Tak-2 x *Mpthe1* spores. A *proMpEF1α::MpPTI*<sup>[R240C]</sup>-RFP construct was transformed into the spores and n = 100 resistant thalli (*i.e.* putative transformants) were isolated from selection plates. Following experiments will include verification of the presence of both, the *Mpthe1* allele and the transformed *MpPTI*<sup>[R240C]</sup>-RFP construct via PCR-based genotyping and the analysis of rhizoid growth in the respective lines. If *MpPTI*<sup>[R240C]</sup>-RFP expression is capable to rescue *Mpthe1*-induced rhizoid bursting, this would indicate that CWI signaling relies on a common signaling module comprised of MLRs and PTI-like genes in both, *Arabidopsis* and *Marchantia* tip-growing cells.

#### 4.1.6. Is *MpPTI*<sup>[R240C]</sup> capable of rescuing the loss of CWI in *fer-4* root hairs and *amiRRALF4/19* pollen tubes?

##### ***MpPTI*<sup>[R240C]</sup> in *fer-4* root hairs**

To further study the degree of signaling conservation between *Arabidopsis thaliana* and *Marchantia polymorpha*, we are planning to express *MpPTI*<sup>[R240C]</sup> in the *Arabidopsis fer-4* mutant, which was described to display excessive RH bursting upon growth initiation (Duan et al., 2010) and to regulate root hair growth upstream of *AtMRI*, as the *fer-4* root hair growth defect was shown before to be rescued by expression of the overactive protein version *AtMRI*<sup>[R240C]</sup> (Boisson-Dernier et al., 2015).

Initially, a *MpPTI*<sup>[R240C]</sup>-YFP fusion under control of *proMRI* (*proAtMRI::MpPTI*<sup>[R240C]</sup>-YFP; see section 4.1.4.2.) was transformed into *fer-4* plants. T1 seeds of transformed *fer-4* plants

were selected on respective plant antibiotics and 8 independent T1 seedlings were isolated (despite the strong and manifold vegetative phenotypes induced by the *fer-4* null mutant allele). YFP-fluorescence was verified in pollen and T1 plants were allowed to self-fertilize. To assess, whether expression of MpPTI<sup>[R240C]</sup>-YFP can rescue *fer-4*-induced root hair bursting, we are planning to select T2 plants for presence of the MpPTI<sup>[R240C]</sup>-YFP fusion construct and to analyze transgenic specimens in a root hair assay. If MpPTI<sup>[R240C]</sup>-YFP expression is capable of rescuing root hair growth in *fer-4*, this would indicate that - not only the function of PTI-likes *per se* - but a signaling module comprised of MLR/PTI-likes as a whole has been evolutionarily conserved to control tip-growth.

#### **MpPTI<sup>[R240C]</sup> in *amiRRALF4/19* pollen tubes**

Similarly, we are planning to test, whether MpPTI<sup>[R240C]</sup> can take over a similar function downstream of AtANX1/2-mediated tip-growth control in pollen tubes. An artificial microRNA line against the AtANX1/2 ligands RALF4/19 (*amiRRALF4/19*) has been described before to lead to pollen bursting *in vitro* and to a reduced seed set, indicated by short siliques. Both of these phenotypes could be rescued by expression of AtMR1<sup>[R240C]</sup> (Mecchia et al., 2017). To test whether MpPTI<sup>[R240C]</sup> is also capable of rescuing *amiRRALF4/19*-induced sterility, a MpPTI<sup>[R240C]</sup>-CFP fusion under control of the pollen-specific *proLAT52* (*proLAT52::MpPTI<sup>[R240C]</sup>-CFP*) was transformed into the *amiRRALF4/19* mutant. Following experiments will include: (i) verification of pollen-localized CFP-expression in T1 plants, (ii) screening for silique elongation (*i.e.* restoration of fertility) in transgenic T1 lines and (iii) analysis of *in vitro* pollen germination of T2 plants homozygously expressing MpPTI<sup>[R240C]</sup>-CFP. If expression of MpPTI<sup>[R240C]</sup>-CFP factually leads to a rescue of male fertility, this would indicate that a MLR/PTI-like signaling module has been universally conserved between life phases (gametophytic pollen tubes and rhizoids vs. sporophytic root hairs) and irrespective of their biological function.

#### **4.1.7. Do *Mppti* and *Mpthe1* govern further functions in *Marchantia*?**

Based on the knowledge that *Arabidopsis* MLR AtFER is known to govern a multitude of functions during plant development, reproduction and pathogen defense (Franck et al., 2018 A), it was hypothesized that MpTHE1 (and possibly also MpPTI) may govern similar pleiotropic functions. Indeed, a first analysis showed that *Mpthe1* and *Mppti* mutants both develop a bent thallus morphology on solid Gamborg B5 growth medium (Fig. 24A) and form

fewer gametangia upon entry in the reproductive phase (Fig. 24B and C), both of which might be secondary effects of their rhizoid growth defect, likely leading to lower nutrient and water uptake, and thus, decreased plant fitness. In order to reveal further potential *Mppti* and *Mpthe1* mutant phenotypes, wild-type plants could be transformed with a *proMpPTI::YFP-NLS* and *proMpTHE1::YFP-NLS* construct, respectively (both received from Susanna Streubel, University of Oxford). This strategy would allow to characterize the expression profile of both, *MpPTI* and *MpTHE1* by screening transgenic lines for cell types which show nuclear YFP-fluorescence. It will be interesting to learn whether *MpTHE1*, besides its putative role as rhizoid growth regulatory gene, may take over a function during reproduction as well. Possible ways of searching for male-specific *Mpthe1*-defects could be (i) the determination of the segregation ratio of Tak-2 and *Mpthe1* sporelings from a Tak-2 x *Mpthe1* crossing event or (ii) the comparison of *Mpthe1* and Tak-1 spermatozoid attraction or perception by Tak-2 archegoniophores in a semi-*in vivo* setup.

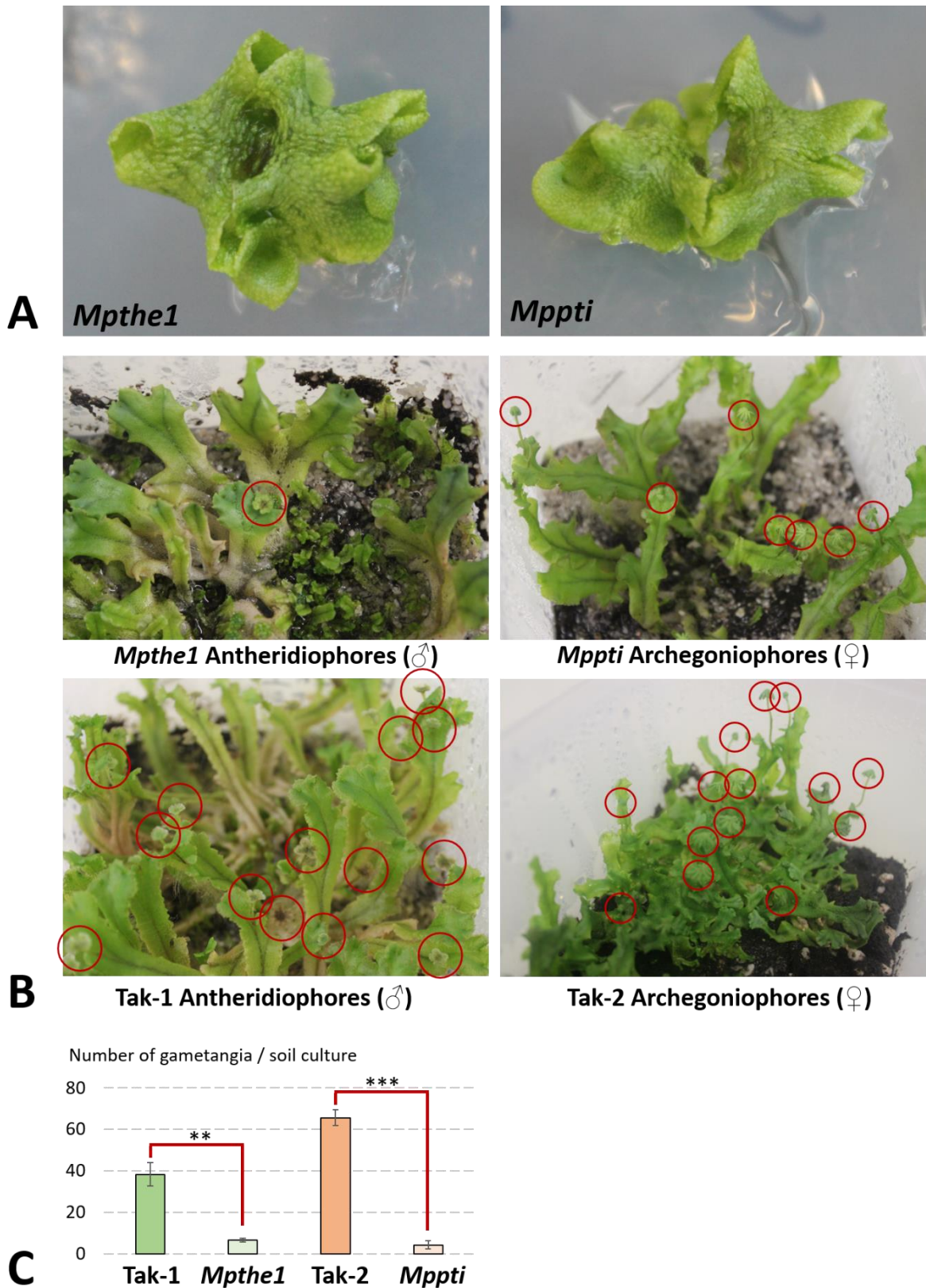


**Fig. 24: Phenotyping of *Mppti* and *Mpthe1*.** (A) Morphology of 3 weeks old thalli of *Mppti* and *Mpthe1* grown on solid Gamborg B5 medium. (B) Gametangia formation shown for mature thalli grown under FR light for 4 weeks. (C) Determination of the number of gametangia per soil culture (two four-weeks-old thalli were transferred onto soil, then incubated under supplemental FR light as described in section 3.2.1.2. After 4 weeks counting was conducted. Significance tested by help of a two-tailed, unpaired student's T-test:  $p < 0.01$  (\*\*) and  $< 0.001$  (\*\*\*)).

## 4.2. The protein phosphatases AUN1/2 regulate cell wall integrity in tip-growing cells

### 4.2.1. Former work

Based on a forward-genetic suppressor screen for rescue of *anx1 anx2* fertility, which was also used to identify the strong positive tip-growth regulator MRI (Boisson-Dernier et al., 2015), an additional weak suppressor was identified, which was named *impotence rescue mutant 7 (ipr7)*. It was shown to display a reduction of *anx1 anx2*-mediated pollen bursting from 100 to 89 % *in vitro* and a restoration of seed set from 2 (*anx1 anx2*) to 8 (*ipr7* heterozygous) and 14 seeds per silique (*ipr7* homozygous). The causal, non-synonymous point mutation was mapped to the *Arabidopsis* locus AT3G05580, coding for a putative type-one protein phosphatase (TOPP), which was named ATUNIS1 (AUN1). The point mutation was found to induce an aspartate to asparagine substitution at residue 94 (D94N) of the AUN1 protein. To test whether the *ipr7* mutation truly refers to a D94N substitution in AUN1, both AUN1 and AUN1<sup>[D94N]</sup> were fused to YFP and expressed in the *anx1-1 anx2-1* mutant under control of the pollen-specific LAT52 promoter (*proLAT52::AUN1-YFP* and *proLAT52::AUN1<sup>[D94N]</sup>-YFP*). While three T2 plants expressing AUN1<sup>[D94N]</sup>-YFP were found to be homozygous for *anx1-1 anx2-1* (n = 127 plants), not a single double-homozygous line expressing AUN1-YFP could be found (n = 141 plants). Furthermore, the expression of AUN1<sup>[D94N]</sup>-YFP in homozygous *anx1-1 anx2-1* reduced pollen bursting and restored seed set to similar levels as *ipr7*, showing that the substitution of D94N is equivalent to the *ipr7* mutation and causative for the observed phenotypic rescue. The work described above was mainly carried out by former doctoral student Dr. Christina Maria Franck and was published recently (Franck et al., 2018 B). In the following, I will only present the data in whose acquisition I was involved.

### 4.2.2. Establishment and phenotypic analysis of the independent mutant alleles *aun1-2* and *aun2-2*

To support the phenotypic analyses on *aun1-1*, *aun2-1*, as well as the double mutant *aun1-1 aun2-1*, two new independent alleles were required. Therefore, the T-DNA lines *aun1-2* (GABI\_600E08) and *aun2-2* (SALK\_125184) were ordered and presence of the allelic T-DNA-insertion was verified by PCR-based genotyping (Fig. 25A). The homozygous single mutants were crossed to generate the double mutant *aun1-2 aun2-2*. Therefore, F1 plants

were genotyped for heterozygosity for both alleles, selfed and F2 plants were genotyped again to detect homozygous lines.

The established single and double mutants were then phenotypically analyzed concerning *in vitro* pollen germination. The *in vitro* pollen germination assays revealed that the single mutants *aun1-2* and *aun2-2* do not show significant changes in either pollen germination or bursting (Fig. 25B), just like *aun1-1* (SALK\_045433C) and *aun2-1* (SALK\_137888) (Franck et al., 2018 B; Fig. 25A). In contrast, the *aun1-2 aun2-2* double mutant revealed a decreased germination rate of 10 %, similarly to the 20 % of germinating pollen observed in *aun1-1 aun2-1*. Data of both double mutants was significantly different from the > 70 % of germinating pollen observed in the Col-0 wild type and the *aun1-2* and *aun2-2* single mutants. In contrast, the fraction of bursting pollen grains was not significantly altered in either of the analyzed lines (Fig. 25B). Microscopic analyses additionally revealed that *aun1 aun2* double mutants frequently display growth inhibition phenotypes and cannot efficiently initiate pollen germination, as depicted by two or more colpi (*i.e.* sites of growth initiation) per pollen grain (Fig. 25C). This growth inhibition phenotype was very reminiscent of the former observations in both, the ANX1- and MRI<sup>[R240C]</sup> overexpression lines (Boisson-Dernier et al., 2013; Boisson-Dernier et al., 2015). Taken together, these results show that AUN1/2 are redundant, negative regulators of pollen tube growth control.



**Fig. 25: Both *aun1 aun2* double mutants, but not *aun1* or *aun2* single mutants, display inhibition of pollen germination *in vitro*.** (A) AUN1/2 gene models with T-DNA insertion sites, *ipr7* SNP and genotyping primers. (B) *In vitro* pollen germination assay.  $n \geq 200$  pollen grains per genotype were analyzed in three independent experiments. Error bars represent the standard error from the mean (SEM). Data of both, the *aun1-1 aun2-1* and *aun1-2 aun2-2* double mutants were significantly different from Col-0 and the *aun1-2* and *aun2-2* single mutants (\*\*:  $p < 0.01$  in a student's T-test). (C) Representative images of the data presented in section (B). White and magenta arrowheads indicate CW material over-accumulations and attempted outgrowth at two colpi per pollen grain, respectively. Scale bars: Upper images and lower left: 80  $\mu\text{m}$ ; lower right: 25  $\mu\text{m}$ . All presented data is from Franck et al., 2018 B; minor changes to the layout have been made.

#### 4.2.3. Cloning of AUN2 ORF and *proAUN1*

In order to complement the *aun1 aun2* pollen-specific phenotypes, both AUN1-YFP and AUN2-YFP expressed under control of *proLAT52* (*proLAT52::AUN1-YFP* and *proLAT52::AUN2-YFP*) would have to be introduced into the *aun1-1 aun2-1* double mutant. Therefore, AUN2 was amplified from pollen-specific cDNA, introduced into a *proLAT52::GW-YFP* destination vector and finally transformed into *aun1-1 aun2-1* plants. Two transgenic T2 lines (from independent T1 plants) were analyzed in a pollen germination assay. Indeed, both, AUN1-YFP and AUN2-YFP expression led to complete restoration of the *aun1-1 aun2-1*-mediated pollen growth inhibition *in vitro* back to wild-type levels of approximately 60 % of germinating pollen grains (shown for AUN2-YFP in Fig. 26A). Fluorescence microscopy of the same lines revealed that AUN2-YFP localizes to the pollen tube cytoplasm, as well as the vegetative nucleus, just as described for AUN1-YFP (Fig. 26B; Franck et al., 2018). These results confirm, that it is indeed the simultaneous disruption of AUN1 and AUN2, which impairs pollen tube growth.

Based on moderate expression of both, *AUN1* and *AUN2*, in root tissue (Franck et al., 2018 B), as well as the knowledge about functional conservation of RLK-mediated tip-growth control via the same kinds of homologs in both, pollen tubes and root hairs (reviewed by Franck et al., 2018 A; Fig. 8), it was questioned whether AUN1/2 also control tip-growth in root hairs. Indeed, the *aun1-1* and *aun2-1* single mutants, as well as the *aun1-1 aun2-1* double mutant were found to display shorter root hairs as compared to the wild type, indicating inhibition of root hair growth (Franck et al., 2018 B). To complement the *aun1-1 aun2-1* root hair phenotype the ~1.5 kb long AUN1 promoter (*proAUN1*) was amplified from Col-0 genomic DNA. It was then fused to either AUN1-YFP or AUN2-YFP (to generate *proAUN1::AUN1-YFP* and *proAUN1::AUN2-YFP*) and transformed into *aun1-1 aun2-1* plants. We obtained 8 and 9 T1 plants expressing AUN1-YFP and AUN2-YFP in pollen. However, none of these 17 lines showed visible YFP fluorescence in root hairs (as observed



under a fluorescence binocular). Closer analysis of two lines per genotype (under an epifluorescence microscope) led to the same observation. Given these results, we hypothesized, that *proAUN1* might drive expression in pollen, but not in root hairs, which impeded further *proAUN1*-based expression studies.

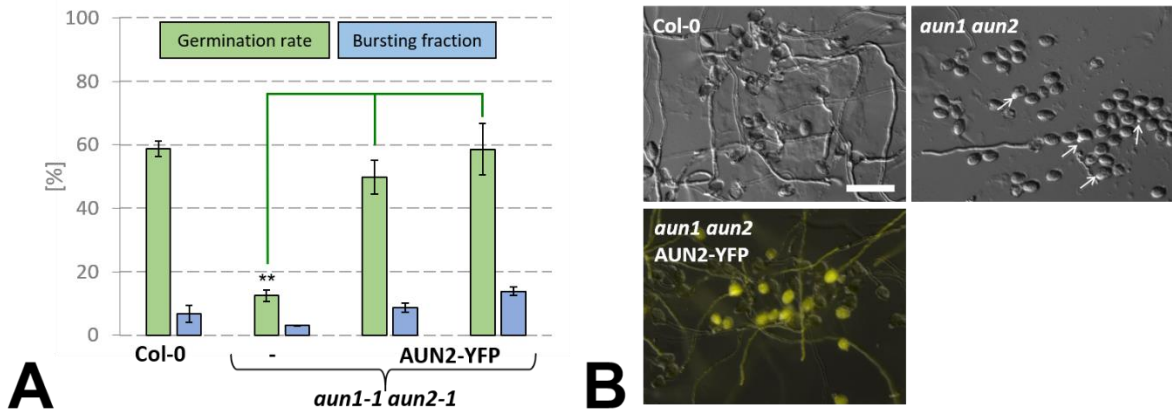


**Fig. 26: Expression of AUN2-YFP complements the *aun1-1 aun2-1* pollen growth inhibition phenotype *in vitro*.** (A) *In vitro* pollen germination assay.  $n \geq 200$  pollen grains per genotype were analyzed in three independent experiments. Error bars represent the standard error from the mean (SEM). Data of the untransformed *aun1-1 aun2-1* double mutant was significantly different from Col-0 and the two independent complemented *aun1-1 aun2-1* lines homozygously expressing *proLAT52::AUN2-YFP* (\*\*:  $p < 0.01$  in a student's T-test). (B) Representative images of the data presented in section (A). White arrowheads indicate CW material overaccumulations of untransformed *aun1-1 aun2-1* pollen. The picture shown for *aun1 aun2* AUN2-YFP shows an overlay of a bright field capture and YFP-fluorescence. Scale bars = 80 μm. All presented data is from Franck et al., 2018 B; minor changes to the layout have been made.

#### 4.2.4. Subsequent work

Based on the intermediary findings presented above (sections 4.2.2. and 4.2.3.), which included my involvement, follow-up experiments led to the following findings: It could be shown that expression of the dominant negative protein version AUN1<sup>[D94N]</sup> (but not of native AUN1 fused to YFP) leads to rescue of pollen bursting, not only in *anx1-1 anx2-1*, but also in *amiRRALF4/19*, *lrx8-11* and *rbohH-3 rbohJ-3*. In contrast, neither AUN1-YFP, nor AUN1<sup>[D94N]</sup>-YFP appeared to be capable of rescuing *mri-1*-induced male sterility. Similarly, MRI<sup>[R240C]</sup>-YFP could not rescue the corresponding phenotypic defects of *lrx8-11* mutant lines (Franck et al., 2018 B). Taken together, these results demonstrate, that AUN1/2 regulate pollen tube growth downstream of LRX8/9/10/11, RALF4/19 and RBOHH/J, possibly in a parallel signaling pathway to MRI.

### 4.3. Role of CNGCs and Ca<sup>2+</sup> signaling in tip-growth control

#### 4.3.1. Loss of CNGC18 function leads to pollen tube bursting *in vitro*.

The ambiguous roles of calcium during tip-growth control in pollen tubes and root hairs have been well-established for many years. Based on the irregularities in intracellular Ca<sup>2+</sup> dynamics observed in pollen tubes of the *rbohH rbohJ* mutant, it appears most likely, that ANX1/2 and RBOHH/J control Ca<sup>2+</sup>-homeostasis during pollen tube growth. However, the quest for one or several calcium-permeable channels, which are directly linked to CWI signaling, is ongoing. In earlier studies, CNGC18 (AT5G14870) has been described as a crucial regulator of pollen germination and growth control (Chang et al., 2007; Frietsch et al., 2007; Gao et al., 2016; Gu et al., 2017; see section 1.5). While the *cngc18-1/CNGC18* loss-of-function mutant, for instance, has been reported to lead to short and 'kinky' pollen tubes (fully reducing the male transmission efficiency of the *cngc18-1* allele), it remains unclear, if the described phenotype factually refers to premature pollen tube bursting. Loss or knockdown of CNGC18 function has furthermore been reported to lead to irregularities in [Ca<sup>2+</sup>]<sub>cyt.</sub>-homeostasis, however, it remains to be elucidated, if and how irregularities in both, Ca<sup>2+</sup> homeostasis and pollen tube growth correlate and collude.

To revise the role of CNGC18 during pollen tube growth control, *in vitro* pollen germination was studied in several independent knockout (*cngc18-1/CNGC18*, *cngc18-2/CNGC18*) and knockdown (*cngc18-17*) lines (Fig. 27). While both, *cngc18-1/CNGC18* and *cngc18-2/CNGC18* represent T-DNA insertion lines, *cngc18-17* was created via EMS-mutagenesis, which led to a CNGC18<sup>[R491Q]</sup> amino acid exchange. The CNGC18 gene model, corresponding mutant alleles and protein structure are depicted in Fig. 27A.

During this study, both *cngc18-1/CNGC18* and *cngc18-2/CNGC18* revealed a drastic and highly significant increase in pollen bursting in the range of 50 - 59 % and 48 - 58 % respectively, just like the *mri-1/MRI* control line whose pollen bursting rate ranged between 53 and 62 %. In contrast, Col-0 (*qrt*) pollen displayed less frequent loss of CWI in the range of 15 - 21 %. The knockout lines *cngc18-1/CNGC18* and *mri-1/MRI* are in the *quartet* (*qrt*) background, which prevents separation of the four meiotic products during pollen development and leads to pollen release in tetrads (Preuss et al., 1994). Tetrads of heterozygous knockout mutants in the *qrt* background allow efficient quantification of *in vitro* pollen germination, as two of four tetrads carry the mutant allele, while the other two express the wild-type allele. Interestingly, the majority of tetrads in both, the *cngc18-1/CNGC18* and the *mri-1/MRI* knockout lines consisted of two (or more) pollen grains which had lost their CWI. Fittingly, not a single one of the 180 analyzed tetrads per line revealed more than two

intact pollen tubes, indicating the strength of the *cngc18-1*- and *mri-1*-induced growth defect. In contrast, the germination rate was not significantly altered between all four lines. These results indicate that, like MRI, CNGC18 is an essential positive regulator of pollen tube CWI.

The *cngc18-17* knockdown mutant homozygously expresses a full-length CNGC18 protein with an arginine to glutamine amino acid substitution at position 491 (R491Q), which was shown to trigger irregular intracellular  $\text{Ca}^{2+}$ -oscillation and impair pollen tube guidance (Gao et al., 2016). The mutated site is situated in the C-terminal cyclic nucleotide-binding domain (CNBD). While it does not abolish CNGC18 pore activity, it was reported to prevent its activation via cyclic nucleotides (Gao et al., 2016; see Fig. 27B). In the course of our experiments, both, the *cngc18-17* and *mri-2* knockdown lines, revealed an increased pollen bursting rate in the range of 56 - 75 % and 50 - 59 %. These rates were significantly different compared to the 11 - 17 % observed in Col-0. The germination rate was not significantly altered between all three lines. These results support that CNGC18 acts as a positive regulator of pollen tube growth control. The phenotypic similarity between *cngc18*- and *mri*-loss-of-function mutants suggests, that CNGC18 and MRI may act in a common signaling pathway.

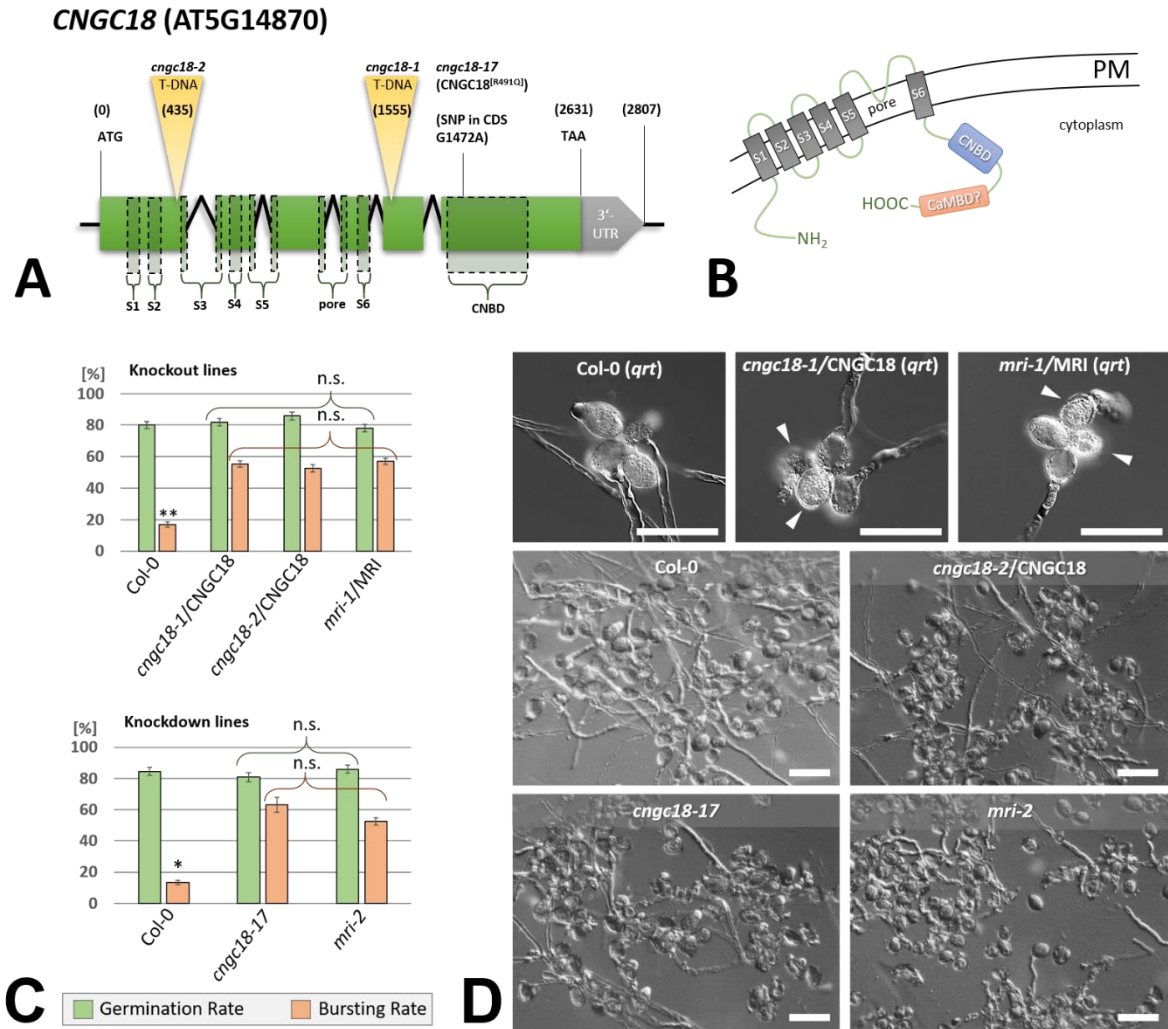


**Fig. 27: Knockdown/- knockout of CNGC18 leads to pollen bursting *in vitro*.** (A) *CNGC18* (AT5G14870) gene model including sites of T-DNA insertion/SNPs, as well as translated protein domains. The scheme is based on the descriptions of Frietsch et al., 2007; Gao et al., 2016 and Fischer et al., 2017. (B) Corresponding protein domain structure of CNGC18, including transmembrane-domains S1-S6, a pore region, cyclic nucleotide-binding domain (CNBD) and a putative CaM-binding domain (CaMBD). The scheme is based on the descriptions of Hua et al., 2003, Frietsch et al., 2007 and Fischer et al., 2017. (C) Summary of three independent *in vitro* pollen germination assays on the knockout lines *cngc18-1/CNGC18 (qrt)* and *cngc18-2/CNGC18* in comparison with *mri-1/MRI (qrt)* and Col-0 (*qrt*) ( $n \geq 187$  pollen grains per genotype in three independent experiments), as well as the knockdown line *cngc18-17* in comparison with *mri-2* and Col-0 ( $n = 240$  pollen grains per genotype in three independent experiments). Error bars show the standard error of the mean (SEM). Significance inferred based on a two-tailed, unpaired Student's T-test (n.s. = not significant, \*\*/\*\*\*: significant at  $p < 0.01/p < 0.001$ ). (D) Representative microscopic captures of the lines shown in section C. White arrowheads indicate pollen grains that precociously lost their CWI. Scale bars: 80  $\mu\text{m}$ .

#### 4.3.2. The CNGC18<sup>[R491Q]</sup> amino acid substitution in *cngc18-17* is truly linked to pollen bursting.

During assessment of pollen germination and pollen tube growth *in vitro*, it became apparent that *cngc18-17* mutants do not only display a pollen-specific defect, but are generally impaired in reproductive and vegetative development, the most striking examples being extreme increase of pistil size before maturation of stamina, leading to a vast decrease of self-pollination and short siliques (supposedly as a result of low fertilization rates) (Fig. 28). We questioned whether potential remaining EMS-induced mutations may cause the observed loss of CWI we observed during *in vitro* germination of *cngc18-17* pollen - amongst the further observed phenotypes - instead of the *cngc18-17* allele itself. Thus, we examined whether the [R491Q] substitution in the CNGC18 amino acid sequence of *cngc18-17* mutants was causative for impaired pollen tube CWI maintenance. Pistils of *cngc18-17* plants were pollinated with Col-0 pollen to circumvent male-induced sterility through impaired function of CNGC18. T1 plants were genotyped for heterozygosity of the *cngc18-17* allele via the dCaps-method (see section 3.2.2.4.). Homozygous *cngc18-17* F2 seedlings from three independent F1 lines were isolated. Homozygosity was confirmed in F3 generation and plants were phenotyped concerning flower development, pollen germination and silique length. Flowers of backcrossed lines were found to display a wild type-like morphology (Fig. 28A), while the pollen germination and bursting rates of backcrossed and non-backcrossed lines did not significantly differ *in vitro* (Fig. 28B and C). However, an increase in silique length of backcrossed plants could be observed (Fig. 28D), which may result from the regained ability for self-pollination in backcrossed *cngc18-17* plants. Taken together, these results confirmed that the CNGC18<sup>[R491Q]</sup> amino acid substitution in the *cngc18-17* allele is indeed causative for pollen tube bursting, but not for the short silique phenotype. We thus proceeded with further experiments on the backcrossed *cngc18-17* allele.

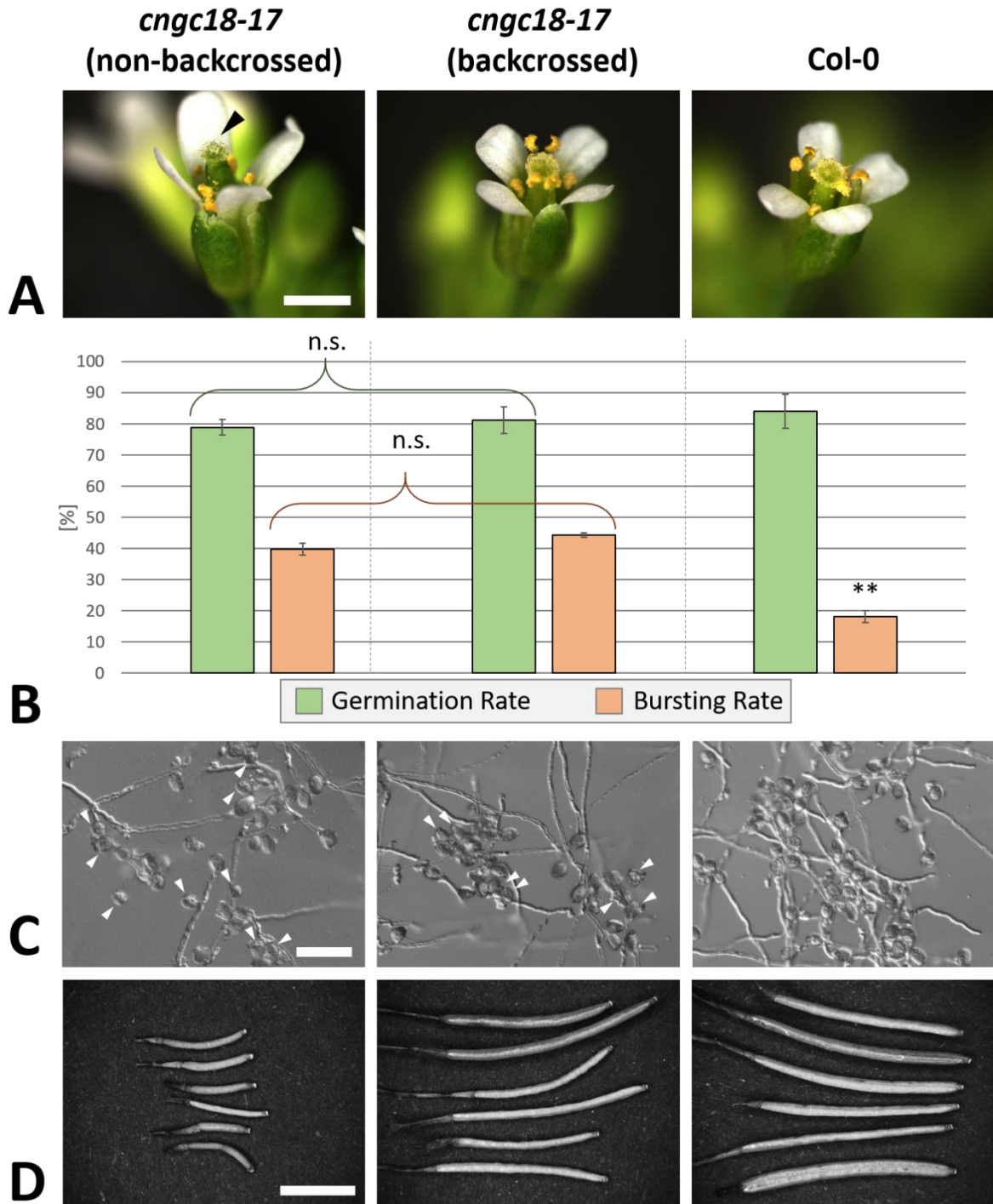


**Fig. 28: Phenotypic analyses of backcrossed and non-backcrossed *cngc18-17* plants.** The three separate columns contain data for *cngc18-17* (non-backcrossed), *cngc18-17* (backcrossed) and Col-0 regarding (A) Development of inflorescences (1-2 d after opening of floral buds). The black arrowhead indicates a representative, non-pollinated pistil, which was characteristic for non-backcrossed *cngc18-17* inflorescences. Scale bar: 2mm; (B) *in vitro* pollen germination. Error bars show the standard error of the mean (SEM). Significance inferred based on a two-tailed, unpaired Student's T-test (n.s. = not significant, \*\* = significant at  $p < 0.01$ ); (C) *in vitro* pollen germination assay; representative images for the data presented in section B. White arrowheads indicate pollen grains that precociously lost their CWI. Scale bar: 80  $\mu$ m. (D) Representative siliques. Scale bar: 5 mm.

#### 4.3.3. Overexpression of GFP-CNGC18 inhibits pollen tube growth *in vitro*.

To assess whether the overexpression of CNGC18 has an opposite phenotypic (*i.e.* growth inhibitory) effect on tip-growth in pollen tubes as compared to the premature loss of CWI observed in the loss-of-function lines analyzed before (section 4.3.1.), a wild-type (CNGC18) line in the *qrt* background hemizygotously expressing GFP-CNGC18 under control of the Autoinhibited  $\text{Ca}^{2+}$  ATPase 9 promoter (*proACA9::GFP-CNGC18*) was recovered from a complemented heterozygous *cngc18-1/CNGC18* line published earlier (Frietsch et al., 2007; line received from Prof. Dr. Jeffrey F. Harper, University of Nevada, Reno, USA). The expressed construct segregated at 64 % ( $n = 66$ ). Plants were genotyped for presence of the *cngc18-1* allele and three wild type individuals (CNGC18/CNGC18) hemizygotously expressing GFP-CNGC18 were analyzed in two independent *in vitro* pollen germination assays. To test if GFP-CNGC18 affects pollen tube germination, the relative amount of fluorescent to non-fluorescent pollen tubes was determined (Tab. 23). The three individuals displayed a reduction of fluorescent pollen tubes to ~9 % ( $n = 380$ ) (as compared to a hypothetical value of 50 % in a line not affected in pollen germination), while the ratio of fluorescent pollen grains remained at 46 % ( $n = 160$  pollen grains) (*i.e.* close to the expectation of 50 % in a hemizygous transgenic line). As microscopic analyses could reveal, transgenic pollen tubes were obviously shorter as compared to wild-type pollen tubes (Fig. 29A). Taken together, these results are consistent with the data presented in section 4.3.1 and thus confirm, that CNGC18 acts as a positive regulator of pollen tube growth control. The CNGC18 growth inhibition phenotype was very reminiscent of the overexpression phenotypes described for other positive CWI regulators, such as ANX1 (Boisson-Dernier et al., 2009) and MRI (Boisson-Dernier et al., 2015), as well as the loss-of-function phenotype of the negative CWI regulators *aun1 aun2* (Franck et al., 2018 B).

**Tab. 23: Determination of relative pollen tube numbers in dependance of GFP-CNGC18 expression.** Numbers of fluorescent and non-fluorescent pollen tubes were determined in three individual CNGC18 *qrt* plants hemizygotously expressing *proACA9::GFP-CNGC18*. The underlying ratio was taken as a proxy for the effect of GFP-CNGC18 overexpression on pollen tube growth. Significance inferred based on a two-tailed, unpaired Student's T-test.

	Round 1			p-value
	Fluorescent PTs	Non-fluorescent PTs	% fluorescent PTs	
Individual 1	2	51	3.9 %	
Individual 2	8	53	15.1 %	
Individual 3	3	60	5.0 %	
	Round 2			
	Fluorescent PTs	Non-fluorescent PTs		
Individual 1	2	56	3.5 %	
Individual 2	8	62	12.9 %	
Individual 3	8	67	11.9 %	
Total	31	349	8.8 %	



Col-0 with *proACA9::GFP-CNGC18* (hemizygous)

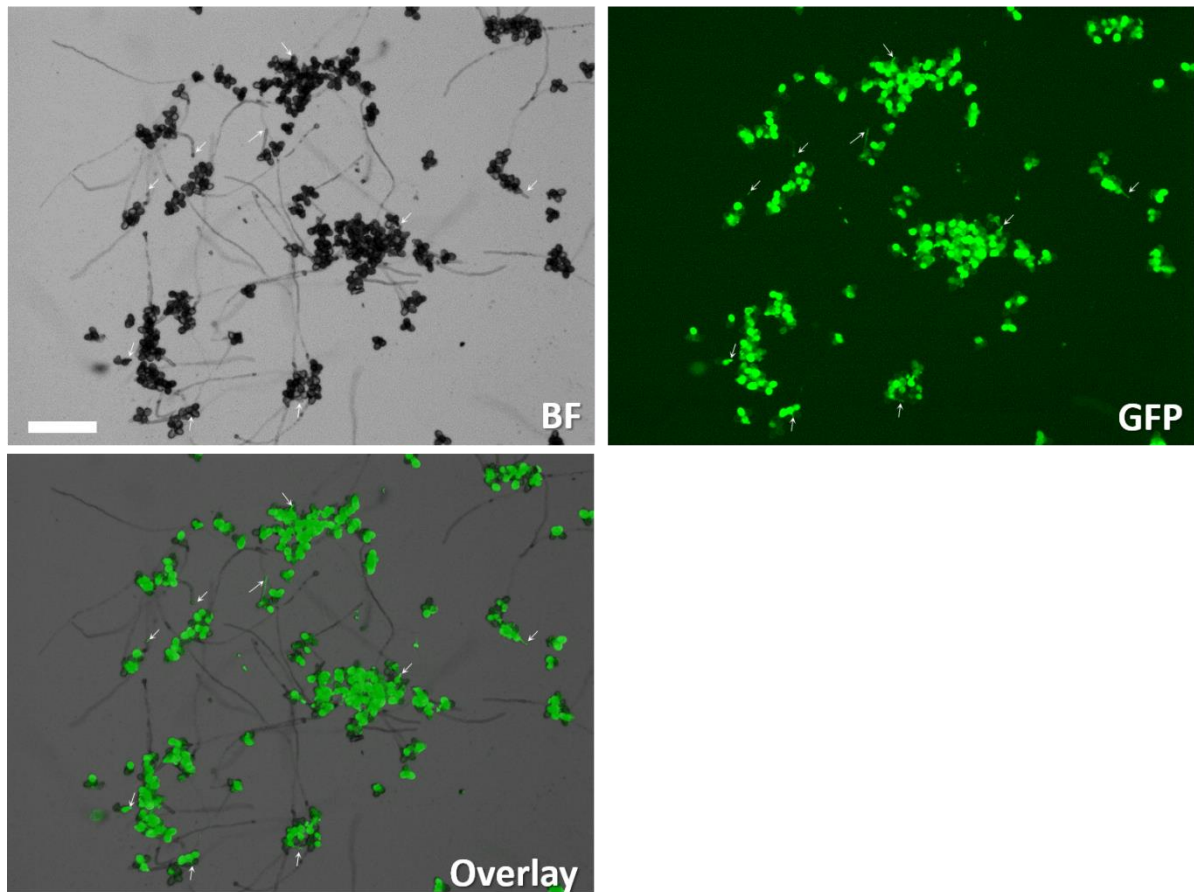


**Fig. 29: *In vitro* pollen germination assay of Col-0 *qrt* hemizygously expressing GFP-CNGC18.** Shown are representative captures of pollen tubes hemizygously expressing *proACA9::GFP-CNGC18*. Arrows mark transgenic pollen tubes. Scale bar: 400  $\mu$ m.

#### 4.3.4. Knockdown of both, CNGC18 and MRI, leads to irregular $[Ca^{2+}]_{\text{cyt.}}$ -oscillations and unsteady pollen tube growth *in vitro*.

CNGC18 knockdown has previously been linked to disturbance of regular  $[Ca^{2+}]_{\text{cyt.}}$ -dynamics, as was reported for the *cngc18-17* (CNGC18<sup>[R491Q]</sup>) and *cngc18-22* (CNGC18<sup>[R578K]</sup>) knockdown mutants (Gao et al., 2016). However, it remains unclear how such irregularities were defined and categorized and if irregular  $[Ca^{2+}]_{\text{cyt.}}$ -dynamics upon *cngc18* knockdown are linked to growth irregularities as has been demonstrated for *rbohH rbohJ* (Boisson-Dernier et al., 2013; Franck et al., 2017). In order to further assess the effects of *cngc18-17* knockdown on  $[Ca^{2+}]_{\text{cyt.}}$ -dynamics and pollen tube growth, a *cngc18-17* line homozygously expressing the Yellow CaMeleon 3.60 (YC3.60) ratiometric biosensor under control of *proLAT52* (*proLAT52::YC3.60*) was studied. It was compared to *mri-2* expressing YC3.60 under control of the Actin1 promoter (*proAct1::YC3.60*), as well as to two Col-0 wild-type lines homozygously expressing either *proLAT52::YC3.60* or *proAct1::YC3.60* (Both, the *cngc18-17* and wild-type lines expressing the YC3.60 biosensor, were received from Prof. Dr. Yong-Fei Wang, Chinese Academy of Sciences, Shanghai, China, while the transgenic *mri-2* line was obtained by crossing with the *proAct1::YC3.60* wild-type line). The same kind of sensor has already been used earlier to reveal the irregularities in intracellular  $Ca^{2+}$  oscillation and steady pollen tube growth in the *rbohH rbohJ* mutant (Boisson-Dernier et al., 2013; Franck et al., 2017).

In consideration of former research linking changes in tip-focused  $Ca^{2+}$ -concentrations to cessation of pollen tube growth (e.g. Frank et al., 2017), we analyzed the *cngc18-17* mutant for similar correlations. Based on kymographs, which illustrate the relative  $Ca^{2+}$  concentration along the longitudinal pollen tube axis over time and distance, pollen tube growth and  $Ca^{2+}$  dynamics were manually classified as follows: (A) strong irregularities and temporal correlations of both,  $Ca^{2+}$  oscillation and growth, (B) moderate, yet correlated irregularities, (C) mild, but temporally non-correlated irregularities in either  $Ca^{2+}$  oscillation or growth and (D) regular, wild type-like growth (Fig. 30). Strikingly, 81 % of all *cngc18-17* pollen tubes displayed irregularities in  $Ca^{2+}$  oscillation and growth rate, while 62 % were found to show strong positive correlation between both phenomena. Similarly, 83 % of *mri-2* pollen tubes displayed irregularities with 60 % showing positive correlations. In contrast, the *proAct1::YC3.60* and *proLAT52::YC3.60* control lines displayed irregular growth in 33 % and 39 % of all cases, with only 11 % and 15 % of pollen tubes showing positive correlations between both phenomena, respectively.

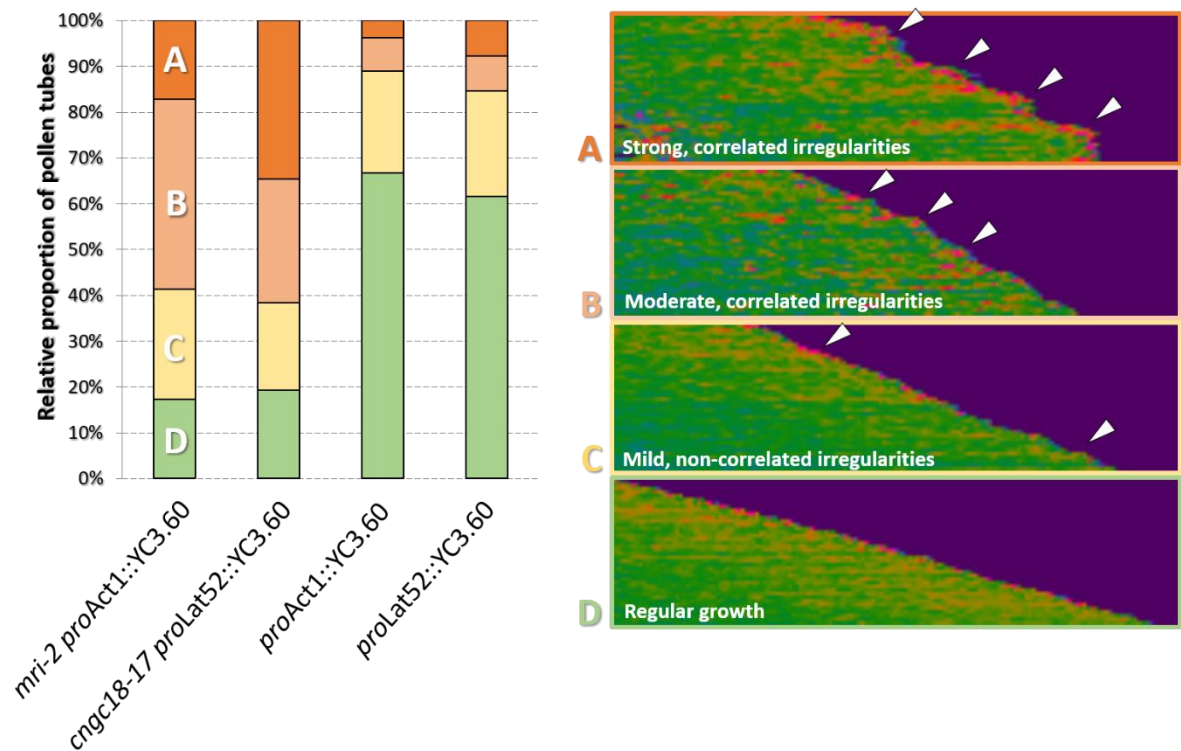


**Fig. 30: Knockdown of both, CNGC18 and MRI, leads to irregular intracellular  $\text{Ca}^{2+}$ -dynamics, which correlate with pollen tube growth rate oscillation.** Shown is the relative proportion of pollen tubes displaying (A) strong irregularities and temporal correlations of both,  $\text{Ca}^{2+}$  oscillation and steady growth, (B) moderate, yet correlated irregularities, (C) mild, but non-correlated irregularities in either  $\text{Ca}^{2+}$ -oscillation or steady growth and (D) regular, wild-type-like growth.  $n \geq 26$  pollen tubes were analyzed for each genotype. Pictures on the right show representative kymographs of the quantified phenomena.

Closer analysis of intracellular  $\text{Ca}^{2+}$  dynamics furthermore revealed that the observed irregularities in frequency and magnitude of  $\text{Ca}^{2+}$  oscillation precede growth cessation in both, *cngc18-17* and *mri-2* specimens (Fig. 31). In contrast to the control lines, which showed comparatively moderate and frequent oscillatory  $\text{Ca}^{2+}$  peaks, which did not affect steady growth, both mutants revealed a lower oscillation frequency. While the oscillations in *cngc18-17* displayed a drastic increase of peak-to-valley-value (*i.e.* the maximal difference between highest and lowest intracellular  $\text{Ca}^{2+}$  concentrations at the same position), this maximal difference tended to decrease in *mri-2*, as compared to wild-type values. Despite these described changes, the relative  $\text{Ca}^{2+}$  concentrations between pollen tube tip and shank region remained at a constant ratio in the range between 1.0 and 1.5 (shown for one exemplary specimen per genotype in Fig. 31). These findings demonstrate, that intracellular  $\text{Ca}^{2+}$ -dynamics are similarly modulated by CNGC18 and MRI, presenting a crucial step in facilitation of steady pollen tube growth. The  $\text{Ca}^{2+}$  responsiveness of *mri-2* and *rbohH rbohJ* indicates, that all three gene classes may act in a common CWI signaling pathway upstream of  $\text{Ca}^{2+}$  homeostasis.

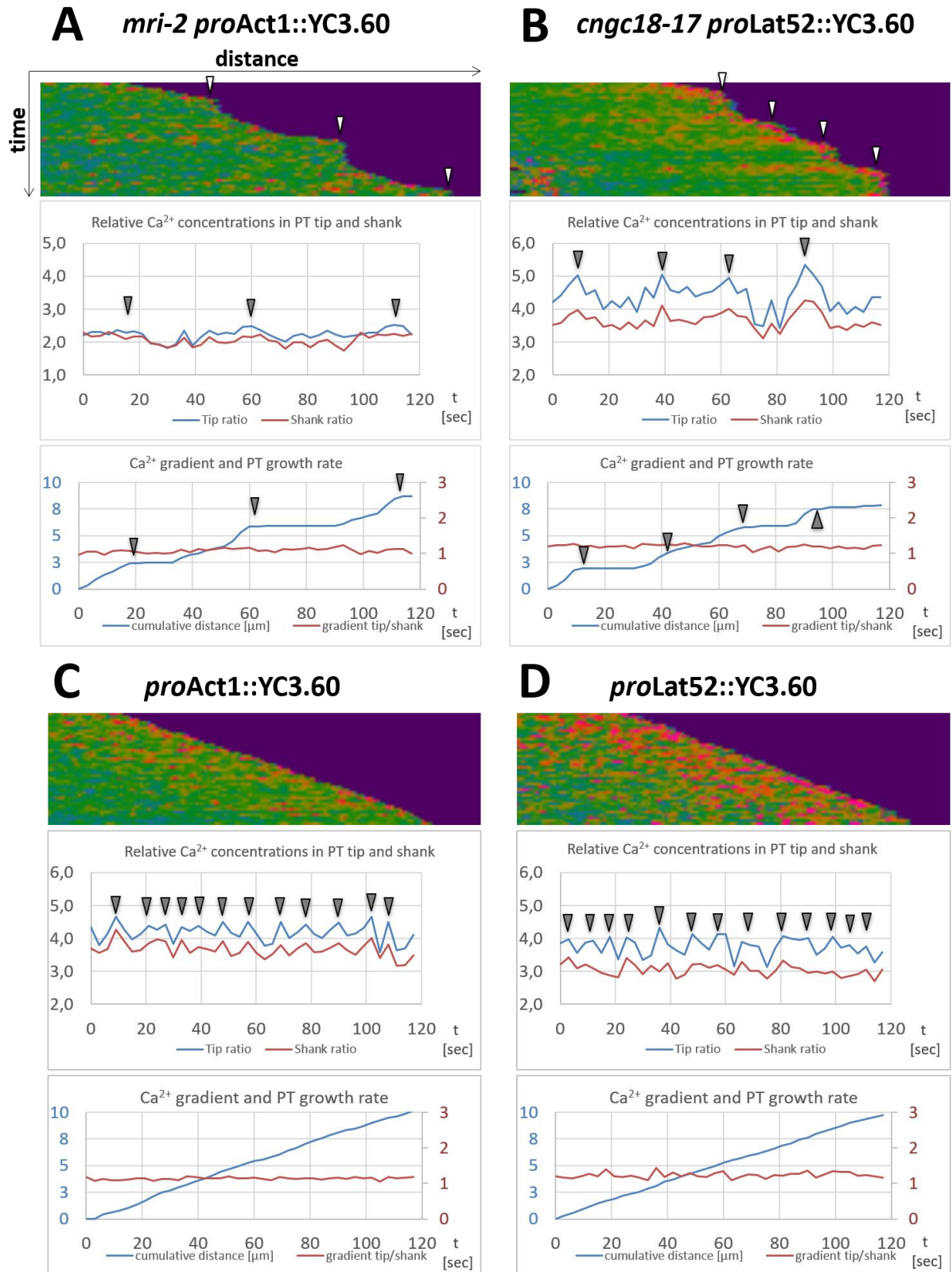


**Fig. 31: Irregular intracellular  $\text{Ca}^{2+}$ -oscillation correlates with and precedes pollen tube growth rate decrease in both, *cngc18-17* and *mri-2*.** Shown are representative kymographs and corresponding quantitative analyses of (i) relative  $\text{Ca}^{2+}$ -concentrations in the pollen tube (PT) tip and shank region (upper graph) and of (ii) tip-to-shank-gradient and growth rate (lower graph) shown for the lines analyzed before (Fig. 30). Arrowheads indicate the correlation between irregular  $\text{Ca}^{2+}$ -oscillation events and growth cessation. Quantitative analyses were carried out as described by Franck et al., 2017.

#### 4.3.5. Expression of YFP-CNGC18 under *proLat52* does not rescue male transmission of the *anx2-2* allele in the *anx1-1/anx1-1 anx2-1/ANX2* background.

Based on the phenotyping results presented above, it was hypothesized whether CNGC18 functions downstream of ANX1/2 and MRI in CWI signaling of tip-growing pollen tubes. To test this hypothesis, the CNGC18 ORF was amplified from floral cDNA and a YFP-CNGC18 protein fusion under control of the pollen-specific *proLAT52* (*proLAT52::YFP-CNGC18*) was transformed into *anx1-1/anx1-1 anx2-1/ANX2*. T1 plants were selected for presence of the transgene, PCR-genotyped for heterozygosity of *anx2-1/ANX2* and pollen was checked for fluorescence to confirm hemizygosity for the transgene. T2 plants were again selected for presence of the transgene using antibiotics and subsequently PCR-genotyped for *anx2-1*. In the untransformed *anx1-1/anx1-1 anx2-1/ANX2* line, the severe (male-specific) loss of CWI phenotype upon pollen germination, mediated by *anx1-1 anx2-1* normally impedes male transmission of both alleles (Boisson-Dernier et al., 2009). Thus, the identification of progeny which is homozygous for *anx1-1 anx2-1* would indicate a putative rescue of the male pollen bursting phenotype.

Within 184 T2 plants originating from 4 independent T1 lines of *anx1-1/anx1-1 anx2-1/ANX2*, all hemi- or homozygously (over)expressing *proLAT52::YFP-CNGC18*, not a single double-homozygous *anx1-1 anx2-1* plant could be found. Strikingly, out of a total number of 184 transgenic lines (hemi- or homozygously expressing *proLAT52::YFP-CNGC18*) only 52 were found to be heterozygous for *anx2-1/ANX2*. While untransformed *anx1-1/anx1-1 anx2-1/ANX2* displayed a male-gametophytic segregation ratio close to 1:1, the segregation ratio of the transformed line differed significantly from a mendelian distribution of 1:2:1, while even falling significantly below the expected ratio of 1:1 assuming a (male) gametophytic transmission defect (Tab. 24). These unusual results indicate that expression of the transformed YFP-CNGC18 construct under *proLat52* does not rescue male transmission of the *anx2-1* allele in the *anx1-1/anx1-1 anx2-1/ANX2* background.

**Tab. 24: Segregation analysis of the *anx2-1* allele in the *anx1-1/anx1-1 anx2-1/ANX2* background transformed with *proLAT52::YFP-CNGC18*.** Shown are the observed numbers of T2 progeny - which were heterozygous for *anx2-1/ANX2* or homozygous for one of the alleles - in dependence of presence/absence of the transformed construct *proLAT52::YFP-CNGC18*. Observed values of the transformed lines were compared by means of a  $\chi^2$  test of independence with the expected values based on a hypothetical mendelian distribution or a (male) gametophytic transmission defect.

	<i>anx1-1/anx1-1</i> <i>ANX2/ANX2</i>	<i>anx1-1/anx1-1</i> <i>anx2-1/ANX2</i>	<i>anx1-1/anx1-1</i> <i>anx2-1/anx2-1</i>	n	Ratio	p-value (two-tailed $\chi^2$ test)
Observed ( <i>anx1-1/anx1-1</i> <i>anx2-1/ANX2</i> )	89	71	0	160	1 : 0.80 : (0)	
Observed ( <i>anx1-1/anx1-1</i> <i>anx2-1/ANX2</i> with YFP- CNGC18)	132	52	0	184	1 : 0.40 : (0)	
Expected (Mendelian distribution)	46	92	46	184	1 : 2 : 1	<0.001
Expected (Male gametophytic defect)	92	92	0	184	1 : 1 : 0	<0.001

Strikingly, out of 52 transgenic lines (*anx1-1/anx1-1 anx2-1/ANX2* with *proLAT52::YFP-CNGC18*), only 5 lines were found to show homozygous expression of YFP-CNGC18 (indicated by 100 % of fluorescent pollen grains), while the remaining 47 lines showed hemizygous expression (50 % of fluorescent pollen grains). This observation was significantly different from the expected (1):2:1 ratio in assumption of mendelian distribution (Tab. 25). It indicates that the transformed construct may segregate in a non-mendelian manner, while the reason remains unclear.

**Tab. 25: Segregation analysis of *proLAT52::YFP-CNGC18* in the *anx1-1/anx1-1 anx2-1/ANX2* background.** Shown are the observed numbers of T2 progeny which was hemi- or homozygous for the transformed construct. The observed values were compared by means of a  $\chi^2$  test of independence with the expected values based on a hypothetical mendelian distribution. The possibility of absence of the transformed construct was excluded by antibiotics-based selection with a transformation vector-specific selection marker.

	<i>anx1-1/anx1-1 anx2-1/ANX2</i> with YFP- CNGC18 (hemiz.)	<i>anx1-1/anx1-1 anx2-1/ANX2</i> with YFP- CNGC18 (homoz.)	n	Ratio	p-value (two-tailed $\chi^2$ test)
Observed	47	5	52	1 : 0.15	0.0003
Expected	34.7	17.3	52	1 : 0.5	



To test whether the apparent incapability of YFP-CNGC18 to rescue male transmission of the *anx2-1* allele results from the inability of YFP-CNGC18 to rescue the associated pollen bursting phenotype, the influence of its expression on pollen germination was analyzed *in vitro*. A preliminary analysis of *in vitro* pollen germination of a single *anx1-1/anx1-1 anx2-1/ANX2* T1 line hemizyously expressing *proLAT52::YFP-CNGC18* revealed an increase in pollen bursting to 86 %, as compared to 66 % in the untransformed *anx1-1/anx1-1 anx2-1/ANX2* line and 28 % in the Col-0 wild-type control (Fig. 32A). Closer analysis showed that none of the intact pollen tubes show YFP-fluorescence and that all fluorescent pollen grains either lose their CWI upon germination or do not germinate at all (Fig. 32B). This result indicates that expression of the transformed YFP-CNGC18 fusion under *proLat52* is incapable of rescuing *anx1 anx2*-mediated pollen bursting *in vitro*. The slight increase in pollen bursting upon expression of the transgene suggests that - on the contrary - it may induce an increase in pollen bursting. This assumption is consistent with the observed non-mendelian segregation ratio of the YFP-CNGC18 fusion construct (Tab. 25), which could, however, also be explained by YFP-CNGC18 overexpression inhibiting pollen tube growth.

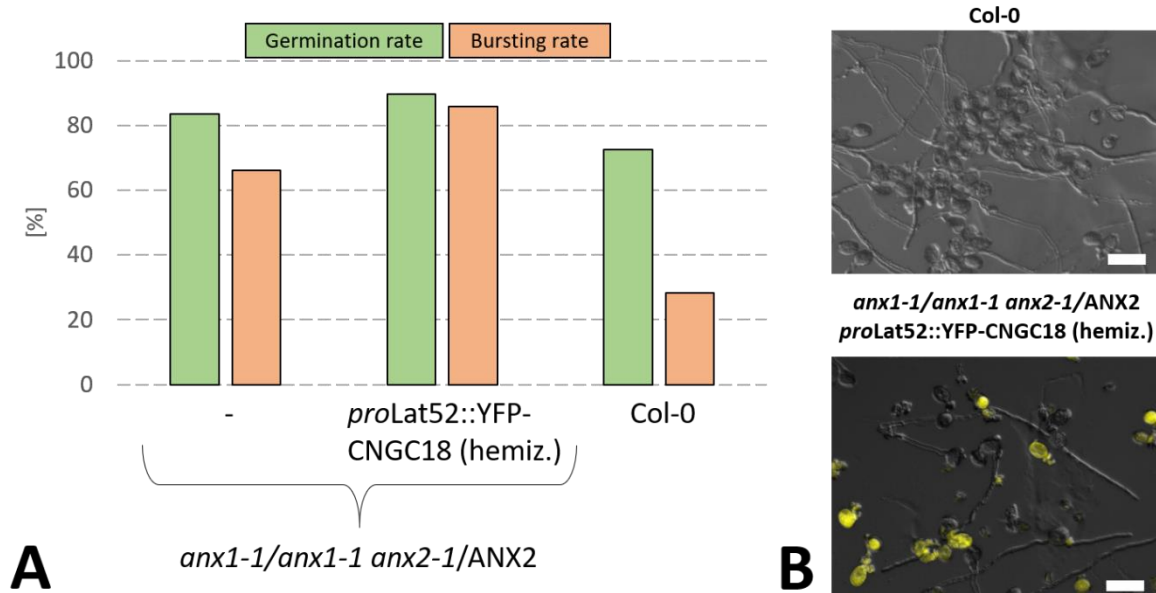


**Fig. 32: *In vitro* pollen germination of *anx1-1/anx1-1 anx2-1/ANX2* expressing YFP-CNGC18.** (A) Pollen germination was tested in a T1 line hemizyously expressing *proLAT52::YFP-CNGC18* and compared to an untransformed *anx1-1/anx1-1 anx2-1/ANX2* line and a Col-0 wild type control.  $n \geq 330$  pollen grains. (B) Left: Representative image of *in vitro* pollen germination in *anx1-1/anx1-1 anx2-1/ANX2* hemizyously expressing YFP-CNGC18; Overlap of bright field image and YFP-fluorescence. Right: Col-0 control line; bright field image. Scale bars = 80  $\mu$ m.

#### 4.3.6. Does introduction of *proACA9::GFP-CNGC18* via crossing rescue male transmission of *anx2-1* in the *anx1-1/anx1-1 anx2-1/ANX2* background?

Based on the conspicuous observations described in section 4.3.5., we questioned whether the observed incapability of YFP-CNGC18 expression under *proLat52* to rescue male transmission of the *anx2-1* allele and to reduce pollen bursting in *anx1-1/anx1-1 anx2-1/ANX2* may be the result of a technical error (e.g. in the transformation vector structure). Therefore, we applied an alternative strategy to test for a putative genetic interaction between CNGC18 and ANX1/2.

Col-0 wild-type plants expressing *proACA9::GFP-CNGC18* (which was shown to be functional before and was originating from the same parental plants as described in section 4.3.3) were crossed with *anx1-1/anx1-1 anx2-1/ANX2* plants. F1 plants were checked for heterozygosity of both, the *anx2-1* allele (PCR-diagnostics) and the GFP-CNGC18 fusion (pollen fluorescence) and allowed to self-fertilize. F2 plants were selected with antibiotics for GFP-CNGC18 and PCR-genotyped for presence of the *anx2-1* allele. Three *anx1-1/anx1-1 anx2-1/ANX2 GFP-CNGC18/-* plants was isolated and allowed to self-fertilize. Out of 174 F3 plants originating from three independent F2 lines and selected for presence of GFP-CNGC18, 4 plants were found to be double-homozygous (*anx1-1 anx2-1*) (Tab. 26). Further analysis is ongoing and will include assessment of potential rescue of plant fertility (pollen germination and seed set assays) in these 4 lines. A similar strategy may be applied using the *mri-1/MRI* knockout mutant to study a putative genetic interaction between MRI and CNGC18. The preliminary results presented here indicate, that CNGC18 may truly act downstream of ANX1 in a common CWI signaling pathway.

**Tab. 26: Segregation of the *anx2-1* allele in the *anx1-1/anx1-1 anx2-1/ANX2* background transformed with *proACA9::GFP-CNGC18*.** Shown are the genotyping results of a total of 174 F2 plants originating from *anx1-1/anx1-1 anx2-1/ANX2* F1 plants hemizygotously expressing GFP-CNGC18. Crossing and genotyping were performed by Dr. Aurélien Boisson-Dernier.

Genotype	<i>proACA9::GFP-CNGC18</i>		
	<i>anx1-1/anx1-1 ANX2/ANX2</i>	<i>anx1-1/anx1-1 anx2-1/ANX2</i>	<i>anx1-1/anx1-1 anx2-1/anx2-1</i>
Number of plants	70	100	4



#### 4.4. The role of the class VII-RLCK VEIVE in plant reproduction

##### 4.4.1. VEIVE is a pollen-expressed member of class VII RLCKs.

The *Arabidopsis* genetic locus AT2G07180 encodes a putative, pollen-expressed RLCK that we named VEIVE (VEI). VEI was shown before to be a homolog of type-VII RLCKs by phylogenetic analysis (Ranf et al., 2014). RLCK subfamily VII genes are known to govern a variety of biological functions, including the roles of the pollen tube guidance genes LOST IN POLLEN TUBE GUIDANCE 1 (LIP1) and 2 (LIP2) (Liu et al., 2013), as well as the well studied plant immunity regulators BOTRYTIS-INDUCED KINASE 1 (BIK1) (Lu et al., 2010) and RPM1-induced protein kinase (RIPK) (Liu et al., 2011). In a former transcriptional study, VEI was shown to be expressed in pollen grains, however expression was only slightly altered after pollen germination and during pollen tube growth (<1.6fold expression change) (Wang et al., 2008). The pollen-specific expression of VEI could be confirmed using the *Arabidopsis* eFP browser (Fig. 33).

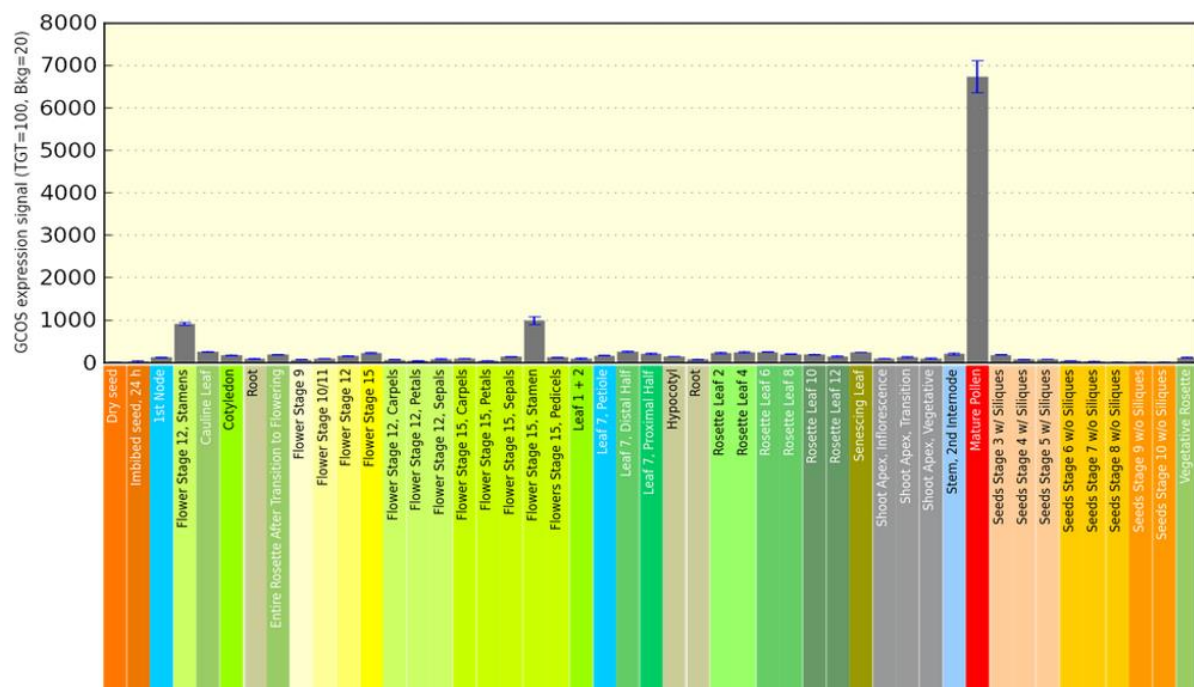


**Fig. 33: VEIVE is an exclusively pollen-expressed gene.** Expression levels of *VEI* (AT2G07180) in different *Arabidopsis* tissues. The pollen expression level is marked in red. Data retrieved from the *Arabidopsis* expression database on <http://bar.utoronto.ca/efp/cgi-bin/efpWeb.cgi>. The y-axis shows the relative level of gene expression (Schmid et al., 2005).

#### 4.4.2. VEIVE loss of function does not cause obvious phenotypes linked to male fertility.

Two T-DNA insertion lines, SK26869 and SK29099, for the VEIVE genomic locus AT2G07180 were ordered from the Salk Institute Genomic Analysis Laboratory (<http://signal.salk.edu/>) and genotyped for presence of the annotated T-DNA. The two independent lines SK26869 and SK29099 were named *vei-1* and *vei-2*, respectively (Fig. 34). Homozygous plants were isolated for both lines via PCR-based genotyping.

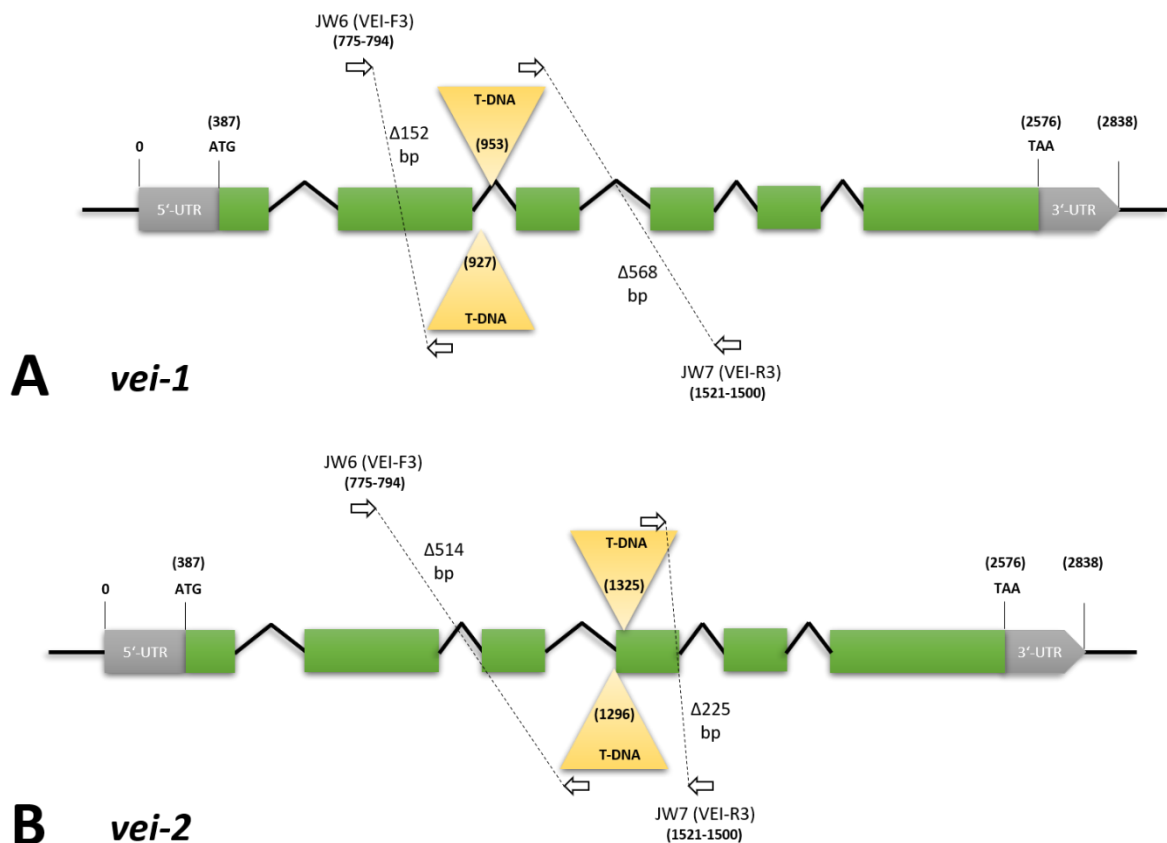


**Fig. 34: VEIVE genetic locus and *vei-1* and *vei-2* T-DNA insertion sites.** Numbers in brackets show the nucleotide positions of transcription start and end for AT2G07180.1, T-DNA insertion sites (that triggered short deletions from nucleotides 927 - 953 (*vei-1*) and from nucleotides 1296 - 1325 (*vei-2*), as well as genotyping primers. Primer binding positions are indicated by white arrows. Both, the *vei-1* (A) and *vei-2* alleles were verified by genotyping PCR and found to possess two T-DNA insertions. Gene model based on the entry for AT2G07180.1 on <https://www.arabidopsis.org/> and T-DNA insertion site verified by genotyping PCR and sequencing.

Homozygous plants of both lines were analyzed for putative pollen germination and growth defects in an *in vitro* pollen germination assay. Neither *vei-1* nor *vei-2* pollen displayed any significant changes in pollen germination or bursting rates as compared to Col-0 wild-type pollen (Fig. 35). These results indicate, that VEI does not participate in the regulation of pollen tube growth.

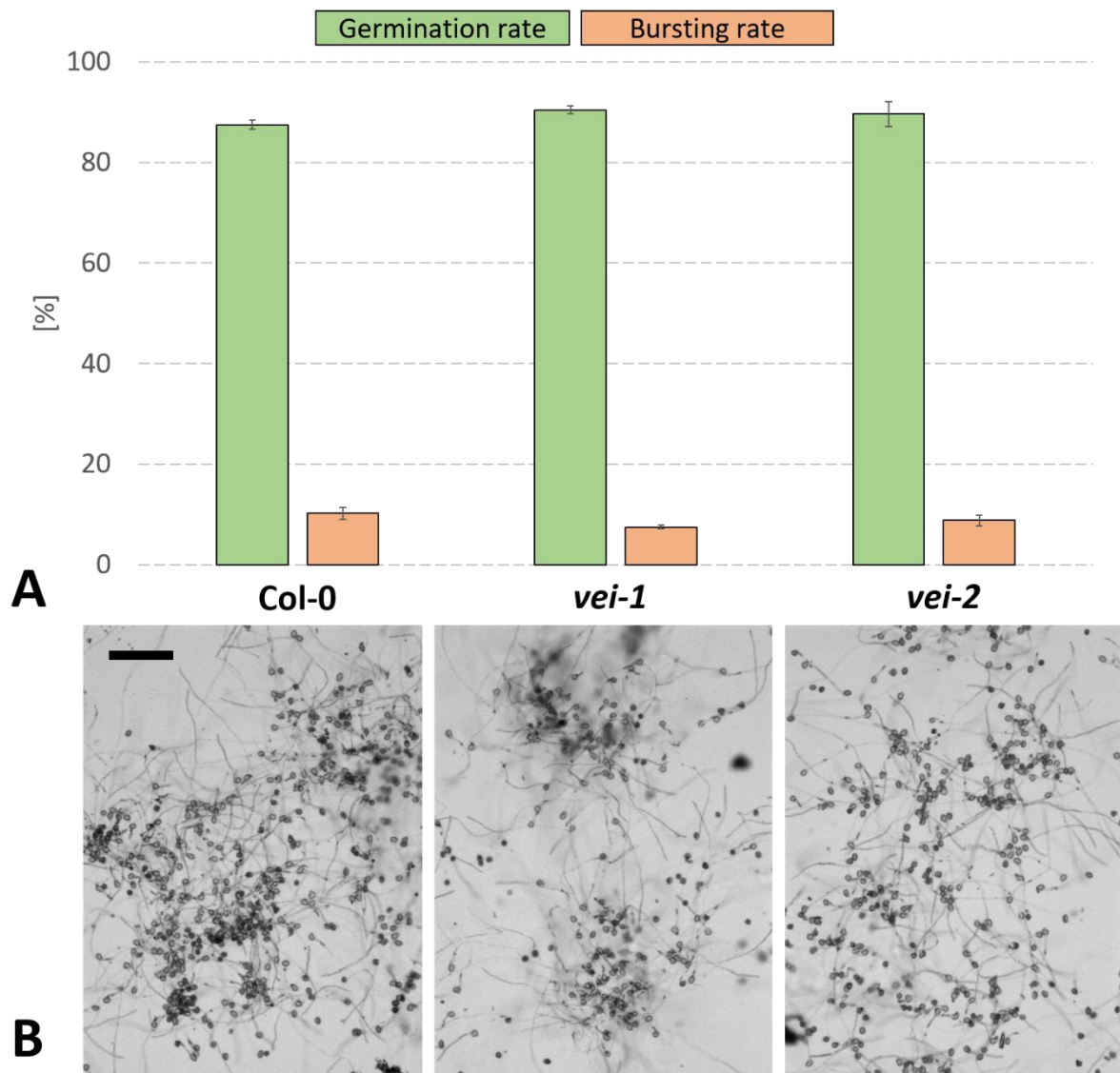


**Fig. 35: *vei-1* and *vei-2* do not display any significant phenotypic deviations concerning *in vitro* pollen germination or bursting.** (A) *In vitro* pollen germination assay.  $n \geq 415$  pollen grains per genotype were analyzed in three independent experiments to compare germination and bursting rates of *vei-1*, *vei-2* and Col-0. Error bars show the standard error of the mean (SEM). Datasets of both *vei-1* and *vei-2* were not significantly different from Col-0 ( $p > 0.05$  in a student's T-test). (B) Representative overview captures of the data presented in section (A). Scale bar: 400 µm.

To exclude a phenotypic effect on pollen tube growth that only becomes visible under *in vivo* conditions (such as pollen tube guidance or perception phenotypes), the seed set of representative homozygous plants of both lines was analyzed. Both, *vei-1* and *vei-2* displayed a mild, but significant decrease of mean seed set to 44.8 and 45.4 seeds per silique, respectively, as compared to a mean value of 54.7 seeds/silique in the Col-0 wild-type control line. Furthermore, the individual measurements for *vei-1* and *vei-2* show a wider distribution than in Col-0, while the *vei-1* allele showed a stronger effect (Fig. 36). These findings contradict the observation, that VEI loss of function does not alter pollen germination or bursting *in vitro*, but may indicate, that VEI indeed controls another aspect of plant fertility.

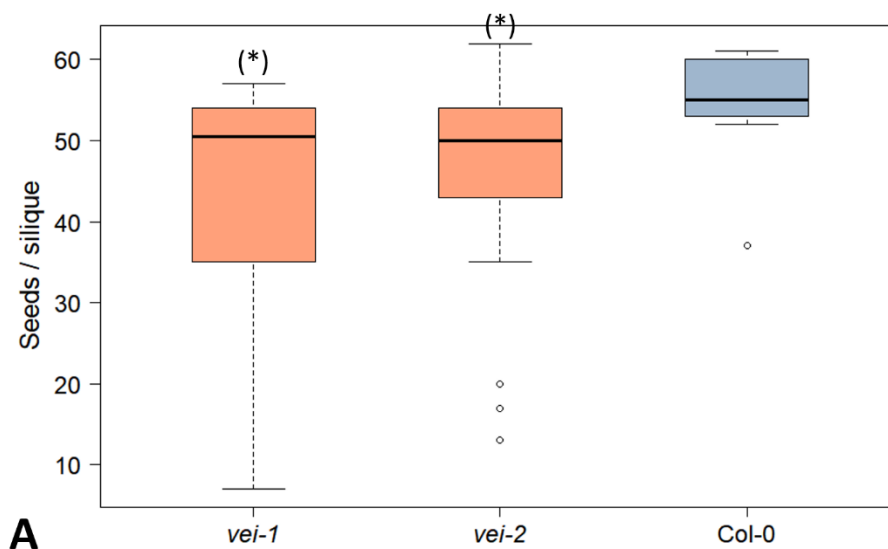


**Fig. 36: *vei-1* and *vei-2* have a mildly decreased seed set.** The number of seeds per silique was determined for  $n \geq 10$  siliques per genotype. Data presented as a boxplot. Significance of *vei-1* and *vei-2* datasets was tested against Col-0 with a student's T-test. (\*):  $p < 0.05$  (0.025 (*vei-1*) and 0.034 (*vei-2*)).

To further test the possibility of a *vei-1/2*-induced male-specific transmission defect, reciprocal crossing experiments with *vei-1* and *vei-2* were carried out. Therefore, Col-0 pistils were pollinated with pollen from heterozygous (*vei-1*/VEI and *vei-2*/VEI) lines. F1 lines revealed a reduced transmission efficiency of 38 % for *vei-1* and 89 % for *vei-2*. In a second experiment *vei-1*/VEI and *vei-2*/VEI pistils were additionally pollinated with Col-0 pollen, which would give indications for a female-specific transmission defect of *vei-1/2*. Male *vei-1* and *vei-2* alleles were transmitted with an efficiency of 55 % and 50 %, respectively. Taken together, these transmission efficiency values indicate a mild to moderate transmission defect of both, the male *vei-1* and *vei-2* alleles. In contrast, the female *vei-1* allele was transmitted with an efficiency of 100 %, depicting the absence of a female-specific

transmission defect. Strikingly, the transmission efficiency of the female *vei-2* allele was reduced to 33 % in the second experiment (Tab. 27).

**Tab. 27: Transmission efficiency of *vei-1* and *vei-2* based on reciprocal crossing experiments.** Transmission efficiency calculated as described in section 3.2.3.4. based on the PCR-genotyping results of  $n \geq 87$  F1 plants (Round 1) and  $n \geq 60$  F1 plants (Round 2).

Crossed lines	TE - Round 1	TE - Round 2
<i>vei-1</i> ♀ x Col-0 ♂	-	100 %
Col-0 ♀ x <i>vei-1</i> ♂	38 %	55 %
<i>vei-2</i> ♀ x Col-0 ♂	-	33 %
Col-0 ♀ x <i>vei-2</i> ♂	89 %	50 %

#### 4.4.3. VEIVE does not have any close *Arabidopsis* homologs.

To exclude the possibility that *vei-1/2* do not display apparent fertility-related phenotypes due to the expression of a structurally similar, functionally redundant homolog, a pBLAST search was performed. However, no close, pollen-expressed homolog could be found, as the 10 best hits displayed a sequence identity of < 68 % (Tab. 28).

**Tab. 28: The *Arabidopsis* genome does not contain any close, pollen-expressed VEIVE homologs.** Homologs were determined via pBLAST against the TAIR10 proteome carried out on the genome database phytozome (<https://phytozome.jgi.doe.gov>) using the VEIVE amino acid sequence as query. Alternative splice variants with alike sequence identity values were filtered from the list. Pollen expression was assessed using the *Arabidopsis* eFP browser (Schmid et al., 2005; <http://bar.utoronto.ca/efp/cgi-bin/efpWeb.cgi>).

Hit #	Gene ID	% identity	E-value	pollen-expression?
1	AT2G07180 (VEIVE)	100	0	yes (exclusive)
2	AT5G01020	67.8	2E-158	no
3	AT2G05940	61.5	1.3E-137	no
4	AT5G56460	61.1	6E-137	weak
5	AT2G28930 (APK1B)	60.7	2.2E-133	no
6	AT5G02290 (NAK)	59.5	4.1E-133	no
7	AT2G26290 (ARSK1)	57.9	4.3E-133	no
8	AT2G39660 (BIK1)	60.7	1.9E-132	no
9	AT5G15080	59.1	1.6E-131	no
10	AT3G01300	62.8	3.4E-130	no

Due to conflicting transmission efficiency analyses and the absence of clear mutant phenotypes, it was decided to not proceed forward with the VEIVE project.

## 5. DISCUSSION

### 5.1. RLK-mediated CWI signaling during tip-growth is conserved amongst land plants.

In the course of the study on the functional conservation of a common MLR- and PTI-like signaling module, loss-of-function mutants of the *Marchantia* MLR-homolog *MpTHE1* and PTI-like homolog *MpPTI* were shown to induce loss of CWI in tip-growing *Marchantia* rhizoids. This is in agreement to the role of their *Arabidopsis* homologs *AtANX1/2/AtFER* and *AtMRI*, respectively, in *Arabidopsis* tip-growth control (Boisson-Dernier et al., 2009; Duan et al., 2010; Boisson-Dernier et al., 2015). Expression of either, *AtMRI* or *MpPTI*, was shown to complement these phenotypic defects in both, pollen tubes and root hairs of the *Arabidopsis mri-1* mutant as well as in rhizoids of the *Marchantia Mppti* mutant. In contrast, overexpression of PTI-like and MLR-homologs led to an opposite (growth-inhibitory) effect in *Arabidopsis* and *Marchantia* tip-growing cells. Based on the knowledge about the hypermorphic variant *AtMRI*<sup>[R240C]</sup> (Boisson-Dernier et al., 2015), a homologous mutation was applied to generate *MpPTI*<sup>[R240C]</sup>. Follow-up experiments will include the expression of *MpPTI*<sup>[R240C]</sup> in *Mpthe1* rhizoids, *fer-4* root hairs and pollen *amiRRALF4/19* tubes to test for the putative general ability of PTI-like genes to control tip-growth downstream of MLRs.

The loss of CWI phenotype in *Mppti* and *Mpthe1* rhizoids (Fig. 12) suggests a crucial function of the corresponding genes *MpPTI* and *MpTHE1* during rhizoid growth control (Honkanen et al., 2015; Honkanen et al., 2016; this study). The complementation of *Mppti* through expression of *MpPTI*-RFP (Fig. 13) proves that the observed loss of CWI phenotype is truly caused by disruption of the *MpPTI* genetic locus. Remarkably, *MpPTI*-YFP is able to clearly rescue *mri-1*-induced loss of CWI in both, *Arabidopsis* pollen tubes (Fig. 15) and root hairs (Fig. 17), while *AtMRI*-RFP is capable of rescuing *Mppti*-induced loss of CWI during rhizoid growth (Fig. 14). The finding that both, *MpPTI* and *AtMRI* share a similar localization pattern, with major localization to the plasma membrane, and less pronounced signal in the cytoplasm and putatively to secretory vesicles (Fig. 13-Fig. 15, Fig. 18 and Fig. 19), suggests that PTI-like genes are transported via a common secretory system, which may be shared by all tip-growing cell types. Taken together, these observations indicate that the regulation of CWI via PTI-like genes has been well conserved in tip-growing cells from descendants of early land plants (such as *Marchantia*) to evolutionarily and developmentally derived flowering plants (such as *Arabidopsis*), despite the estimated independent evolution of both lineages for >470 my.

This conclusion is reflected by a notable degree of structural identity between the *AtMRI* and *MpPTI* amino acid sequences (Fig. 14). As the phylogenetic analyses of this study indicate, *AtMRI* and bryophytic PTI-like homologs from *Physcomitrella* and *Marchantia* all cluster in an *AtMRI*-like subgroup (Fig. 22). Thus, all these members share a higher sequence identity as compared to five further *AtPTI*-like homologs which cluster in a distinct group. Accordingly, *AtMRI* and its close homologs may represent the well-conserved successors of an ancient PTI-like genetic progenitor, which has been established early during land plant evolution (*i.e.* before bryophytes diverged from the lineage which gave rise to extant seed plants). Intriguingly, former research reported that neither one of the preferentially pollen-expressed *Arabidopsis* PTI-like homologs (*AtPTI1-2* (AT2G30740), *AtPTI1-3* (AT3G59350), *AtPTI1-4* (AT2G47060) and *AtPTI1-7* (AT2G43230)) were able to rescue the *mri*-induced male transmission defect (Liao et al., 2016). This may have several reasons: (i) The four *AtMRI*-like genes may represent more diverged PTI-like genes (*i.e.* their regulatory sites and domains may have been reconfigured during evolution). However, all PTI-like sequences analyzed in this study share a highly conserved serine-/threonine kinase domain, which includes an ultra-conserved STR-motif that is thought to be crucial for kinase function. Thus, such changes may have occurred elsewhere, *e.g.* in the N-terminal and C-terminal protein regions, neither of which have been extensively studied to date. (ii) The four *AtMRI*-like genes may have evolved to respond to different upstream regulators (*e.g.* they may be able to bind to a different set of proteins). This, in turn, could be the consequence of their adaptation to different biological functions. (iii) The moderate bootstrap value (50 %) at the junction between bryophytic PTI-likes and the *Arabidopsis* MRI-like group indicates that *MpPTI* and *AtMRI* may be structurally and functionally closer related than the cladogram suggests. This, in turn, is reflected by the fact that *AtMRI* and the closest *MpPTI* homolog AT2G30740 share comparable amino acid similarities to *MpPTI*, both on the whole protein level (76 and 79 %) and by only comparing their kinase domains (86 and 89 %) (Tab. S1), indicating the close structural identity of homologs of the MRI-like group (Fig. 22). Taken together, all these observations emphasize the close functional correlation and conservation between *MpPTI* and *AtMRI* regarding regulation of CWI during tip-growth.

According to the highly similar loss-of-function phenotypes observed for both, *MpPTI* and *AtMRI*, as well as their upstream regulators *MpTHE1* and *AtFER/AtANX1/AtANX2*, we expected to observe similar growth inhibitory phenotypes upon their overexpression in both, *Marchantia* and *Arabidopsis* wild-type tip-growing cells. Indeed, overexpression of all tested PTI-like (*AtMRI*, *MpPTI*) and MLR (*AtANX1*, *AtFER*) sequences led to growth inhibition (Fig. 18 - Fig. 20) further underpinning the conserved function of both gene subfamilies in tip-



growth control. One could argue, that PTI-likes, representing PM-localized proteins without extracellular domains that transduce intracellular signals, may have naturally been well conserved as they do not necessarily need to confer extracellular signal specificity. The extracellular domain of upstream-regulatory MLRs, in contrast, is thought to confer regulatory specificity via binding of different (sets of) ligands and co-factors such as RALFs and LRXs (Ge et al., 2017; Mecchia et al., 2017). The fact, that overexpression of both, *AtANX1* and *AtFER* (which govern distinct functions in *Arabidopsis* developmental and immunity signaling) leads to growth inhibition in *Marchantia* rhizoids may be explained by: (i) the high degree of structural similarity between *MpTHE1* and the MLR-subgroup comprised of *AtANX1/2* (59 % amino acid similarity) and its closest homolog *AtFER* (63 % amino acid similarity) (Tab. S2) or (ii) a lower stringency of the three *MpRALFs* as compared to the 36 family members in *Arabidopsis* (Murphy and De Smet, 2014), which may be able to bind to not only one, but several MLRs, as they may represent evolutionarily less derived RALF gene copies. Scenario (i) could be further tested by overexpression of (structurally and functionally) more distantly related *Arabidopsis* MLRs in *Marchantia* rhizoids, while scenario (ii) could be tested by comparison of the effects of *MpRALF* and *AtRALF*-treatment on tip-growth in *Arabidopsis* and *Marchantia*, as well as physical interaction assays between *MpRALFs* and *AtMLRs* and *vice versa*. Such future projects may also be helpful to link *MpTHE1* expression to further functions, possibly through differential gene regulation via tissue-/ cell type-specific *MpRALF* activity. To find such differential (tissue-specific) expression in *Marchantia* would not be surprising, given the fact that pleiotropic roles have been reported for *Arabidopsis* RALFs and MLRs (such as the function of RALF34 in THE1- and FER-dependent lateral root development (Gonneau et al., 2018) and putatively in paracrine induction of pollen tube rupture during fertilization via competition with RALF4/19 (Ge et al., 2017; Mecchia et al., 2017)).

The capability of bryophytic and spermatophytic MLR homologs, which evolved independently for >470 my, to trigger similar effects in different kinds of tip-growing cells also indicates that the general CW composition and principles of CW remodeling, are likely to share basic commonalities. This is based on the assumption, that MLRs confer extracellular cues to (intra)cellular responses, one outcome of which may be the alteration and remodeling of primary CW composition to fine-tune tip-growth control. Indeed, a series of common CW components (e.g. cellulose and a basic set of CW polysaccharides, including hemicellulose) and similarities in CW synthesis/remodeling (e.g. CESA activity, differential methyl esterification of homogalacturonans (such as pectins) in CW microdomains and their Ca<sup>2+</sup>-dependent crosslinking) has been described for different taxa throughout the plant kingdom, including charophycean green algae. Despite the fact, that our knowledge about

the evolution of land plant cell walls is still fragmentary, it has been hypothesized before that many cell wall components may have been established prior to the conquest of terrestrial environments by plants and elaborated to more specialized forms in response to specific evolutionary selection-pressures, often in a species- and tissue-specific manner (Sorensen et al., 2010).

It will be of great importance to learn, whether *MpPTI*<sup>[R240C]</sup> is capable of rescuing *Mpthe1*-induced loss of CWI in *Marchantia* rhizoids. This would demonstrate that *MpPTI* functions downstream of *MpTHE1* during *Marchantia* rhizoid growth, possibly via similar signal transduction mechanisms as known for RLK-mediated *Arabidopsis* PT and RH growth control. It would also demonstrate that the STR motif of PTI-likes represents a well-conserved regulatory site that is universally crucial for tip-growth control. If a similar rescue effect through *MpPTI*<sup>[R240C]</sup> will be observed in *Arabidopsis fer-4* root hairs and *amiRRALF4/19* pollen tubes, this would further underpin the high degree of evolutionary conservation between the described *Arabidopsis* and *Marchantia* CWI signaling module – which may have been universally conserved throughout land plant evolution (Fig. 37A).

### 5.1.1. The evolution of tip-growth – Homology or convergence?

Evolutionary developmental studies have a great potential to answer crucial questions regarding how regulatory genes, cell types or whole species evolved over time. One major question of plant evolution is to understand how early land plants adapted to the terrestrial habitat and its highly different environmental conditions. One example is the development of rooting cells to guarantee sufficient nutrient and water uptake from the substrate against the gravitropic vector. Against this background, one central question is how tip-growing cells such as rooting cells evolved: Two major concepts in evolutionary biology are the principles of homology and convergence. Homologous body plans arise from the same progenitor and thus are directly related to each other. Homologous structures can serve the same plesiomorphic (ancestral) purpose or fulfill apomorphic (derived) functions. An example is the evolution of floral organs in angiosperms which derive from and are homologous to leaves. On a microevolutionary scale, floral development is regulated by evolutionary related (homologous) genetic networks in related species (Dornelas and Dornelas, 2005). Convergence, in contrast, describes the independent evolution of similar body structures through similar selective pressure. Accordingly, convergent structures usually serve very similar functions, yet in distantly related species. One example for convergence on the

macroevolutionary level is the development of edible fruits to facilitate seed dispersal by herbivores (Lorts and Briggeman, 2008). However, such macroevolutionary principles have also been observed on the molecular level, an example being the convergent evolution of C4-photosynthesis which is thought to have evolved independently more than 40 times in distantly related taxa (Osborne and Beerling, 2006).

With respect to tip-growing cells, it has been reasoned that roots and rooting cells may have evolved independently for several times during land plant evolution. One major argument is the fact that (gametophytic) rhizoids and (sporophytic) root hairs are produced during different life phases of the plant and thus, may not be structurally correspondent (Scotland, 2010). Following this argumentation, similar selective pressures (*i.e.* the demand for water and nutrient uptake) may have fostered the evolution of anatomically alike, yet analogous structures, namely rhizoids and root hairs. Strikingly, the extinct rhyniophytes possessed rhizoids on both, the gametophyte and sporophyte, while some extant plant taxa, including monilophytes and lycophytes possess both, gametophytic rhizoids and sporophytic root hairs (Jones and Dolan, 2012). With this regard, separation by life phase does not necessarily exclude the possibility that the genetic program regulating rooting cell development may have been transferred from one life phase to the other.

Indeed, homologous genetic functions in rooting cell development across species have been described for several times (Menand et al., 2007 B; Hwang et al., 2010; Ito et al., 2014; Breuninger et al., 2016; Otani et al., 2018). In this study, it could be shown that *Marchantia* rhizoids, as well as *Arabidopsis* root hairs and pollen tubes all respond similarly to disruption and overexpression of PTI-like and MLR genes, which favors the scenario of homologous evolution. This would also suggest that PTI-like genes have been conserved as central regulators of tip-growth phase control across life phases and irrespectively of cell function. Based on the presented results, they may function in a conserved signaling module, comprised of MLRs, PTI-like genes and likely further up- and downstream components. The most likely scenario (Fig. 37B) that can be pictured based on these findings, is the establishment of a genetic signaling pathway or network that was used to regulate tip-growth and CWI integrity in early tip-growing cells such as gametophytic rhizoids. During the evolution of sporophyte dominance, the shift from an obligate gametophyte-dependent to a free-living lifestyle led to the demand of autonomous nutrition. Hence, rhizoid-like rooting cells developed at the sporophyte-substrate interface. Development and growth control of these rhizoid-like cells likely made use of a genetic program that was derived from gametophytic rhizoids and co-opted by the sporophyte. The fossil record of rhyniophytes may depict an early stage of this process. The sporophyte of the younger tracheophyte

lineage, comprised of lycophytes, monilophytes and seed plants, then developed multicellular water-conducting root tissues as a strategy for fast and efficient uptake of liquids. These roots developed root hairs for surface area extension, which supposedly conserved the genetic program used for gametophytic and sporophytic rhizoid growth control. Interestingly, rhizoids of leafy mosses possess multicellular rhizoids, while those of liverworts and hornworts are unicellular. Hence, it can be speculated that moss rhizoids might portrait early evolutionary tendencies towards root multicellularity. In the course of seed plant evolution, the gametophyte lost its free-living lifestyle and development of rhizoids became obsolete. This process went hand in hand with the evolution of targeted sperm delivery, which represented a major evolutionary advantage, as it guaranteed fertilization in a terrestrial habitat (*i.e.* in the absence of watery environments), as opposed to water-dependent delivery via free-swimming (flagellate) sperm. However, it required an efficient transport mechanism to actively deliver the non-flagellate male sperm cells to the female egg cell. The process was realized by development of pollen tubes (Rudall and Bateman, 2007), likely accompanied by a second co-option of the genetic tip-growth control module. The sole PTI-like homolog *MpPTI* may represent a comparatively ancient state of PTI-like genes in the last common ancestor of early-diverging land plants and seed plants. Hence, it may reflect the ancient structural and functional qualities of the PTI-like gene family. Following the hypothetical scenario described above, pollen tubes and rhizoids may be more distantly related structures, than it is true for rhizoids and root hairs. This is consistent with the observation that *MpPTI* expression in *Arabidopsis* is capable of rescuing defective root hair growth more efficiently (Fig. 17), than pollen tube growth (Fig. 15).

### 5.1.2. Future directions

#### **When did tip-growth control emerge?**

Rhizoids are thought to be one of the earliest tip-growing cells of land plants as they represent crucial adaptations to the terrestrial environment. However, the need for CWI sensing has already been present in algal progenitors of the first land plants. A recent study on the charophycean green alga *Closterium* demonstrates that the MLR homolog *CpRLK1* is necessary to facilitate fertilization via conjugatory papillae formation between two single-celled algae (Hirano et al., 2014). While it has not been shown that such papillae-formation is the result of tip-growth, *CpRLK1* represents the evolutionary most ancient CWI sensor in the streptophytic clade known to date. It will be interesting to learn whether CWI signaling in polarly growing algal structures already relied on the same regulatory module composed of a

MLR and a PTI-like. A promising approach towards that question would be the study of protonemata. In bryophytes, they represent the juvenile gametophyte, to some extent they resemble the morphology of filamentous green algae (including anisotropic growth) (Reski, 1998) and they have been demonstrated to expand by tip-growth (Menand et al., 2007 A). Thus, protonemata may resemble one of the earliest kinds of tip-growing cells which arose during land plant evolution. Accordingly, they may represent an additional promising model to study functional conservation of tip-growth control in land plants, which could be studied in the leafy moss *Physcomitrella patens*, for example. It will be exciting to learn whether growth regulators of rooting cell development, such as MLRs and PTI-likes can also be found in putatively even more ancient cell types.

### **How did tip-growth control evolve?**

Based on the observation that PTI-like and MLR homologs work in a conserved signaling module, it seems to be likely that further up- and downstream components (mainly known from research on *Arabidopsis*) may also play a role in CWI signaling of *Marchantia* rhizoids. This may include RALF peptides (3 homologs), LRXs (2 homologs), RBOHs (2 homologs), TOPPs (2 homologs) or CNGCs (5 homologs) (values obtained by pBlast with amino acid sequences of the respective *Arabidopsis* homologs RALF1, LRX8, RBOHH, AUN1 and CNGC14; pBlast performed on <https://phytozome.jgi.doe.gov> against the *M. polymorpha* 3.1 proteome using standard settings). Finding more common tip-growth regulators and understanding how they function on a mechanistic level would further aid our understanding of the role of CWI signaling in the first terrestrial plants and how it evolved afterwards.

### **Has tip-growth control evolved convergently during emergence of roots and seed-bearing plants?**

Phylogenetic and morphological analyses that consider both fossil data and extant species, strongly suggest that roots evolved (at least) twice during land plant evolution - once in the lycophyte and once in the euphyllophyte lineage (together building the tracheophyte taxon) (Friedman et al., 2004; Hetherington and Dolan, 2018), one distinguishing feature being the mode of root branching. This would mean that roots cannot be considered homologous structures throughout the land plant clade (Fig. 37B). Following this scenario, it can be assumed that (i) either the underlying genetic program regulating tip-growth differs significantly between euphyllophytes (such as *Arabidopsis*) and lycophytes as it evolved after the lycophyte-euphyllophyte split, or (ii) despite the convergent evolution of roots in both lineages, the same genes may have been co-opted analogously. Thus, future studies could include assessment of lycophyte PTI-like homologs, both structurally and functionally. A promising model may be *Selaginella moellendorffii*, as it possesses a fully sequenced

genome with at least 4 PTI-like homologs with a sequence identity in the range of 66 to 72 % to *AtMRI* (Values obtained by pBlast using *AtMRI* amino acid sequence as query; pBlast performed on <https://phytozome.jgi.doe.gov> against the *Selaginella moellendorffii* v1.0 proteome using standard settings). Such a study would aid our understanding on whether root hair growth control has been universally conserved in all tracheophytes (*i.e.* between leucophytes and euphyllophytes).

Interestingly, phylogenetic analyses indicate that the principle of siphonogamy (transfer of male sperm cells to female egg cells via pollen tubes) may have evolved convergently, as well – once in the angiosperm and once in the gymnosperm lineage (Doyle, 2006). Taken together, these findings indicate that land plant evolution may have frequently led to convergent evolution of alike structures in distinct lineages to adapt to the same environmental challenges. One of the main questions regarding these processes is whether such adaptations include similar regulatory genetic processes: Did convergent evolution of roots (and rooting cells), as well as siphonogamy (and pollen tubes), make use of homologous sets of genetic regulators?

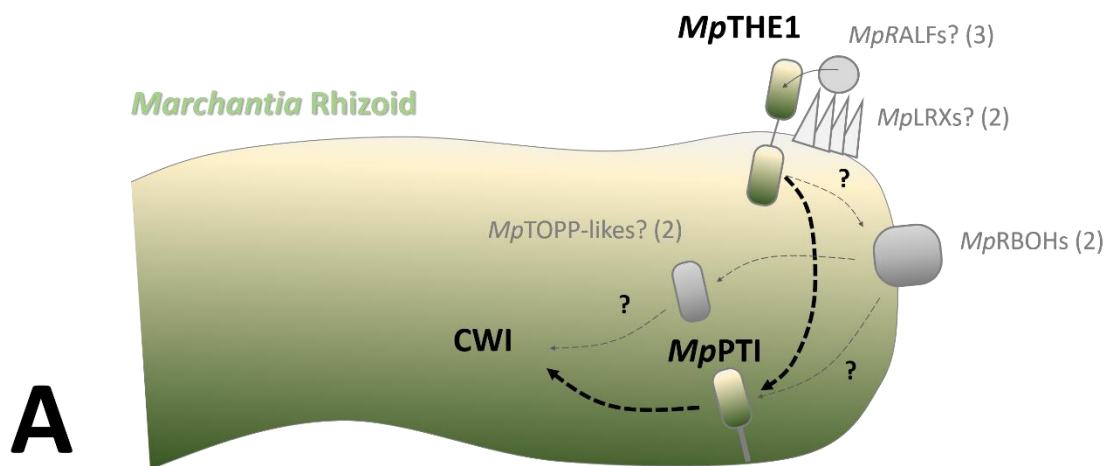
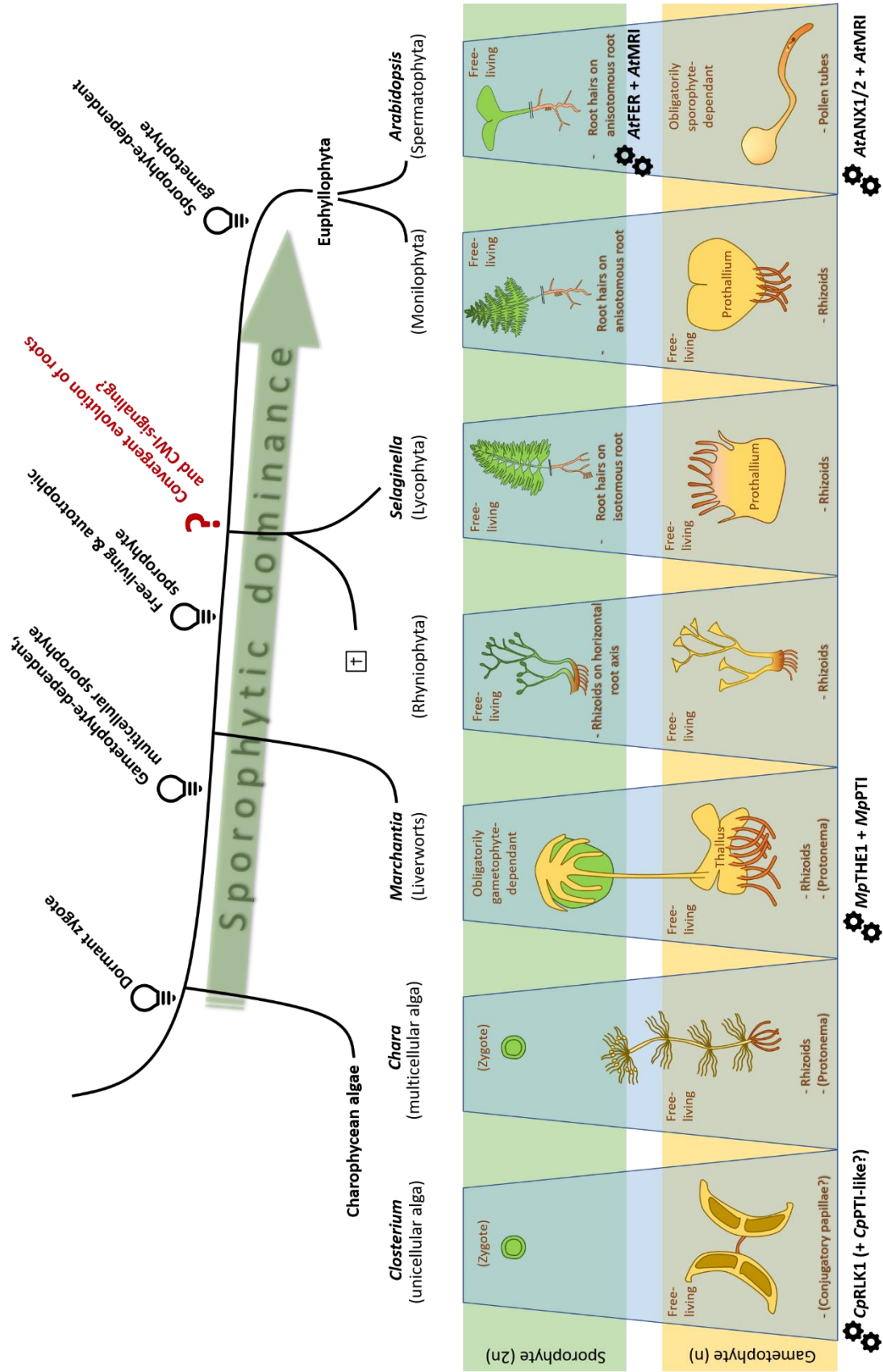


**Fig. 37: The evolution of tip-growth control.** (A) The conserved CWI signaling pathway in *Marchantia* rhizoids is comprised of *MpTHE1* and *MpPTI*. Further putative up- and downstream targets (based on the knowledge about *Arabidopsis* tip-growth control) are shown in gray. (B) see next page. A combined model of the evolution of land plants, roots and rooting cells and the sporophytic dominance, as well as underlying MLR and PTI-like genes for tip-growth control (based on the descriptions in section 5.1 to 5.3). The divergence times shown on the junction between two branches represent the median divergence time of all relevant studies (carried out on <http://timetree.org/>).



## 5.2. The protein phosphatases AUN1/2 negatively regulate MLR-mediated tip-growth control.

AUN1/2 are two type-one Ser/Thr-protein phosphatases (TOPP) which share 90 % sequence identity. The fact that the *aun1-1 aun2-1* double mutant, but neither of the four single mutants (*aun1-1*, *aun1-2*, *aun2-1* or *aun2-2*) reduce pollen germination *in vitro* (Fig. 25), indicates that AUN1/2 represent redundant negative regulators of tip-growth control in pollen tubes. The above-mentioned alleles truly impair function of AUN1/2, as could be proven by complementation of the growth inhibitory phenotype of *aun1-1 aun2-1* pollen (tubes) through pollen-specific expression of either AUN1-YFP (Franck et al., 2018 B) or AUN2-YFP (Fig. 26).

In contrast to the functional redundancy of AUN1/2 in pollen tubes, the *aun1-1* and *aun2-1* single mutants and the *aun1-1 aun2-1* double mutant displayed the same degree of growth inhibition in root hairs, suggesting that both genes regulate root hair growth in a non-redundant manner. The observation that *proAUN1* only drove expression in pollen, but not in root hairs, is unexpected, given the fact that the *AUN1* gene is significantly expressed in root tissue (Franck et al., 2018 B). However, it is consistent with the observation that the *MRI* gene (whose promoter was proven to be functional before (Boisson-Dernier et al., 2015)) is expressed approximately up to 10 times higher in the root elongation and early maturation zone, than found for *AUN1* (absolute maximal expression signals of 2665.21 (*MRI*) to 340.97 (*AUN1*); <http://bar.utoronto.ca/efp/cgi-bin/efpWeb.cgi>; 'Root' expression database of Brady et al., 2007). This would explain the absence of (visible) AUN1/2-YFP expression. Further explanations could be (i) the putatively insufficient promoter length of ~1.5 kb, which may allow for upregulation of expression in pollen, but not in root hairs, or (ii) the (random) insertion of the transformed protein fusion into genomic regions which are amenable to the intracellular expression machinery of pollen, but not of root hairs.

Finally, the growth-inhibitory effect on Col-0 wild-type pollen germination, together with the rescue of the pollen bursting phenotypes of *anx1-1 anx2-1*, *lrx8-11*, *amiRRALF4/19* and *rbohH-3 rbohJ-3* via expression of AUN1<sup>[D94N]</sup>-YFP, but not via its native form AUN1-YFP (Franck et al., 2018 B), shows that (i) AUN1/2 regulate pollen tube growth downstream of the ANX1/2-mediated CWI signaling pathway described before (Boisson-Dernier et al., 2013; Mecchia et al., 2017) and that (ii) AUN1/2 are negative regulators in this pathway, while AUN1<sup>[D94N]</sup> represents a dominant negative protein version. While the overactive protein version MRI<sup>[R240C]</sup> has been demonstrated before to rescue fertility of *anx1-1 anx2-1*, *rbohH*



*rbohJ* and *amiRRALF4/19* (Boisson-Dernier et al., 2015; Mecchia et al., 2017), the incapability of AUN<sup>[D94N]</sup>-YFP to rescue *mri-1*-induced male sterility shows that AUN1 does not control pollen tube CWI maintenance downstream of MRI (Franck et al., 2018 B; Fig. 38). One explanation may be that ANX1/2-mediated CWI signaling branches downstream of RBOHH/J. Thus, the MRI kinase and the AUN1/2 phosphatases may represent opposing factors which allow fine-tuning of the intracellularly transduced signal. It is conceivable that they may in fact target the same downstream elements. The incapability of MRI<sup>[R240C]</sup>-CFP to rescue *lrx8-11* sterility (Franck et al., 2018 B), while representing a downstream target of ANX1/2 (Boisson-Dernier et al., 2015) and RALF4/19 (Mecchia et al., 2017), may indicate that intracellular signal transduction via AUN1/2 and MRI may be differentially regulated by the extracellular LRX8-11-RALF4/19-ANX1/2-(BUPS1/2) receptor-ligand complex, possibly in dependence on the participation of a different combination of the single complex components. However, direct binding has only been demonstrated for some, but not all of the hypothetical complex partners. Thus, such simultaneous and/or differential binding would have to be tested in close detail and would require the analysis of MRI kinase/AUN1/2 phosphatase activity in response to extracellular complex formation.

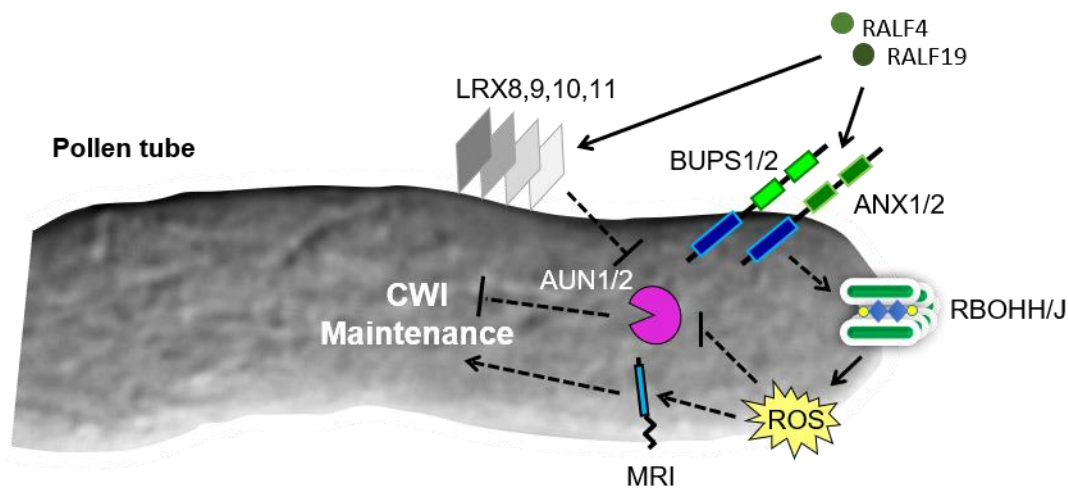


**Fig. 38: Schematic model of the pollen tube CWI signaling pathway including the hypothetical positions of AUN1/2.** The figure is based on the conclusions of section 5.2. and Franck et al., 2018 B and is shown as published by Franck et al., 2018 B.

### 5.2.1. AUN1/2 and their putative up- and downstream targets

#### **Antagonistic phosphatase- versus kinase signaling**

The results presented above strongly indicate that AUN1/2 and MRI are not part of a linear signaling pathway (Franck et al., 2018 B). In fact, it seems more likely that NADPH-dependent signaling leads to differential regulation of AUN1/2 and MRI activity in a parallel pathway, which may alter the phospho-state of a (common) target protein. Such subtle changes may allow fine-tuning of associated downstream processes such as the rate of vesicular secretion, CW remodeling, turgor-pressure and, ultimately, growth. Experimental strategies for the identification of such downstream targets may include (i) a forward genetic approach in form of a suppressor screen for rescue of *aun1 aun2*-induced growth inhibition or *mri*-induced loss of integrity phenotypes in pollen tubes or root hairs, (ii) phosphoproteomic studies which could identify downstream targets that may be differentially regulated, e.g. in response to treatment with (artificial) RALF4/19 peptides, (iii) a (co)immunoprecipitation of AUN1-YFP or MRI-YFP, to find physical interaction partners - representing putative downstream targets -, or (iv) a Yeast Two-hybrid(Y2H)-screen of an *Arabidopsis* cDNA library with AUN1 or MRI as bait.

#### **Inhibition of phosphatase activity via ROS**

Phosphatase activity is known to be directly regulated in a negative manner via ROS throughout eukaryotes (e.g. via modification of thiol residues of cystein) (reviewed by Apel and Hirt, 2004; Ray et al., 2012; Waszczak et al., 2018). AUN1/2 act genetically downstream of the ROS-producing NADPH oxidases RBOHH/J during tip-growth control (Franck et al., 2018 B). It is conclusive that AUN1/2 may be targeted via a similar ROS-dependent signaling process. It will be interesting to learn whether AUN1/2 function factually depends on ROS activity, e.g. via live-imaging of intracellular ROS dynamics or analysis of putative ROS-effects on pollen germination in presence or absence of AUN1/2. Interestingly, former research demonstrated that pharmacological protein phosphatase inhibition leads to increased ROS-production via RBOHH/J (Kaya et al., 2014), thus it may also be possible that AUN1/2 negatively feed back on RBOHH/J, instead of or in addition to signal transduction to further downstream constituents.

#### **Regulation of ion homeostasis**

It has been demonstrated several times that posttranslational modification of K<sup>+</sup>-channels and transporters via de-/phosphorylation is crucial for K<sup>+</sup>-channel activity and K<sup>+</sup>-affinity (reviewed by Wang and Wu, 2017). In rice (*Oryza sativa*), the MLR homolog RUPTURED

POLLEN (OsRUPO) interacts with potassium transporters (OsHAKs) to regulate pollen tube growth (Liu et al., 2017), but a link between RLK-mediated tip-growth control and potassium signaling remains to be discovered. It is an intriguing question, whether tip-growth control in the *Arabidopsis* pollen tube (or root hair) relies on similar interactions between ANX1/2 (or FER) and AtHAKs and, if so, whether antagonistic kinase/phosphatase signaling (e.g. via MRI and AUN1/2) may fine-tune K<sup>+</sup>-channel activity.

An inverse scenario may be the targeting of AUN1/2 (*i.e.* its regulatory subunit(s)) via cation (Ca<sup>2+</sup>- and K<sup>+</sup>-) dependent proteins, possibly in response to changes in trans-PM cation flux via channel or transporter proteins. A direct or indirect influence of Ca<sup>2+</sup>-signaling on type-one protein phosphatase activity remains to be tested, but has been described for other phosphatase classes. Prominent examples are direct targeting of the Ca<sup>2+</sup>-dependent phosphatase calcineurin or indirect regulation through Ca<sup>2+</sup>-dependent Calmodulin activity (review by Bush, 1995; Ermak and Davies, 2002; Hashimoto and Kudla, 2011; Kudla et al., 2018). Based on the intracellular Ca<sup>2+</sup>- and growth irregularities observed in *rbohH rbohJ* (Franck et al., 2017), *mri-2* and *cngc18-17* pollen tubes (this study; see section 4.3.4), it can be assumed that RLK-dependent CWI signaling relies on integration and close regulation of intracellular Ca<sup>2+</sup>-dynamics. Consequently, further research on the mechanistic integration of AUN1/2 into the CWI pathway could include assessment of Ca<sup>2+</sup>-signatures in loss-of-function or overexpression mutants (e.g. via crossing of a YC3.60 expression line with an *aun1 aun2* mutant line). It will be fascinating to learn if AUN1/2 are part of the Ca<sup>2+</sup>-responsive branch of RLK-mediated tip-growth control, and, if so, how Ca<sup>2+</sup>-signaling is generally integrated in negative regulation of tip-growth.

### 5.3. Do CNGCs regulate the tip-focused $\text{Ca}^{2+}$ -gradient in response to RLK-mediated CWI signaling?

The loss of CWI phenotype observed in three independent CNGC18 loss-of-function-/knockdown mutants confirms its crucial role as a positive regulator of CWI maintenance during pollen tube growth (Fig. 27). The fact, that loss of function of root hair-expressed CNGC14 leads to comparable phenotypic defects during root hair growth (Zhang et al., 2017) indicates the functionally conserved role of CNGCs in tip-growth control. In accordance to the loss-of-function phenotypes described before, overexpression of CNGC18 leads to growth inhibition in *Arabidopsis* wild-type pollen tubes (Fig. 29). Taken together, these results show that CNGC18 is a positive regulator of tip-growth control in *Arabidopsis* pollen tubes.

The strong phenotypic resemblance upon loss of function of CNGC18, MRI (Fig. 27, Fig. 30 and Fig. 31) and further CWI regulators such as RBOHH/J and ANX1/2 prompted us to investigate a potential role of CNGC18 in RLK-mediated CWI signaling in the growing *Arabidopsis* pollen tube. Indeed, expression of GFP-CNGC18 under *proACA9* in the *anx1-1/anx1-1 anx2-1/ANX2* mutant was capable of rescuing male transmission of the *anx2-1* allele (Tab. 26), supporting the hypothesis that CNGC18 controls  $\text{Ca}^{2+}$ -homeostasis downstream of ANX1 in a common pollen tube CWI pathway. It is intriguing, that the expression of YFP-CNGC18 under *proLAT52* did not lead to a corresponding rescue effect (Tab. 24). As the analysis of *in vitro* pollen germination revealed, *proLat52::YFP-CNGC18* seemed to impede pollen tube growth, as indicated by the absence of YFP-fluorescence in intact pollen tubes of *anx1-1/anx1-1 anx2-1/ANX2* plants hemizygotously expressing YFP-CNGC18 (Fig. 32). This observation is surprising, as the functionality of *proLAT52* in other models, including *Arabidopsis*, has been demonstrated many times (e.g. Twell et al., 1990; Franck et al., 2018 B). Possible explanations may be: (i) a technical error, e.g. in the *proLat52::YFP-CNGC18* sequence or the expression vector, which will need to be tested by verification of the vector nucleotide sequence, (ii) protein-misfolding or mislocalization, the latter of which could only be tested in the presence of transgenic pollen tubes expressing YFP-CGNC18 (which could not be observed). (ii) Given the existence of three further pollen-expressed CNGC7/8/16, it is reasonable that CNGC18 may not be the (only)  $\text{Ca}^{2+}$ -channel acting in a RLK-mediated CWI signaling pathway in the growing *Arabidopsis* pollen tube. However, it seems unlikely, that another pollen-expressed CNGC regulates pollen tube CWI (in a RLK-mediated manner): CNGC16 was described to be important for heat and drought stress tolerance during pollen development (Tunc-Ozdemir, 2013 B), but not for pollen tube

growth *per se*. CNGC7-GFP was described to localize to the flanks of the growing pollen tube (Tunc-Ozdemir et al., 2013 A), not the apical PM. Thus, it is improbable, that CNGC7/8 (both of which share the highest sequence identity of 74 % amongst *Arabidopsis* CNGCs) mediate a tip-focused calcium influx. Despite these observations, it cannot be excluded, that  $\text{Ca}^{2+}$ -mediated tip-growth control requires more than one  $\text{Ca}^{2+}$ -channel or transporter. With this respect it is also noteworthy that CNGCs are thought to function in tetramers. It is thus possible, that tip-growth control requires heterotetrameric CNGC-formations.

### 5.3.1. Alternative models for RLK-dependent and -independent $\text{Ca}^{2+}$ -signaling

#### **NADPH-oxidases may induce positive, $\text{Ca}^{2+}$ -dependent feedback signaling.**

ROS-producing NADPH oxidases of the RBOH subfamily possess  $\text{Ca}^{2+}$ -binding EF-hand motifs. Both, presence of  $\text{Ca}^{2+}$  and functionality of EF-hand motifs, were demonstrated to be necessary for oxidase activity (Kaya et al., 2009) and may thus be targeted via one or several  $\text{Ca}^{2+}$ -channels such as CNGCs. Irrespective of CNGC18 being the predominant  $\text{Ca}^{2+}$ -channel regulating CWI maintenance in response to RLKs or not, the ability of RBOHH/J to bind and respond to  $\text{Ca}^{2+}$  would support a model in which RLK-mediated signal transduction activates a  $\text{Ca}^{2+}$ -channel to regulate  $\text{Ca}^{2+}$ -influx, while changes in intracellular  $\text{Ca}^{2+}$ -concentrations feed back to RBOHH/J to regulate their activity. This would explain, why we see irregular  $\text{Ca}^{2+}$ -signatures and growth behavior not only in *cngc18-17* (*i.e.* the  $\text{Ca}^{2+}$ -channel mutant itself), but in all of its putative upstream regulators analyzed so far. It would also represent an explanation for the incapability to rescue loss of CWI through abundant expression of CNGC18 under a strong promoter such as *proLAT52*. Assuming a positive feedback loop between RBOHH/J and CNGC18, such abundant expression of CNGC18 may lead to excessive ROS-production via RBOHH/J, which may alter downstream activity and, in turn, imbalance control of CWI maintenance. To further test the dose dependency of CNGC18 and  $[\text{Ca}^{2+}]_{\text{cyt.}}$ , follow-up experiments could include assessment of the influence of different extracellular  $\text{Ca}^{2+}$ -concentrations on *in vitro* pollen germination in both, CNGC18 loss-of-function lines and overexpression lines in the mutant backgrounds described before. This may aid our understanding of how and to what extent  $\text{Ca}^{2+}$  influences CWI maintenance, both, in response to and absence of CNGC18. If it is true, that RBOHH/J are the junction of positive  $\text{Ca}^{2+}$ -dependent feedback, one would also expect absence of irregular  $\text{Ca}^{2+}$ -dynamics in a knockdown mutant of upstream effectors, such as ANX1/2, RALF4/19 or LRX8-11, which could be tested via ratiometric  $\text{Ca}^{2+}$ -imaging. However, such

experiments are difficult to be conducted in strong loss-of-function mutants such as *anx1* *anx2*, given their early loss of CWI phenotype upon pollen germination (Boisson-Dernier et al., 2013). It will be interesting to learn, whether CNGC18 acts in a common CWI signaling pathway as RBOHH/J and its upstream regulators.

**The function of CNGCs may be modulated by a (trans)membrane multi-protein complex.**

Recently, it has been demonstrated, that not only the MLRs ANX1/2 regulate pollen tube CWI in response to RALFs, but that signaling relies on further constituents, namely the two MLRs BUPS1/2 and the LRR-extensin chimera LRX8-11, all of which may interact in a multi-protein complex at the interface between extracellular signal perception and transmembrane signal transduction (Ge et al., 2017; Mecchia et al., 2017). It is conceivable that this multi-protein complex may represent a molecular switch which directs CWI signaling into different ways, possibly via steric antagonism in the complex and/or binding of different ligands (such as RALFs), as it was suggested before (Ge et al., 2017). Thus, it may not be unlikely, that such differential (*i.e.* 'early-branching') signaling may regulate CNGC18 activity independently from certain complex partners, such as ANX1/2. To test this, one could assess, whether CNGC18 overexpression can restore male fertility in *lrx8-11*, *bups1 bups2* or *ralf4 ralf19* loss-of-function mutants.

**Tip-growth control may rely on an interplay of ion channels, together with Ca<sup>2+</sup>-responsive cytosolic regulators.**

*Medicago truncatula* (*Mt*) CNGC15, ortholog to *At*CNGC15, has been demonstrated to physically interact with the K<sup>+</sup>-permeable channel *Mt*DMI1 at the nuclear envelope to modulate Ca<sup>2+</sup>-oscillations and subsequently mediate plant-bacterial symbiosis. Interestingly, *Mt*DMI1 functionality is required for regular Ca<sup>2+</sup>-oscillations. Furthermore, it could be demonstrated via mathematical modeling that the combination of a CNGC, a K<sup>+</sup>-channel and a Ca<sup>2+</sup>-ATPase is able and sufficient to modulate Ca<sup>2+</sup>-oscillations *in silico*, which are equivalent to those observed in plant cells (Charpentier et al., 2016). A similar interaction of a CNGC and a K<sup>+</sup>-channel, possibly together with further ion transport proteins, may be conceivable for the regulation of transmembrane Ca<sup>2+</sup>-flux and cytosolic Ca<sup>2+</sup>-oscillations in tip-growing cells. Several *Arabidopsis* CPKs were shown to phosphorylate K<sup>+</sup>-channels to regulate K<sup>+</sup>-influx and control stomatal opening, both in a Ca<sup>2+</sup>-dependent (Corratge-Faillie et al., 2017) and -independent manner (Ronzier et al., 2014). Interestingly, it has also been shown that the calcium-dependent kinase 32 (CPK32) interacts with and activates CNGC18 to promote pollen tube growth (Zhou et al., 2014). CPK32 overexpression was furthermore described to lead to a swollen pollen tube apex (Zhou et al., 2014), just like observed for

several other tip-growth regulators before (e.g. *AtROP1* (Li et al., 1999; Gu et al., 2005; Hwang et al., 2010) or PTI-likes (see section 4.1.3)). Taken together, these observations may well point to a model in which CNGC18-mediated  $\text{Ca}^{2+}$ -influx regulates  $\text{K}^{+}$ -channel activity via CPKs, while CNGC18-activity itself is fostered by a positive feedback loop through  $\text{Ca}^{2+}$ -activated CPK32.  $\text{Ca}^{2+}$ - and anion homeostasis may be functionally connected, as anion channels have been demonstrated to be recruited to the pollen tube apex in a  $\text{Ca}^{2+}$ - and CPK2/6/20-dependent manner, while  $\text{Ca}^{2+}$ - and anion channels have been suggested to oscillate in an antagonistic pattern (Gutermuth et al., 2018). Imbalance between CNGC-, CPK- and downstream target activity may explain why the equilibrium between  $\text{Ca}^{2+}$ - and growth dynamics collapses in the *cngc18-17* mutant. It will be interesting to learn whether or not  $\text{Ca}^{2+}$ -flux, mediated by  $\text{Ca}^{2+}$ -permeable channels such as CNGCs, may target (further) ion channels to control maintenance of cytosolic turgor pressure and tip-growth control.

Another layer of  $\text{Ca}^{2+}$ -signaling regulation could be the indirect autoinhibition of CNGC18 via  $\text{Ca}^{2+}$ -binding CaM. It has been recently demonstrated that CaM is able to physically interact with the C-terminus of most of the 20 *Arabidopsis* CNGCs, including RH- and PT-expressed CNGC6/9/14/18 (Fischer et al., 2017). Furthermore, CNGC2/4 and the  $\text{Ca}^{2+}$ -ATPases ACA8/10 are known to be common targets of CaM-binding in plant immunity signaling. Whereas CNGC-mediated  $\text{Ca}^{2+}$ -influx leads to an (auto)-inhibitory effect on CNGC2/4 via  $\text{Ca}^{2+}$ /CaM-binding,  $\text{Ca}^{2+}$ -efflux is promoted via ACA8/10-activation through  $\text{Ca}^{2+}$ /CaM, in turn negatively feeding back on CaM-activity (Hua et al., 2003; Cheval et al., 2013). A similar mode of action could be envisioned for CNGC18/ACA9-mediated tip-growth control in the *Arabidopsis* pollen tube, however, such interaction remains to be tested.

The information and ideas discussed in this section (5.3.1) have been summarized in a putative model explaining how CNGC18 may be linked to CWI signaling and the intracellular growth machinery in pollen tubes (Fig. 39).

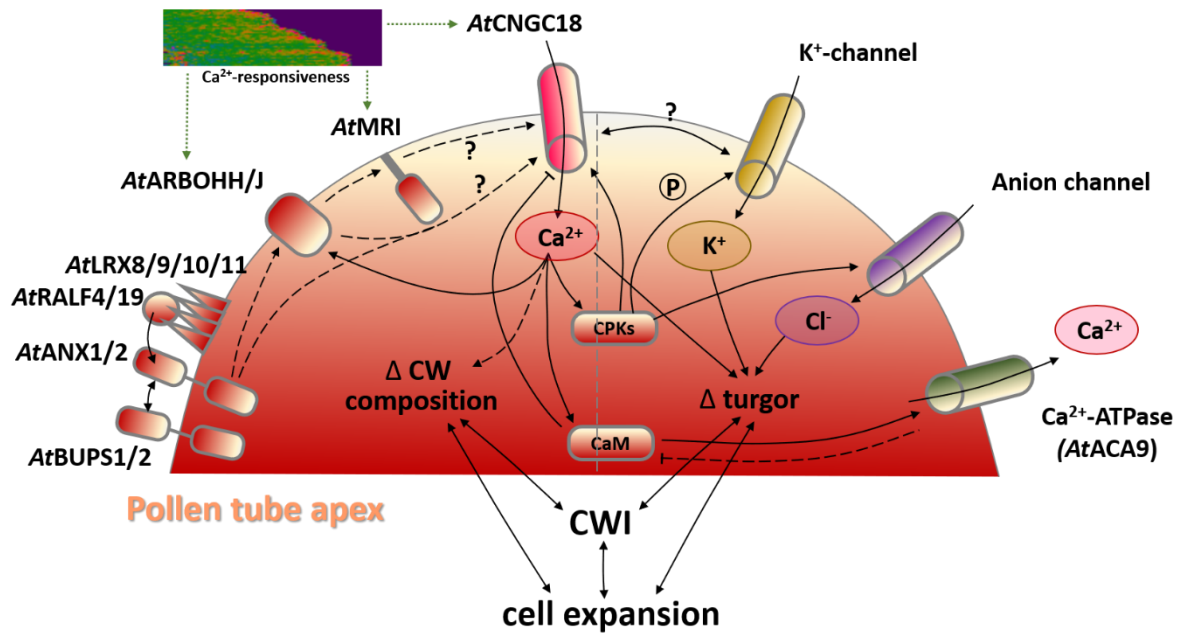


**Fig. 39: How may CNGCs and  $\text{Ca}^{2+}$ -dynamics be connected to CWI signaling and tip-growth control?** Shown is a model depicting possible links between CNGC-mediated  $\text{Ca}^{2+}$ -flux and putative up- and downstream regulators. The model is based on the descriptions of sections 5.3. and 5.3.1. Dashed arrows: Genetic/indirect interaction; Continuous arrows: physical/direct interaction; double-arrows: Binding or mutual dependence.



#### 5.4. May Rho-GTPases be the missing link between the establishment of pollen tube polarity and the Ca<sup>2+</sup>-dependent regulation of growth speed?

Results from several independent *in vitro* pollen germination experiments clearly indicate that *AtROP1* overexpression abolishes tip-focused growth in pollen tubes leading to enlarged pollen tube tips (Li et al., 1999; Gu et al., 2005; Hwang et al., 2010). Similarly, overexpression of either *PpROP2* or its guanine exchange factor *PpRopGEF3* induces loss of anisotropic growth behaviour and inflation of apical protonema cells in *Physcomitrella*, while overexpression of *PpROP2* additionally leads to malformation of protonemal cross walls (Ito et al., 2014). This strongly reminds of the role of ROPs in regulation of cell polarization and asymmetric cell division of stomatal cells in maize (*Zea mays*) (Humphries et al., 2011). Altogether, these findings support a general, functionally conserved role of ROPs in establishment of polarity. It is conclusive that *AtROP1* is crucial for the determination of a defined polar growth region in the *Arabidopsis* pollen tube and that establishment and maintenance of such a region may be strongly dose-dependent. Interestingly, *AtROP1* depletion via anti-*AtROP1* antibodies was shown to lead to disruption of the tip-localized Ca<sup>2+</sup>-influx and tip-focused Ca<sup>2+</sup>-gradient (Li et al., 1999), which is known to be crucial for steady tip-growth (e.g. Franck et al., 2017; this study, see section 4.3.4). Such influx was shown to be mediated by CNGCs (e.g. Leng et al., 1999). It was hypothesized before that a ROP1-governed regulatory pathway may couple the determination of tip-growth sites with the regulation of growth speed via Ca<sup>2+</sup>-influx (Li et al., 1999). Consequently, pollen tube growth and CWI may be regulated in a common signaling pathway that incorporates both, Rho-like GTPases such as *AtROP1* and Ca<sup>2+</sup> influx channels such as CNGCs.

With this respect, it is remarkable that overexpression of the PTI-like genes *MpPTI* and *AtMRI* in the Col-0 wild-type background led to the same (partial) depolarization phenotypes as described for *AtROP1*. Furthermore, *mri-2* pollen tubes were found to display similar irregular Ca<sup>2+</sup>-oscillations as *cngc18-17* pollen tubes (this study). One explanation for these commonalities might be that CNGCs and PTI-like genes may interact with ROPs to synchronize both, the establishment of pollen tube polarity and the Ca<sup>2+</sup>-dependent regulation of growth speed. This assumption goes along with the observation that tip-growing cells share a common set of regulatory components and processes (including ROP- and Ca<sup>2+</sup> -signaling (Palanivelu and Preuss, 2000)). Interestingly, in *Fusarium*, low Ca<sup>2+</sup> concentrations have been demonstrated to directly influence cell polarity by induction of

hyphal branching (Robson et al., 1991), reminding of the *Arabidopsis* pollen tube phenotypes observed upon expression of *MpPTI* (Fig. 15).

Based on this knowledge, interesting future experiments could include: (i) the study of intracellular  $\text{Ca}^{2+}$ -dynamics in tip-growing cells of *AtROP1* mutants and comparison with known  $\text{Ca}^{2+}$ -associated mutants of the PTI-like-, RBOH- or CNGC subfamilies (Franck et al., 2017; this study), (ii) Genetic and physical interaction tests between ROPs and known tip-growth regulatory genes in *Arabidopsis*: The *CrRLK1L* member FER is known to physically interact with *AtROP2* and RopGEFs to control root hair growth and CWI (Duan et al., 2010). It is imaginable, that *Arabidopsis* *CrRLK1L*s, PTI-like RLCKs and/or CNGCs interact via intermediary signaling components, such as ROPs, to control tip-growth. Findings on similar ROP functions throughout land plants may indicate that tip-growing cells share a common RLK/ROP-governed signaling mechanism.

## 5.5. VEIVE does not exert an obvious pollen-specific function during plant reproduction.

VEI is an *Arabidopsis* RLCK homolog, which is encoded by locus AT2G07180. It was shown before to be strongly pollen-expressed (Wang et al., 2008), as supported by the presented eFP expression profile (Fig. 33). RLCKs are known to be important downstream regulatory proteins in various processes, including the role of PTI-likes in both, pollen tube, root hair and rhizoid growth (Boisson-Dernier et al., 2015; this study) or the roles of RIPK and BIK1 in plant defense (Lu et al., 2010; Liu et al., 2011; reviewed by Franck et al., 2018 A). Despite the mild seed set reduction in ripe *vei-1* and *vei-2* siliques (Fig. 36), no obvious irregularities and defects in pollen germination or premature loss of CWI could be observed *in vitro* (Fig. 35). This may be in agreement with the absence of strong upregulation of VEI gene expression upon pollen germination or pollen tube growth (Wang et al., 2008). However, an earlier developmental function of VEIVE, *i.e.* in pollen development and viability, is highly unlikely, as pollen was shown to germinate normally *in vitro*. The mild decrease of seed set (Fig. 36) and moderate decrease of transmission efficiency observed for both *vei-1* and *vei-2* (Tab. 27), however, could point towards a function later during reproduction, (*e.g.* in pollen tube guidance or fertilization). Thus, future phenotyping experiments could focus on the study of pollen tube growth and perception in a (semi-) *in vivo*-system.

According to the TAIR10 annotations, VEI has two splice variants (AT2G07180.1 = VEI.1 and AT2G07180.2 = VEI.2). However, the T-DNAs of both, *vei-1* and *vei-2*, insert in the coding sequence of VEI, while VEI.1 and VEI.2 only differ in the presence of an intron that inserts in the 5'-UTR. Thus, protein function should be equally affected in both splice variants. A phylogenetic analysis of type-VII RLCKs that was published earlier on indicates that VEI has a sister gene, AT5G01020 (Ranf et al., 2014), with moderate sequence identity of 67.8 % on the amino acid level. However, neither AT5G01020, nor any of the 9 closest VEIVE homologs in *Arabidopsis* appeared to be highly expressed in pollen (Tab. 28). Thus, functional redundancy to a close VEI homolog, which might compensate for putative *vei-1/2*-induced phenotypic defects, is unlikely. Nevertheless, a future experiment could include the generation of a complementary microRNA line to exclude such possibility. An alternative would be the generation of a double mutant with its closest homolog AT5G01020.

## 6. SUPPLEMENTAL FIGURES AND TABLES

**Tab. S1: The 10 closest *MpPTI* homologs of *Arabidopsis thaliana*.** Shown is the output of a pBlast using the *MpPTI* (Mapoly0051s0094) amino acid sequence as query against the Araport11 transcript database (carried out on <https://www.arabidopsis.org/Blast/> using standard settings). (A) Comparison of full length amino acid sequences; (B) Comparison of kinase domain only.

(A) Full length amino acid sequences			
Gene	% identity	% similarity	E-value
AT2G30740	70	79	e-147
AT3G59350	69	79	e-145
AT2G43230	69	79	e-144
AT2G47060	69	77	e-143
AT1G06700	68	77	e-141
AT3G17410	73	81	e-141
AT3G62220	67	78	e-141
AT1G48210	67	76	e-138
AT2G30730	69	82	e-133
<b>AT2G41970 (AtMRI)</b>	64	76	e-133
(B) Kinase domain amino acid sequences			
Gene	% identity	% similarity	E-value
AT2G43230	81	89	e-137
AT3G59350	80	89	e-137
AT2G30740	81	88	e-137
AT1G06700	81	88	e-136
AT3G17410	81	87	e-134
AT2G47060	79	86	e-130
AT3G62220	77	86	e-129
AT1G48210	77	85	e-128
AT2G30730	74	85	e-126
<b>AT2G41970 (AtMRI)</b>	73	86	e-124

**Tab. S2: The 10 closest *MpTHE1* homologs of *Arabidopsis thaliana*.** Shown is the output of a pBlast using the *MpTHE1* (Mapoly0869s0001.1) amino acid sequence as query against the Araport11 transcript database (carried out on <https://www.arabidopsis.org/Blast/> using standard settings).

Gene	% identity (length of homology)	% similarity	E-value
AT5G54380 (THESEUS1)	47 (403/853)	60	0
<b>AT3G51550 (FERONIA)</b>	48 (390/803)	63	0
AT5G61350 (ERULUS/CAP1)	47 (384/808)	60	0
AT3G46290 (HERK1)	46 (359/778)	61	0
AT5G59700	46 (353/765)	61	0
AT2G21480 (BUPS2)	46 (362/779)	60	0
AT1G30570 (HERK2)	47 (344/731)	61	0
AT4G39110 (BUPS1)	46 (362/786)	59	0
<b>AT5G28680 (ANX2)</b>	45 (368/802)	59	0
<b>AT3G04690 (ANX1)</b>	45 (360/791)	59	0

## 7. REFERENCES

- Althoff, F., Kopischke, S., Zobell, O., Ide, K., Ishizaki, K., Kohchi, T., & Zachgo, S. (2014). Comparison of the MpEF1 $\alpha$  and CaMV35 promoters for application in *Marchantia polymorpha* overexpression studies. *Transgenic research*, 23(2), 235-244.
- Ambrose, B. A., & Purugganan, M. D. (Eds.). (2012). *Annual Plant Reviews, The Evolution of Plant Form* (Vol. 45). John Wiley & Sons.
- Anthony, R. G., Henriques, R., Helfer, A., Meszaros, T., Rios, G., Testerink, C., ... & Bögre, L. (2004). A protein kinase target of a PDK1 signalling pathway is involved in root hair growth in *Arabidopsis*. *The EMBO journal*, 23(3), 572-581.
- Anthony, R. G., Khan, S., Costa, J., Pais, M. S., & Bögre, L. (2006). The *Arabidopsis* protein kinase PTI1-2 is activated by convergent phosphatidic acid and oxidative stress signaling pathways downstream of PDK1 and OXI1. *Journal of Biological Chemistry*, 281(49), 37536-37546.
- Apel, K., & Hirt, H. (2004). Reactive oxygen species: metabolism, oxidative stress, and signal transduction. *Annu. Rev. Plant Biol.*, 55, 373-399.
- Bateman, R. M., Crane, P. R., DiMichele, W. A., Kenrick, P. R., Rowe, N. P., Speck, T., & Stein, W. E. (1998). Early evolution of land plants: phylogeny, physiology, and ecology of the primary terrestrial radiation. *Annual Review of Ecology and Systematics*, 29(1), 263-292.
- Baumberger, N., Ringli, C., & Keller, B. (2001). The chimeric leucine-rich repeat/extensin cell wall protein LRX1 is required for root hair morphogenesis in *Arabidopsis thaliana*. *Genes & development*, 15(9), 1128-1139.
- Baumberger, N., Doesseger, B., Guyot, R., Diet, A., Parsons, R. L., Clark, M. A., ... & Keller, B. (2003). Whole-genome comparison of leucine-rich repeat extensins in *Arabidopsis* and rice. A conserved family of cell wall proteins form a vegetative and a reproductive clade. *Plant physiology*, 131(3), 1313-1326.
- Bedinger, P. (2018). Coordinating Cell Walls and Cell Growth: A Role for LRX Extensin Chimeras. *Plant physiology*, 176(3), 1890-1891.
- Bernal, A. J., Yoo, C. M., Mutwil, M., Jensen, J. K., Hou, G., Blaukopf, C., ... & Willats, W. G. (2008). Functional analysis of the cellulose synthase-like genes CSLD1, CSLD2, and CSLD4 in tip-growing *Arabidopsis* cells. *Plant Physiology*, 148(3), 1238-1253.
- Bibikova, T. N., Jacob, T., Dahse, I., & Gilroy, S. (1998). Localized changes in apoplastic and cytoplasmic pH are associated with root hair development in *Arabidopsis thaliana*. *Development*, 125(15), 2925-2934.
- Bischler, H. (1986). *Marchantia polymorpha* L. s. lat. karyotype analysis. *Journal of the Hattori Botanical Laboratory*.

- Boavida, L. C., & McCormick, S. (2007). TECHNICAL ADVANCE: Temperature as a determinant factor for increased and reproducible in vitro pollen germination in *Arabidopsis thaliana*. *The Plant Journal*, 52(3), 570-582.
- Bogdanove, A. J., & Martin, G. B. (2000). AvrPto-dependent Pto-interacting proteins and AvrPto-interacting proteins in tomato. *Proceedings of the national academy of sciences*, 97(16), 8836-8840.
- Boisson-Dernier, A., Roy, S., Kritsas, K., Grobei, M. A., Jaciubek, M., Schroeder, J. I., & Grossniklaus, U. (2009). Disruption of the pollen-expressed FERONIA homologs ANXUR1 and ANXUR2 triggers pollen tube discharge. *Development*, 136(19), 3279-3288.
- Boisson-Dernier, A., Lituiev, D. S., Nestorova, A., Franck, C. M., Thirugnanarajah, S., & Grossniklaus, U. (2013). ANXUR receptor-like kinases coordinate cell wall integrity with growth at the pollen tube tip via NADPH oxidases. *PLoS biology*, 11(11), e1001719.
- Boisson-Dernier, A., Franck, C. M., Lituiev, D. S., & Grossniklaus, U. (2015). Receptor-like cytoplasmic kinase MARIS functions downstream of CrRLK1L-dependent signaling during tip growth. *Proceedings of the National Academy of Sciences*, 112(39), 12211-12216.
- Bosch, M., & Hepler, P. K. (2005). Pectin methylesterases and pectin dynamics in pollen tubes. *The Plant Cell*, 17(12), 3219-3226.
- Bowman, J. L., Kohchi, T., Yamato, K. T., Jenkins, J., Shu, S., Ishizaki, K., ... & Adam, C. (2017). Insights into land plant evolution garnered from the *Marchantia polymorpha* genome. *Cell*, 171(2), 287-304.
- Brady, S. M., Orlando, D. A., Lee, J. Y., Wang, J. Y., Koch, J., Dinneny, J. R., ... & Benfey, P. N. (2007). A high-resolution root spatiotemporal map reveals dominant expression patterns. *Science*, 318(5851), 801-806.
- Brand, A. C., Morrison, E., Milne, S., Gonias, S., Gale, C. A., & Gow, N. A. (2014). Cdc42 GTPase dynamics control directional growth responses. *Proceedings of the National Academy of Sciences*, 111(2), 811-816.
- Breuninger, H., Thamm, A., Streubel, S., Sakayama, H., Nishiyama, T., & Dolan, L. (2016). Diversification of a transcription factor family led to the evolution of antagonistically acting genetic regulators of root hair growth. *Current biology*, 26(12), 1622-1628.
- Brewbaker, J. L., & Kwack, B. H. (1963). The essential role of calcium ion in pollen germination and pollen tube growth. *American Journal of Botany*, 50(9), 859-865.
- Burkart, G. M., Baskin, T. I., & Bezanilla, M. (2015). A family of ROP proteins that suppress actin dynamics and are essential for polarized growth and cell adhesion. *J Cell Sci*, jcs-172445.
- Bush, D. S. (1995). Calcium regulation in plant cells and its role in signaling. *Annual review of plant biology*, 46(1), 95-122.
- Cai, G., Faleri, C., Del Casino, C., Emons, A. M. C., & Cresti, M. (2011). Distribution of callose synthase, cellulose synthase, and sucrose synthase in tobacco pollen tube is

controlled in dissimilar ways by actin filaments and microtubules. *Plant Physiology*, 155(3), 1169-1190.

Cai, G., Parrotta, L., & Cresti, M. (2015). Organelle trafficking, the cytoskeleton, and pollen tube growth. *Journal of integrative plant biology*, 57(1), 63-78.

Cai, G., & Cresti, M. (2008). Organelle motility in the pollen tube: a tale of 20 years. *Journal of experimental botany*, 60(2), 495-508.

Camacho, L., & Malhó, R. (2003). Endo/exocytosis in the pollen tube apex is differentially regulated by Ca<sup>2+</sup> and GTPases. *Journal of Experimental Botany*, 54(380), 83-92.

Candéo, A., Doccia, F. G., Valentini, G., Bassi, A., & Costa, A. (2017). Light sheet fluorescence microscopy quantifies calcium oscillations in root hairs of *Arabidopsis thaliana*. *Plant and Cell Physiology*, 58(7), 1161-1172.

Cárdenas, L., Lovy-Wheeler, A., Wilsen, K. L., & Hepler, P. K. (2005). Actin polymerization promotes the reversal of streaming in the apex of pollen tubes. *Cell motility and the cytoskeleton*, 61(2), 112-127.

Cárdenas, L., Lovy-Wheeler, A., Kunkel, J. G., & Hepler, P. K. (2008). Pollen tube growth oscillations and intracellular calcium levels are reversibly modulated by actin polymerization. *Plant physiology*, 146(4), 1611-1621.

Carol, R. J., & Dolan, L. (2002). Building a hair: tip growth in *Arabidopsis thaliana* root hairs. *Philosophical Transactions of the Royal Society of London B: Biological Sciences*, 357(1422), 815-821.

Carroll, S. B. (2008). Evo-devo and an expanding evolutionary synthesis: a genetic theory of morphological evolution. *Cell*, 134(1), 25-36.

Certal, A. C., Almeida, R. B., Carvalho, L. M., Wong, E., Moreno, N., Michard, E., ... & Feijó, J. A. (2008). Exclusion of a proton ATPase from the apical membrane is associated with cell polarity and tip growth in *Nicotiana tabacum* pollen tubes. *The Plant Cell*, 20(3), 614-634.

Chang, F., Yan, A., Zhao, L. N., Wu, W. H., & Yang, Z. (2007). A putative calcium-permeable cyclic nucleotide-gated channel, CNGC18, regulates polarized pollen tube growth. *Journal of Integrative Plant Biology*, 49(8), 1261-1270.

Chang, F., Gu, Y., Ma, H., & Yang, Z. (2013). AtPRK2 promotes ROP1 activation via RopGEFs in the control of polarized pollen tube growth. *Molecular plant*, 6(4), 1187-1201.

Charpentier, M., Sun, J., Martins, T. V., Radhakrishnan, G. V., Findlay, K., Soumpourou, E., ... & Oldroyd, G. E. (2016). Nuclear-localized cyclic nucleotide-gated channels mediate symbiotic calcium oscillations. *Science*, 352(6289), 1102-1105.

Cheung, A. Y., Duan, Q. H., Costa, S. S., de Graaf, B. H., Di Stilio, V. S., Feijo, J., & Wu, H. M. (2008). The dynamic pollen tube cytoskeleton: live cell studies using actin-binding and microtubule-binding reporter proteins. *Molecular plant*, 1(4), 686-702.



- Cheval, C., Aldon, D., Galaud, J. P., & Ranty, B. (2013). Calcium/calmodulin-mediated regulation of plant immunity. *Biochimica et Biophysica Acta (BBA)-Molecular Cell Research*, 1833(7), 1766-1771.
- Clough, S. J., & Bent, A. F. (1998). Floral dip: a simplified method for *Agrobacterium*-mediated transformation of *Arabidopsis thaliana*. *The plant journal*, 16(6), 735-743.
- Corratgé-Faillie, C., Ronzier, E., Sanchez, F., Prado, K., Kim, J. H., Lanciano, S., ... & Xiong, T. C. (2017). The *Arabidopsis* guard cell outward potassium channel GORK is regulated by CPK33. *FEBS letters*, 591(13), 1982-1992.
- Cosgrove, D. J. (2005). Growth of the plant cell wall. *Nature reviews molecular cell biology*, 6(11), 850.
- Cosgrove, D. J. (2016). Catalysts of plant cell wall loosening. *F1000Research*, 5.
- DeFalco, T. A., Moeder, W., & Yoshioka, K. (2016). Opening the gates: insights into cyclic nucleotide-gated channel-mediated signaling. *Trends in plant science*, 21(11), 903-906.
- Demidchik, V., Shabala, S., Isayenkov, S., Cuin, T. A., & Pottosin, I. (2018). Calcium transport across plant membranes: mechanisms and functions. *New Phytologist*.
- Dornelas, M. C., & Dornelas, O. (2005). From leaf to flower: revisiting Goethe's concepts on the "metamorphosis" of plants. *Brazilian Journal of Plant Physiology*, 17(4), 335-344.
- Doyle, J. A. (2006). Seed ferns and the origin of angiosperms. *The Journal of the Torrey Botanical Society*, 169-209.
- Draeger, C., Fabrice, T. N., Gineau, E., Mouille, G., Kuhn, B. M., Moller, I., ... & Ringli, C. (2015). *Arabidopsis* leucine-rich repeat extensin (LRX) proteins modify cell wall composition and influence plant growth. *BMC plant biology*, 15(1), 155.
- Dresselhaus, T., & Franklin-Tong, N. (2013). Male–female crosstalk during pollen germination, tube growth and guidance, and double fertilization. *Molecular plant*, 6(4), 1018-1036.
- Duan, Q., Kita, D., Li, C., Cheung, A. Y., & Wu, H. M. (2010). FERONIA receptor-like kinase regulates RHO GTPase signaling of root hair development. *Proceedings of the National Academy of Sciences*, 107(41), 17821-17826.
- Ermak, G., & Davies, K. J. (2002). Calcium and oxidative stress: from cell signaling to cell death. *Molecular immunology*, 38(10), 713-721.
- Fabrice, T. N., Vogler, H., Draeger, C., Munglani, G., Gupta, S., Herger, A. G., ... & Ringli, C. (2018). LRX Proteins play a crucial role in pollen grain and pollen tube cell wall development. *Plant physiology*, 176(3), 1981-1992.
- Fagard, M., Desnos, T., Desprez, T., Goubet, F., Refregier, G., Mouille, G., ... & Höfte, H. (2000). PROCUSTE1 encodes a cellulose synthase required for normal cell elongation specifically in roots and dark-grown hypocotyls of *Arabidopsis*. *The plant cell*, 12(12), 2409-2423.

- Feijó, J. A., Sainhas, J., Hackett, G. R., Kunkel, J. G., & Hepler, P. K. (1999). Growing pollen tubes possess a constitutive alkaline band in the clear zone and a growth-dependent acidic tip. *The Journal of cell biology*, 144(3), 483-496.
- Felsenstein, J. (1985). Confidence limits on phylogenies: an approach using the bootstrap. *Evolution*, 39(4), 783-791.
- Mang, H., Feng, B., Hu, Z., Boisson-Dernier, A., Franck, C., Meng, X., ... & Shan, L. (2017). Differential regulation of two-tiered plant immunity and sexual reproduction by ANXUR receptor-like kinases. *The Plant Cell*, tpc-00464.
- Fischer, C., DeFalco, T. A., Karia, P., Snedden, W. A., Moeder, W., Yoshioka, K., & Dietrich, P. (2017). Calmodulin as a Ca<sup>2+</sup>-sensing subunit of Arabidopsis cyclic nucleotide-gated channel complexes. *Plant and Cell Physiology*, 58(7), 1208-1221.
- Foreman, J., & Dolan, L. (2001). Root hairs as a model system for studying plant cell growth. *Annals of Botany*, 88(1), 1-7.
- Fort, P. (2017). Rho signaling: An historical and evolutionary perspective. *Rho Gtpases: Molecular Biology In Health And Disease*, 1.
- Forzani, C., Carreri, A., van Bentem, S. D. L. F., Lecourieux, D., Lecourieux, F., & Hirt, H. (2011). The Arabidopsis protein kinase Pto-interacting 1-4 is a common target of the oxidative signal-inducible 1 and mitogen-activated protein kinases. *The FEBS journal*, 278(7), 1126-1136.
- Franck, C. M., Westermann, J., & Boisson-Dernier, A. (2017). Imaging Ca<sup>2+</sup> Dynamics in Wild-Type and NADPH Oxidase-Deficient Mutant Pollen Tubes with Yellow Cameleon and Confocal Laser Scanning Microscopy. In *Plant Germline Development* (pp. 103-116). Humana Press, New York, NY.
- Franck, C. M. (2018). Characterisation and functional analysis of receptor-like cytoplasmic kinase MARIS and protein phosphatases ATUNIS1 and ATUNIS2 in tip-growing plant cells (*Doctoral dissertation*, Universität zu Köln).
- Franck, C. M., Westermann, J., & Boisson-Dernier, A. (2018). Plant Malectin-Like Receptor Kinases: From Cell Wall Integrity to Immunity and Beyond. *Annual review of plant biology*, 69, 301-328. (A)
- Franck, C. M., Westermann, J., Bürssner, S., Lentz, R., Lituiev, D. S., & Boisson-Dernier, A. (2018). The Protein Phosphatases ATUNIS1 and ATUNIS2 Regulate Cell Wall Integrity in Tip-Growing Cells. *The Plant Cell*, 30(8), 1906-1923. (B)
- Friedman, W. E. (1993). The evolutionary history of the seed plant male gametophyte. *Trends in ecology & evolution*, 8(1), 15-21.
- Friedman, W. E., Moore, R. C., & Purugganan, M. D. (2004). The evolution of plant development. *American Journal of Botany*, 91(10), 1726-1741.
- Frietsch, S., Wang, Y. F., Sladek, C., Poulsen, L. R., Romanowsky, S. M., Schroeder, J. I., & Harper, J. F. (2007). A cyclic nucleotide-gated channel is essential for polarized tip growth of pollen. *Proceedings of the National Academy of Sciences*, 104(36), 14531-14536.

- Fry, S. C. (1989). Cellulases, hemicelluloses and auxin-stimulated growth: a possible relationship. *Physiologia Plantarum*, 75(4), 532-536.
- Fry, A. M., O'Regan, L., Sabir, S. R., & Bayliss, R. (2012). Cell cycle regulation by the NEK family of protein kinases. *J Cell Sci*, jcs-111195.
- Fujisawa, M., Hayashi, K., Nishio, T., Bando, T., Okada, S., Yamato, K. T., ... & Ohyama, K. (2001). Isolation of X and Y chromosome-specific DNA markers from a liverwort, *Marchantia polymorpha*, by representational difference analysis. *Genetics*, 159(3), 981-985.
- Galindo-Trigo, S., Gray, J. E., & Smith, L. M. (2016). Conserved roles of CrRLK1L Receptor-Like Kinases in cell Expansion and reproduction from algae to angiosperms. *Frontiers in plant science*, 7, 1269.
- Galway, M. E., Eng, R. C., Schiefelbein, J. W., & Wasteneys, G. O. (2011). Root hair-specific disruption of cellulose and xyloglucan in AtCSLD3 mutants, and factors affecting the post-rupture resumption of mutant root hair growth. *Planta*, 233(5), 985-999.
- Gao, Q. F., Fei, C. F., Dong, J. Y., Gu, L. L., & Wang, Y. F. (2014). Arabidopsis CNGC18 is a Ca<sup>2+</sup>-permeable channel. *Molecular plant*, 7(4), 739-743.
- Gao, Q. F., Gu, L. L., Wang, H. Q., Fei, C. F., Fang, X., Hussain, J., ... & Wang, Y. F. (2016). Cyclic nucleotide-gated channel 18 is an essential Ca<sup>2+</sup> channel in pollen tube tips for pollen tube guidance to ovules in Arabidopsis. *Proceedings of the National Academy of Sciences*, 113(11), 3096-3101.
- Ge, Z., Bergonci, T., Zhao, Y., Zou, Y., Du, S., Liu, M. C., ... & Hou, S. (2017). Arabidopsis pollen tube integrity and sperm release are regulated by RALF-mediated signaling. *Science*, 358(6370), 1596-1600.
- Geitmann, A., & Ortega, J. K. (2009). Mechanics and modeling of plant cell growth. *Trends in plant science*, 14(9), 467-478.
- Gibson, M. (2006). Introducing bryophytes. *Victorian Naturalist, The*, 123(4), 192.
- Goriely, A., & Tabor, M. (2003). Self-similar tip growth in filamentary organisms. *Physical review letters*, 90(10), 108101.
- Govindaraghavan, M., Anglin, S. L. M., Shen, K. F., Shukla, N., De Souza, C. P., & Osmani, S. A. (2014). Identification of interphase functions for the NIMA kinase involving microtubules and the ESCRT pathway. *PLoS genetics*, 10(3), e1004248.
- Gu, Y., Fu, Y., Dowd, P., Li, S., Vernoud, V., Gilroy, S., & Yang, Z. (2005). A Rho family GTPase controls actin dynamics and tip growth via two counteracting downstream pathways in pollen tubes. *J Cell Biol*, 169(1), 127-138.
- Gu, F., & Nielsen, E. (2013). Targeting and regulation of cell wall synthesis during tip growth in plants. *Journal of Integrative Plant Biology*, 55(9), 835-846.
- Gu, L. L., Gao, Q. F., & Wang, Y. F. (2017). Cyclic nucleotide-gated channel 18 functions as an essential Ca<sup>2+</sup> channel for pollen germination and pollen tube growth in Arabidopsis. *Plant signaling & behavior*, 12(11), e1197999.

- Guerriero, G., Hausman, J. F., & Cai, G. (2014). No stress! Relax! Mechanisms governing growth and shape in plant cells. *International journal of molecular sciences*, 15(3), 5094-5114.
- Gutermuth, T., Herbell, S., Lassig, R., Brosché, M., Romeis, T., Feijó, J. A., ... & Konrad, K. R. (2018). Tip-localized Ca<sup>2+</sup>-permeable channels control pollen tube growth via kinase-dependent R- and S-type anion channel regulation. *New Phytologist*, 218(3), 1089-1105.
- Harrison, C. J. (2017). Development and genetics in the evolution of land plant body plans. *Phil. Trans. R. Soc. B*, 372(1713), 20150490.
- Haruta, M., Sabat, G., Stecker, K., Minkoff, B. B., & Sussman, M. R. (2014). A peptide hormone and its receptor protein kinase regulate plant cell expansion. *Science*, 343(6169), 408-411.
- Hashimoto, K., & Kudla, J. (2011). Calcium decoding mechanisms in plants. *Biochimie*, 93(12), 2054-2059.
- Hématy, K., Sado, P. E., Van Tuinen, A., Rochange, S., Desnos, T., Balzergue, S., ... & Höfte, H. (2007). A receptor-like kinase mediates the response of Arabidopsis cells to the inhibition of cellulose synthesis. *Current Biology*, 17(11), 922-931.
- Hepler, P. K., Kunkel, J. G., Rounds, C. M., & Winship, L. J. (2012). Calcium entry into pollen tubes. *Trends in plant science*, 17(1), 32-38.
- Hetherington, A. J., & Dolan, L. (2018). Bilaterally symmetric axes with rhizoids composed the rooting structure of the common ancestor of vascular plants. *Phil. Trans. R. Soc. B*, 373(1739), 20170042.
- Hirano, N., Marukawa, Y., Abe, J., Hashiba, S., Ichikawa, M., Tanabe, Y., ... & Sekimoto, H. (2015). A Receptor-Like Kinase, Related to Cell Wall Sensor of Higher Plants, is Required for Sexual Reproduction in the Unicellular Charophycean Alga, *Closterium peracerosum-strigosum-littorale* Complex. *Plant and Cell Physiology*, 56(7), 1456-1462.
- Hoffmann, R. D., Olsen, L. I., Ezike, C. V., Pedersen, J. T., Manstretta, R., Lopez-Marques, R. L., & Palmgren, M. (2018). Roles of plasma membrane proton ATPases AHA2 and AHA7 in normal growth of roots and root hairs in *Arabidopsis thaliana*. *Physiologia plantarum*.
- Holdaway-Clarke, T. L., Feijó, J. A., Hackett, G. R., Kunkel, J. G., & Hepler, P. K. (1997). Pollen tube growth and the intracellular cytosolic calcium gradient oscillate in phase while extracellular calcium influx is delayed. *The Plant Cell*, 9(11), 1999-2010.
- Holdaway-Clarke, T. L., & Hepler, P. K. (2003). Control of pollen tube growth: role of ion gradients and fluxes. *New Phytologist*, 159(3), 539-563.
- Honkanen, S. (2015). *Genetic basis of rhizoid development in the liverwort Marchantia polymorpha* (Doctoral dissertation, University of Oxford).
- Honkanen, S., Jones, V. A., Morieri, G., Champion, C., Hetherington, A. J., Kelly, S., ... & Dolan, L. (2016). The mechanism forming the cell surface of tip-growing rooting cells is conserved among land plants. *Current Biology*, 26(23), 3238-3244.

- Hua, B. G., Mercier, R. W., Zielinski, R. E., & Berkowitz, G. A. (2003). Functional interaction of calmodulin with a plant cyclic nucleotide gated cation channel. *Plant Physiology and Biochemistry*, 41(11-12), 945-954.
- Humphries, J. A., Vejlpkova, Z., Luo, A., Meeley, R. B., Sylvester, A. W., Fowler, J. E., & Smith, L. G. (2011). ROP GTPases act with the receptor-like protein PAN1 to polarize asymmetric cell division in maize. *The Plant Cell*, tpc-111.
- Hwang, J. U., Wu, G., Yan, A., Lee, Y. J., Grierson, C. S., & Yang, Z. (2010). Pollen-tube tip growth requires a balance of lateral propagation and global inhibition of Rho-family GTPase activity. *Journal of cell science*, jcs-039180.
- Ishizaki, K., Shimizu-Ueda, Y., Okada, S., Yamamoto, M., Fujisawa, M., Yamato, K. T., ... & Ohyama, K. (2002). Multicopy genes uniquely amplified in the Y chromosome-specific repeats of the liverwort *Marchantia polymorpha*. *Nucleic acids research*, 30(21), 4675-4681.
- Ishizaki, K., Chiyoda, S., Yamato, K. T., & Kohchi, T. (2008). Agrobacterium-mediated transformation of the haploid liverwort *Marchantia polymorpha* L., an emerging model for plant biology. *Plant and cell physiology*, 49(7), 1084-1091.
- Ishizaki, K., Nishihama, R., Yamato, K. T., & Kohchi, T. (2015). Molecular genetic tools and techniques for *Marchantia polymorpha* research. *Plant and Cell Physiology*, 57(2), 262-270.
- Ito, K., Ren, J., & Fujita, T. (2014). Conserved function of Rho-related Rop/RAC GTPase signaling in regulation of cell polarity in *Physcomitrella patens*. *Gene*, 544(2), 241-247.
- Jaffe, L. A., Weisenseel, M. H., & Jaffe, L. F. (1975). Calcium accumulations within the growing tips of pollen tubes. *The Journal of cell biology*, 67(2), 488-492.
- Jiang, L., Yang, S. L., Xie, L. F., San Puah, C., Zhang, X. Q., Yang, W. C., ... & Ye, D. (2005). VANGUARD1 encodes a pectin methylesterase that enhances pollen tube growth in the Arabidopsis style and transmitting tract. *The Plant Cell*, 17(2), 584-596.
- Jones, V. A., & Dolan, L. (2012). The evolution of root hairs and rhizoids. *Annals of Botany*, 110(2), 205-212.
- Kaya, H., Nakajima, R., Iwano, M., Kanaoka, M. M., Kimura, S., Takeda, S., ... & Takayama, S. (2014). Ca<sup>2+</sup>-activated reactive oxygen species production by Arabidopsis RbohH and RbohJ is essential for proper pollen tube tip growth. *The Plant Cell*, tpc-113.
- Kenrick, P., & Crane, P. R. (1997). *The origin and early diversification of land plants. A cladistic study* (Vol. 560). Smithsonian Institution Press Washington DC.: A cladistic study. Smithsonian Institution Press.
- Kim, H. S., Czymmek, K. J., Patel, A., Modla, S., Nohe, A., Duncan, R., ... & Kang, S. (2012). Expression of the Cameleon calcium biosensor in fungi reveals distinct Ca<sup>2+</sup> signatures associated with polarized growth, development, and pathogenesis. *Fungal genetics and biology*, 49(8), 589-601.
- Kramer, E. M., Kong, H., & Rausher, M. D. (2017). Plant evolutionary developmental biology. Introduction to a special issue. *New Phytologist*, 216(2), 335-336.

- Kroeger, J. H., Geitmann, A., & Grant, M. (2008). Model for calcium dependent oscillatory growth in pollen tubes. *Journal of Theoretical Biology*, 253(2), 363-374.
- Kroeger, J., & Geitmann, A. (2012). The pollen tube paradigm revisited. *Current opinion in plant biology*, 15(6), 618-624.
- Kubota, A., Ishizaki, K., Hosaka, M., & Kohchi, T. (2013). Efficient Agrobacterium-mediated transformation of the liverwort *Marchantia polymorpha* using regenerating thalli. *Bioscience, biotechnology, and biochemistry*, 77(1), 167-172.
- Kudla, J., Becker, D., Grill, E., Hedrich, R., Hippler, M., Kummer, U., ... & Schumacher, K. (2018). Advances and current challenges in calcium signaling. *New Phytologist*, 218(2), 414-431.
- Kühnreiter, W. M., & Jaffe, L. F. (1990). Detection of extracellular calcium gradients with a calcium-specific vibrating electrode. *The Journal of cell biology*, 110(5), 1565-1573.
- Kumar, S., Stecher, G., & Tamura, K. (2016). MEGA7: molecular evolutionary genetics analysis version 7.0 for bigger datasets. *Molecular biology and evolution*, 33(7), 1870-1874.
- Kwack, B. H. (1967). Studies on cellular site of calcium action in promoting pollen growth. *Physiologia Plantarum*, 20(4), 825-833.
- Kwon, T., Sparks, J. A., Liao, F., & Blancaflor, E. B. (2018). ERULUS Is a Plasma Membrane-Localized Receptor-Like Kinase That Specifies Root Hair Growth by Maintaining Tip-Focused Cytoplasmic Calcium Oscillations. *The Plant Cell*, 30(6), 1173-1177.
- Lassig, R., Gutermuth, T., Bey, T. D., Konrad, K. R., & Romeis, T. (2014). Pollen tube NAD (P) H oxidases act as a speed control to dampen growth rate oscillations during polarized cell growth. *The Plant Journal*, 78(1), 94-106.
- Lee, Y. J., Szumlanski, A., Nielsen, E., & Yang, Z. (2008). Rho-GTPase-dependent filamentous actin dynamics coordinate vesicle targeting and exocytosis during tip growth. *The Journal of cell biology*, 181(7), 1155-1168.
- Lei, M. J., Wang, Q., Li, X., Chen, A., Luo, L., Xie, Y., ... & Xie, Z. P. (2015). The small GTPase ROP10 of *Medicago truncatula* is required for both tip growth of root hairs and nod factor-induced root hair deformation. *The Plant Cell*, tpc-114.
- Leng, Q., Mercier, R. W., Yao, W., & Berkowitz, G. A. (1999). Cloning and first functional characterization of a plant cyclic nucleotide-gated cation channel. *Plant Physiology*, 121(3), 753-761.
- Li, Y. Q., Zhang, H. Q., Pierson, E. S., Huang, F. Y., Linskens, H. F., Hepler, P. K., & Cresti, M. (1996). Enforced growth-rate fluctuation causes pectin ring formation in the cell wall of *Lilium longiflorum* pollen tubes. *Planta*, 200(1), 41-49.
- Li, H., Lin, Y., Heath, R. M., Zhu, M. X., & Yang, Z. (1999). Control of pollen tube tip growth by a Rop GTPase-dependent pathway that leads to tip-localized calcium influx. *The Plant Cell*, 11(9), 1731-1742.

- Liao, H. Z., Zhu, M. M., Cui, H. H., Du, X. Y., Tang, Y., Chen, L. Q., ... & Zhang, X. Q. (2016). MARIS plays important roles in Arabidopsis pollen tube and root hair growth. *Journal of integrative plant biology*, 58(11), 927-940.
- Ligrone, R., Duckett, J. G., & Renzaglia, K. S. (2012). Major transitions in the evolution of early land plants: a bryological perspective. *Annals of botany*, 109(5), 851-871.
- Liu, J., Elmore, J. M., Lin, Z. J. D., & Coaker, G. (2011). A receptor-like cytoplasmic kinase phosphorylates the host target RIN4, leading to the activation of a plant innate immune receptor. *Cell host & microbe*, 9(2), 137-146.
- Liu, J., Zhong, S., Guo, X., Hao, L., Wei, X., Huang, Q., ... & Qu, L. J. (2013). Membrane-bound RLCKs LIP1 and LIP2 are essential male factors controlling male-female attraction in Arabidopsis. *Current Biology*, 23(11), 993-998.
- Liu, L., Zheng, C., Kuang, B., Wei, L., Yan, L., & Wang, T. (2016). Receptor-like kinase RUPO interacts with potassium transporters to regulate pollen tube growth and integrity in rice. *PLoS genetics*, 12(7), e1006085.
- Lorts, C. M., & Briggeman, T. (2008). Evolution of fruit types and seed dispersal: a phylogenetic and ecological snapshot. *Journal of systematics and evolution*, 46(3), 396-404.
- Lu, D., Wu, S., Gao, X., Zhang, Y., Shan, L., & He, P. (2010). A receptor-like cytoplasmic kinase, BIK1, associates with a flagellin receptor complex to initiate plant innate immunity. *Proceedings of the National Academy of Sciences*, 107(1), 496-501.
- Malho, R., & Trewavas, A. J. (1996). Localized apical increases of cytosolic free calcium control pollen tube orientation. *The Plant Cell*, 8(11), 1935-1949.
- Mangano, S., Juárez, S. P. D., & Estevez, J. M. (2016). ROS regulation of polar growth in plant cells. *Plant physiology*, 171(3), 1593-1605.
- McKenna, S. T., Kunkel, J. G., Bosch, M., Rounds, C. M., Vidali, L., Winship, L. J., & Hepler, P. K. (2009). Exocytosis precedes and predicts the increase in growth in oscillating pollen tubes. *The Plant Cell*, 21(10), 3026-3040.
- Mecchia, M. A., Santos-Fernandez, G., Duss, N. N., Somoza, S. C., Boisson-Dernier, A., Gagliardini, V., ... & Grossniklaus, U. (2017). RALF4/19 peptides interact with LRX proteins to control pollen tube growth in Arabidopsis. *Science*, 358(6370), 1600-1603.
- Menand, B., Calder, G., & Dolan, L. (2007). Both chloronemal and caulonemal cells expand by tip growth in the moss *Physcomitrella patens*. *Journal of experimental botany*, 58(7), 1843-1849. (A)
- Menand, B., Yi, K., Jouannic, S., Hoffmann, L., Ryan, E., Linstead, P., ... & Dolan, L. (2007). An ancient mechanism controls the development of cells with a rooting function in land plants. *Science*, 316(5830), 1477-1480. (B)
- Messerli, M., & Robinson, K. R. (1997). Tip localized Ca<sup>2+</sup> pulses are coincident with peak pulsatile growth rates in pollen tubes of *Lilium longiflorum*. *Journal of Cell Science*, 110(11), 1269-1278.

Michard, E., Lima, P. T., Borges, F., Silva, A. C., Portes, M. T., Carvalho, J. E., ... & Feijó, J. A. (2011). Glutamate receptor-like genes form Ca<sup>2+</sup> channels in pollen tubes and are regulated by pistil D-serine. *Science*, 1201101.

Michard, E., Simon, A. A., Tavares, B., Wudick, M. M., & Feijó, J. A. (2017). Signaling with ions: the keystone for apical cell growth and morphogenesis in pollen tubes. *Plant Physiology*, 173(1), 91-111.

Miller, D. D., Callaham, D. A., Gross, D. J., & Hepler, P. K. (1992). Free Ca<sup>2+</sup> gradient in growing pollen tubes of Lillium. *Journal of Cell Science*, 101(1), 7-12.

Monshausen, G. B., Bibikova, T. N., Messerli, M. A., Shi, C., & Gilroy, S. (2007). Oscillations in extracellular pH and reactive oxygen species modulate tip growth of Arabidopsis root hairs. *Proceedings of the National Academy of Sciences*, 104(52), 20996-21001.

Monshausen, G. B., Messerli, M. A., & Gilroy, S. (2008). Imaging of the Yellow Cameleon 3.6 indicator reveals that elevations in cytosolic Ca<sup>2+</sup> follow oscillating increases in growth in root hairs of Arabidopsis. *Plant physiology*, 147(4), 1690-1698.

Monshausen, G. B., Bibikova, T. N., Weisenseel, M. H., & Gilroy, S. (2009). Ca<sup>2+</sup> regulates reactive oxygen species production and pH during mechanosensing in Arabidopsis roots. *The Plant Cell*, 21(8), 2341-2356.

Motose, H., Tominaga, R., Wada, T., Sugiyama, M., & Watanabe, Y. (2008). A NIMA-related protein kinase suppresses ectopic outgrowth of epidermal cells through its kinase activity and the association with microtubules. *The Plant Journal*, 54(5), 829-844.

Motose, H., Hamada, T., Yoshimoto, K., Murata, T., Hasebe, M., Watanabe, Y., ... & Takahashi, T. (2011). NIMA-related kinases 6, 4, and 5 interact with each other to regulate microtubule organization during epidermal cell expansion in Arabidopsis thaliana. *The Plant Journal*, 67(6), 993-1005.

Murphy, E., & De Smet, I. (2014). Understanding the RALF family: a tale of many species. *Trends in plant science*, 19(10), 664-671.

Miyazaki, S., Murata, T., Sakurai-Ozato, N., Kubo, M., Demura, T., Fukuda, H., & Hasebe, M. (2009). ANXUR1 and 2, sister genes to FERONIA/SIRENE, are male factors for coordinated fertilization. *Current Biology*, 19(15), 1327-1331.

Nakazato, T., Kadota, A., & Wada, M. (1999). Photoinduction of spore germination in Marchantia polymorpha L. is mediated by photosynthesis. *Plant and cell physiology*, 40(10), 1014-1020.

Okada, S., Sone, T., Fujisawa, M., Nakayama, S., Takenaka, M., Ishizaki, K., ... & Fukuzawa, H. (2001). The Y chromosome in the liverwort Marchantia polymorpha has accumulated unique repeat sequences harboring a male-specific gene. *Proceedings of the National Academy of Sciences*, 98(16), 9454-9459.

Ono, K., Ohyama, K., & Gamborg, O. L. (1979). Regeneration of the liverwort Marchantia polymorpha L. from protoplasts isolated from cell suspension culture. *Plant Science Letters*, 14(3), 225-229.



- Osborne, C. P., & Beerling, D. J. (2006). Nature's green revolution: the remarkable evolutionary rise of C4 plants. *Philosophical Transactions of the Royal Society of London B: Biological Sciences*, 361(1465), 173-194.
- Otani, K., Ishizaki, K., Nishihama, R., Takatani, S., Kohchi, T., Takahashi, T., & Motose, H. (2018). An evolutionarily conserved NIMA-related kinase directs rhizoid tip growth in the basal land plant *Marchantia polymorpha*. *Development*, 145(5), dev154617.
- Palanivelu, R., & Preuss, D. (2000). Pollen tube targeting and axon guidance: parallels in tip growth mechanisms. *Trends in cell biology*, 10(12), 517-524.
- Park, S., Szumlanski, A. L., Gu, F., Guo, F., & Nielsen, E. (2011). A role for CSLD3 during cell-wall synthesis in apical plasma membranes of tip-growing root-hair cells. *Nature cell biology*, 13(8), 973.
- Persson, S., Paredez, A., Carroll, A., Palsdottir, H., Doblin, M., Poindexter, P., ... & Somerville, C. R. (2007). Genetic evidence for three unique components in primary cell-wall cellulose synthase complexes in *Arabidopsis*. *Proceedings of the National Academy of Sciences*, 104(39), 15566-15571.
- Picton, J. M., & Steer, M. W. (1983). Membrane recycling and the control of secretory activity in pollen tubes. *Journal of Cell Science*, 63(1), 303-310.
- Pina, C., Pinto, F., Feijó, J. A., & Becker, J. D. (2005). Gene family analysis of the *Arabidopsis* pollen transcriptome reveals biological implications for cell growth, division control, and gene expression regulation. *Plant physiology*, 138(2), 744-756.
- Preuss, D., Rhee, S. Y., & Davis, R. W. (1994). Tetrad analysis possible in *Arabidopsis* with mutation of the QUARTET (QRT) genes. *Science*, 264(5164), 1458-1460.
- Qi, Z., Stephens, N. R., & Spalding, E. P. (2006). Calcium entry mediated by GLR3. 3, an *Arabidopsis* glutamate receptor with a broad agonist profile. *Plant Physiology*, 142(3), 963-971.
- Ranf, S., Eschen-Lippold, L., Fröhlich, K., Westphal, L., Scheel, D., & Lee, J. (2014). Microbe-associated molecular pattern-induced calcium signaling requires the receptor-like cytoplasmic kinases, PBL1 and BIK1. *BMC plant biology*, 14(1), 374.
- Raven, J. A., & Edwards, D. (2001). Roots: evolutionary origins and biogeochemical significance. *Journal of experimental botany*, 52(suppl\_1), 381-401.
- Ray, P. D., Huang, B. W., & Tsuji, Y. (2012). Reactive oxygen species (ROS) homeostasis and redox regulation in cellular signaling. *Cellular signalling*, 24(5), 981-990.
- Reece-Hoyes, J. S., & Walhout, A. J. (2018). Gateway recombinational cloning. *Cold Spring Harbor Protocols*, 2018(1), pdb-top094912.
- Rensing, S. A. (2016). Plant Evo–Devo: How Tip Growth Evolved. *Current Biology*, 26(23), R1228-R1230.
- Reski, R. (1998). Development, genetics and molecular biology of mosses. *Botanica Acta*, 111(1), 1-15.

- Robson, G. D., Wiebe, M. G., & Trinci, A. P. (1991). Low calcium concentrations induce increased branching in *Fusarium graminearum*. *Mycological Research*, 95(5), 561-565.
- Röckel, N., Wolf, S., Kost, B., Rausch, T., & Greiner, S. (2008). Elaborate spatial patterning of cell-wall PME and PME1 at the pollen tube tip involves PME1 endocytosis, and reflects the distribution of esterified and de-esterified pectins. *The Plant Journal*, 53(1), 133-143.
- Ronzier, E., Corratgé-Faillie, C., Sanchez, F., Prado, K., Brière, C., Leonhardt, N., ... & Xiong, T. C. (2014). CPK13, a non-canonical CPK, specifically inhibits KAT2 and KAT1 Shaker channels and reduces stomatal opening. *Plant physiology*, pp-114.
- Rounds, C. M., & Bezanilla, M. (2013). Growth mechanisms in tip-growing plant cells. *Annual review of plant biology*, 64, 243-265.
- Roy, S. J., Holdaway-Clarke, T. L., Hackett, G. R., Kunkel, J. G., Lord, E. M., & Hepler, P. K. (1999). Uncoupling secretion and tip growth in lily pollen tubes: evidence for the role of calcium in exocytosis. *The Plant Journal*, 19(4), 379-386.
- Rubinstein, A. L., Marquez, J., Suarez-Cervera, M., & Bedinger, P. A. (1995). Extensin-like glycoproteins in the maize pollen tube wall. *The Plant Cell*, 7(12), 2211-2225.
- Rudall, P. J., & Bateman, R. M. (2007). Developmental bases for key innovations in the seed-plant microgametophyte. *Trends in plant science*, 12(7), 317-326.
- Saitou, N., & Nei, M. (1987). The neighbor-joining method: a new method for reconstructing phylogenetic trees. *Molecular biology and evolution*, 4(4), 406-425.
- Sakai, T., Honing, H. V. D., Nishioka, M., Uehara, Y., Takahashi, M., Fujisawa, N., ... & Smirnov, N. (2008). Armadillo repeat-containing kinesins and a NIMA-related kinase are required for epidermal-cell morphogenesis in *Arabidopsis*. *The Plant Journal*, 53(1), 157-171.
- Schallus, T., Jaeckh, C., Fehér, K., Palma, A. S., Liu, Y., Simpson, J. C., ... & Pieler, T. (2008). Malectin: a novel carbohydrate-binding protein of the endoplasmic reticulum and a candidate player in the early steps of protein N-glycosylation. *Molecular biology of the cell*, 19(8), 3404-3414.
- Schiøtt, M., Romanowsky, S. M., Bækgaard, L., Jakobsen, M. K., Palmgren, M. G., & Harper, J. F. (2004). A plant plasma membrane Ca<sup>2+</sup> pump is required for normal pollen tube growth and fertilization. *Proceedings of the National Academy of Sciences*, 101(25), 9502-9507.
- Schmid, M., Davison, T. S., Henz, S. R., Pape, U. J., Demar, M., Vingron, M., ... & Lohmann, J. U. (2005). A gene expression map of *Arabidopsis thaliana* development. *Nature genetics*, 37(5), 501.
- Schoenaers, S., Balcerowicz, D., Costa, A., & Vissenberg, K. (2017). The Kinase ERULUS Controls Pollen Tube Targeting and Growth in *Arabidopsis thaliana*. *Frontiers in plant science*, 8, 1942.
- Scotland, R. W. (2010). Deep homology: a view from systematics. *Bioessays*, 32(5), 438-449.

- Sede, A. R., Borassi, C., Wengier, D. L., Mecchia, M. A., Estevez, J. M., & Muschietti, J. P. (2018). Arabidopsis pollen extensins LRX are required for cell wall integrity during pollen tube growth. *FEBS letters*, 592(2), 233-243.
- Shiu, S. H., & Bleecker, A. B. (2001). Receptor-like kinases from Arabidopsis form a monophyletic gene family related to animal receptor kinases. *Proceedings of the National Academy of Sciences*, 98(19), 10763-10768.
- Song, L. F., Zou, J. J., Zhang, W. Z., Wu, W. H., & Wang, Y. (2009). Ion transporters involved in pollen germination and pollen tube tip-growth. *Plant signaling & behavior*, 4(12), 1193-1195.
- Stegmann, M., Monaghan, J., Smakowska-Luzan, E., Rovenich, H., Lehner, A., Holton, N., ... & Zipfel, C. (2017). The receptor kinase FER is a RALF-regulated scaffold controlling plant immune signaling. *Science*, 355(6322), 287-289.
- Sun, J., Eklund, D. M., Montes-Rodriguez, A., & Kost, B. (2015). In vivo Rac/Rop localization as well as interaction with Rho GAP and Rho GDI in tobacco pollen tubes: analysis by low-level expression of fluorescent fusion proteins and bimolecular fluorescence complementation. *The Plant Journal*, 84(1), 83-98.
- Steinhorst, L., & Kudla, J. (2013). Calcium-a central regulator of pollen germination and tube growth. *Biochimica et Biophysica Acta (BBA)-Molecular Cell Research*, 1833(7), 1573-1581. (A)
- Steinhorst, L., & Kudla, J. (2013). Calcium and ROS rule the waves of signaling. *Plant Physiology*, pp-113. (B)
- Takeshita, N., Manck, R., Grün, N., de Vega, S. H., & Fischer, R. (2014). Interdependence of the actin and the microtubule cytoskeleton during fungal growth. *Current opinion in microbiology*, 20, 34-41.
- Thompson, J. D., Gibson, T. J., & Higgins, D. G. (2003). Multiple sequence alignment using ClustalW and ClustalX. *Current protocols in bioinformatics*, (1), 2-3.
- Tian, G. W., Chen, M. H., Zaltsman, A., & Citovsky, V. (2006). Pollen-specific pectin methylesterase involved in pollen tube growth. *Developmental biology*, 294(1), 83-91.
- Tunc-Ozdemir, M., Rato, C., Brown, E., Rogers, S., Mooneyham, A., Frietsch, S., ... & Harper, J. F. (2013). Cyclic nucleotide gated channels 7 and 8 are essential for male reproductive fertility. *PLoS One*, 8(2), e55277. (A)
- Tunc-Ozdemir, M., Tang, C., Ishka, M. R., Brown, E., Groves, N. R., Myers, C. T., ... & Mittler, R. (2013). A cyclic nucleotide-gated channel (CNGC16) in pollen is critical for stress tolerance in pollen reproductive development. *Plant physiology*, 161(2), 1010-1020.
- Twell, D., Yamaguchi, J., & McCORMICK, S. H. E. I. L. A. (1990). Pollen-specific gene expression in transgenic plants: coordinate regulation of two different tomato gene promoters during microsporogenesis. *Development*, 109(3), 705-713.

- Véry, A. A., & Davies, J. M. (2000). Hyperpolarization-activated calcium channels at the tip of Arabidopsis root hairs. *Proceedings of the National Academy of Sciences*, 97(17), 9801-9806.
- Wang, Y., Zhang, W. Z., Song, L. F., Zou, J. J., Su, Z., & Wu, W. H. (2008). Transcriptome analyses show changes in gene expression to accompany pollen germination and tube growth in Arabidopsis. *Plant physiology*, 148(3), 1201-1211.
- Wang, W., Wang, L., Chen, C., Xiong, G., Tan, X. Y., Yang, K. Z., ... & Chen, L. Q. (2011). Arabidopsis CSLD1 and CSLD4 are required for cellulose deposition and normal growth of pollen tubes. *Journal of experimental botany*, 62(14), 5161-5177. (A)
- Wang, Z. Y., Li, Z. B., Yang, Y. X., Huang, J. Y., Dong, C. H., & Liu, S. Y. (2011). Silencing of BnROP1 homologue gene leads to male sterility in Arabidopsis [J]. *Chinese Journal of Oil Crop Sciences*, 1, 002. (B)
- Wang, Y., & Wu, W. H. (2017). Regulation of potassium transport and signaling in plants. *Current opinion in plant biology*, 39, 123-128.
- Waszczak, C., Carmody, M., & Kangasjärvi, J. (2018). Reactive oxygen species in plant signaling. *Annual review of plant biology*, 69, 209-236.
- Weisenseel, M. H., Nuccitelli, R., & Jaffe, L. F. (1975). Large electrical currents traverse growing pollen tubes. *The Journal of cell biology*, 66(3), 556-567.
- Yoo, C. M., Quan, L., & Blancaflor, E. B. (2012). Divergence and redundancy in CSLD2 and CSLD3 function during Arabidopsis thaliana root hair and female gametophyte development. *Frontiers in plant science*, 3, 111.
- Zhang, S., Pan, Y., Tian, W., Dong, M., Zhu, H., Luan, S., & Li, L. (2017). Arabidopsis CNGC14 mediates calcium influx required for tip growth in root hairs. *Molecular plant*, 10(7), 1004-1006.
- Zheng, L., Baumann, U., & Reymond, J. L. (2004). An efficient one-step site-directed and site-saturation mutagenesis protocol. *Nucleic acids research*, 32(14), e115-e115.
- Zhou, L., Lan, W., Jiang, Y., Fang, W., & Luan, S. (2014). A calcium-dependent protein kinase interacts with and activates a calcium channel to regulate pollen tube growth. *Molecular plant*, 7(2), 369-376.
- Zonia, L., & Munnik, T. (2011). Understanding pollen tube growth: the hydrodynamic model versus the cell wall model. *Trends in plant science*, 16(7), 347-352.

## 8. INDEX OF ABBREVIATIONS

Abbreviation	Full name
AB	Antibiotic(s)
ACA9	Autoinhibited Ca <sup>2+</sup> ATPase 9
ad.	Fill up to
AUN1/2	ATUNIS1/2, two protein phosphatases
ANX1/2	ANXUR1/2, two malectin-like receptors
<i>An</i>	<i>Aspergillus nidulans</i> ; a filamentous fungus
ARK1	Armadillo repeat-containing kinesin 1
<i>At</i>	<i>Arabidopsis thaliana</i> ; an angiosperm
ATP	Adenosine triphosphate
bp	Base pair
bHLH	Basic helix loop helix transcription factors
BIK1	BOTRYTIS-INDUCED KINASE1
BUPS1/2	BUDDHA'S PAPER SEAL1/2; two Malectin-like receptors
C/N-term.	Carboxy-/Amino-terminal
Ca <sup>2+</sup> /[Ca <sup>2+</sup> ] <sub>cyl</sub>	Calcium ion/cytoplasmic Calcium concentration
CaM(BD)	Calmodulin-(binding domain)
CESA	Cellulose synthase
CFP	Cyan fluorescent protein
CLSM	Confocal laser scanning microscope
CNBD	Cyclic nucleotide-binding domain
Col-0	Columbia-0; an <i>Arabidopsis</i> ecotype
<i>Cp</i>	<i>Closterium peracerosum-strigosum-littorale</i> -complex of unicellular charophycean green algae
CNGCs	Cyclic nucleotide-gated ion channels
CPK	Calcium-dependent protein kinase
CRISPR/Cas system	Clustered Regularly Interspaced Short Palindromic Repeat/ endonuclease system; a genome editing method
CSL	CESA-like
CW	Cell wall
CWI	Cell wall integrity
d	Day(s)
dCAPS	Derived cleaved amplified polymorphism sequence

ddH <sub>2</sub> O	Double-distilled water; <i>i.e.</i> millipore water
dNTPs	Deoxynucleotide triphosphates
ECM	Extracellular matrix
<i>e.g.</i>	(lat.) <i>exempli gratia</i> ; for example
ER	Endoplasmic reticulum
<i>etc.</i>	(lat.) <i>et cetera</i> ; and so forth
F1; -2; -3	Filial generation 1; -2; -3
FER	FERONIA, a malectin-like receptor
Fig.	Figure
FR	Far-red (light)
FRET	Förster resonance energy transfer
gDNA	Genomic DNA
GE	Gel electrophoresis
GEF	Guanine exchange factor
GFP	Green fluorescent protein
GLR	Glutamate-receptor like ion channel
GTP	Guanosine triphosphate
GUS	Glucuronidase
GW	Gateway
h	Hour(s)
H <sup>+</sup>	Hydrogen ion, <i>i.e.</i> a proton
<i>i.e.</i>	(lat) <i>id est</i> ; namely, in other words
<i>ipr</i>	<i>Impotence rescue</i>
kb	Kilo base pair
LB	Lysogeny broth; a common bacteria cultivation medium
LIP1	LOST IN POLLEN TUBE GUIDANCE1; a receptor-like cytoplasmic kinase
LRL	<i>Lotus japonicus</i> -ROOTHAIRLESS-LIKE transcription factor
LRX1/2	Leucin-rich-repeat extensin chimera 1/2
μm	Micrometer
μM	Micromolar
M	Molar
mm	Millimeter
min	Minute(s)
MLR	Malectin-like receptor

mM	Millimolar
<i>Mp</i>	<i>Marchantia polymorpha</i> ; a liverwort
MRI	MARIS, a receptor-like cytoplasmic kinase
MS	Murashige-Skoog; a plant growth medium
my(a)	Million years (ago)
NADP(H)	Nicotinamide adenine dinucleotide phosphate
NEKs	NEVER IN MITOSIS A (NIMA)-RELATED KINASEs
NLS	Nuclear localization site
<i>NtAHA</i>	<i>Nicotiana tabacum</i> Autoinhibited plasma membrane H <sup>+</sup> -ATPase
OD <sub>600</sub>	Optical density at wavelength of 600 nanometers
ORF	Open reading frame
OsRUPO	<i>Oryza sativa</i> RUPTURED POLLEN; a rice Malectin-like receptor
ox	Overexpression
PCR	Polymerase chain reaction
PM	Plasma membrane
PME(I)	Pectin methylesterase (inhibitor)
<i>Pp</i>	<i>Physcomitrella patens</i> ; a leafy moss
PPFD	Photosynthetically active photon flux density
PRK	POLLEN-SPECIFIC RECEPTOR KINASE
<i>pro</i>	Promoter
P <sub>t</sub>	Turgor pressure
PT	Pollen tube
PTI	Pto-interacting protein
<i>qrt</i>	<i>Quartet</i> mutant background
RALFs	RAPID ALKALINIZATION FACTORs; signaling peptides
R <sub>b</sub>	Bursting rate
RBOHH/J	RESPIRATORY BURST OXIDASE H/J; two NADPH oxidases
RFP	Red fluorescent protein
RE	Restriction enzyme
R <sub>g</sub>	Germination rate
RH	Root hair
RHD	ROOT HAIR DEFECTIVE; a group of root hair growth regulators
RIPK	RPM1-INDUCED PROTEIN KINASE
RLCK	Receptor-like cytoplasmic kinase

RLK	Receptor-like kinase
ROP	Rho-family GTPases of plants
ROS	Reactive oxygen species
rpm	Rounds per minute
RS	Restriction site
RSL	RHD6-LIKE; a transcription factor
RT	Reverse transcriptase
RZ	Rhizoid
Sac	A restriction enzyme
SDM	Site-directed mutagenesis
SEM	Standard error of the mean value
Ser	Serine; a proteinogenic amino acid
SNP	Single nucleotide polymorphism
Spe	A restriction enzyme
T-DNA	Transfer DNA
T1; -2; -3	Transformed (filial) generation 1; -2; -3
Tab.	Table
Tak-1/2	Takaragaike-1/2; <i>Marchantia</i> ecotypes
T <sub>E</sub>	Transmission efficiency
THE1	THESEUS1, a Malectin-like receptor
Thr	Threonine; a proteinogenic amino acid
TOPP	Type-one protein phosphatase
UTR	Untranslated region
VEI	VEIVE, a receptor-like cytoplasmic kinase
VGD1	VANGUARD1, a pectin methylesterase
YC3.60	Yellow Cameleon 3.60; a Ca <sup>2+</sup> biosensor
YFP	Yellow fluorescent protein



## 9. INDEX OF FIGURES

Fig. 1	The variety of growth modes in plant cells.
Fig. 2	The functions of root hairs and pollen tubes in flowering plants.
Fig. 3	Structural composition of the extracellular matrix and intracellular cytoskeleton of the tip-growing cell.
Fig. 4	The internal growth machinery relies on close interplay between exocytosis and ion fluxes.
Fig. 5	Occurrence of tip-growing cells during land plant evolution.
Fig. 6	Phylogeny of Malectin-like receptors.
Fig. 7	Phylogeny of <i>Arabidopsis</i> and bryophytic PTI-like homologs.
Fig. 8	Cell wall integrity signaling in tip-growing cells of <i>Arabidopsis</i> and <i>Marchantia</i> .
Fig. 9	<i>Marchantia polymorpha</i> developmental stages.
Fig. 10	Fluorescence spectra of used fluorophores.
Fig. 11	CLSM-based detection of RFP signals in autofluorescent tissue of <i>M. polymorpha</i> .
Fig. 12	The T-DNA mutant lines ST13-3 and ST14-3 display defects in rhizoid growth.
Fig. 13	<i>MpPTI</i> -RFP complements ST13-3 ( <i>Mppti</i> )-induced loss of CWI in growing <i>Marchantia</i> rhizoids.
Fig. 14	Structural and functional conservation between <i>AtMRI</i> and <i>MpPTI</i> .
Fig. 15	Expression of <i>MpPTI</i> -YFP rescues <i>mri-1</i> -induced loss of CWI during <i>in vitro</i> pollen germination.
Fig. 16	Expression of <i>MpPTI</i> -YFP partially restores the <i>mri-1/mri-1</i> seed set.
Fig. 17	Expression of <i>MpPTI</i> -YFP rescues CWI in growing <i>mri-1/mri-1</i> root hairs.
Fig. 18	Overexpression of <i>MpPTI</i> -3xCitrine leads to growth inhibition in <i>Marchantia</i> wild-type rhizoids.
Fig. 19	Overexpression of <i>AtMRI</i> -3xCitrine leads to growth inhibition in <i>Marchantia</i> wild-type rhizoids.
Fig. 20	Overexpression of <i>AtANX1</i> -3xCitrine and <i>AtFER</i> -3xCitrine leads to growth inhibition in <i>Marchantia</i> rhizoids.
Fig. 21	Expression of <i>MpPTI</i> -YFP leads to decrease of PT length <i>in vitro</i> .
Fig. 22	Phylogenetic analysis of PTI-like proteins from <i>Arabidopsis</i> and bryophytes.
Fig. 23	Expression of <i>MpPTI</i> <sup>[R240C]</sup> -YFP leads to growth inhibition in Col-0 root hairs.
Fig. 24	Phenotyping of <i>Mppti</i> and <i>Mpthe1</i> .
Fig. 25	Both <i>aun1 aun2</i> double mutants, but not <i>aun1</i> or <i>aun2</i> single mutants, display inhibition of pollen germination <i>in vitro</i> .
Fig. 26	Expression of <i>AUN2</i> -YFP complements the <i>aun1-1 aun2-1</i> pollen growth inhibition phenotype <i>in vitro</i> .
Fig. 27	Knockdown-/ knockout of <i>CNGC18</i> leads to pollen bursting <i>in vitro</i> .
Fig. 28	Phenotypic analyses of backcrossed and non-backcrossed <i>cngc18-17</i> plants.
Fig. 29	<i>In vitro</i> pollen germination assay of Col-0 <i>qrt</i> hemizygotously expressing GFP-CNGC18.
Fig. 30	Knockdown of both, <i>CNGC18</i> and <i>MRI</i> , leads to irregular intracellular Ca <sup>2+</sup> -dynamics, which correlate with pollen tube growth rate oscillation.
Fig. 31	Irregular intracellular Ca <sup>2+</sup> -oscillation correlates with and precedes pollen tube growth rate decrease in both,

	<i>cngc18-17</i> and <i>mri-2</i> .
Fig. 32	<i>In vitro</i> pollen germination of <i>anx1-1/anx1-1 anx2-1/ANX2</i> expressing YFP-CNGC18.
Fig. 33	VEIVE is an exclusively pollen-expressed gene.
Fig. 34	VEIVE genetic locus and <i>vei-1</i> and <i>vei-2</i> T-DNA insertion sites.
Fig. 35	<i>vei-1</i> and <i>vei-2</i> do not display any significant phenotypic deviations concerning <i>in vitro</i> pollen germination or bursting.
Fig. 36	<i>vei-1</i> and <i>vei-2</i> have a mildly decreased seed set.
Fig. 37	The evolution of tip-growth control.
Fig. 38	Schematic model of the pollen tube CWI signaling pathway including the hypothetical positions of AUN1/2.
Fig. 39	How may CNGCs and Ca <sup>2+</sup> -dynamics be connected to CWI signaling and tip-growth control?

## 10. INDEX OF TABLES

Tab. 1	Genetically modified <i>Arabidopsis thaliana</i> lines.
Tab. 2	Genetically modified <i>Marchantia polymorpha</i> lines.
Tab. 3	Entry vectors and clones.
Tab. 4	Destination vectors.
Tab. 5	Expression vectors.
Tab. 6	Oligonucleotide sequences.
Tab. 7	Common media.
Tab. 8	Antibiotics.
Tab. 9	Preparation kits.
Tab. 10	Software.
Tab. 11	Standard Genotyping-PCR mix.
Tab. 12	Standard PCR protocol.
Tab. 13	Amplicon sizes for dCAPS-based genotyping of the <i>cngc18-17</i> and CNGC18 alleles.
Tab. 14	cDNA synthesis protocol.
Tab. 15	PCR-mix for promoter and ORF amplification.
Tab. 16	PCR protocol for promoter and ORF amplification.
Tab. 17	T4-Ligase-based DNA ligation protocol.
Tab. 18	Protocol for analytical restriction digestion reactions.
Tab. 19	Sequencing reaction protocol.
Tab. 20	Mendelian segregation ratios in a reciprocal crossing experiment absent from allelic transmission defects.
Tab. 21	Segregation analysis of the <i>mri-1</i> allele in the <i>mri-1</i> /MRI background transformed with <i>proMRI::MpPTI-YFP</i> .
Tab. 22	Expression of <i>MpPTI-YFP</i> does not inhibit Col-0 wild-type pollen germination.
Tab. 23	Determination of relative pollen tube numbers in dependance of GFP-CNGC18 expression.
Tab. 24	Segregation analysis of the <i>anx2-1</i> allele in the <i>anx1-1/anx1-1 anx2-1/ANX2</i> background transformed with <i>proLAT52::YFP-CNGC18</i> .
Tab. 25	Segregation analysis of <i>proLAT52::YFP-CNGC18</i> in the <i>anx1-1/anx1-1 anx2-1/ANX2</i> background.
Tab. 26	Segregation of the <i>anx2-1</i> allele in the <i>anx1-1/anx1-1 anx2-1/ANX2</i> background transformed with <i>proACA9::GFP-CNGC18</i> .
Tab. 27	Transmission efficiency of <i>vei-1</i> and <i>vei-2</i> based on reciprocal crossing experiments.
Tab. 28	The <i>Arabidopsis</i> genome does not contain any close, pollen-expressed VEIVE homologs.
Tab. S1	The 10 closest <i>MpPTI</i> homologs of <i>Arabidopsis thaliana</i> .
Tab. S2	The 10 closest <i>MpTHE1</i> homologs of <i>Arabidopsis thaliana</i> .

## 11. ACKNOWLEDGEMENTS

I would like to thank

- **Dr. Aurélien Boisson-Dernier** for accepting me as a doctoral student in his research group and for being the first referee of my dissertation. Thanks for your very helpful and appreciative supervision throughout the project, for encouragement and permission to engage in scientific and academic events and for the manifold of new things I was able to learn during the last three years thanks to you.
- **Prof. Dr. Martin Hülskamp** (University of Cologne) for hosting our research group in the botanical institute and for agreeing to be the second referee of my dissertation. Thank you for the possibility to participate in activities in- and outside of the lab and making us feel like part of the whole group.
- **Prof. Dr. Siegfried Roth** (University of Cologne) for agreeing to chair my PhD defense.
- **Dr. Swen Schellmann** for agreeing to be part of the doctoral committee.
- **Prof. Dr. Liam Dolan** (University of Oxford, United Kingdom) and his whole research group for kindly hosting me for six weeks in their research group and giving me the possibility to learn everything about utilization of *Marchantia* as a genetic model organism and to work on our collaborative project. Thank you for making my visit insightful, informative and highly enjoyable. Special thanks go to **Susanna Streubel**, who did a great job introducing me to the lab, to *Marchantia*-related work and to Oxford life.
- **Prof. Dr. Ute Höcker** (University of Cologne) and her research group for kindly granting me access to their far-red light plant chamber.
- **Prof. Dr. Jeffrey F. Harper** (University of Nevada, Reno, USA) for provision of the *cngc18-1/CNGC18*, *cngc18-2/CNGC18* and GFP-CNGC18 *Arabidopsis* lines (Frietsch et al., 2007).
- **Prof. Dr. Yong-Fei Wang** (Shanghai Academy of Sciences, China) for provision of the *Arabidopsis* YC3.60 expression lines and the *Arabidopsis cngc18-17* mutant line (Gao et al., 2016).
- **Prof. Dr. Hiroyasu Motose** (University of Okayama, Japan) for valuable advice on imaging of rhizoid growth in liquid systems.
- **Roswitha Lentz** for her truly awesome work as a lab technician in our research group: Thank you for your everyday motivation that exceeded everything one could have expected by far. Thanks for your helpful advice and ideas, your pleasant and kind nature and for constantly expanding my knowledge on the best North Rhine-Westphalian hiking trails and weekend destinations.
- Our former practical students **Iqra**, **Pilar**, **Sebastian** and **Simon** for enriching the Boisson-Dernier group with your presence. It was fun working with you and having you around.
- **Dr. Lisa Stephan** and **Dr. Christina Maria Franck** for detailed proof-reading of the thesis draft.

- The **whole Hülskamp working group** for a nice working environment, helpful advice, 'open ears', occasional chats and discussions about 'everything and anything', summerly 'Mauerbier', and the nice evenings outside of the lab.
- I would like to thank **my mother** and **my grandmother** for supporting me throughout my life in every possible way. Thank you for everything you have done for me!
- Last, but surely not least, thank you **Christina** for our awesome 'long-term collaboration' in- and outside of the lab. Thank you for having shared two wonderful years in Cologne with me. Thank you for all the support, shared laughter, cheer-up and so many good moments we have already shared so far. You're out of this world!

## 12. EIGENSTÄNDIGKEITSERKLÄRUNG

(Declaration of authenticity)

Ich versichere, dass ich die von mir vorgelegte Dissertation selbständig angefertigt, die benutzten Quellen und Hilfsmittel vollständig angegeben und die Stellen der Arbeit – einschließlich Tabellen, Karten und Abbildungen –, die anderen Werken im Wortlaut oder dem Sinn nach entnommen sind, in jedem Einzelfall als Entlehnung kenntlich gemacht habe; dass diese Dissertation noch keiner anderen Fakultät oder Universität zur Prüfung vorgelegen hat; dass sie – abgesehen von unten angegebenen Teilpublikationen – noch nicht veröffentlicht worden ist, sowie, dass ich eine solche Veröffentlichung vor Abschluss des Promotionsverfahrens nicht vornehmen werde. Die Bestimmungen der Promotionsordnung sind mir bekannt. Die von mir vorgelegte Dissertation ist von Dr. Aurélien Boisson-Dernier betreut worden.

Teilpublikationen:

Die in den Abschnitten 4.2. und 5.2. dargestellten Daten wurden bereits vor Fertigstellung der vorgelegten Dissertation publiziert; siehe Literaturverzeichnis (Abschnitt 7), Publikation von Franck et al., 2018 B.

---

(Jens Westermann)

## 13. LEBENS LAUF

(Curriculum vitae)

Persönliche Daten	
Name:	Westermann
Vorname:	Jens
Geburtsdatum:	26.09.1989
Geburtsort:	Schwalmstadt, Hessen, Deutschland
Nationalität:	Deutsch
Ausbildung	
03/2016 – heute	<b>Promotion in Botanik</b> Universität zu Köln (Deutschland)
10/2017 – 12/2017	<b>Forschungsaufenthalt als Gaststudent</b> Universität zu Oxford (Vereinigtes Königreich) Arbeitsgruppe von Prof. Dr. Liam Dolan  mithilfe eines Kurzzeitstipendiums für Doktoranden des Deutschen Akademischen Austauschdienstes (DAAD)
04/2014 – 02/2016	<b>Master of Science in Molekular- und Zellbiologie</b> Philipps-Universität (Marburg, Deutschland)  Durchschnittsnote: 1,3  Titel der schriftlichen Abschlussarbeit: "Optimization of gene targeting efficiency and cytogenetic determination of the chromosome number of <i>Physcomitrella patens</i> "  durchgeführt in der Arbeitsgruppe von Prof. Dr. Stefan Rensing, 'Zellbiologie der Pflanzen'
11/2013 – 01/2014	<b>Freiwilliges Praktikum</b> Max-Planck-Institut für molekulare Zellbiologie und Genetik (Dresden, Deutschland)  Schwerpunkte: vergleichende Genomik, Evolutionsbiologie und angewandte Bioinformatik  durchgeführt in der Arbeitsgruppe von Dr. Michael Hiller, 'Computational Biology and Evolutionary Genomics'
10/2010 – 09/2013	<b>Bachelor of Science in Biologie</b> Philipps-Universität (Marburg, Deutschland)  Durchschnittsnote: 1,7

	<p>Titel der schriftlichen Abschlussarbeit: "Sprouties as possible regulators of the MAP-kinase pathway during budding in <i>Hydra vulgaris</i>"</p> <p>durchgeführt in der Arbeitsgruppe von Prof. Dr. Monika Hassel, 'Molekulare Evolution der Wirbellosen'</p>
10/2009 – 06/2010	<p><b>Zivildienst</b> AWO Altenzentrum (Stadtallendorf, Deutschland)</p>
09/2006 – 06/2009	<p><b>Gymnasiale Oberstufe (Abitur)</b> Alfred-Wegener-Schule (Kirchhain, Deutschland)</p> <p>Leistungskurse: Biologie, Englisch</p>
08/2000 - 07/2006	<p><b>Gymnasiale Mittelstufe</b> Georg-Büchner-Schule (Stadtallendorf, Deutschland)</p>